

Impingement in total hip replacements

Mr Simon Williams

Submitted in accordance with the requirements for the degree of
PhD and Master of Science

The University of Leeds
School of Mechanical Engineering

November, 2022

The candidate confirms that the work submitted is his/her own and that appropriate credit has been given where reference has been made to the work of others.

This copy has been supplied on the understanding that it is copyright material and that no quotation from the thesis may be published without proper acknowledgement.

© 2022 The University of Leeds and Simon Williams

Abstract

Dislocation is the most common reason for early failure in total hip replacements (THRs) and occurs following impingement. Impingement is the unwanted contact between either the component and/or bone around the THR. This thesis investigates the effect of factors such as patient bony anatomy, patient activity and cup orientation on impingement likelihood and severity to provide an understanding of how these factors and their interplay may be used to reduce impingement in THRs.

Geometric models were developed of bony geometries from different subjects so that variation in anatomy affecting impingement could be investigated, these were implanted with THRs. Kinematic datasets from different subjects were applied to the models to investigate the effects of subject activity and cup orientation. An in vitro simulator study was carried out which developed kinematic activity data for use in a hip simulator to investigate the consequences of impingement damage.

Variation in bony anatomy, patient activity and cup orientation affected the likelihood and severity of impingement. The anterior inferior iliac spine and anteversion angle of the natural acetabulum significantly affected impingement outcomes and could be used to predict bone-on-bone impingement. The variation in subject's kinematic data resulted in varying impingement occurrences at different cup orientations. This suggests that clinically recommended implantation positions should be patient-specific. A hip simulator test was developed which applied clinically-relevant motions and loads to generate impingement damage and compared three subject's squat activities. Findings correlated with geometric model predictions.

The variation in individual subject bone and motion suggest a subject-specific impingement-free range of motion, therefore to minimise impingement and potential dislocation, implantation targets for component orientation should be patient-specific. The methods developed in this thesis could be developed for a preoperative planning tool and aid the design of new implants by providing clinically relevant tools to assess for impingement.

Acknowledgements:

I would like to acknowledge the Engineering and Physical Research Council (EPSRC) and DePuy Synthes UK for funding my position at the Institute of Medical and Biological Engineering while I completed this PhD. I would also like to thank DePuy Synthes UK for supplying the component drawings and physical test samples.

I would like to express my deepest gratitude to Professor Sophie Williams for her continuous encouragement, inspiration and support throughout my PhD. I would also like to thank my supervisors Professor Graham Isaac, Dr. Alison Jones, Professor Ruth Wilcox, Professor Tim Board and Ms Alison Traynor for their help and guidance throughout this work. Thank you to all of you for the inspiration and learning opportunities you have all provided.

I would like to personally thank Dr. David Jiminez-Cruz, Dr. Gregory Pryce, Mr Nicholas Cooper and Dr. Robin Layton for their technical support and guidance throughout the practical work. I would also like to thank all of the technicians in iMBE for their assistance and support as well as my fellow PhD students who have helped motivate and inspire me.

I would like to thank my friends and family - Dad, Mum, Christopher and Nicola for your support and encouragement through the tough times. I would like to finally thank María for all of your support over these last five years, this wouldn't have been possible without you.

Conference Proceedings

Chapter Three of this thesis is based on the publication at the British Orthopaedic Research Society 2020 conference proceeding entitled: The effect of anterior inferior iliac spine anatomy on the range of motion to impingement in total hip replacements.

Chapter Four of this thesis is based on the publication at the European Society of Biomechanics 2021 conference proceeding entitled: Effect of bony geometry on impingement in total hip replacements during dislocation-prone activities.

Chapter Five of this thesis is based on the publication at the Orthopaedic Research Society 2022 conference proceeding entitled: Impingement risk in total hip replacement: effect of patient activity differences on recommended cup position.

Table of Contents

Abstract.....	iii
Acknowledgements:	iv
Conference Proceedings	v
Table of Contents	vi
List of Tables	xiv
List of Figures.....	xvii
List of Abbreviations.....	xxix
Chapter One : Literature Review	1
1.1 Introduction	1
1.2 Failure modes of total hip replacements.....	4
1.2.1 The role of impingement and edge loading in failure.....	6
1.3 Causes of impingement.....	7
1.3.1 Implant factors which contribute towards impingement.....	7
1.3.1.1 Femoral head diameter	7
1.3.1.1.1 Jumping distance	10
1.3.1.1.2 Head to neck ratio	11
1.3.1.2 Acetabular liner design	13
1.3.1.3 Offset, leg-length and neck-shaft angle	14
1.3.2 Activities of daily living prone to impingement.....	15
1.3.2.1 Dislocation-prone activities of daily living (Nadzadi, et al., 2003).....	16
1.3.2.2 Impingement-prone activities of daily living (Layton, et al., 2021)	19
1.3.3 Surgical Factors risking impingement	23
1.3.3.1 Surgical Approach.....	23
1.3.3.2 Acetabular cup orientation	26
1.3.3.3 Current THR preoperative planning methods.....	27
1.3.4 Patient factors that influence impingement	28
1.3.4.1 Geometry of pelvis and femur	28
1.3.4.2 Pelvic (sagittal) tilt	32
1.4 Evidence and consequences of impingement.....	33
1.5 Impingement studies using computational models of THR's.....	36
1.5.1 Finite Element Analysis models	38
1.5.2 Geometric analysis models	40

1.6	Hip simulator studies investigating impingement.....	41
1.7	Project rationale	47
1.8	Project aim	50
1.9	Project objectives	50
Chapter Two : Development of nine geometric models of a total hip replacement with individual bony morphology		51
2.1	Introduction	51
2.2	Method development.....	53
2.2.1	Requirements of the geometric models.....	53
2.2.2	Overview of method development.....	53
2.2.3	CT scan selection and bony geometry characterisation.....	53
2.2.4	Segmentation of the CT scans.....	55
2.2.5	Conversion of surface meshes to 3D solid geometry	58
2.2.6	Removal of osteophytes.....	61
2.2.7	Defining the Centre of Rotation.....	64
2.2.8	Defining the coordinate systems	66
2.2.9	Scaling of the geometric models	69
2.2.10	Virtual total hip replacement.....	70
2.2.10.1	Femoral component assembly	70
2.2.10.2	Acetabular component assembly	73
2.2.10.3	Complete geometric model	74
2.2.11	Bony geometry measurements	75
2.2.12	Cardan sequences to input known rotations	82
2.2.13	Outputs of the geometric model	85
2.2.14	Verification of the geometric model.....	86
2.3	Discussion.....	87
2.3.1	Limitations.....	88
2.4	Summary.....	89
Chapter Three : Identifying anatomical bony features and their effect on patient's with THR's		90
3.1	Introduction	90
3.2	Method	92
3.2.1	Overview of method	92
3.2.2	Classification analysis (Hetsroni, et al., 2013).....	92
3.2.3	Assessing range of motion.....	93
3.2.4	Statistical analysis.....	94

3.3	Results	95
3.3.1	Overview of results.....	95
3.3.2	The effect of the location of the peak of the AIIIS on the range of motion	95
3.3.3	Impingement locations	98
3.3.4	Amount of difference in range of motion across the geometric models.....	99
3.3.5	AIIIS combination measures	101
3.3.6	Classification analysis (Hetsroni, et al., 2013).....	102
3.4	Discussion.....	103
3.4.1	The effect of the location of the peak of the AIIIS on the range of motion of the geometric models	103
3.4.2	Location and type of impingement	105
3.4.3	Range of motion difference across the geometric models	106
3.4.4	AIIIS combination measures	106
3.4.5	Hetsroni classification analysis.....	107
3.4.6	Limitations.....	108
3.5	Summary	108
Chapter Four : Effect of bony geometry on impingement in Total Hip Replacement during dislocation-prone activities.....		110
4.1	Introduction	110
4.2	Method	112
4.2.1	Overview of method	112
4.2.2	Geometric models and the dislocation-prone activities of daily living (Nadzadi, et al., 2003)	113
4.2.3	Bony features for comparison	113
4.2.4	Outcome measures of impingement	114
4.2.5	Statistical analysis.....	115
4.3	Results	115
4.3.1	Overview of results.....	115
4.3.2	Occurrence and types of impingement across different bony geometries.....	116
4.3.3	Severity of bone-on-bone impingement for the anterior dislocation-prone activities	117
4.3.3.1	The effect of different bony geometries.....	117
4.3.3.2	The effect of the anteversion angle of the natural acetabulum.....	120

4.3.4	Severity of bone-on-bone impingement for the posterior dislocation-prone activities	122
4.3.4.1	The effect of bony geometries.....	123
4.3.4.2	The effect of the location of the anterior inferior iliac spine	125
4.3.5	Bone-on-bone impingement sites.....	132
4.4	Discussion.....	135
4.4.1	Occurrence and types of impingement across differing bony geometries.....	135
4.4.2	Effect of the anteversion angle of the natural acetabulum on the severity of impingement	136
4.4.3	Effect of the location of the AIIS on the severity of impingement.....	137
4.4.4	Effect of different activities on the severity of impingement.....	138
4.4.5	Bone-on-bone impingement sites.....	140
4.4.6	The severity of impingement measures	142
4.4.7	Clinical significance.....	143
4.4.8	Limitations of the study	144
4.5	Summary.....	145
Chapter Five : Subject-specific kinematic activities of daily living and their effect on impingement in THR's		147
5.1	Introduction	147
5.2	Method	149
5.2.1	Overview of study design	149
5.2.2	Individual kinematic activity data (Layton, et al., 2021)	149
5.2.3	Initial testing	153
5.2.4	Severity of impingement during a squat activity	154
5.2.5	Cup orientation grids for each activity	155
5.2.6	Cup orientation grids for each subject.....	156
5.2.7	Statistical analysis.....	156
5.3	Results	157
5.3.1	Overview of results.....	157
5.3.2	Initial testing	157
5.3.2.1	28mm THR components	157
5.3.2.2	Impingement occurrences in a malpositioned acetabular cup.....	158
5.3.3	Severity of impingement during a squat activity	159

5.3.4 Cup orientation grids for each activity	161
5.3.4.1 Occurrence and type of impingement during the anterior impingement-prone activities	162
5.3.4.2 Occurrence and type of impingement during the posterior impingement-prone activities.....	162
5.3.4.3 Number of occurrences of impingement for each activity to demonstrate severity	163
5.3.5 Cup orientation grids for individual subjects and their subject-specific impingement-prone activities	165
5.3.5.1 Impingement occurrences across subjects	165
5.3.5.2 Analysis of the cup orientation grids of the different subjects	166
5.3.5.3 Comparison of the subjects with the greatest and smallest number of occurrences of impingement.....	170
5.4 Discussion.....	173
5.4.1 Comparison of the impingement-prone activities (Layton, et al., 2021) with the literature	173
5.4.2 Effect of the impingement-prone activities	174
5.4.3 Cup orientation and its effect on impingement	176
5.4.4 The effect of range of motion on impingement occurrence during the impingement-prone activities for different subjects	178
5.4.5 The effect of the subject variation on impingement occurrence during the impingement-prone activities.....	178
5.4.6 Dynamic assessment and THR surgical preoperative planning potential.....	179
5.4.7 Limitations.....	180
5.5 Summary.....	181
Chapter Six : <i>In vitro</i> consequences of impingement in total hip replacements during clinically-relevant motions	183
6.1 Introduction	183
6.2 Method	185
6.2.1 Overview of method	185
6.2.2 THR components	185
6.2.3 Development of <i>in vitro</i> impingement test inputs.....	186
6.2.3.1 Selection of the three squat kinematics	186
6.2.3.2 Component orientation.....	188
6.2.3.3 Using the incorrect sequence of rotations in the simulator	188

6.2.3.3.1	Mitigations taken for using the incorrect order of rotations in the hip simulator	190
6.2.3.3.2	Comparisons of the equivalent rotations of the simulator inputs with the previous kinematic dataset (Layton, et al., 2021)	191
6.2.3.4	Development of kinematic simulator inputs.....	193
6.2.3.5	Effect of smoothing on the impingement event ...	195
6.2.3.6	Angular sliding distance during impingement.....	197
6.2.3.7	Simulator force input	199
6.2.4	Test Setup.....	201
6.2.4.1	Simulator details and capabilities	201
6.2.4.2	Simulator setup	204
6.2.4.3	Fixtures and mounting of components	207
6.2.4.4	Sensitivity analysis for cementing process.....	210
6.2.4.5	Lubrication of components	212
6.2.4.6	Calibrations	212
6.2.5	Test Outputs.....	212
6.2.5.1	Pre-testing CMM measurements	212
6.2.5.2	Processing of CMM data.....	213
6.2.5.3	Displacement of the CoR in the ML and AP directions.....	213
6.2.5.4	Frequency of data collection from the simulator..	215
6.2.6	Predictions from the geometric model	215
6.2.6.1	Volumetric overlap of impingement.....	215
6.2.6.2	Location of impingement damage around the liner rim	216
6.3	Results	219
6.3.1	Overview of results.....	219
6.3.2	Damage to the acetabular liner rim	219
6.3.3	Location of impingement	220
6.3.4	Displacement of the femoral head away from the CoR of the simulator in the ML and AP directions	222
6.3.5	Forces acting in the simulator comparing the kinematics of subjects A and B	225
6.3.6	Analysis of the bearing surface	227
6.3.7	Comparison with geometric model predictions	227
6.3.7.1	Location of impingement.....	228

6.3.7.2	Severity of impingement.....	230
6.4	Discussion.....	232
6.4.1	Development of <i>in vitro</i> impingement test inputs.....	232
6.4.1.1	Effect of the order of rotations.....	233
6.4.1.2	Effect of the size of the forces on the impingement damage.....	233
6.4.1.3	Force inputs in comparison to a previous dataset (Layton, et al., 2021).....	234
6.4.2	Measurable damage outputs.....	235
6.4.2.1	Penetration damage to the liner rims for the three squat activities	235
6.4.2.2	The displacement of the femoral head away from the CoR and its association with the damage to the acetabular liner rim.....	235
6.4.2.3	Bearing surface changes	236
6.4.3	Geometric model predictions with the given kinematic inputs	237
6.4.4	Comparison with current impingement test methods and standards	238
6.4.5	Clinical significance.....	239
6.4.6	Limitations.....	241
6.5	Summary.....	242
	Chapter Seven : Discussion and future work	243
7.1	Introduction	243
7.1.1	Project aim	245
7.2	Bony features which have an effect on impingement in total hip replacements.....	245
7.2.1	Anterior inferior iliac spine.....	245
7.2.2	Anteversion angle of the natural acetabulum	246
7.3	The kinematic activities of patients can affect impingement.....	246
7.4	The potential of the use of the geometric models as a THR preoperative planning tool.....	248
7.5	<i>In vitro</i> consequences of impingement during clinically-relevant motions.....	250
7.6	Limitations.....	252
7.7	Future Work	253
7.8	Conclusions.....	254

List of References	256
Appendix A: Engineering drawings for hip simulator study (Chapter Six)	268

List of Tables

Table 1.1 Retrieval studies with evidence of clinical impingement detailed from the literature.	34
Table 1.2 Computational modelling studies investigating impingement from the literature.	37
Table 1.3 Impingement studies using <i>in vitro</i> hip simulators from the literature.	43
Table 2.1 A comparison of the distance measures to bony features used to investigate the effect of the number of faces to create a 3D geometric model from a mesh between a medium and high detailed geometric model using bony geometry ID number 1. The distance measures to bony features were from the origin of the acetabulum to the bony features indicated for the medium and high detailed pelvises which were in an identical position.....	59
Table 2.2 The acetabulum diameter before and after the scaling process including the ratio which was used to scale the models.	69
Table 2.3 Components used in the virtual total hip replacements of the nine geometric models. All components were commercially available products manufactured by DePuy Synthes which were provided as drawings.	70
Table 2.4 Acetabular component orientations for each of the nine geometric models including the radiographic inclination, radiographic anteversion and the amount of medialisation. The medialisation reaming line was 45° radiographic inclination and 20° radiographic anteversion.....	74
Table 2.5 The AIIIS measures in the nine geometric models following the scaling process including the anterior, superior and lateral AIIIS measures as well as the anteversion angles of the natural acetabulum.....	82
Table 3.1 Anterior, superior and lateral measures of the peak of the most anterior point on the anterior inferior iliac spine. The classification was also determined using a previously defined system (Hetsroni, et al., 2013).....	93
Table 3.2 The internal rotation angle in the hip before impingement in a series of THR geometric models at different fixed angles of flexion and comparing across the three location measures of the AIIIS. The statistical test was a Pearson’s chi-squared test for correlation.	98

Table 3.3 The ranges of internal rotation at each of the fixed flexion angles for the entire series of geometric models. The colours denote the type of impingement found during the range of motion testing. Yellow is when the range of motion was restricted by bone-on-bone impingement. Blue is when the range of motion was restricted by implant-on-bone impingement.....	99
Table 3.4 The p values of the Pearson’s chi-squared test for correlation comparing the combinations of AIIIS location measures and the RoM across the series of nine geometric models at varying degrees of fixed high flexion.	101
Table 5.1 Components used in the virtual THR of the one bony geometry used in Chapter Five. All components were commercially available products manufactured by DePuy Synthes which were provided as drawings.	154
Table 6.1 Product names and sizes of the total hip replacement components (DePuy Synthes, Leeds, UK) used in the hip simulator study.	186
Table 6.2 The motion and load specifications of the Simsol Prosim six axis, single station anatomical hip simulator.	203
Table 6.3 The acetabular cup orientation in the geometric model in terms of the radiographic inclination and anteversion. The values include the orientation of the acetabular cup in the femoral coordinate system at the starting position in the geometric model and the orientation of the acetabular cup in the femoral coordinate system after the femur has been flexed 40°. The pre-flexed 40° cup orientation is the orientation of the cup used for the simulator setup.....	205
Table 6.4 The geometric model predictions of the volumetric overlap of impingement for subjects A, B and F. Two orders of rotations were included in the predictions including the original FE-AA-IE order and the hip simulator order of AA-FE-IE. These were measured by rotating the femur into the greatest range of motion during the activity and measuring the volumetric overlap of components giving an indication to the severity of impingement. The expected order of severity of impingement is the AA-FE-IE rotation order which was carried out in the simulator.....	216
Table 6.5 The geometric model predictions of the location of impingement around the liner rim. These were measured by rotating the femur into the greatest range of motion during the activity and measuring the angle of rotation at the deepest point of impingement from the anterior axis on the liner. This was carried out in the AA-FE-IE rotation order.	217

Table 6.6 The predicted location of impingement for the three kinematic squat activities which highlight the area of volumetric overlap as well as the location of the deepest part of the impingement.....	218
Table 6.7 The location of impingement measurements taken from the predictions of the geometric model and the results from the CMM measurements of the simulator study. A comparison was made between the prediction of the geometric model and the outcomes of the simulator tests.....	228

List of Figures

- Figure 1.1** Labelled components of a total hip replacement implanted in a femur and acetabulum. The acetabulum on the pelvis has been reamed. The acetabular shell is press-fit or screwed into the reamed acetabulum and the acetabular liner is press-fit into the shell. The femur has gone through an osteotomy at the femoral neck. The femoral stem is press-fit into the shaft of the femur and a femoral head is press-fit onto the stem. The femoral head is then placed into the acetabular liner. 2
- Figure 1.2** A simplified diagram of a THR undergoing implant-on-implant impingement. The femoral head and stem are being levered out of an acetabular liner component as the femoral stem impinges on the rim of the acetabular liner (as it follows the rotation of the blue arrows). 4
- Figure 1.3** The reasons for revisions in primary total hip replacements up to one year post-surgery demonstrated as the number of revisions per 1,000 prosthesis years at risk. Data from the 17th annual report National Joint Registry in England, Wales and Northern Ireland, 2020 (National Joint Registry, 2020)..... 5
- Figure 1.4** A simplified diagram of a THR demonstrating the range of motion advantage with a larger femoral head (the neck diameter of the femoral stem is the same for both THR's)..... 8
- Figure 1.5** The range of motion before implant-on-implant impingement for different sized acetabular liners and femoral head diameters demonstrating the increase in range of motion with a larger femoral head. These results are from a finite element analysis study (Crowninshield, et al., 2004). 9
- Figure 1.6** A simplified diagram of a THR displaying the 'jumping distance' which is the distance needed for the head to displace out of the acetabular liner until it would dislocate (measurement A-B shown in purple). Where φ is the cup inclination angle..... 11
- Figure 1.7** A simplified diagram of a Total Hip Replacement with the measurements needed for the equation which calculates the theoretical range of motion. Where θ is the range of motion before implant-on-implant impingement, A is the maximum ROM of the acetabular liner, n is the neck diameter of the femoral stem at the point of impingement and r is the radius of the femoral head. 12
- Figure 1.8** A DePuy Pinnacle® standard neutral liner (32mm) next to a DePuy Pinnacle® lipped liner (32mm) demonstrating the elevation in the liner rim. Lipped liners are used to increase the surface area of the bearing to reduce the likelihood of dislocation. 14

Figure 1.9 A simplified DePuy Corail® standard size 12 stem with a 36mm femoral head. The femoral offset and neck-shaft angle have been labelled.	15
Figure 1.10 Kinematic data from the literature (Nadzadi, et al., 2003) demonstrating the flexion/extension angle of the femur around a fixed pelvis over time for seven dislocation-prone activities.....	18
Figure 1.11 Kinematic data from the literature (Nadzadi, et al., 2003) demonstrating the adduction/abduction angle of the femur around a fixed pelvis over time for seven dislocation-prone activities.....	18
Figure 1.12 Kinematic data from the literature (Nadzadi, et al., 2003) demonstrating the internal/external rotation angle of the femur around a fixed pelvis over time for seven dislocation-prone activities.....	19
Figure 1.13 Average kinematic data of up to 18 subjects from the literature (Layton, et al., 2021) demonstrating the flexion/extension angle of the femur relative to the pelvis over time for eight activities of daily living potentially prone to impingement.....	22
Figure 1.14 Average kinematic data of up to 18 subjects from the literature (Layton, et al., 2021) demonstrating the adduction/abduction angle of the femur relative to the pelvis over time for eight activities of daily living potentially prone to impingement.....	22
Figure 1.15 Average kinematic data of up to 18 subjects from the literature (Layton, et al., 2021) demonstrating the internal/external rotation angle of the femur relative to the pelvis over time for eight activities of daily living potentially prone to impingement.	23
Figure 1.16 The three most common approaches for a surgeon to perform a total hip replacement including: A) the posterior approach shown from a posterior view of the hip, B) the anterior approach shown from an anterior view of the hip and C) the lateral approach shown from a lateral view of the hip. Each approach includes a first image including notable muscles around the hip joint and a red line to mark the approximate location of the incision. The second image for each approach includes the notable muscles as transparent to understand the direction that the hip is accessed from in relation to the bones.....	25
Figure 1.17 The three types of AHS (“Hetsroni classification”) as previously defined by a study (Hetsroni, et al., 2013), demonstrated on a hemi-pelvis of different geometric models.	31

Figure 1.18 A sagittal view of three total hip replacements demonstrating a rotation in the pelvic tilt angle of +15°, 0° and -15°. The cup orientation is visibly changing across the three pelvic tilt angles demonstrating the change in functional cup orientation as the pelvis rotates.	33
Figure 2.1 The Anterior Inferior Iliac Spine (AIIS) and the ischium of the pelvis labelled on bony geometry ID number 4. A) the coronal view of the pelvis and B) the sagittal view of the pelvis.	52
Figure 2.2 A coronal view of one of the CT scan images used for this study in the Simpleware ScanIP software including just the bone (this was included in the segmentation process which highlighted a pre-set range of the greyscale denoting cortical bone).....	55
Figure 2.3 A transverse plane view of three 2D slices of the same CT scan image of one of the CT scans used in this study including all of the tissue shown as a greyscale in the Simpleware ScanIP software. A) The greyscale tissue with no highlighting. B) The same CT scan image after it has been highlighted by the greyscale range which highlighted cortical bone and demonstrates the inner cancellous bone which was not highlighted during this step. C) The same CT scan image following the manual highlighting of the cancellous bone in the pelvis.....	57
Figure 2.4 A coronal view of a full pelvis mask in the Simpleware ScanIP software following all of the steps of segmentation and smoothing ready for exporting as an STL file for one of the CT scans used in this study.	57
Figure 2.5 A coronal plane view of one of the geometric models in Solidworks which includes the origin from the CT scan and the five distance measures to bony features used to investigate the effect of the number of faces to create a 3D geometric model from a mesh between a medium and high detailed geometric model. Bony geometry ID number 1 was used.....	60
Figure 2.6 An osteophyte found on bony geometry ID number 5 for A) a coronal view B) A 45° angle to the coronal view and C) A view of the acetabulum from an inferior-superior view in line with the transverse acetabular ligament.....	62
Figure 2.7 Bony geometry ID number 5 with the osteophyte removed from A) a coronal view B) A 45° angle to the coronal view and C) A view of the acetabulum from an inferior-superior view in line with the transverse acetabular ligament.....	63
Figure 2.8 A coronal view of one of the left femurs in Solidworks with a sphere added in order to define the centre of rotation of the femur. The centre of rotation is at the centre of the sphere in blue. The femoral head was measured and an average taken to draw the size of the sphere.....	64

Figure 2.9 A coronal view of one of the left pelvises in Solidworks with a sphere added in order to define the centre of rotation of the acetabulum. The centre of rotation is at the centre of the sphere in blue. The inside of the acetabulum was measured and an average taken to draw the size of the sphere.	65
Figure 2.10 A coronal view of one of the pelvises in Solidworks including the bony landmarks used to define the anterior pelvic plane (APP). The APP was defined using the left anterior superior iliac spine point (LASIS), the right anterior superior iliac spine point (RASIS) and the midpoint of the pubic symphysis (MPS).	67
Figure 2.11 The plane and bony features used to align the femurs to an existing femur with a correct coordinate system. To align the femurs, the shaft axis and the centre of rotation of the femoral head were used.	68
Figure 2.12 Coronal views in Solidworks of a left femur from one of the geometric models used in this study. The process used to carry out the osteotomy on the femur and the insertion of the femoral THR components is demonstrated. A) A 45° angle to the shaft axis was used for the angle of the osteotomy. B) A circle was drawn which covered the size of the femoral head and was extruded into the femoral head to remove it. C) The final femur bony geometry following the osteotomy. D) The CoR of the femoral head was then restored and the stem inserted along the shaft axis at an anteversion angle of 15°.	72
Figure 2.13 A coronal view in Solidworks of the final setup of the geometric model with bony geometry ID number 1 for a left hip including the relevant global coordinate system.	75
Figure 2.14 The anterior AIIIS measure demonstrated in a sagittal view of bony geometry ID number 1, of a left hip. The blue line is the plane parallel with the coronal plane and coincident with the anterior peak point of the AIIIS. The dotted black line is the inferior/superior axis which is coincident with the centre of rotation of the THR. The red arrowed line denotes the anterior measure of the AIIIS.....	77
Figure 2.15 The superior AIIIS measure demonstrated in a coronal view of bony geometry ID number 1, of a left hip. The blue line is the plane parallel with the transverse plane and coincident with the anterior peak point of the AIIIS. The dotted black line is the medial/lateral axis which is coincident with the centre of rotation of the THR. The red arrowed line denotes the superior measure of the AIIIS.....	78

- Figure 2.16** The lateral AIIIS measure demonstrated in a coronal view of bony geometry ID number 1, of a left hip. The blue line is the plane parallel with the sagittal plane and coincident with the anterior peak point of the AIIIS. The dotted black line is the inferior/superior axis which is coincident with the centre of rotation of the THR. The red arrowed line denotes the lateral measure of the AIIIS..... 79
- Figure 2.17** The anteversion angle measurement of the natural acetabulum. A) A coronal view of a left pelvis in Solidworks of one of the geometric models used in this study demonstrating a plane over the face of the acetabulum. B) The pelvis is rotated around the inferior-superior axis until the face of the plane is perpendicular to the view. The rotation around the inferior-superior axis is the anteversion angle of the natural acetabulum. The anteversion angle of the natural acetabulum was measured in each of the nine geometric models. 81
- Figure 2.18** A coronal view in Solidworks of a left geometric model used in the current study. A typical Cardan rotation sequence of flexion/extension, adduction/abduction followed by internal/external rotation is applied in steps from the neutral starting position to the final position. The rotations applied were 80° flexion, 30° adduction and then 30° internal rotation. The black dotted line represents the vector which controls the flexion and adduction/abduction of the femur. The orange plane demonstrates the rotation by the vector which is attached to the coronal plane of the femoral component assembly. This vector controls the internal/external rotation. 83
- Figure 2.19** A view at a 45° angle to the coronal and sagittal plane of the left hip of one of the geometric models. The volumetric overlap (outlined in red) is demonstrated between the femur and the pelvic bone in the region of the AIIIS..... 86
- Figure 3.1** The three previously defined types of AIIIS (Hetsroni, et al., 2013) demonstrated on a hemi-pelvis of different geometric models from this study. A) Type 1 AIIIS – Bony geometry ID number 4 at 45° to the coronal plane (bony geometry ID number 4 is a left hip however it has been mirrored in this figure for comparison purposes). B) Type 2 AIIIS – Bony geometry ID number 1 at 45° to the coronal plane. C) Type 3 AIIIS – An edited version of bony geometry ID number 1 with the AIIIS artificially extended to demonstrate a type 3 AIIIS at 45° to the coronal plane..... 91
- Figure 3.2** The effect of the lateral measure of the anterior inferior iliac spine on the internal rotation angle before impingement at varying degrees of fixed high flexion. Each point represents one of the nine geometric models at each fixed flexion angle. Only the correlation lines that were significant have been added. 96

Figure 3.3 A) The effect of the superior measure of the anterior inferior iliac spine on the internal rotation angle before impingement at varying degrees of fixed flexion. B) The effect of the anterior measure of the anterior inferior iliac spine on internal rotation angle before impingement at varying degrees of fixed flexion. Each point represents one of the nine geometric models at each fixed flexion angle. No significant correlations were found.	97
Figure 3.4 A) The internal rotation angle before impingement at a fixed flexion of 90° for all of the nine geometric models in descending order of range of motion. 3.4 B) The internal rotation angle before impingement at a fixed flexion of 100° for all of the nine geometric models in descending order of range of motion. 3.4 C) The internal rotation angle before impingement at a fixed flexion of 110° for all of the nine geometric models in descending order of range of motion.....	100
Figure 3.5 A comparison of internal rotation angle before impingement between the two different types of AIIIS found in the series of geometric models at varying degrees of fixed high flexion. The black lines represent the range of motion for each individual model.....	102
Figure 4.1 Occurrence and type of impingement found in the series of nine geometric models during the seven dislocation-prone activities of daily living. The type of impingement was defined as the solid bodies which were first to impinge in the model during the activity.	117
Figure 4.2 The severity of bone-on-bone impingement as measured by the volume of overlapping bones found for each of the nine geometric models of a THR during anterior dislocation-prone activities (PIVOT and ROLL). The severity of impingement was defined by measuring the volumetric overlap of the pelvic bones and femur at the greatest volume of impingement. Only severity of bone-on-bone impingement has been assessed this way (and not other types of impingement).....	118
Figure 4.3 The difference in external rotation angle at the initial bone-on-bone impingement contact and maximum rotation of the activity in each of the nine geometric models of a THR during the anterior dislocation-prone activities (PIVOT and ROLL). Only severity of bone-on-bone impingement has been assessed this way (and not other types of impingement).....	119
Figure 4.4 Effect of the anteversion angle of the natural acetabulum on the severity of bone-on-bone impingement during the PIVOT and ROLL activities. Each point represents one of the series of nine geometric models of a THR which encountered bone-on-bone impingement (i.e. six models as shown for the PIVOT activity (blue) in Figure 4.4).....	121

Figure 4.5 Effect of the anteversion angle of the natural acetabulum on the difference in external rotation angle at the initial bone-on-bone impingement contact and maximum rotation of the PIVOT and ROLL activities. Each point represents one of the series of nine geometric models of a THR which encountered bone-on-bone impingement (i.e. six models as shown for the PIVOT activity (blue) in Figure 4.5).	122
Figure 4.6 Volume of bone-on-bone impingement for each of the nine geometric models of a THR during the STOOP activity. The impingement is recorded as zero if bone-on-bone impingement wasn't the first type of impingement encountered.	124
Figure 4.7 The difference in flexion angle at the initial bone-on-bone impingement contact and maximum rotation of the STOOP activity for each of the series of nine geometric models of a THR. Only the geometric models which encountered bone-on-bone impingement as the first impingement contact during the STOOP activity are displayed here.	125
Figure 4.8 Effect of the lateral measure of the AIIS on the severity of bone-on-bone impingement as measured by the volume of overlapping bones during the STOOP activity. Each point represents one of the series of nine geometric models of a THR that encountered bone-on-bone impingement (i.e. four models as shown in Figure 4.8) (note; five of the geometric models did not show impingement).	127
Figure 4.9 Effect of the lateral measure of the AIIS on the severity of bone-on-bone impingement as measured by the difference in flexion angle at the initial bone-on-bone impingement contact and maximum rotation of the STOOP activity. Each point represents one of the series of nine geometric models of a THR that encountered bone-on-bone impingement (i.e. four models as shown in Figure 4.9). (note; five of the geometric models did not show impingement).	127
Figure 4.10 The effect of the anterior measure of the AIIS on the severity of bone-on-bone impingement as measured by the volume of overlapping bones during the STOOP activity. Each point represents one of the series of nine geometric models of a THR which encountered bone-on-bone impingement (i.e. four models as shown in Figure 4.10). (note; five of the geometric models did not show impingement).	129
Figure 4.11 The effect of the anterior measure of the AIIS on the severity of bone-on-bone impingement as measured by the difference in flexion angle at the initial impingement contact and maximum rotation of the STOOP activity. Each point represents one of the series of nine geometric models of a THR which encountered bone-on-bone impingement (i.e. four models as shown in Figure 4.11). (note; five of the geometric models did not show impingement).	129

Figure 4.12 The effect of the superior measure of the AIIIS on the severity of bone-on-bone impingement as measured by the volume of overlapping bones during the STOOP activity. Each point represents one of the series of nine geometric models which encountered bone-on-bone impingement (i.e. four models as shown in Figure 4.12). (note; five of the geometric models did not show impingement).	131
Figure 4.13 The effect of the superior measure of the AIIIS on the severity of bone-on-bone impingement as measured by the difference in flexion angle at the initial impingement contact and maximum rotation of the STOOP activity. Each point represents one of the series of nine geometric models which encountered bone-on-bone impingement. (i.e. four models as shown in Figure 4.13). (note; five of the geometric models did not show impingement).	131
Figure 4.14 A coronal view of the same left hip geometric model demonstrating typical bone-on-bone impingement sites for the PIVOT and ROLL activities. (A) Bone-on-bone impingement at the posterior side of the hip between the ischium and the lesser trochanter for bony geometry ID number 1 during the PIVOT activity. The impingement site included the lesser trochanter. (B) Bone-on-bone impingement at the posterior side of the hip between the ischium and the intertrochanteric crest of the femur for bony geometry ID number 1 during the ROLL activity.	133
Figure 4.15 A view at a 45° angle to the coronal and sagittal plane of the left hip of the bony geometry ID number 1 during the STOOP activity. Typical bone-on-bone impingement site demonstrating the volumetric overlap (outlined in red) between the femur and the pelvic bone in the region of the AIIIS.	134
Figure 5.1 Consort diagram of how the individual kinematic activity data (Layton, et al., 2021) was focussed for each study section and analysed. The blue boxes label the results section of the study which the data was used in.	152
Figure 5.2 The occurrences and types of impingement during the eight impingement-prone activities for the eighteen subjects in geometric model with bony geometry ID number 8 with the 28mm sized THR components. The impingement type was recorded as the first contact to occur between solid bodies in the geometric model. The component orientation of the cup was 45° radiographic inclination and 25° radiographic anteversion.	158

Figure 5.3 The occurrences and types of impingement found during the eight impingement-prone activities for the eighteen subjects in bony geometry ID number 8 with malpositioned 28mm sized THR components. The malposition was 30° radiographic inclination and 0° radiographic anteversion. The impingement type was recorded as the first contact to occur between solid bodies in the geometric model..... 159

Figure 5.4 The change in severity of impingement as measured by the volume of overlap of the stem and liner in the THR geometric model for each of the available squat activities of the different subjects. The subject's which did not register a squat activity are not included in the figure. 160

Figure 5.5 The greatest registered flexion angle during a squat activity compared to the severity of impingement as measured by the volume of overlap of the stem and liner in the geometric THR model. Each marker represents an individual kinematic squat activity by a different subject. 161

Figure 5.6 Cup orientation grids for each activity. This includes the THR geometric model results for all of the impingement-prone activities of the available subject's data at each acetabular cup orientation. Each individual box represents the number of impingement occurrences at each respective acetabular cup orientation. The number of subjects included for each activity is displayed in the top left corner of each activity cup orientation grid. The cup orientation boxes are individually coloured based on the type of impingement found as well as the total number of impingement occurrences. Walk turn and Golf swing were prone to posterior impingement, all other activities were prone to anterior impingement..... 164

Figure 5.7 Cup orientation grids for each subject. The THR geometric model results for the eight impingement-prone activities of the six subjects at each acetabular cup orientation. Each individual box represents the number of impingement occurrences at each respective acetabular cup orientation. The cup orientation grids for all of the six subjects included all eight of their activities at each cup orientation and the number of impingement occurrences at each of the acetabular cup orientations. The cup orientation boxes are individually coloured based on the type of impingement found as well as the total number of impingement occurrences..... 169

Figure 5.8 A comparison of the six anterior impingement-prone activities for Subject B and Subject N demonstrating the difference in the flexion for their activities. 171

Figure 5.9 A comparison of the golf swing activity (posterior impingement-prone activity) from the impingement-prone activity data for Subject B and Subject N demonstrating the difference in the rotations for their respective golf swings. This included the three rotations (flexion/extension, adduction/abduction and internal/external rotation) that were followed for the activity. 172

Figure 6.1 All of the raw kinematic squat data from the previous kinematic dataset (Layton, et al., 2021) for the subjects which resulted in impingement in the malpositioned geometric model used in Chapter Five (Section 5.3.2.2). The subjects which were chosen were all the maximums of each individual rotation. Subject F had the highest flexion angle, subject A had the highest adduction angle and subject B had the highest internal rotation angle. 187

Figure 6.2 A consort diagram demonstrating the process used to calculate a rotational matrices from a set of three rotations and move the femur component in relation to the fixed acetabular component. A) to achieve the joint orientation positions which were recorded in the gait lab study (Layton, et al., 2021). This was the process used for the geometric model in Chapters Three, Four and Five. B) The process which was carried out in the hip simulator where the incorrect order of rotations was applied. 189

Figure 6.3 The process used to calculate the equivalent FE-AA-IE rotational angles for what was carried out in the hip simulator study. 191

Figure 6.4 The three rotational angles for the three squat activities which were applied in the simulator in an equivalent FE-AA-IE order of rotations when compared to the Layton et al. (2021) dataset of squat activities. The grey lines represent the squat activities in the previous kinematic dataset (Layton, et al., 2021). The raw data consisted of 101 discrete time points, however the simulator software required 128 discrete time points hence the difference in time points between the raw data and simulator inputs..... 192

Figure 6.5 The final kinematic simulator inputs for subjects A) A, B) B and C) F with the raw data overlaid for comparison. SI=smoothed simulator input; RD=raw data. The simulator inputs for flexion started at 40° due to the setup of the simulator which is described in detail in section 6.2.4.2. 194

Figure 6.6 The volumetric overlap of impingement measured from the geometric model for the impingement event in the raw data compared with the smoothed kinematic squat activities of A) subject A, B) subject B and C) subject F. SI=simplified simulator input; RD=raw data . The order of rotations for the geometric model was AA-FE-IE. 196

Figure 6.7 The sliding distance for the impingement event during the raw data of the squat activity of Subject A. The green liner on the left is demonstrating the location of impingement at the initial impingement contact. The green liner on the right is demonstrating the impingement contact at the end of the impingement event. The graph demonstrates the volumetric overlap of impinging solids in the geometric model over the impingement event.	198
Figure 6.8 The axial force data measured in the previous kinematic dataset (Layton, et al., 2021) for Subject's B and F (Subject A's data was not registered in the study).....	200
Figure 6.9 The loading profile used in the hip simulator for the impingement testing for both the axial load and the medial-lateral load. The peak of the force was positioned so that this was the point in the kinematics where the greatest range of motion was.	200
Figure 6.10 Simsol Prosim six axis hip simulator (AHS) schematic drawing of the working area and height of the centre of rotation. The pink lines indicate the size of the working space in the simulator and the height needed for the design of the fixtures to achieve the correct centre of rotation. Note: the components in this diagram are test dummy components and were not used in the current study. In the current study, the femoral stem and head were fixed to the top of the simulator and the acetabular cup attached to the bottom of the simulator.....	202
Figure 6.11 Geometric models demonstrating the process of pre-flexing the femur 40° and the mounting of the components into the fixtures. Followed by the components being flipped upside down so that the force direction is correct during the impingement testing. A) A sagittal view of the original setup of the bony geometries and components. B) The femur is flexed 40°. C) The relative position of the femur and pelvis is rotated so that the femur is in its original position. D) The bony geometries are removed leaving just the stem, liner and head. E) The components are mounted in fixtures. F) The fixtures are rotated 180° resulting in the final setup in the hip simulator.	206
Figure 6.12 The fixtures which were used in the current study including those that already existed and those that needed to be developed.	209
Figure 6.13 A sensitivity analysis for the cementing process measured in the geometric model including A) the effect on the volumetric overlap of impingement between components when the anteversion of the stem was varied and B) the effect on the volumetric overlap of impingement between components when the adduction of the stem was varied. The original orientation of the femoral stem was 0° anteversion and 10° adduction (at the y axes).	211

- Figure 6.14** The displacement measurements of the femoral head away from the CoR of the simulator in the A) anterior-posterior view and B) medial-lateral view. The acetabular cup would rotate and make impingement contact on the femoral stem, pushing the femoral head away from the CoR of the simulator. Figure includes the impingement test setup demonstrating the rotation of the acetabular fixture, location of impingement contact and the direction of the measurement of the displacement of the femoral head after impingement contact.... 214
- Figure 6.15** The mean penetration depth of the three squat activities. The penetration depth was recorded as the greatest deviation from the unworn liners. There were three repeats for each subject and the error bars demonstrate the standard deviation of the three repeats. 220
- Figure 6.16** The location of the impingement for the three individual squat activities. The three liners in this figure were from the first round of repeats of each of the squat activities however were typical of the damage observed on the acetabular liner. A) Subject A, B) Subject B, C) Subject F. A burr is visible to the right side of the impingement damage in dark red for subjects A and B. 221
- Figure 6.17** The displacement of the femoral head away from the centre of rotation in the medial-lateral direction for all of the subjects and all of the repeats. The values were taken every 1k cycles between 10k and 40k cycles..... 223
- Figure 6.18** The displacement of the femoral head away from the centre of rotation in the anterior-posterior direction for all of the subjects and all of the repeats. The values were taken every 1k cycles between 10k and 40k cycles. 223
- Figure 6.19** The average displacement of the femoral head away from the centre of rotation of the simulator in a resultant direction of the anterior-posterior and medial-lateral direction. The values were averages of the three repeat tests taken every 1k cycles between 10k and 40k cycles..... 224
- Figure 6.20** An average of the medial force applied to the femoral head by the simulator during one cycle. The average was taken from the three repeats between cycles 10k-40k (at 1k intervals). 226
- Figure 6.21** An average of the anterior-posterior force applied to the femoral head by the impingement event during one cycle. The average was taken from the three repeats between cycles 10k-40k (at 1k intervals)..... 226

List of Abbreviations

THR – Total Hip Replacement

CoR – Centre of Rotation

APP – Anterior Pelvic Plane

ASIS – Anterior Superior Iliac Spine

AIIS – Anterior Inferior Iliac Spine

DICOM - Digital Imaging and Communications in Medicine (image file type used for CT scans)

RoM – Range of motion

PIVOT – Dislocation-prone activity of twisting one leg through external rotation whilst in a standing position (Nadzadi, et al., 2003).

ROLL - Dislocation-prone activity of rolling over in bed whilst in a supine position (Nadzadi, et al., 2003).

STOOP - Dislocation-prone activity of picking an object up off the floor whilst in a standing position (Nadzadi, et al., 2003).

XLG – Dislocation-prone activity of crossing one leg over the other whilst in a seated position (Nadzadi, et al., 2003).

SSN – Dislocation-prone activity of standing up from a normal-height seated chair (Nadzadi, et al., 2003).

SSL – Dislocation-prone activity of standing up from a low-height seated chair (Nadzadi, et al., 2003).

TIE – Dislocation-prone activity of tying shoes whilst in a seated position (Nadzadi, et al., 2003).

CMM - Coordinate measuring machine

Chapter One : Literature Review

1.1 Introduction

Osteoarthritis of the hip is the degradation of cartilage and the underlying bone causing a loss of structure and reduced function of the joint (Hunter & Felson, 2006; Kapoor, et al., 2011). It affects an estimated 8.75 million people over the age of 45 years in the UK (Arthritis Research UK, 2013). The most common reason for patients needing to undergo a primary total hip replacement is for osteoarthritis (NHS, 2019; National Joint Registry, 2020). There were 95,677 procedures reported in 2019 across England, Wales and Northern Ireland (National Joint Registry, 2020) (the 2019 data is quoted because the number of procedures carried out in 2020 and 2021 were reduced due to the COVID-19 pandemic). A total hip replacement consists of replacing the hip joint with a mechanical 'ball and cup' socket joint (Figure 1.1). The procedure involves the reaming of the bony acetabulum and replacing it with an acetabular shell and liner. The femoral head is also removed and replaced with a femoral stem which is positioned inside the shaft of the femur, and a head component attached to the superior region of the stem. The femoral head and liner then act as the hip joint. A successful hip replacement aims to restore function to the hip and reduce pain for the patient (Crawford & Murray, 1997).

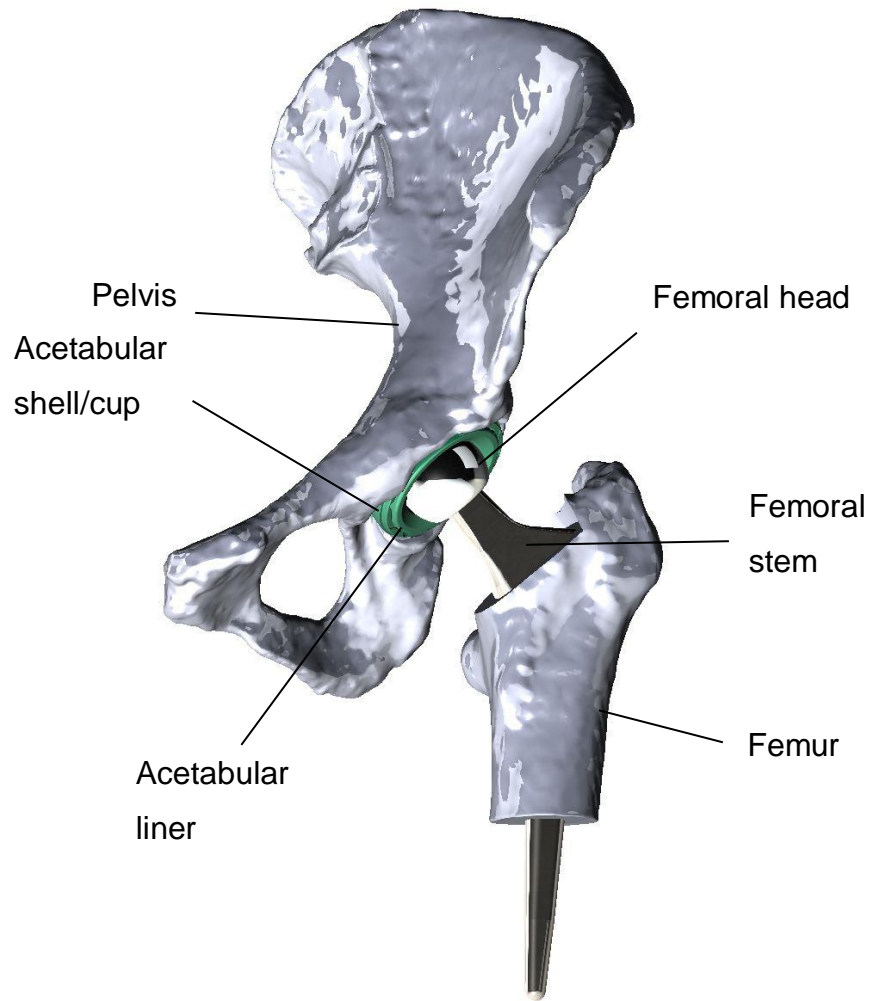


Figure 1.1 Labelled components of a total hip replacement implanted in a femur and acetabulum. The acetabulum on the pelvis has been reamed. The acetabular shell is press-fit or screwed into the reamed acetabulum and the acetabular liner is press-fit into the shell. The femur has gone through an osteotomy at the femoral neck. The femoral stem is press-fit into the shaft of the femur and a femoral head is press-fit onto the stem. The femoral head is then placed into the acetabular liner.

The most common bearings used in THR's in England, Wales and Northern Ireland is the metal-on-polyethylene bearing combination (National Joint Registry, 2020). Polyethylene has a history of good mechanical properties and wear resistance, however the wear particles can cause a biological response which can lead to osteolysis (Barrack, 2003). The most commonly used

polymer in THR liners is the ultra-high molecular weight polyethylene (UHMWPE) which has outstanding wear resistance and because of developments in the stabilisation and sterilisation process of the polyethylene, also has good mechanical properties (Singh, et al., 2018).

Total hip replacements have a cumulative revision across all total hip replacements in England, Wales and Northern Ireland up to 17 years of 7.78% (National Joint Registry, 2020). The most common reason for revision up to one year post-surgery was dislocation. Dislocation in THR's occur because of impingement which is the undesired contact between either the components (the femoral stem and the acetabular liner) and/or bones (femur and pelvis), and can also occur between soft tissues around the hip (Malik, et al., 2007; Hayashi, et al., 2012). There are a number of factors which can affect the likelihood of impingement occurring in a THR, including factors attributed to the implant design, surgical technique (and resultant implant position) and the patient (Malik, et al., 2007).

There are three types of impingement which can occur with a total hip replacement (Malik, et al., 2007; Brown, et al., 2014). Implant-on-implant impingement is the unwanted contact between the femoral neck of the implant and the rim of the acetabular liner. Implant-on-bone impingement is between the femoral stem and the bone around the acetabulum. Bone-on-bone impingement is between bones and/or soft tissues around the hip (Bartz, et al., 2000). This mechanical impingement can cause subluxation via a levering out mechanism which can also lead to dislocation (Figure 1.2).

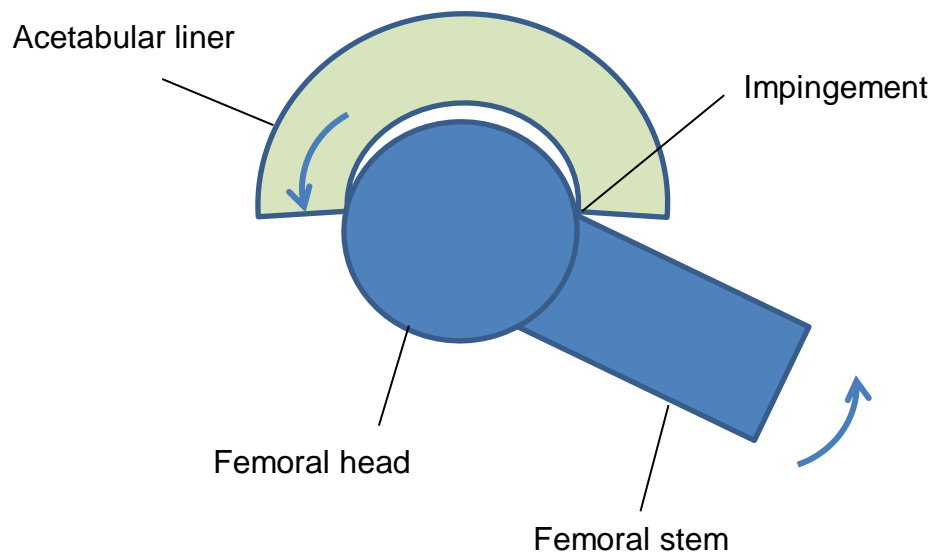


Figure 1.2 A simplified diagram of a THR undergoing implant-on-implant impingement. The femoral head and stem are being levered out of an acetabular liner component as the femoral stem impinges on the rim of the acetabular liner (as it follows the rotation of the blue arrows).

1.2 Failure modes of total hip replacements

There are a number of failure modes that can occur in a THR which can result in revision surgery. The most common reasons for revision include dislocation, aseptic loosening, adverse soft tissue reaction to wear debris, peri-prosthetic fracture and infection (Figure 1.3).

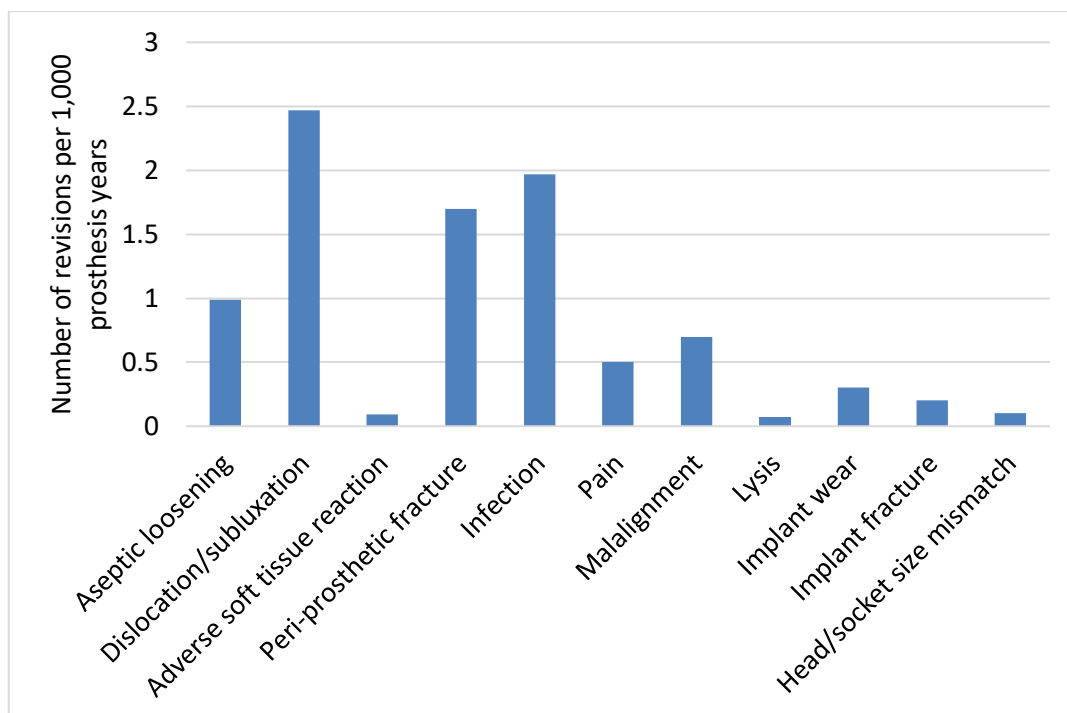


Figure 1.3 The reasons for revisions in primary total hip replacements up to one year post-surgery demonstrated as the number of revisions per 1,000 prosthesis years at risk. Data from the 17th annual report National Joint Registry in England, Wales and Northern Ireland, 2020 (National Joint Registry, 2020).

Dislocation is the occurrence of the femoral head coming out of the acetabular cup through a levering out mechanism caused by impingement (Brown, et al., 2014). Patients are at the greatest risk of dislocation in the first six weeks after their THR surgery (Sikes, et al., 2008). The most common form of dislocation is in the posterior direction after the occurrence of impingement at the anterior of the hip due to the high ranges of flexion angle associated with some activities of daily living (Nadzadi, et al., 2003; Di Schino, et al., 2009). There are also some dislocations which occur in the anterior direction (Nadzadi, et al., 2003). The most common surgical approach to THR surgery is the posterior approach which disrupts the muscles and ligaments at the posterior of the hip (National Joint Registry, 2020). This could be the reason behind the increased rates of posterior dislocation as there have been a number of studies which have found an increase in the dislocation rate in THR's which have been carried out by the posterior surgical approach (Byström, et al.,

2003; Enocson, et al., 2009; Hailer, et al., 2012; Cebatorius, et al., 2015; Zijlstra, et al., 2017). The surgical approaches are described in detail in Section 1.3.3.1.

Aseptic loosening is the loss of stability at the interface between the bone and the implant (Abu-Amer, et al., 2007). The constant motion between the bearings in a hip replacement can cause a large build-up of wear debris over time. Wear can be accelerated through mechanisms such as impingement and edge loading (Fisher, 2011). The immune response to this wear debris can cause bone resorption around the THR components and cause loosening (Mellon, et al., 2013). It is a failure which usually occurs over many years of use (Abu-Amer, et al., 2007). As well as leading to aseptic loosening, the generation of wear debris, particularly from metallic components can have an adverse soft tissue reaction around the hip leading to failure.

Peri-prosthetic fracture can also occur in total hip replacements which is the fracture of the bone which surrounds the THR components. This failure is usually related to a low-energy traumatic event such as the patient falling over and breaking the bones around the prosthesis (Patsiogiannis, et al., 2021). Infection is also a common surgical reason for failure in total hip replacement due to the potential of bacteria at the time of surgery and the use of foreign materials being placed inside the body (Lopez, et al., 2017).

1.2.1 The role of impingement and edge loading in failure

Impingement causes dislocation and/or subluxation in THRs (Malik, et al., 2007; Brown, et al., 2014). Impingement can also cause an acceleration in the generation of wear debris which can lead to further complications such as aseptic loosening and adverse reactions to the soft tissue (Malik, et al., 2007; Fisher, 2011; Mellon, et al., 2013). The high ranges of motion which lead to impingement could also cause edge loading on the acetabular liner. Edge loading is the increase in the applied stress because of the reduction in the contact area as the femoral head approaches the rim of the bearing surface of the liner which can result in an increase in wear (Williams, et al., 2003). This acceleration of wear to the acetabular liner bearing surface can be increased

by subsequent impingement and potential subluxation of the femoral head (Brown, et al., 2014). A number of computational models have demonstrated this increase in force concentration due to edge loading (Hua, et al., 2014; Liu, et al., 2015; Leng, et al., 2017; Jahani, et al., 2021). This increase in wear from edge loading has also been demonstrated experimentally in both hard-on-hard and hard-on-soft bearings under edge loading conditions in hip simulators (Leslie, et al., 2009; Al-Hajjar, et al., 2013a; Al-Hajjar, et al., 2013b; Williams, et al., 2013; O'Dwyer Lancaster-Jones, et al., 2018; Ali, et al., 2019).

1.3 Causes of impingement

There are a number of variables in a THR that can affect the likelihood of impingement. The clinical data demonstrates a number of different variables which all relate to the risk of impingement and dislocation such as neuromuscular disorders, obesity, dementia, peri-prosthetic fracture, head-to-neck ratio, small femoral heads, weak abductor muscles, surgical approach, choice of material and age etc. (Malik, et al., 2007; Sikes, et al., 2008). All of these variables related to impingement can be broken down into three categories: patient factors, surgical factors and implant factors. Due to the large amount of variability in total hip replacements, the aim of reducing the number of revisions includes aiming to reduce impingement in THR's by identifying and limiting factors which could lead to impingement occurrence (Malik, et al., 2007; Brooks, 2013).

1.3.1 Implant factors which contribute towards impingement

There are different design characteristics of total hip replacements which can have an effect on the likelihood of impingement including femoral head sizes, component orientation, offset, head-to-neck ratios, neck angles, elevated liner rims etc. (Barrack, 2003; Padgett, et al., 2006; Malik, et al., 2007).

1.3.1.1 Femoral head diameter

The femoral head diameter affects the range of motion and therefore the outcomes of impingement in total hip replacements (Cho, et al., 2016). The

size of the most frequently used femoral head diameter used by surgeons over time has slowly increased from 22mm in the 1960's to 28mm in the 1990's and more recently 32mm in the 2000's (Tsikandylakis, et al., 2018). Currently, the most used implant head size is the 32mm diameter femoral head (National Joint Registry, 2020). The reasoning for the smaller head sizes used in the past have been because of the lower volumetric wear rates associated with small femoral heads (Lachiewicz, et al., 2009), however this allowed for a smaller range of motion. As the materials used in THR's such as highly-crosslinked ultra-high molecular weight polyethylene improved, these provided lower wear rates. Hence, there was an increase in the use of larger femoral heads to provide the larger range of motion and therefore a reduction in dislocation (Cooper & Della Valle, 2014).

There have been a number of studies which have investigated the size of femoral heads and its effect on the range of motion. By increasing the femoral head size with the same femoral neck diameter, the impingement-free range of motion would be higher (Figure 1.4). This was demonstrated in an FEA study, finding that an increase in the femoral head size resulted in an increase in the RoM (Figure 1.5) (Crowninshield, et al., 2004).

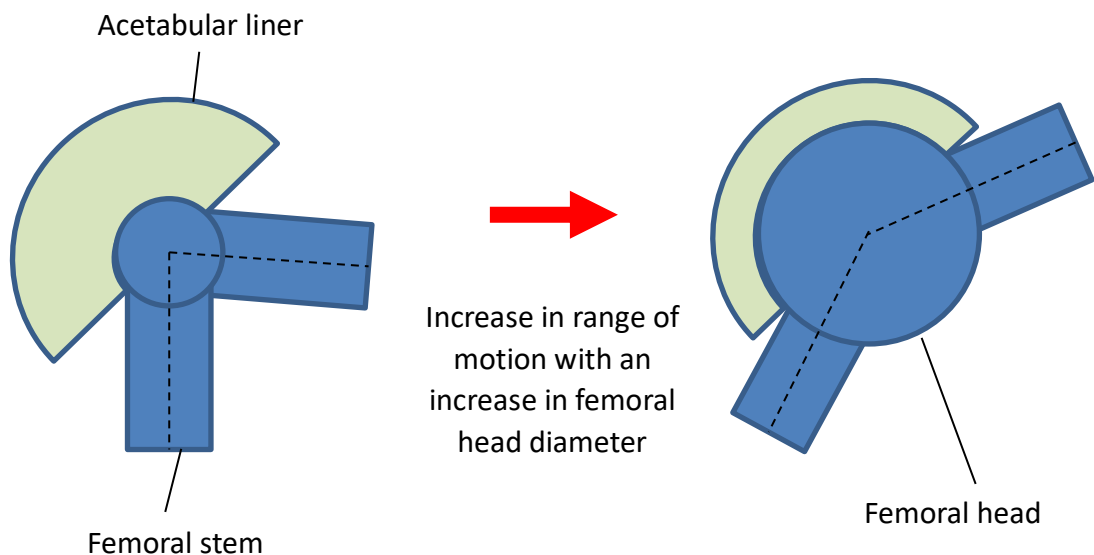


Figure 1.4 A simplified diagram of a THR demonstrating the range of motion advantage with a larger femoral head (the neck diameter of the femoral stem is the same for both THR's).

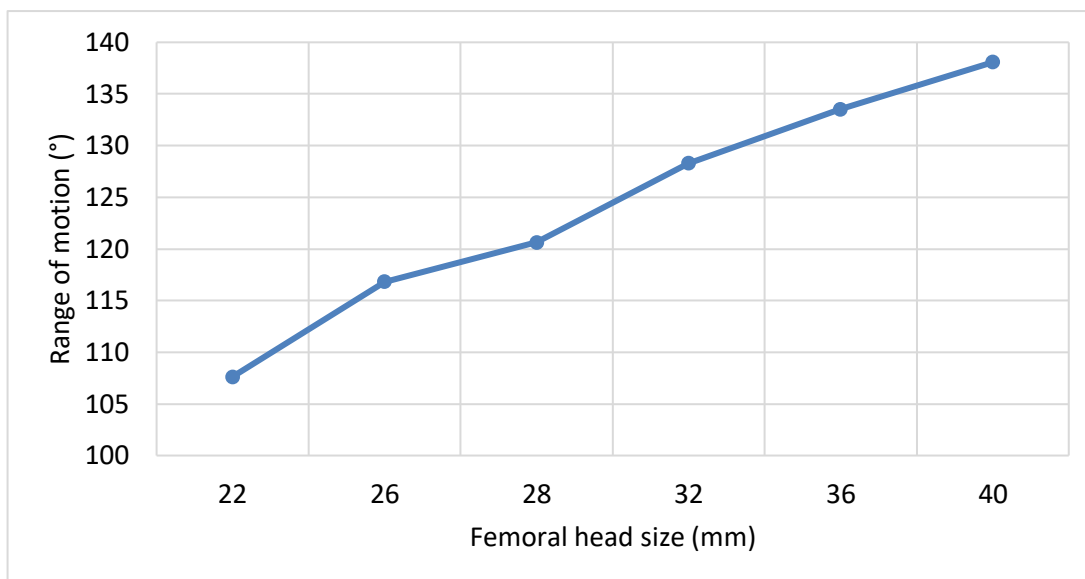


Figure 1.5 The range of motion before implant-on-implant impingement for different sized acetabular liners and femoral head diameters demonstrating the increase in range of motion with a larger femoral head. These results are from a finite element analysis study (Crowninshield, et al., 2004).

Clinical studies have investigated the effect of femoral head sizes on revisions, particularly related to impingement and dislocation. One study (Waddell, et al., 2018) investigated 97 liners retrieved from revision surgeries which were analysed for evidence of impingement. It was found that impingement was lessened in the larger femoral heads however it was not completely eliminated. There have also been a number of clinical retrospective studies which found that larger femoral heads also resulted in a reduced amount of dislocations (Cuckler, et al., 2004; Jameson, et al., 2011; Stroh, et al., 2013).

An increase in femoral head size has been demonstrated to increase the RoM and cause less impingement and dislocation clinically, however there is a limit to the increase in the size of the femoral head because of bone-on-bone impingement (Burroughs, et al., 2005). As larger head sizes are used, the implant-on-implant impingement stops being the restrictive factor for RoM and instead bone-on-bone impingement becomes the restricting factor to RoM

(Elkins, et al., 2012). One study (Burroughs, et al., 2005) investigated the RoM until impingement and recorded the types of impingement with different femoral head sizes. They used a table-top rig consisting of a fiberglass femur parallel to the floor and a plastic hemi-pelvis at 90° flexion. The pelvis was then rotated through flexion until impingement occurred. It was found that implant-on-implant impingement was almost completely eliminated and replaced with bone-on-bone impingement when increasing the femoral head size. A computational study also investigated the RoM in different sized femoral heads and found that bone-on-bone impingement restricted RoM at femoral head sizes above 32mm diameter (Cinotti, et al., 2011). These studies however only included one hip geometry, and therefore different patients and different shaped bony geometries could have resulted in different outcomes.

1.3.1.1.1 Jumping distance

Jumping distance is a measure used to characterise a THR for risk of dislocation, which is directly related to femoral head size. Jumping distance is the amount of lateral translation of the femoral head centre needed for dislocation to occur. The shorter the distance before dislocation, the more at risk the implant is of dislocating. The femoral head affects the jumping distance and therefore the risk of dislocation.

The equation to calculate the jumping distance has been previously demonstrated (Sariali, et al., 2009):

$$Jumping\ Distance = 2R \sin \left[\frac{(\pi/2) - \varphi - \sin^{-1}(femoral\ head\ offset/R)}{2} \right]$$

Where R is the femoral head radius, φ is the cup inclination angle and 'femoral head offset' is the distance between the centre of the femoral head and the acetabular liner opening plane (Figure 1.6). As seen in the equation for jumping distance, the femoral head diameter is directly related to the jumping distance with an increase in jumping distance being associated with a larger

femoral head size. A diagram of the mechanics associated with jumping distance is displayed in Figure 1.6.

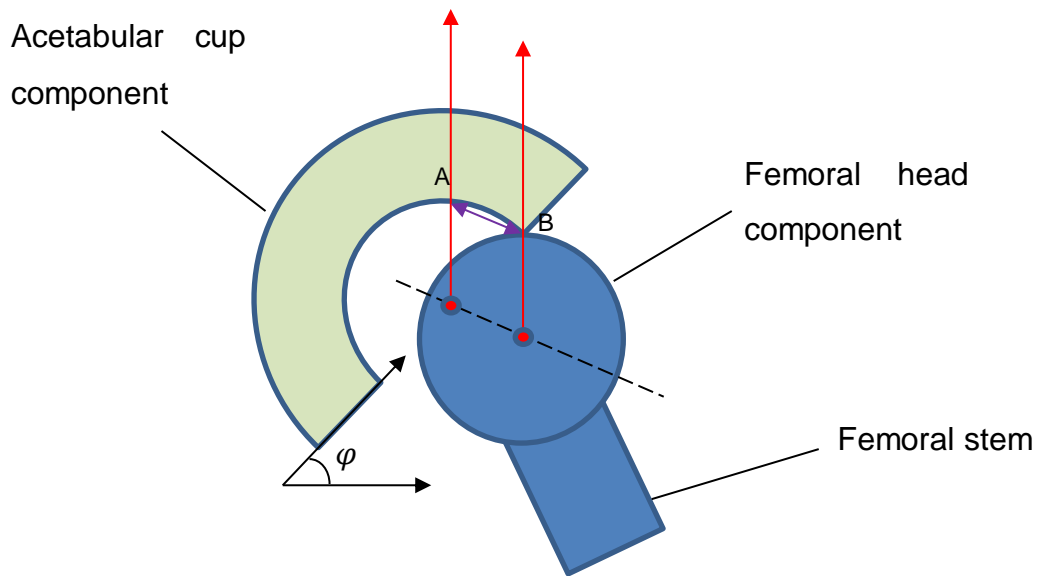
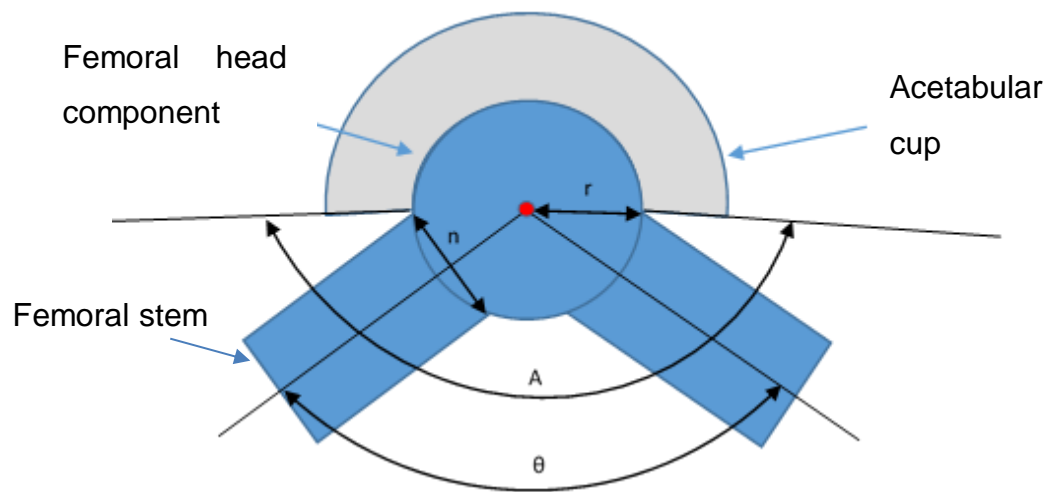


Figure 1.6 A simplified diagram of a THR displaying the ‘jumping distance’ which is the distance needed for the head to displace out of the acetabular liner until it would dislocate (measurement A-B shown in purple). Where φ is the cup inclination angle.

1.3.1.1.2 Head to neck ratio

The head to neck ratio affects the range of motion of the THR and therefore the likelihood of impingement. The head to neck ratio is the ratio between the femoral head diameter and the femoral neck diameter. There are many different designs of implants available with differing head-to-neck ratio's all of which may affect the RoM and therefore the likelihood of impingement. The mechanics behind the RoM in a simple ball and cup joint before implant-on-implant impingement in relation to the head-to-neck ratio can be calculated using an equation (Figure 1.7) (Yoshimine & Ginbayashi, 2002).



$$\theta = A - 2 \sin^{-1} \left(\frac{n/2}{r} \right) = A - 2 \sin^{-1} \left(\frac{1}{\text{head diameter to neck diameter ratio}} \right)$$

Figure 1.7 A simplified diagram of a Total Hip Replacement with the measurements needed for the equation which calculates the theoretical range of motion. Where θ is the range of motion before implant-on-implant impingement, A is the maximum ROM of the acetabular liner, n is the neck diameter of the femoral stem at the point of impingement and r is the radius of the femoral head.

As demonstrated in the equation, an increase in the head to neck ratio would increase the theoretical RoM. Therefore to increase the RoM, the aim would be to implant a larger head and a smaller neck diameter. There is however a limit to the reduction in size of the stem neck due to mechanical stress during the function of the hip implant (Ro, et al., 2018). Other theoretical and computational studies have analysed the head to neck ratio and have found that a larger head to neck ratio results in a larger range of motion (D'Lima, et al., 2000; Barrack, et al., 2001; Yoshimine & Ginbayashi, 2002; Lin, et al., 2015; Ro, et al., 2018). This also agreed with a clinical study which investigated 111 retrieved components for impingement and it was found that there was a significant difference in the head to neck ratio between the

retrieved liners which showed signs of impingement and those that didn't (Yamaguchi, et al., 2000).

1.3.1.2 Acetabular liner design

To reduce post-operative instability failures in total hip replacements, elevated rims were introduced to decrease dislocations in high-risk patients (Cobb, et al., 1996). An elevated rim consists of a small elevation built onto the acetabular cup rim to provide extra surface area for the bearing surface (Figure 1.8). The elevation is usually added to the posterior side as this is the direction that results in the greatest number of dislocations (Di Schino, et al., 2009). The elevated liner provides additional contact area for the femoral head during high ranges of motion to reduce the maximum stress at the edge of the liner (edge loading) and improve stability (Krushell, et al., 1991; Cobb, et al., 1996; Kaku, et al., 2020).

Clinical studies have found reduced dislocation rates with lipped liners when comparing with neutral liners (Cobb, et al., 1996; Sierra, et al., 2005; Wyatt, et al., 2020). However another study disagreed and found increased dislocation rates with lipped liners (Girard, et al., 2013). Other studies also found high levels of impingement in explanted lipped liners compared with neutral liners (Shon, et al., 2005; Waddell, et al., 2018). While the lipped liner allows for increased stability, it decreases the impingement-free range of motion around the elevated lip of the lipped liner possibly leading to increased impingement around the elevation of the lip. There is not much guidance in the literature for the orientation of the lip which could have caused the discrepancies in clinical outcomes. One study (Williams, et al., 2022) investigated the direction of the lip and how this affected the impingement occurrence in a computational geometric model and found that no matter the orientation of the lip, there was reduced range of motion for the lipped liner, however placed in an appropriate lip orientation, this range of motion loss could be minimised whilst still providing additional joint stability.

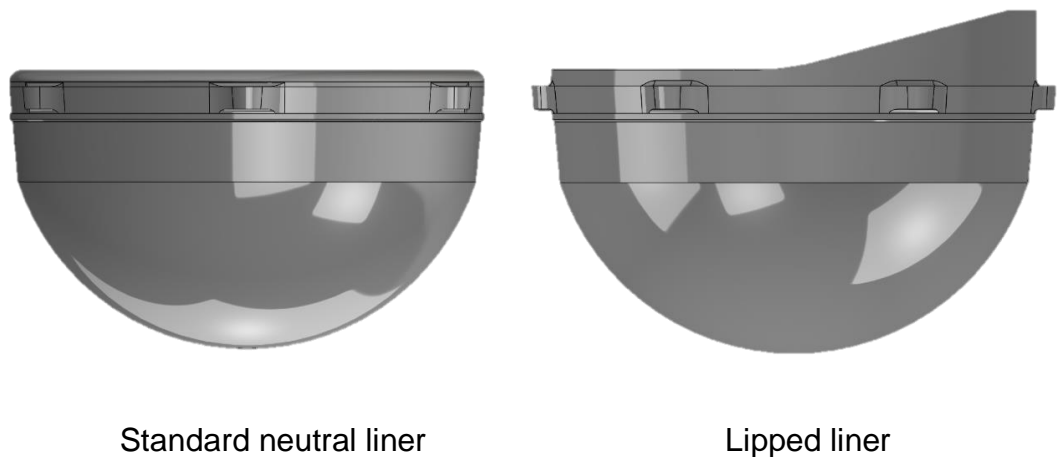


Figure 1.8 A DePuy Pinnacle® standard neutral liner (32mm) next to a DePuy Pinnacle® lipped liner (32mm) demonstrating the elevation in the liner rim. Lipped liners are used to increase the surface area of the bearing to reduce the likelihood of dislocation.

1.3.1.3 Offset, leg-length and neck-shaft angle

The aim of a THR is to restore the biomechanics of a patient's hip. The offset and leg-length need to be adequately restored to maximise RoM and soft tissue tension (Lecerf, et al., 2009). These parameters can be controlled by the neck-shaft angle which can apply varying levels of offset and leg length. The femoral offset is the perpendicular distance from the CoR of the femoral head to a line bisecting the long axis of the femoral stem (Lecerf, et al., 2009; Flecher, et al., 2016) (Figure 1.9).

Not restoring femoral offset in THR's have been shown to affect dislocation outcomes particularly in terms of not restoring sufficient soft-tissue tension around the hip leading to instability (Takao, et al., 2016; Ogawa, et al., 2018). There have been studies which have investigated femoral offset and found that increasing the offset resulted in an increase in the RoM before impingement in the THR (Matsushita, et al., 2009; Shoji, et al., 2016; Jinno, et al., 2017). Inadequate restoration of the leg length has been shown to

potentially cause lower back pain, instability and discomfort for the patient (Wylde, et al., 2009). The neck-shaft angle itself can also have an effect on the RoM (Widmer & Majewski, 2005).

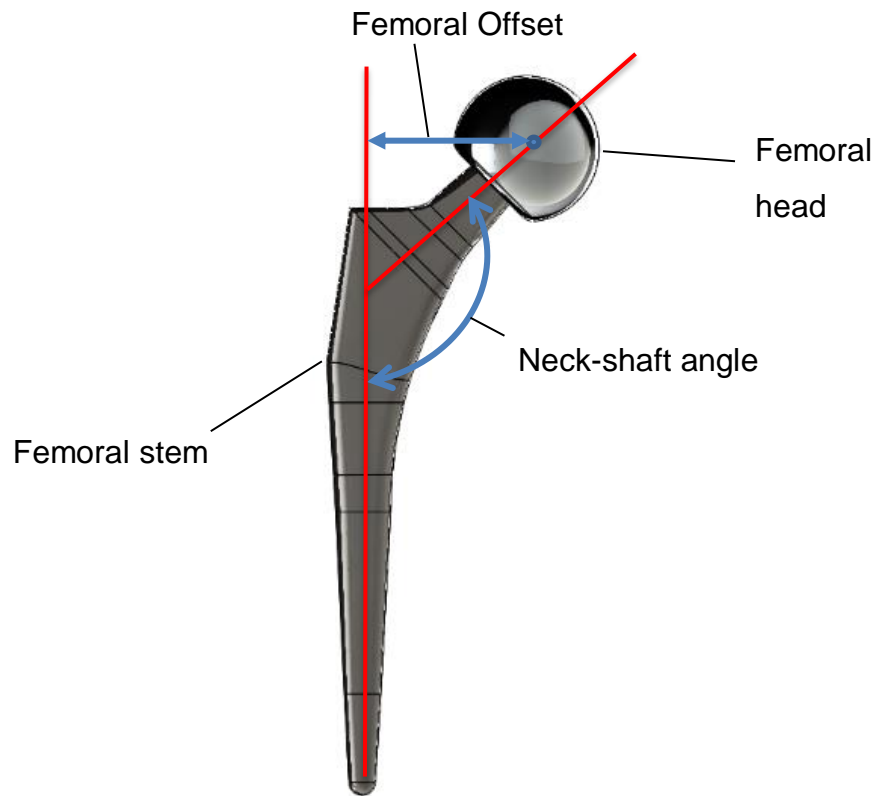


Figure 1.9 A simplified DePuy Corail® standard size 12 stem with a 36mm femoral head. The femoral offset and neck-shaft angle have been labelled.

1.3.2 Activities of daily living prone to impingement

Clinically, the mechanical occurrence of impingement is caused by the patient carrying out activities of daily living which have a high range of motion resulting in contact between either the implants or bones (Malik, et al., 2007). Most activities of daily living are at a low risk of impingement, for example walking and climbing stairs which have low ranges of motion, however there

are a number of activities of daily living which frequently have a high range of motion which could result in an impingement event in a THR (for example bending over to tie shoes) (Nadzadi, et al., 2003; Saputra, et al., 2013; Zhou, et al., 2013; Layton, et al., 2021). Increasing the possible RoM of the hip implant is the best way to avoid impingement during activities of daily living which are potentially prone to impingement and dislocation (Pedersen, et al., 2005).

To identify the activities which could cause impingement events in THR's, one clinical study investigated which activities of daily living caused 100 patient's THRs to dislocate (Smith, et al., 2012). The most common causes of dislocations were bed transfers, twisting and turning in bed, putting shoes or socks on and getting on or off the toilet; however there were 17 different activities which had resulted in dislocations.

There were two sources in the literature of recorded activities of daily living which could potentially be used in a computational model (Nadzadi, et al., 2003; Layton, et al., 2021). One study (Nadzadi, et al., 2003) recorded a set of activities in 10 subjects with the aim of gathering activity data which was associated with dislocation. The other study (Layton, et al., 2021) recorded a set of activities in 18 subjects with the aim of analysing joint forces and therefore was not produced in relation to impingement or dislocation. There was also some kinematic data gathered by another study (Sugano, et al., 2012), however the kinematic data was not included in any of the published reports which used this data.

1.3.2.1 Dislocation-prone activities of daily living (Nadzadi, et al., 2003)

One dataset, highlighted in the literature, measured the kinematics and kinetics of seven activities of daily-living which had been linked to dislocation (Nadzadi, et al., 2003). Ten healthy adults aged 44-59 (mean 49.7 years) who had not undergone a total hip replacement were used as the test subjects and each performed seven daily activities associated with posterior and anterior dislocation ("dislocation-prone activities"). The activities were: standing up

from a low-height seat (SSL), standing up from a normal-height seat (SSN), crossing their legs from a seated position (XLG), tying their shoes from a seated position (TIE), picking an object up off the floor from a standing position (STOOP), externally rotating one leg from a standing position (PIVOT) and rolling over in bed whilst laying on their back (ROLL). The method used to gather the data was carried out using LED skin markers on approximate bony features and captured via a motion capture system. A ground reaction force was also measured using a force plate during data collection which was positioned beneath the subject's right foot. The seven activities were recorded for each subject and then one out of the ten subject's data which was at the median of the 10 subjects was chosen to represent each activity. The kinematic wave profiles consisted of three cardan rotations which represent the movements of the femur relative to the pelvis in the three anatomical planes of motion in the specific order of flexion/extension, adduction/abduction and internal/external rotation (Figures 1.10-1.12). There was also published kinetic data with this study which expressed the loads in each direction.

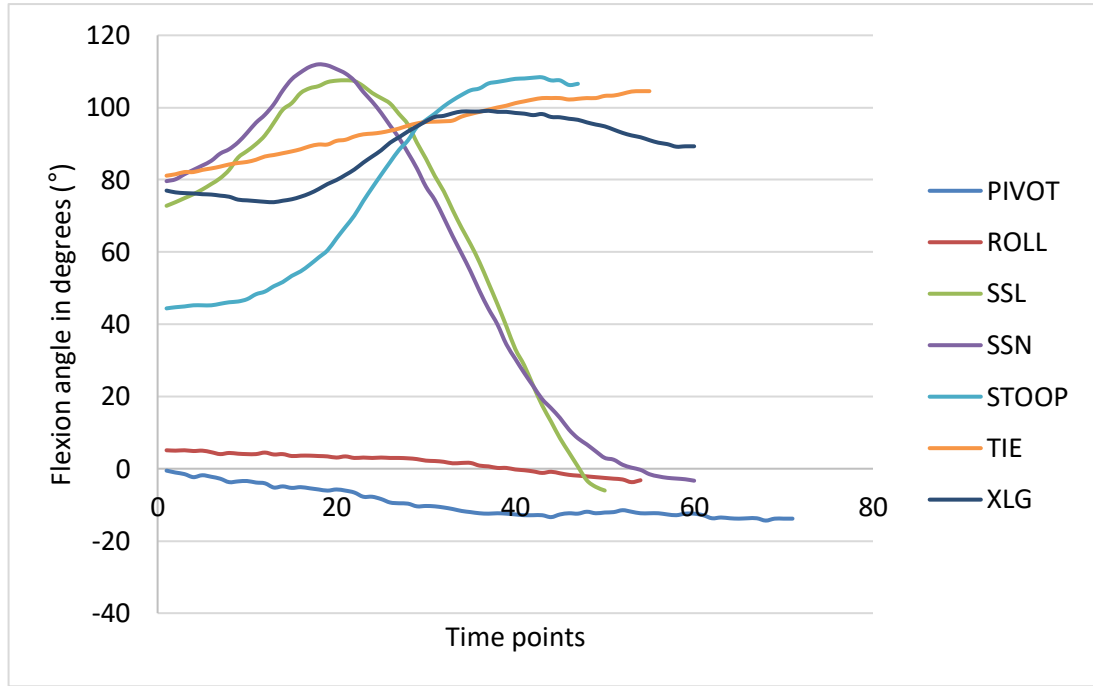


Figure 1.10 Kinematic data from the literature (Nadzadi, et al., 2003) demonstrating the flexion/extension angle of the femur around a fixed pelvis over time for seven dislocation-prone activities.

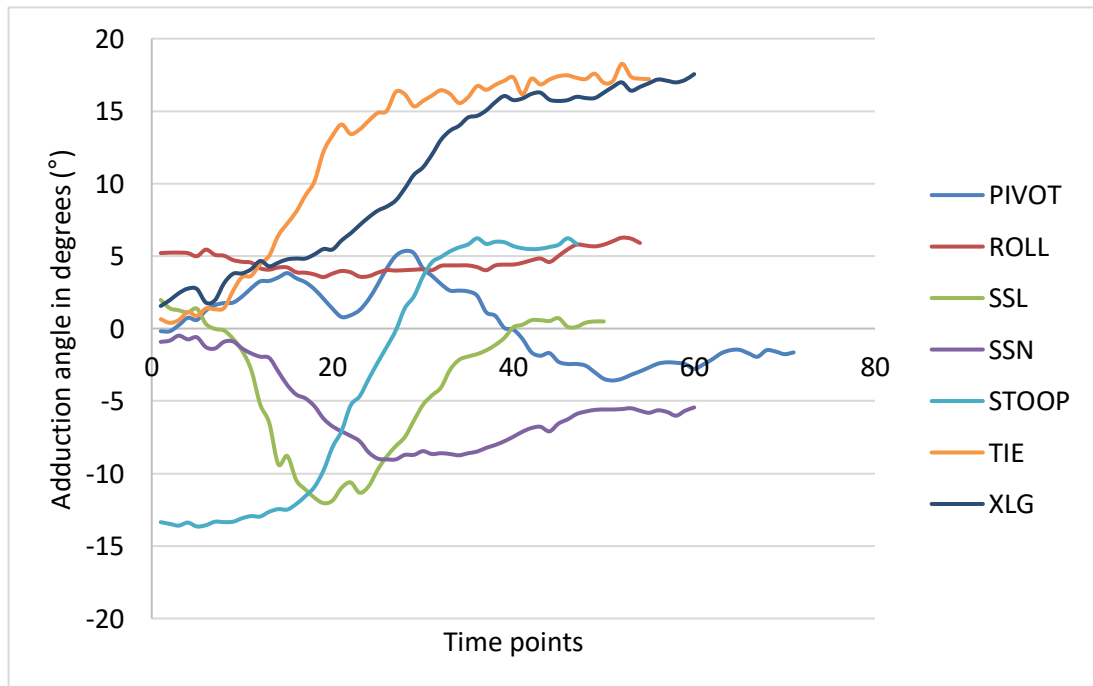


Figure 1.11 Kinematic data from the literature (Nadzadi, et al., 2003) demonstrating the adduction/abduction angle of the femur around a fixed pelvis over time for seven dislocation-prone activities.

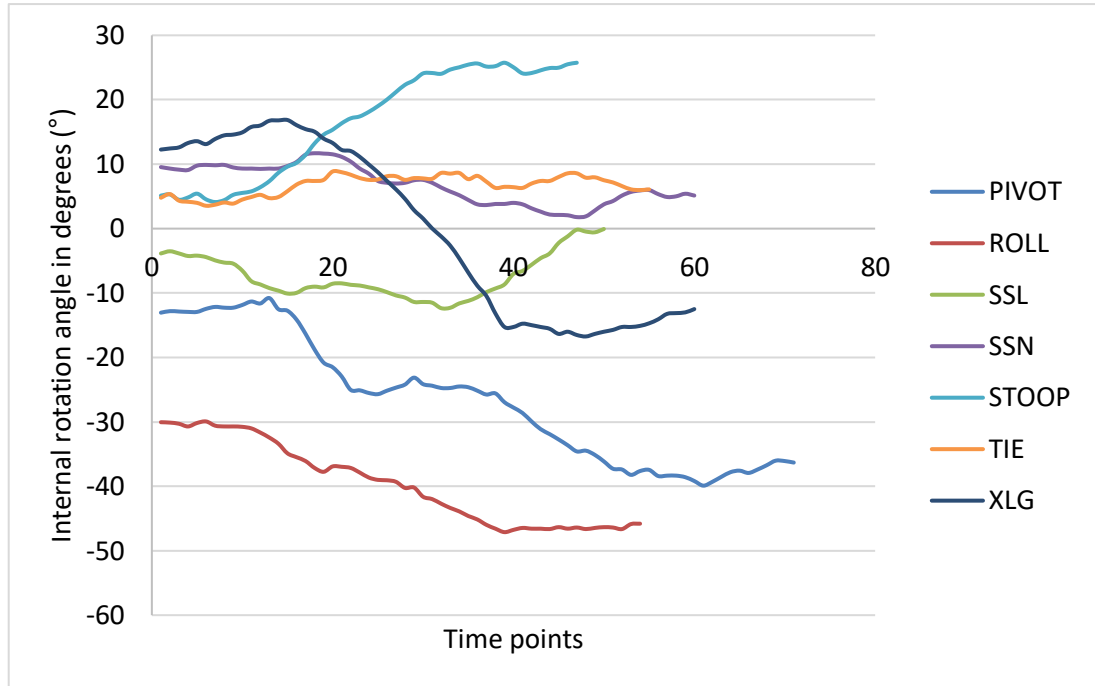


Figure 1.12 Kinematic data from the literature (Nadzadi, et al., 2003) demonstrating the internal/external rotation angle of the femur around a fixed pelvis over time for seven dislocation-prone activities.

This kinematic dataset is an input which can be used to investigate mechanics of impingement and dislocation using typical ranges of motion of activities of daily living, however it has limitations. Firstly, the kinematic data presented consists of one subject's activity data representing the ten subjects for each activity, therefore there was no subject variability in the data. The other subjects could have carried out the same activities with different ranges of motion. Secondly, there was a lack of data on the pelvic movements of the subjects carrying out the activities. There was no consistency across the activities about how much pelvic tilt was in the system because the activities were from different subjects.

1.3.2.2 Impingement-prone activities of daily living (Layton, et al., 2021)

One dataset highlighted in the literature included the kinematics and kinetics of eighteen subjects carrying out thirteen activities of daily living (Layton, et al., 2021). The subjects were non-THR subjects aged between 20-70 years (mean 44.2 years). Each of the eighteen subjects carried out the thirteen

activities for five trials each, however due to errors in data collection, some of the data was missing for some of the subjects. Of the thirteen activities, eight were considered by the authors to be potentially prone to impingement in a THR (“impingement-prone activities”). The activities which were potentially prone to impingement were identified by the size of the RoM. High RoM in flexion was an indicator that a patient/activity would be more likely to impinge such as the stand reach, lunge and squat activities. Another indicator was a large external rotation angle at low flexion angles, indicating an external rotation movement which could possibly impinge at the posterior of the hip such as the walk turn and the golf swing activities.

The impingement-prone activities were: reaching forward from a standing position, reaching forward from a kneeling position, crossing legs whilst seated, walking forwards and then turning (femur rotates through external rotation), sitting down from a standing position, squat, lunge and a golf swing. Unlike the dataset previously described (Nadzadi, et al., 2003), the activity data included all of the subject variability in the dataset. The activity data was captured by using a motion capture system which used skin markers attached to bony landmarks. The force data was also captured using two force platforms on the ground. The kinematic wave profiles consisted of three cardan rotations which represented the movements of the femur relative to the pelvis in the three anatomical planes of motion in the specific order of flexion/extension, adduction/abduction and internal/external rotation (Figures 1.13-1.15). There was also published kinetic data with this study which expressed the loads in each direction.

All of the kinematic data for each activity were the rotation angles for the right side hip. For the walk turn activity, the subject placed their right foot forward as a first step and then turned 90° to the left for the subject’s second step, opening the right hip through external rotation as the subject turned. For the golf swing activity, the subject was given a driver golf club and raised it into a back swing and then followed a golf swing to hit an imaginary ball. For the reaching forward whilst standing activity, the subject stood and reached as far to the floor as possible whilst keeping straight legs. For the reaching forward

from a kneeling position, the subject sat in a kneeling position and then reached as far forwards as possible. For the crossing legs whilst seated activity, the subject sat on a 0.47m stool and crossed the right leg, resting the ankle on the left thigh for one second and then returning to the original sitting position. There were no arms or back support for the chair. For the sitting down from a standing position, the subject sat down onto a chair with no arm or back support and was at a height of 0.47m. For the squat activity, the subject was asked to go from a standing position to a squat position at $\sim 90^\circ$ knee flexion and then return to the standing position. For the lunge activity, the subject was asked to step forward with their left foot, followed by a forward lunge with the right foot, and then stepping out of the lunge again with the left foot.

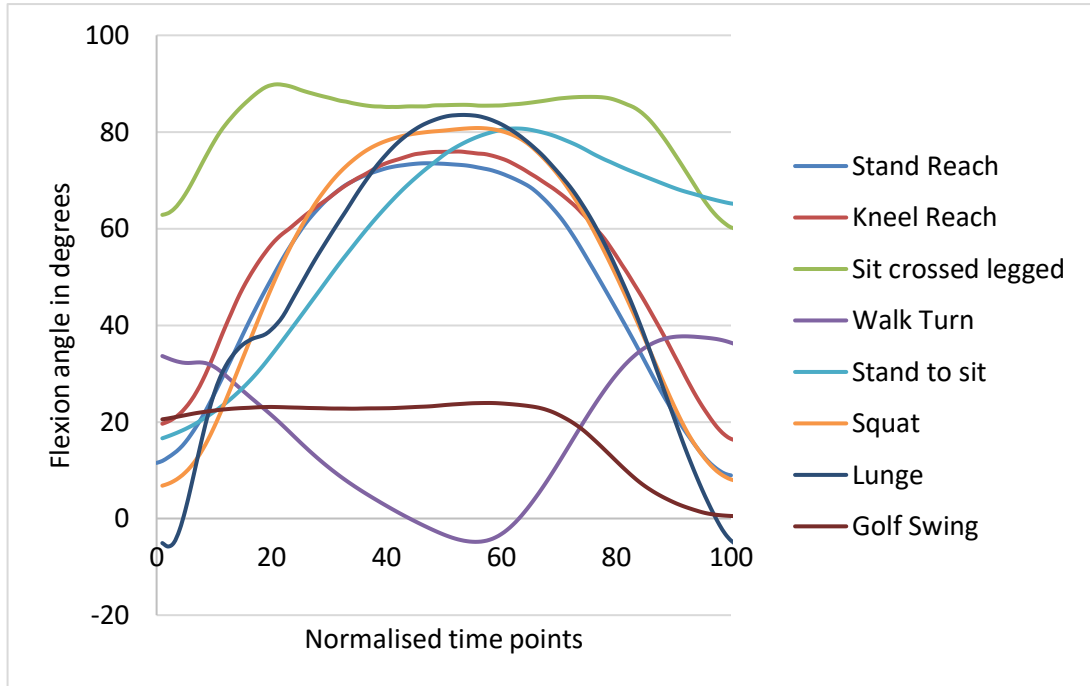


Figure 1.13 Average kinematic data of up to 18 subjects from the literature (Layton, et al., 2021) demonstrating the flexion/extension angle of the femur relative to the pelvis over time for eight activities of daily living potentially prone to impingement.

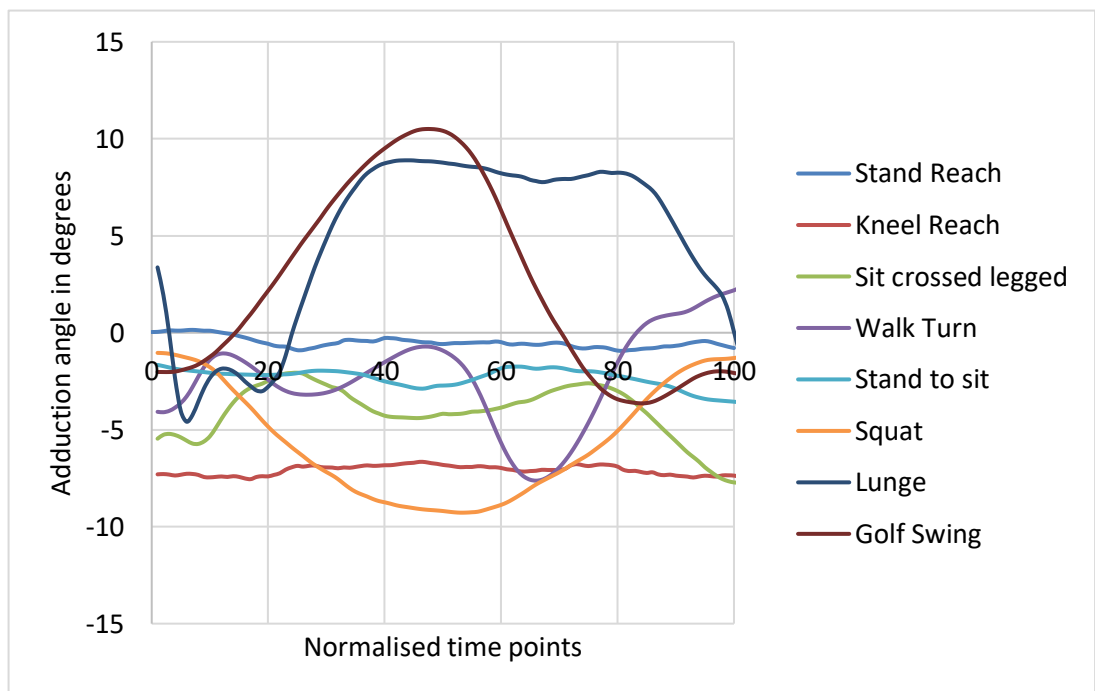


Figure 1.14 Average kinematic data of up to 18 subjects from the literature (Layton, et al., 2021) demonstrating the adduction/abduction angle of the femur relative to the pelvis over time for eight activities of daily living potentially prone to impingement.

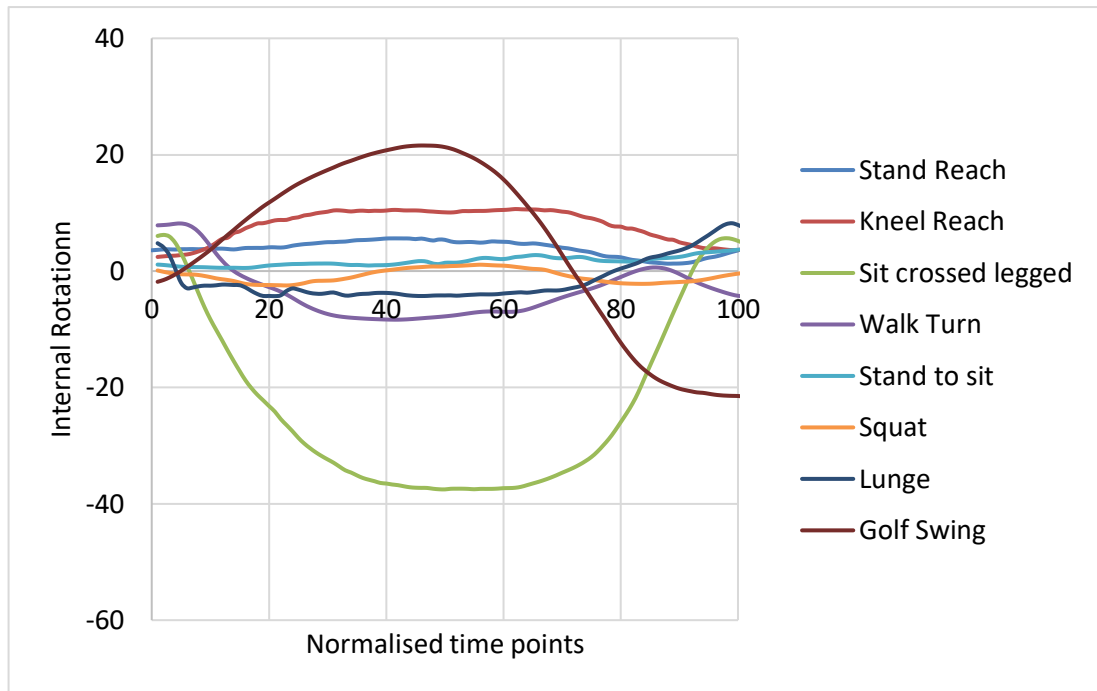


Figure 1.15 Average kinematic data of up to 18 subjects from the literature (Layton, et al., 2021) demonstrating the internal/external rotation angle of the femur relative to the pelvis over time for eight activities of daily living potentially prone to impingement.

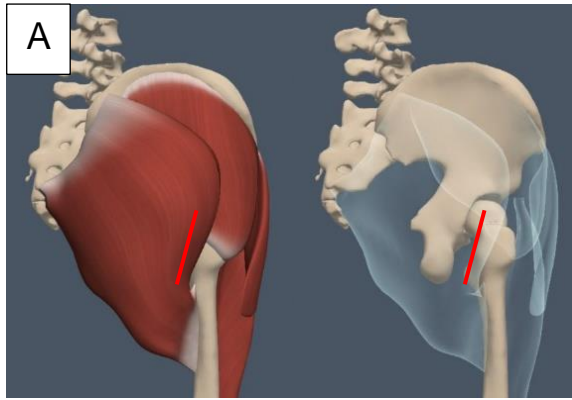
1.3.3 Surgical Factors risking impingement

1.3.3.1 Surgical Approach

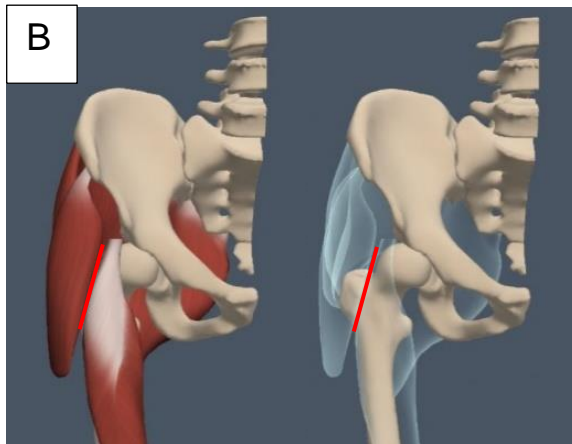
There are a number of different surgical approaches which a surgeon can take to carry out a total hip replacement surgery (Figure 1.16). The largest difference between approaches is the location of incision and the soft tissue which is disturbed to access the hip. The three main types of approach are the posterior approach, anterior approach and lateral approach with the posterior approach being the most common method (54.5%) in England, Wales and Northern Ireland (National Joint Registry, 2020). Surgeons will usually choose the approach based on their experience and personal preference.

The posterior approach to a THR includes an incision made along the posterior outline of the greater trochanter and the hip is exposed by an incision along the longitude of the gluteus maximus muscle to access the hip (Figure

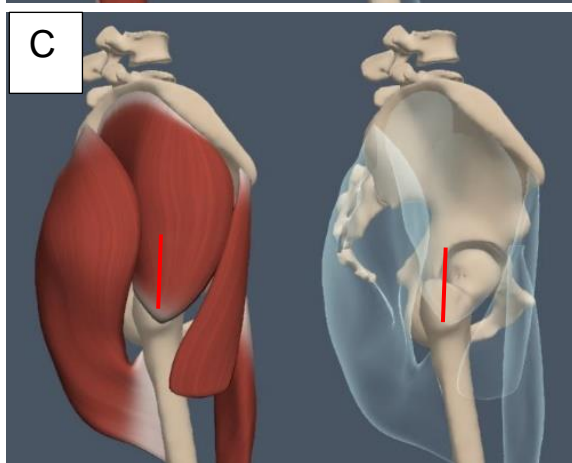
1.16). The posterior approach allows for a greater exposure to the hip providing the surgeon with greater visibility, however some muscle and soft tissue is disrupted (Moretti & Post, 2017). The anterior approach to a THR includes an incision 3 cm lateral and distal to the anterior superior iliac spine (ASIS) and does not need to disrupt any muscle to access the hip. This approach allows for reduced visibility of the hip and therefore is more technically challenging for the surgeon, however it spares the disruption of any muscles surrounding the hip (Moretti & Post, 2017). The lateral approach to a THR includes an incision which is lateral to the hip joint where the hip is accessed by disrupting the longitude of the gluteus medius (Moretti & Post, 2017).



Posterior approach



Anterior approach



Lateral approach

Figure 1.16 The three most common approaches for a surgeon to perform a total hip replacement including: A) the posterior approach shown from a posterior view of the hip, B) the anterior approach shown from an anterior view of the hip and C) the lateral approach shown from a lateral view of the hip. Each approach includes a first image including notable muscles around the hip joint and a red line to mark the approximate location of the incision. The second image for each approach includes the notable muscles as transparent to understand the direction that the hip is accessed from in relation to the bones.

There have been a number of studies which have found that the posterior approach has resulted in a higher dislocation rate (Byström, et al., 2003; Enocson, et al., 2009; Hailer, et al., 2012; Cebatorius, et al., 2015; Zijlstra, et al., 2017) although there have been some studies which have found no difference in the surgical approach in relation to dislocation rates (Palan, et al., 2009; Ji, et al., 2012; Maratt, et al., 2016; Mjaaland, et al., 2017). This increase in the dislocation rate when using the posterior approach is thought to be reduced with sufficient capsular repair (Weeden, et al., 2003; Sierra, et al., 2005; Browne & Pagnano, 2012; Ji, et al., 2012). During the posterior approach, the hip is accessed from the posterior of the hip, disrupting the gluteus maximus muscle and the hip capsule at the rear of the hip. This results in weakened muscles and ligaments at the posterior of the hip and can have an effect on the stability of the joint. Therefore capsular repair is a way to strengthen the ligaments and muscles around the hip to reduce this dislocation risk. The posterior approach continues to be the most popular choice for THR surgery due to the technical ease of the surgery compared to other approaches as well as providing better visibility.

1.3.3.2 Acetabular cup orientation

Acetabular cup orientation affects the risk of impingement and dislocation in THR's (Lewinnek, et al., 1978; Pedersen, et al., 2005; Abdel, et al., 2016; Danoff, et al., 2016). Clinically, acetabular cup orientations have been found to be positioned between 18°-80° inclination and (-)17°-48° anteversion in one study of 1289 THRs which were radiographically assessed following posterior approach surgery (Danoff, et al., 2016). Another study found clinically that acetabular cup orientations were positioned between 25°-66° inclination and 0°-37° anteversion in 834 THRs following surgery by one surgeon using the posterior approach which were measured by radiographs (Minoda, et al., 2006). These values may not be exact as there are difficulties in measuring anteversion on 2D radiographs.

Historically, a safe zone was initially defined (Lewinnek, et al., 1978) which found a range of acetabular cup orientations which had a reduced risk of dislocation. The safe zone was between 30° and 50° radiographic inclination

and 5° and 25° radiographic anteversion. The dislocation rate of 300 THR's was 1.5% inside the safe zone and 6.1% outside the safe zone. Multiple studies however have disagreed with this safe zone and have investigated the numbers of dislocations found clinically inside and outside the defined safe zone and found that large percentages of dislocations had occurred in THR patients whose acetabular cup orientation was within the defined Lewinnek et al. safe zone (McLawn, et al., 2015; Abdel, et al., 2016; Danoff, et al., 2016).

There have been computational studies which have investigated the effect of acetabular cup orientation and its effect on impingement in THR's (Pedersen, et al., 2005; Ghaffari, et al., 2012; Pryce, et al., 2022). These studies varied the acetabular cup orientation in a computational model of a THR and investigated the effect on impingement. There was general agreement across these studies. A low inclination and anteversion angle resulted in lower flexion ranges of motion and increased impingement occurrences during high flexion activities of daily living. A high inclination and anteversion angle resulted in lower external rotation ranges of motion and increased impingement occurrences during high external rotation activities of daily living. These studies demonstrated that small changes to the acetabular cup orientation can have an effect on impingement in a THR.

The consensus in the literature of the effect of implantation angles and safe zones demonstrates that there is still no clear definition as to what the implantation orientations should be or whether there even exists a safe zone that would fit all patients. The safe zone that was previously defined (Lewinnek, et al., 1978) should be used with caution as a rough guide. There is a need for a patient-specific approach to be taken for acetabular cup orientation targets.

1.3.3.3 Current THR preoperative planning methods

It has been shown that with surgical preoperative planning of THR's, up to 50% of THR failures could have been avoided (Novikov, et al., 2019). To attempt to restore the biomechanics and anatomy of the natural hip to maintain stability, the surgeon typically uses templating or preoperative

planning to improve the decision-making for the patient's THR surgery (Lecerf, et al., 2009; Flecher, et al., 2016; Lakstein, et al., 2016). The most common form of preoperative planning is using 2D radiographs of the patient's hip to plan surgical decisions such as the depth of reaming, leg length, offset, component size and component inclination angle. This method of preoperative planning has been shown to be relatively effective in the prediction of the component size, with predictions having a relatively effective level of accuracy to within one size of the final component size (Valle, et al., 2005; Efe, et al., 2011; Stigler, et al., 2017; Holzer, et al., 2019; Kristoffersson, et al., 2021). However this method relies on the accuracy of the radiographs and some studies have shown that there can be large discrepancies with the decisions made during preoperative planning on a radiograph and the final decisions on the patient during surgery (Efe, et al., 2011; Holzer, et al., 2019). Certain decisions such as the acetabular anteversion of the cup can also not be decided accurately from a 2D radiograph. These inaccuracies can be improved with 3D preoperative planning of patient's surgery. One study found that the accuracy in component size of the stem and the acetabular cup was 16% for the 2D templating and 96% for the 3D templating (Sariali, et al., 2012) which agreed with another study which found accuracies of up to 83.6% for the 2D templating and up to 94% for the 3D templating (Schiffner, et al., 2018). Preoperative planning has been shown to be necessary to improve outcomes of THR's, with a 3D preoperative planning showing much higher prediction accuracies to the final decisions made in surgery. The 3D preoperative planning does come at a cost however as it is time consuming and more expensive than a simple radiograph templating (Schiffner, et al., 2018). There is a need for a dynamic 3D templating assessment to improve outcomes of THR' s in relation to impingement and how the patient's activities of daily living can affect impingement.

1.3.4 Patient factors that influence impingement

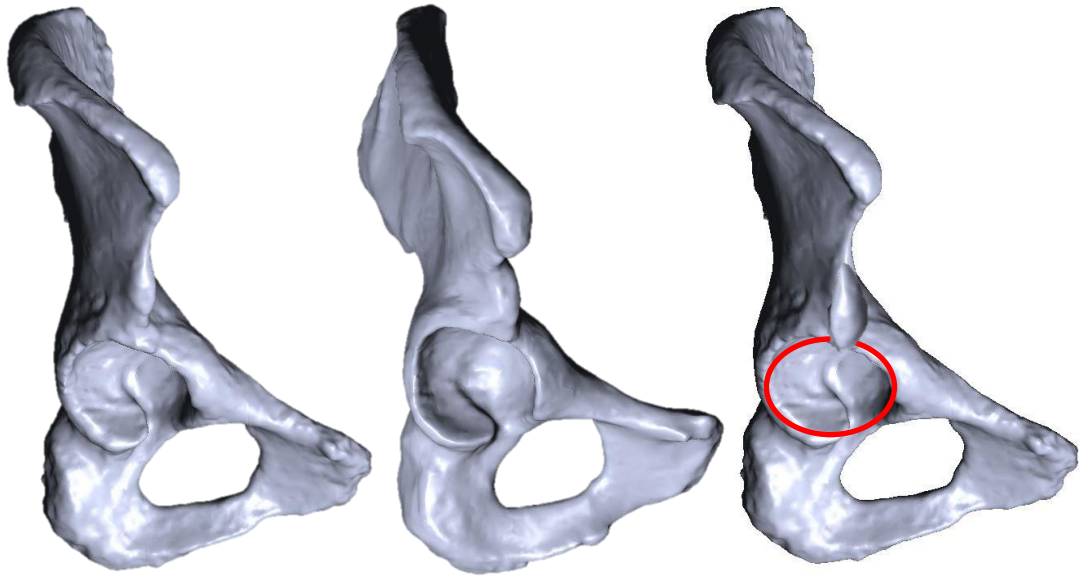
1.3.4.1 Geometry of pelvis and femur

Bone-on-bone impingement has been shown to be a limiting factor to the range of motion of larger head sizes (>32mm) (Burroughs, et al., 2005; Elkins,

et al., 2012). Therefore, the shape of a patient's bony anatomy would be a factor in the range of motion to impingement. The location of bone-on-bone impingement contact limiting range of motion has been found to occur at various locations including between: the anterior inferior iliac spine and the anterior side of the greater trochanter, the lesser trochanter and the ischium, and the intertrochanteric crest of the femur and the ischium (Kessler, et al., 2008; Patel, et al., 2010; Nakahara, et al., 2011; Shoji, et al., 2016; Tabata, et al., 2019). No studies reporting the effect of dislocation-prone activities of daily living on different bony geometries were found in the literature.

At the anterior side of the hip, the anterior inferior iliac spine ("AIIS") has been shown to be involved in bone-on-bone impingement by a number of studies (Hetsroni, et al., 2013; Shoji, et al., 2016; Tabata, et al., 2019). A classification system ("Hetsroni classification") has previously been produced to categorise a patient's AIIS morphology into three variants to help identify problematic AIIS bony geometries in the natural hip (Hetsroni, et al., 2013). These three types consisted of type 1, which was when there was smooth wall between the acetabulum and the acetabular rim, type 2, which was when the AIIS met the acetabular rim and finally type 3, which was when the AIIS extended distally below the level of the top of the acetabular rim (Figure 1.18). The study found that there was a statistically significant difference in the RoM depending on the type of AIIS in a series of 78 natural hips as measured by CT scan data with type 1 allowing for the greatest RoM and type 3 allowing for the lowest RoM. This was investigated further in patients with a THR by another study, which measured the RoM in a cohort of 14 CT scans which were used in the preoperative planning of the patient's THR and which contained hips from all three types of the Hetsroni classification (Tabata, et al., 2019). It was found that there were no statistically significant differences between the types of AIIS in relation to the RoM, however the RoM on average decreased from type 1 to type 2 to type 3. The lack of statistical significance could be because the differences in the three types were subtle. Another study investigated the AIIS morphology by measuring a series of length and angular measurements of the AIIS in 85 THR patients to investigate the effect of the bony morphology

of the AIIIS on the RoM (Shoji, et al., 2016). The length and angular measurements were taken of the AIIIS in relation to the CoR in 85 CT scans and compared to the RoM of the hips. It was found that a number of AIIIS measurements were statistically significant to the reduction in the range of motion of the THR including the lateral measure, anterior measure, lateral inclination angle, anterior inclination angle and the axial straight distance. Some of the measurements used in this study however were also statistically significant when compared to the height of the patients, therefore the measurements identified in this study could have just identified the largest patients who would have larger bony geometries. The same THR components were implanted into each patient with the shell being resized depending on the size of the patient meaning there was not consistency between patients.



A) Type 1 AIIS – Type 1 has a smooth part of ilium wall between the acetabular rim and the AIIS.

B) Type 2 AIIS - Type 2 has the base of the AIIS start at the acetabular rim with no ilium wall in between.

C) Type 3 AIIS – the AIIS extends distally below the rim of the acetabulum.

Figure 1.17 The three types of AIIS (“Hetsroni classification”) as previously defined by a study (Hetsroni, et al., 2013), demonstrated on a hemi-pelvis of different geometric models.

At the posterior side of the hip, the locations of bone-on-bone impingement have been found to be between the ischium of the pelvis and either the lesser trochanter or the intertrochanteric crest of the femur (Kessler, et al., 2008; Patel, et al., 2010; Nakahara, et al., 2011; Shoji, et al., 2016). One study analysed the effect of the acetabulum angle and its effect on the RoM (Nakahara, et al., 2011). The CT scans of 106 elderly subjects were measured for the anteversion angle of the natural acetabulum and the RoM during external rotation. It was found that the anteversion angle of the natural acetabulum significantly affected the RoM of the natural hips in external rotation. A number of studies have found that bone-on-bone impingement becomes the restricting factor to RoM when using larger femoral heads and

is prevalent at the posterior of the hip during external rotation (Burroughs, et al., 2005; Elkins, et al., 2012). Some other studies investigated external rotation activities in THR's, however did not relate this to the anteversion angle of the natural acetabulum (Kessler, et al., 2008; Patel, et al., 2010; Shoji, et al., 2017). Therefore there is a need to investigate the anteversion angle of the natural acetabulum and its relation to the RoM of THR's and further its relation to impingement during activities of daily-living which are prone to bone-on-bone impingement at the posterior of the hip.

1.3.4.2 Pelvic (sagittal) tilt

Pelvic tilt is the rotation of the pelvis in the sagittal plane about an axis which runs through the CoR of the femoral heads (Figure 1.17) and affects the functional positioning of the implants in a THR (Pierrepont, et al., 2017; Lee, et al., 2019). When a total hip replacement is implanted, the surgeons aim to implant the acetabular cup at a specific implantation orientation (Lewinnek, et al., 1978). However, during the movement of a patient's pelvis during activities of daily living, the 'functional' orientation of the acetabular cup in relation to the femoral component can change which will also change the RoM to impingement (Kanazawa, et al., 2016; McCarthy, et al., 2017; Ike, et al., 2018; Pierrepont, et al., 2017). Pelvic tilt has been shown to vary from -30.2° to 27.9° whilst standing (Pierrepont, et al., 2017). One study found that a change of 1° of pelvic tilt can result in a change in 0.5° of cup anteversion (Anda, et al., 1990), while another found that a pelvic tilt of 1° can result in a change of 0.75° of cup anteversion (Schwarz, et al., 2022). Patients with degenerative spinal problems, particularly elderly patients who have reduced pelvic rotation, have been shown to be at an increased risk of dislocation (Blizzard Daniel, et al., 2017). These patients have less pelvic rotation, creating increased demand for femoral rotation, increasing the risk of impingement and dislocation during activities of daily living (Ike, et al., 2018; Lee, et al., 2019).

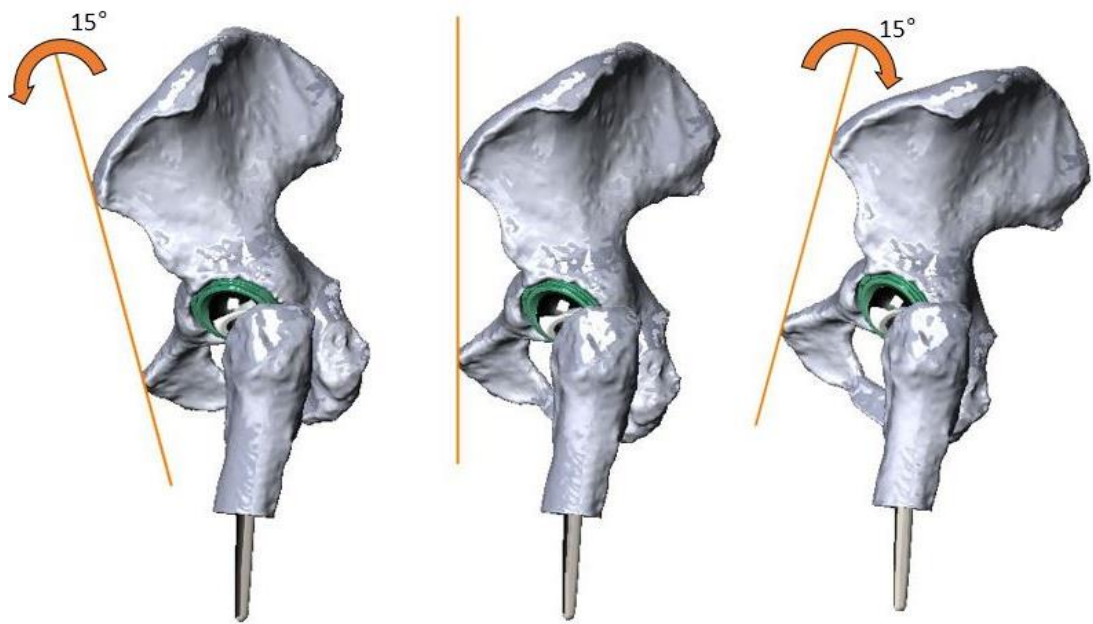


Figure 1.18 A sagittal view of three total hip replacements demonstrating a rotation in the pelvic tilt angle of +15°, 0° and -15°. The cup orientation is visibly changing across the three pelvic tilt angles demonstrating the change in functional cup orientation as the pelvis rotates.

1.4 Evidence and consequences of impingement

The consequences of impingement are evident in retrieved liners following revision surgery (Birman, et al., 2005; Shon, et al., 2005; Usrey, et al., 2006; Lee, et al., 2011; Marchetti, et al., 2011; Waddell, et al., 2018). In polyethylene liners, this impingement evidence is in the form of notching and deformation of the liner rim where the stem has contacted the rim under load and caused damage. In hard-on-hard bearings such as ceramic liners, the impingement evidence was in the form of black staining and macroscopic cracks on the liner rim. This is because of the brittleness of the ceramic material when compared to the polyethylene, meaning damage to the polyethylene liners were visually more obvious and included greater deformation. The details of the retrieval studies are described in Table 1.1.

Table 1.1 Retrieval studies with evidence of clinical impingement detailed from the literature.

Author	Number of retrievals	Liner material analysed	Femoral head sizes	Lipped liner use	Follow-up time (months)	Reasons for revision	Percentage of liners with evidence of impingement damage
(Birman, et al., 2005)	120	Poly-ethylene	N/A	No	Mean follow-up of 80 (range of 2 - 204)	Aseptic loosening (22%), infection (16%), dislocation (25%), wear (20%), pain (4%), and osteolysis (8%).	71/120 (59%). With 38/120 (32%) labelled as having 'moderate' or 'severe' impingement (defined as the radial width of the impingement scar greater than 4mm or significant material loss of the component secondary to impingement). Cracking was also found in 48/120 (40%).
(Shon, et al., 2005)	170	Poly-ethylene	22mm (n=14), 26mm or 28mm (n=75), 32mm (n=19)	47/170 had an elevated rim	Median follow-up of 84 (range of 2 - 240)	Aseptic loosening (92 hips), recurrent dislocation (48 hips), infection (19 hips), cup dissociation (1 hip), stem fracture (1 hip), and osteolysis (1 hip).	96/170 liners (56%). Of these, 20/170 (12%) had "moderate or severe" impingement which had an impingement notch extending >1mm into the liner rim. 38/47 elevated rims (81%) had impingement damage.
(Usrey, et al., 2006)	113	Poly-ethylene	28mm (n=67), 32mm (n=46)	85/113 had an elevated portion	Mean follow-up of 84 months (range of 2 - 192 months)	Aseptic loosening (21%), dislocation (18%), infection (18%), wear (14%), osteolysis (13%) and pain (4%).	68/113 (60%) showed signs of impingement. Of these, 36/113 (32%) were labelled as having 'moderate' or 'severe' impingement (defined as the radial width of the impingement scar greater than 4mm or significant material loss of the component secondary to impingement). 51/85 (60%) elevated liners had signs of moderate or severe impingement.
(Lee, et al., 2011)	16	Ceramic (Alumina)	28mm	No	Mean follow-up of 51.8 (12 - 99)	Head fracture (4 hips), Liner fracture (3 hips), infection (3 hips), acetabular component loosening (2 hips), implant malposition (1 hip), dislocation (1 hip), squeaking (1 hip), osteolysis (1 hip).	4/16 (25%) had signs of impingement (macroscopic notching and black stained liner rim as well as V-shaped notching on the stem).
(Marchetti, et al., 2011)	416	Ceramic (6), Metal (11), Poly-ethylene (399)	22mm (n=51), 28mm (n=195), 32mm (n=146), 26,27,35, 37mm (n=24)	51/416 had an elevated rim	Mean follow-up of 92.4 ± 66 (range of 2 - 312)	Aseptic loosening (131 hips), infection (43 hips), dislocation (56 hips), osteolysis (28 hips), miscellaneous (48 hips), impingement (5 hips).	214/416 liners (51.4%). Of these, 130/416 (31.3%) of the cups being deemed 'severe' (contained an impingement notch >1mm).
(Waddell, et al., 2018)	97	Poly-ethylene	28mm (n=12), 32mm (n=46), 36mm (n=39)	12/97 had an elevated rim (n=4 at 28mm, n=5 at 32mm and n=3 at 36mm)	Mean follow-up data: 28mm heads: 69.6 ± 60 (9.6 - 180) 32mm heads: 28.8 ± 36 (0.36 - 144) 36mm heads: 16.8 ± 24 (0.24 - 96)	Dislocation (55 hips), infection (14 hips), loosening (11 hips), pain/allergy/other (13 hips), leg length discrepancy (3 hips), fracture (1 hip).	75/97 (77%) Of these, 21/97 had signs of "severe" impingement (defined as damage deformation >1mm into liner rim). The impingement damage was lessened by the use of larger femoral heads but not completely eliminated.

The percentage of retrievals which had signs of impingement damage ranged between 25%-77% (Table 1.1). There were a number of different reasons given for the revision surgeries in the patients analysed in these studies, meaning that impingement damage was found in explanted liners which were not revised specifically for impingement or dislocation. This indicates that impingement damage continues to be a common occurrence in THR's.

These studies mostly included explanted polyethylene liners and each had a grading system to determine the severity of the impingement damage. The grading systems differed between studies however were determined by either the depth of the impingement damage into the liner (Shon, et al., 2005; Marchetti, et al., 2011; Waddell, et al., 2018) or the angular size of the damage along the rim (Birman, et al., 2005; Usrey, et al., 2006). Many of the liners across the studies were found to have "moderate" or "severe" impingement damage which were the two most severe grades out of four of impingement damage according to the studies. This included 38/120 (32%) for one study (Birman, et al., 2005) where the "moderate or severe" impingement damage was described as the radial width extending more than 4mm on the rim or significant material loss due to impingement respectively. Another study (Usrey, et al., 2006) used the same grading system and found that 68/113 (60%) of retrieved liners showed signs of moderate or severe impingement. One study (Shon, et al., 2005) found 20/170 (12%) had "moderate or severe" impingement which was described as the impingement damage notch on the rim extending more than 1mm into the rim. Another study (Marchetti, et al., 2011) found 130/416 (31%) had "grade 2 or 3" impingement damage which was defined as the impingement damage notch on the rim extending more than 1mm into the rim. Another study (Waddell, et al., 2018) 21/97 (22%) found "severe" impingement, which was defined as the impingement damage notch on the rim extending more than 1mm into the rim.

Some of the studies included retrieval data from lipped liners. There was a high percentage (60% - 85%) of lipped liners which had evidence of impingement damage (Shon, et al., 2005; Usrey, et al., 2006; Marchetti, et al., 2011; Waddell, et al., 2018). This could have been because of the lower RoM

associated with lipped liners (discussed in more detail in Section 1.3.1.2). The effect of the femoral head size on the impingement damage found clinically was also analysed in the retrieval studies. Only one study found that there was a decrease in the incidence and severity of impingement as the head size was increased (Waddell, et al., 2018). Other studies which investigate head size found no correlation between head size and impingement damage (Shon, et al., 2005; Usrey, et al., 2006; Marchetti, et al., 2011). The effect of femoral head size is discussed in more detail in Section 1.3.1.1.

From the evidence in the literature on the retrieved liners, it was clear that impingement occurred in a large percentage of THR's regardless of the reasons for revision. Impingement can also cause damage to acetabular liners in different bearing materials. The failure of implants directly through impingement has been reported as rare (Marchetti, et al., 2011; National Joint Registry, 2020), however the number of retrievals with evidence of impingement is concerning especially in those retrieved liners whose reason for retrieval had no link to impingement or dislocation.

1.5 Impingement studies using computational models of THR's

There have been a number of studies which have used computational models of THR's to investigate the RoM until impingement (Barsoum, et al., 2007; Kessler, et al., 2008; Ji, et al., 2010; Ezquerro, et al., 2017). There have also been a number of computational studies which have investigated activities of daily living which were prone to impingement (Nadzadi, et al., 2003; Pedersen, et al., 2005; Patel, et al., 2010; Elkins, et al., 2012; Ghaffari, et al., 2012; Pryce, et al., 2022). The details of these studies have been described in Table 1.2.

Table 1.2 Computational modelling studies investigating impingement from the literature.

Author	Type of computational model	Bony geometry included	Activities or range of motion	Force data included
(Nadzadi, et al., 2003)	FEA	No	Activities gathered in this study (Nadzadi et al. (2003) activity dataset)	Kinetic data measured in the study and used to measure resisting moment during the activities
(Pedersen, et al., 2005)	FEA	No	Nadzadi et al. (2003) activity dataset	Force data from Nadzadi et al. (2003) dataset used to find dislocation which was defined as the point where the resultant load was pointed outside of the bearing surface.
(Barsoum, et al., 2007)	Geometric analysis	One bony geometry from online repository	RoM	No
(Kessler, et al., 2008)	Geometric analysis	One bony geometry from online repository	RoM	No
(Ji, et al., 2010)	Geometric analysis	No	RoM	No
(Patel, et al., 2010)	Geometric analysis	Eight bony geometries from an online repository	RoM with the motions based on activities from the Nadzadi et al. (2003) activity dataset	No
(Elkins, et al., 2012)	FEA	One bony geometry from an online repository	Nadzadi et al. (2003) activity dataset as well as pure flexion and a squat exercise	Force data from Nadzadi et al. (2003) used to measure resisting moment during the activities.
(Ghaffari, et al., 2012)	FEA	No	Four of the activities from the Nadzadi et al. (2003) activity dataset	Force data from Nadzadi et al. (2003) used to measure resisting moment during the activities.
(Ezquerro, et al., 2017)	FEA	No	RoM	Resisting moment measured.
(Pryce, et al., 2022)	Geometric analysis	One bony geometry from an online repository	Nadzadi et al. (2003) activity dataset	No

The computational models which have investigated impingement can be split into Finite Element Analysis (FEA) models and geometric analysis models. Due to the computing power and complexity of modelling bony geometries, the majority of FEA models did not include any bone in the computational models, meaning that bone-on-bone impingement could not be recorded. Only one study used an FEA model which included bony geometry to investigate impingement with dislocation-prone activities (Elkins, et al., 2012). The majority of the geometric models could include bony geometries in their analysis, however most of the studies only included one bony geometry, limiting the results to that one bony geometry used in each study.

The activity data used in the computational modelling studies were all the same kinematic dataset from the literature (Nadzadi, et al., 2003). This included the force data used in the FEA models alongside the kinematic dataset. Therefore all of the results from these studies were limited to the one subject which was selected for each activity in this dataset (kinematic dataset described in more detail in section 1.3.2.1). There is a need for other kinematic datasets to be investigated using computational models to strengthen the conclusions made from these studies. Some of the computational models solely used RoM to investigate impingement. While this was an effective way of quickly measuring differences in impingement-free motion, the use of activity data provided a more clinically-relevant way of analysing impingement conditions in THR's.

1.5.1 Finite Element Analysis models

Using FEA can be useful as it detects the forces and contact between the THR components and therefore has the ability to study edge loading, applied stress and dislocation risks, however without any bones or soft tissue, the models are limited in their relevancy because they only capture implant-on-implant impingement and their conclusions around impingement likelihood under different conditions is limited.

Most of the impingement studies which have replicated activities of daily living have been FEA models (Nadzadi, et al., 2003; Pedersen, et al., 2005; Elkins,

et al., 2012; Ghaffari, et al., 2012). The majority of these studies found occurrences of impingement and dislocation using the same kinematic dataset (Nadzadi, et al., 2003). One of the FEA studies (Nadzadi, et al., 2003) used a worst case scenario model which included the use of a 22mm femoral head size and a simple acetabular cup which was positioned at an unfavourable angle (30° inclination and 0° anteversion for the activities prone to posterior dislocation and 70° inclination and 40° anteversion for the activities prone to anterior dislocation). It was found that there were high incidences of dislocations for all of the activities measured by the study with the risk of dislocation being dependant on the activity, however this was a worst case scenario and the model had no bony geometries which limited the clinical relevance of this study. Similarly, another study (Pedersen, et al., 2005) used the same kinematic dataset to investigate cup orientation in an FEA model. The cup orientation was varied between 30°-70° inclination and 0°-40° anteversion. Out of the 175 scenarios which included an activity at each cup orientation (7 activities coupled with 25 cup orientations), impingement occurred in 96 scenarios (55%) and dislocation and impingement occurred in 51 situations (29%). This study included varied cup orientations which provided a more useful insight into the likelihood of impingement and dislocation using a previous kinematic dataset (Nadzadi, et al., 2003), however again included no bony geometries. A similar study (Ghaffari, et al., 2012) used simple shapes to represent the THR components and investigated different acetabular cup orientations. This study did not give very meaningful output data in regards to the effect of acetabular cup orientation or the risk of dislocation. The main output was the impingement data which tracked the angle of impingement throughout the activity. This was an effective method of measuring the risk of impingement as it captured the severity of impingement even in the scenarios which did not result in an impingement event. This study had many limitations including the use of simplified shapes to replicate the THR which were not clinically relevant. Another study (Elkins, et al., 2012) used a previous kinematic dataset (Nadzadi, et al., 2003) as well as a squat exercise with one bony geometry taken from a CT scan in an online repository and clinically-relevant THR components including a 36mm femoral head. No

impingement was found for any of the dislocation-prone activities and only the squatting activity resulted in bone-on-bone impingement. This disagreed with the other FEA studies on impingement occurrences with these dislocation-prone activities, however this study included a large femoral head size and a well-positioned acetabular cup in contrast to the other studies which included malpositioned and smaller components. The squatting exercise was investigated further with the FEA model and found that when the acetabular cup was malpositioned, there was found to be implant-on-implant impingement. Following this, an analysis of the differences between bone-on-bone impingement and implant-on-implant impingement were compared. The resisting moments in the FEA model as well as the contact stresses following an impingement event were measured in different sized femoral heads. The peak edge loading forces in the implant were higher in the implant-on-implant impingement event which was expected as there was no subluxation allowed in the model and therefore this measured the greater RoM needed for implant-on-implant impingement as bone-on-bone impingement would precede implant-on-implant impingement. There was also a measured peak dislocation resisting moment about the cup centre which resulted in lower resisting moments for the implant-on-implant impingement event which again would have been because of the higher RoM needed to reach the implant-on-implant event which was not a fair comparison. This study was limited because there was no movement of the femoral head allowed in the model, therefore the conclusions around dislocation were limited. There was also the use of only one bony geometry, with different shaped bony geometries possibly leading to different results.

1.5.2 Geometric analysis models

The other computational studies to investigate impingement using activities of daily living have used geometric models (Patel, et al., 2010; Pryce, et al., 2022). One study produced eight geometric models with different bony geometries and simplified generic THR component geometries (Patel, et al., 2010). This study used simplified versions of a previous kinematic dataset (Nadzadi, et al., 2003) measuring the RoM of the most dominant rotation. For

the posterior dislocation-prone activities, the flexion was measured alongside values of adduction/abduction and internal/external rotation associated with the particular activity being measured. For the anterior dislocation-prone activities, the external rotation was measured alongside values of flexion/extension and adduction/abduction associated with the particular activity being measured. It was found that the majority of activities prone to posterior dislocation resulted in implant-on-implant impingement and there was found to be bone-on-bone impingement during the activities prone to anterior dislocation. The main output of this study was the RoM, therefore the use of the previous kinematic dataset (Nadzadi, et al., 2003) was unnecessary and it would have been more relevant if the full activities had been used. This study had an effective method of investigating different bony geometries and its effect on the impingement, however the comparison across bony geometries was not discussed. The other geometric model study (Pryce, et al., 2022) which used a geometric model with dislocation-prone activities used a single bony geometry and THR components with a previous kinematic dataset (Nadzadi, et al., 2003) and a walking activity. The study investigated cup orientation and its effect on impingement during these dislocation-prone activities. Impingement was found in at least one cup orientation during all of the activities apart from walking. Bone-on-bone impingement was detected for some of the cup orientations in the STOOP and ROLL activities. There were limitations to this study which included the use of only one bony geometry which could have generated different results with different shaped bony geometries. There was also no way of measuring the severity of the impingement detected by the model and instead only had a “pass/fail” for impingement during each activity. Again, the same kinematic dataset was used and therefore limited the outcomes of the study.

1.6 Hip simulator studies investigating impingement

There have been some studies in the literature which have investigated impingement using *in vitro* hip simulators. These studies have been described

in Table 1.3 (Burroughs, et al., 2005; Holley, et al., 2005; McCarthy, et al., 2017; Pryce, 2019; ASTM F2582, 2020).

Table 1.3 Impingement studies using *in vitro* hip simulators from the literature.

Author	Kinematic motion	Cyclic or non-cyclic test	Component setup	Force application
(Burroughs, et al., 2005)	Pure flexion, internal rotation at 90° flexion, external rotation at 0° flexion. Motions rotated until impingement and dislocation.	Noncyclic test	A table-top rig of a fiberglass femur and a plastic hemi-pelvis. The pelvis is rotated depending on the motion tested.	Force applied as 2-3 times body weight in accordance with another study. Literature not clear what this value was.
(Holley, et al., 2005)	Orbital motion	Cyclic test for 5 million cycles	Femoral head with stem-like feature attached to top of simulator and acetabular cup attached to the bottom of the simulator. Stem and cup articulate so that there is impingement contact during each cycle.	Load profile with a maximum of 2000N.
(McCarthy, et al., 2017)	Three activities: squatting, object pickup and low chair sit to stand. Activities applied until impingement.	Noncyclic test	The acetabular cup is fixed to the top of the table-top jig and the femoral stem is attached to the bottom.	No load applied
(Pryce, 2019)	Object pick-up (STOOP - Nadzadi et al. (2003) data). Simplified version of STOOP activity with reduced RoM.	Cyclic test for 40k cycles	Femoral stem fixed to the top of the simulator and acetabular cup rotates around stem. Initial position includes the stem and liner not in impingement contact.	Simple wave profile of 300N to 800N at the greatest RoM, applied to the femoral stem from above.
(ASTM F2582, 2020)	Simple wave profile of 0° - 10° extension, 0° - 5° abduction, (-5°) - 5° rotation. Liner rim and stem under constant impingement contact.	Cyclic test for 1 million cycles	Acetabular cup fixed to the top of the simulator and femoral stem rotates around liner. Initial position is the stem rotated through abduction until there is impingement contact.	Constant 600N force applied to acetabular cup from above.

The hip simulator studies included a wide range of kinematic motion to simulate impingement conditions. The standard for impingement testing (ASTM F2582, 2020) used a simple wave profile while the components were under constant impingement. This is not a clinically-relevant method for assessing impingement in THR's as the kinematic motion is not how impingement occurs *in vivo*. Another study (Holley, et al., 2005) used "orbital motion" to investigate impingement which is also not clinically-relevant to impingement *conditions in vivo*. Three of the studies did use activities of daily living which were of clinical relevance, however the noncyclic tests did not measure impingement damage and instead only measured RoM (Burroughs, et al., 2005; McCarthy, et al., 2017). One study (Pryce, 2019) used simplified activity data which had reduced RoM and measured impingement damage. The study used the STOOP activity from a previous kinematic dataset (Nadzadi, et al., 2003) and simplified it by smoothing the wave profile and reducing the peak RoM for use in the simulator. The peak RoM was applied so that there was 2.5° and 5° of impingement to compare the difference in damage. This meant that with the reduction in RoM and the change in the peak RoM to apply different severities of impingement, the kinematics had been manipulated to something that was different than that of the original data. This study also only included one activity.

The cyclic tests measured impingement damage after a certain number of cycles. One study (Holley, et al., 2005) included five million cycles of impingement testing. While the number of times patients carry out impingement-prone activities of daily living is not known, five million times is thought to be excessive. As a reference, one study (Tateuchi, et al., 2017) found that a group of 50 patients with secondary hip osteoarthritis walked on average 6596 steps in a day over a one month period which would be 2.4 million steps in a year. Therefore to simulate dislocation-prone activities which happen a few times a day for five million cycles would be considered excessive.

The way in which damage was measured differed across the cyclic tests. The standard for impingement testing (ASTM F2582, 2020) uses visual

assessment of damage including analysing for cracks, fracture, deformation, delamination and wear. Another study (Pryce, 2019) used a Coordinate Measuring Machine (CMM) to analyse the penetration depth of the impingement damage on the liner rim. Another study (Holley, et al., 2005) ran for five million cycles and therefore could use gravimetric wear testing by measuring the weight of the acetabular liner before and after testing to find the wear rate. This method was not considered effective as the test could not differentiate the gravimetric weight loss between impingement damage and bearing wear. The use of five million cycles is thought to be excessive for impingement testing and the gravimetric wear testing method would not be effective on low numbers of cycles.

The setup of components was different for each cyclic test. The standard for impingement testing (ASTM F2582, 2020) included a starting position of the acetabular cup parallel to the floor at the top and then the stem at the bottom was rotated through abduction until there was impingement contact. This meant that the components were not in a clinically-relevant position. Another study (Holley, et al., 2005) used spigots with a femoral head at the top and an acetabular cup at the bottom so that the acetabular cup had a steep cup angle to enable impingement to occur with simple orbital motion. The use of spigots meant that clinically-relevant femoral stems were not used in the setup. The acetabular cup was malpositioned at 50° inclination (no anteversion included) to ensure impingement with each cycle. This was a simple setup which did not include a clinically-relevant stem component and the cup was malpositioned. Another study (Pryce, 2019) used THR components and was setup with the femoral stem above the acetabular cup underneath. The orientation of the acetabular cup included 0° anteversion and 45° inclination and the stem was orientated at 10° adduction and 0° anteversion. This meant that the THR components were considered malpositioned.

The forces applied in the hip simulator tests are also different. The standard for impingement testing (ASTM F2582, 2020) includes a constant 600N force applied to the acetabular cup at the top of the simulator however the use of a constant force is not considered clinically-relevant. One study used a peak

800N axial force which resembled the application of forces found during high flexion activities (Pryce, 2019). These peak forces of 800N are smaller than those used during other simulator testing with gait analysis and edge loading which use up to a peak of 3kN (Leslie, et al., 2009; Al-Hajjar, et al., 2013a). Another study (Holley, et al., 2005) used loads up to 2kN which was more clinically-relevant than the previous two studies, however this study had a non-clinical setup and did not risk dislocation in the simulator.

The two non-cyclic tests measured RoM using table-top jigs (Burroughs, et al., 2005; McCarthy, et al., 2017). One study (McCarthy, et al., 2017) mounted THR components in a clinically-relevant setup and could measure the RoM. This was an effective way of measuring RoM in THR components at various component orientations. This study however was only used for validating a simplistic computational model of impingement and did not simulate impingement damage. The other study (Burroughs, et al., 2005) used a table-top setup of a plastic hemi-pelvis and a fiberglass femur which replicated a generic pelvis and femur shape. THR components were inserted into the plastic pelvis and femur and were attached to a goniometer to measure the RoM. The table-top rig could also simulate dislocation. The femur was attached to a hydraulic mechanical testing machine which could apply a uniaxial force to the femur. The pelvis was then rotated through flexion until the THR components dislocated. While this method was a good way of gaining data on dislocation as it could allow dislocation in the simulation, the outputs on impingement damage were limited due to the sole impingement output being RoM.

In summary, the standard for impingement testing (ASTM F2582, 2020) does not position the THR components in a clinically-relevant way, the kinematic motions used for the standard are also not clinically-relevant, simulating a simple wave profile under constant load which is not clinically-relevant conditions of impingement. The standard also does not allow for comparison of different acetabular cup designs. The conditions of the test are exactly the same for a neutral liner and the design of an acetabular liner to reduce dislocation such as a lipped liner with similar results expected for both designs

of the same material. One study (Holley, et al., 2005) did not include clinically-relevant THR components. The kinematic motions applied were also “orbital motion” which is not a clinically-relevant representation of the conditions of impingement. While this study did apply high loads which would be expected *in vivo*, it was run for five million cycles which is thought to be excessive for impingement damage during dislocation-prone activities of daily living. One study (Pryce, 2019) applied activity kinematics to THR components under load and measured the impingement damage. However the component orientations were malpositioned and the kinematic activity was simplified and had a reduced RoM. This study also only simulated one activity. The loads used in this study were also lower than would be expected *in vivo*. The non-cyclic tests (Burroughs, et al., 2005; McCarthy, et al., 2017) were an effective way of measuring RoM and dislocation, however they did not simulate impingement conditions which included damage. There is a need to develop and improve cyclic impingement testing using hip simulators with an increased number of activities and analysis with a clinically-relevant method.

1.7 Project rationale

Dislocation is the occurrence of the femoral head coming out of the acetabular cup through a levering out mechanism caused by impingement (Brown & Callaghan, 2008) and is the most common reason for failure in the first year after surgery (National Joint Registry, 2020). Impingement in total hip replacements is the undesired contact between either the femoral component, acetabular component or the bones around the hip joint, but can also occur between soft tissues around the hip (Malik, et al., 2007). As well as dislocation, impingement can cause other failures in THR's including the acceleration of impingement related wear damage and aseptic loosening (Fisher, 2011; Marchetti, et al., 2011). Impingement damage has been observed in between 25%-77% of explanted liners including liners which were not revised due to impingement or dislocation (Birman, et al., 2005; Shon, et al., 2005; Marchetti, et al., 2011; Lee, et al., 2011; Waddell, et al., 2018). To reduce impingement

related failures in THR, these factors must be investigated and reduced as much as possible.

There are many factors which effect impingement including factors related to the implant design, surgical technique and patient characteristics (Malik, et al., 2007). The reported patient characteristics which could affect impingement are the variation in the shape of a patient's bone, the kinematic movements of a patient during activities of daily living, rotation of the pelvis (pelvic tilt) and soft tissue tension of the muscles around the hip (Nadzadi, et al., 2003; Malik, et al., 2007; Shoji, et al., 2016; Takao, et al., 2016; Pierrepont, et al., 2017). There has been limited research on the effect that patient factors have on impingement likelihood in THR including the variation of a patient's bony geometry, the variation in kinematic activities of daily living and the investigation into patient-specific implantation targets for cup orientation.

To investigate impingement conditions particularly during activities of daily living, a number of different computational models of THR's exist in the literature (Nadzadi, et al., 2003; Pedersen, et al., 2005; Patel, et al., 2010; Ghaffari, et al., 2012; Pryce, et al., 2022). These can be split into FEA models and geometric models. The FEA models mostly did not include any bony geometry due to the computing power and run times associated with FEA models. Therefore to develop multiple bony geometries for analysis, FEA would not be an appropriate option. There were some limitations to the existing geometric models from the literature. Firstly, only one of the geometric model studies used more than one bony geometry, however the conclusions were limited to only RoM and there was no comparison across different bony geometries. Secondly, all of the models have been able to incorporate activities of daily living into their assessment using the models, however the activities used in every study have all come from one source which is a dataset produced to investigate dislocation-prone activities (Nadzadi, et al., 2003). The dataset consists of seven dislocation-prone activities performed by ten non-THA subjects with one subject whose data was at the median representing each activity. Kinematic data was provided as a cardan sequence consisting of three angles of motion (flexion/extension,

adduction/abduction, internal/external rotation) for the femur relative to the fixed pelvis. Only one kinematic profile exists for each activity which was the typical median subject, therefore there was no patient variation in this data and all of the results of the modelling studies which used this kinematic dataset would only be relevant for the one subject, with other subjects potentially changing the results of the studies. Therefore there is a need to assess other kinematic datasets from the literature which include subject variation in the kinematics (Layton, et al., 2021) to assess the conditions around multiple subjects carrying out these activities.

There are a limited number of studies in the literature assessing impingement damage *in vitro* through the use of hip simulators. Some studies have assessed the impingement-free range of motion (Burroughs, et al., 2005; McCarthy, et al., 2017) with no analysis of any wear or damage. A simulator study carrying out an impingement-related wear test was carried out, however it used orbital motion to simulate impingement and a constant load which were not clinically relevant (Holley, et al., 2005). The standard for impingement testing (ASTM F2582, 2020) aims to test acetabular components for impingement component fatigue, deformation and wear which uses a simple waveform profile under constant impingement and a constant load to simulate impingement conditions, which is not clinically relevant. One study (Pryce, 2019) loosely replicated one of the activities in a previous kinematic dataset (Nadzadi, et al., 2003) which provided a clinically-relevant method of simulating impingement damage in a hip simulator, however there is scope to improve this testing method with more activities of daily living, assessing subluxation in multiple directions and reducing the simplification of the activities (Pryce, 2019). Practically, impingement can be difficult to mechanically simulate due to the potential risk of dislocation in the hip simulator which can be abrupt and damaging to the components and simulators.

1.8 Project aim

The aim of this thesis was to analyse factors (such as patient bony anatomy, patient activity and acetabular cup orientation) affecting the likelihood and severity of impingement in order to inform on the conditions of impingement and reduction of impingement related failure rates in total hip replacements.

1.9 Project objectives

The objectives of this thesis project are:

- To produce a number of THR geometric models from CT scans which have a range of bony features for investigation into impingement.
- To investigate the geometric models to analyse the effects that bony features have on the impingement-free range of motion.
- To apply clinically-relevant dislocation-prone activities to the geometric models to investigate the effect of bony features on the likelihood and severity of impingement.
- To apply a kinematic dataset of activities of daily living which include subject-variation to one of the geometric models to investigate the effect of kinematic subject variation and acetabular cup orientation.
- To develop a clinically-relevant impingement test which can simulate an activity carried out by multiple subjects repetitively in a hip simulator to assess the *in vitro* consequences of impingement and assess the variation in damage between subjects.
- To recommend future work in this area which could continue to inform on the reduction of impingement and impingement-related failures.

Chapter Two : Development of nine geometric models of a total hip replacement with individual bony morphology

2.1 Introduction

The geometry of a patient's bone has been demonstrated to effect the RoM to impingement in total hip replacements (Kessler, et al., 2008; Shoji, et al., 2016). The majority of computational modelling studies which have investigated THRs for impingement in the literature have only used one bony geometry with the results limited to that particular bony geometry (Barsoum, et al., 2007; Kessler, et al., 2008; Elkins, et al., 2012; Pryce, et al., 2022). Therefore there is a need to develop computational models with multiple bony geometries to understand the effect this has on impingement including the effect of individual bony features during activities of daily living. This chapter outlines the method development of a series of geometric models which include THR components and subject-specific femur and pelvis anatomies.

To characterise the differences in the bony geometries, bony features which could affect the occurrences of impingement were identified in the literature. One of these, identified as being an impingement site for high flexion activities of daily living, was the anterior inferior iliac spine (AIIS) (Figure 2.1) (Elkins, et al., 2012; Hetsroni, et al., 2013; Shoji, et al., 2016; Davidovitch, et al., 2015; Tabata, et al., 2019). Another bony feature identified in the literature as being an impingement site at the posterior of the hip for high external rotation activities of daily living was the ischium of the pelvis (Figure 2.1) (Kessler, et al., 2008; Patel, et al., 2010; Nakahara, et al., 2011). The latter would be affected by the anteversion angle of the natural acetabulum. Due to the high incidences of posterior dislocation caused by anterior impingement (Nadzadi, et al., 2003; Di Schino, et al., 2009; Smith, et al., 2012), the geometry of the AIIS was prioritised as a method of characterising the differences in the bony geometries (described in more detail in section 2.2.11). To achieve a range of defined bony features for the geometric models, a series of 56 CT scans were measured for their AIIS and the three smallest, closest to the mean and largest

were selected for a total of nine geometric models (described in more detail in section 2.2.3).

The aim of this chapter was to develop a series of nine geometric models of THR's which included clinically-relevant THR components and different bony geometries so that the effect of bony geometry could be understood and investigated for impingement analysis.

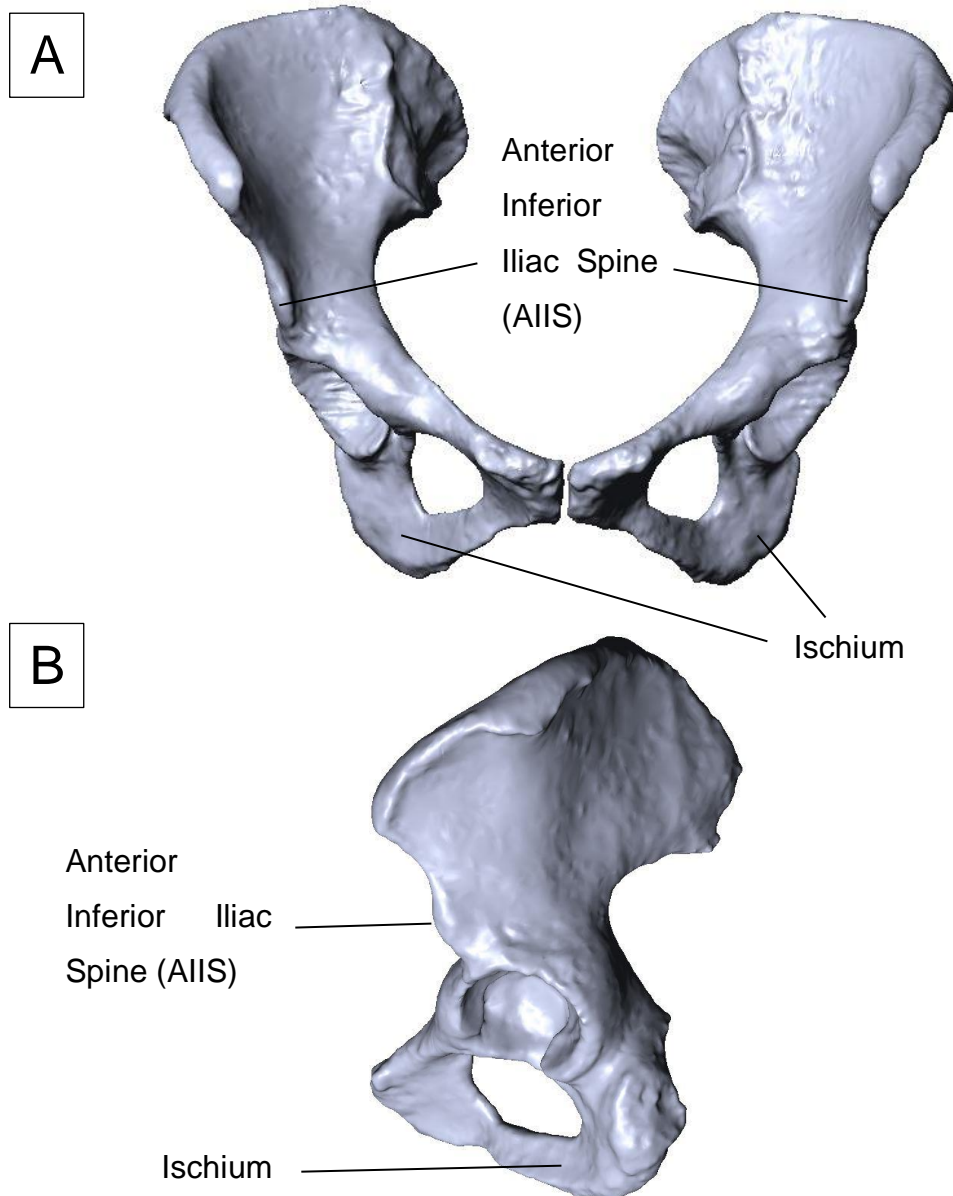


Figure 2.1 The Anterior Inferior Iliac Spine (AIIS) and the ischium of the pelvis labelled on bony geometry ID number 4. A) the coronal view of the pelvis and B) the sagittal view of the pelvis.

2.2 Method development

2.2.1 Requirements of the geometric models

The requirements of the geometric models were:

- To consist of clinically-relevant bony structures from CT scan images.
- To be able to include clinically-relevant THR components.
- To be set up in appropriate coordinate systems for the pelvis and femur.
- To be able to detect impingement.
- To measure the range of motion.
- To process kinematic data including kinematic datasets from the literature of activities of daily living.
- To measure the severity of impingement.
- To represent a range of sizes of AHS bony geometry.

2.2.2 Overview of method development

This chapter describes the development of a series of geometric models of total hip replacements. In summary, nine CT scans were segmented and processed using Synopsis Simpleware ScanIP (Version 2017, Mountainview, California, United States). The pelvis and femur from each CT scan were then imported into Solidworks (Version 2019, Dassault Systèmes, Vélizy-Villacoublay, France). Each pelvis and femur then underwent a virtual THR using components from DePuy Synthes (DePuy Synthes, St. Anthony's Road, Leeds, LS11 8DT, UK) resulting in nine THR geometric models with different bony geometries. The collision detection system in Solidworks, which identifies when solid geometries are in contact in the model, was used to detect when impingement occurred.

2.2.3 CT scan selection and bony geometry characterisation

The CT scans used for the geometric models were taken from an online repository of CT scans of colon cancer patients (Johnson, et al., 2008). There were 56 CT scans (112 hips) in total, comprising of 27 males and 29 females

which were downloaded from a previous ongoing project. The CT images were focussed on the abdomen and colon area (Figure 2.2). Consequently, the CT images consisted of the lower part of the spine, the whole pelvis and the top half of each femur. Some of the 56 CT scans could not be selected as they did not contain a sufficient portion of the femur shaft below the lesser trochanter which was needed to define the coordinate system when creating the geometric models (section 2.2.8). Those CT scans which did not include the entire greater trochanter were excluded. The cohort of 56 CT scans (112 hips) were reduced down to 25 CT scans (50 hips).

A requirement of the method development of the geometric models was to establish a set of models which were as representative as possible of the range of AIIIS sizes, while controlling the total number of geometric cases to be analysed. The models also aimed to include the same THR components and therefore all needed to be the same size, therefore to ensure that the selection wasn't only identifying the largest and smallest pelvises, the CT scans were height-adjusted so that a range of AIIIS sizes would be achieved following a scaling process.

Preliminary measurements were initially taken to identify bony geometries so that geometric models could be generated which included a range of AIIIS sizes, therefore once the geometric models were created, more accurate measurements of the bony features were taken (section 2.2.11). To select the bony geometries to achieve a range of AIIIS measures, the anterior protrusion of the AIIIS was roughly measured in the CT scan of each of the 50 hips which was defined as the distance between the coronal plane at the CoR and the coronal plane at the most anterior point on the AIIIS. The values were then height-adjusted to the size of the pelvises by taking measurements of the height of the pelvis and dividing by the value for the anterior peak of the AIIIS, so that the size of the pelvis did not affect the selection. The measurements of the AIIIS anterior distances were then compared across the 50 hips.

To achieve a range of AIIIS measures, the three smallest, three closest to the mean and the three largest AIIIS anterior protrusion measurements were selected and the corresponding bony geometry chosen. The side of the hip

chosen to develop into a geometric model was chosen as the side which was either the smallest, closest to the mean or largest depending on the group which was selected. No bony geometry was selected twice, if the same pelvis (left and right) was required to be selected, then the next hip was selected.

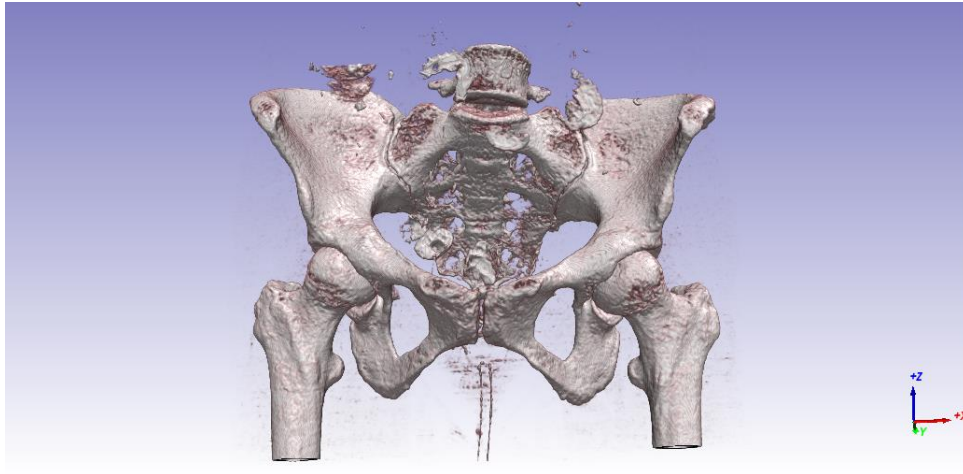


Figure 2.2 A coronal view of one of the CT scan images used for this study in the Simpleware ScanIP software including just the bone (this was included in the segmentation process which highlighted a pre-set range of the greyscale denoting cortical bone).

2.2.4 Segmentation of the CT scans

For segmentation of the CT scans, the whole pelvis was segmented into surface geometry, no matter the hip side to be used. The whole pelvis was needed because of the way that the coordinate system was set up later in the development of the models (section 2.2.8). Only the selected femur to be investigated was required to be segmented and processed.

The Synopsis Simpleware ScanIP (Version 2017, Mountainview, California, United States) software was used to process the CT scans into surface geometries. The CT scan images were imported as DICOM files into the software. The voxel sizes of the CT scans were 0.7mm x 0.7mm x 0.7mm. Once in the software, the DICOM files were displayed as a series of 2D

greyscale images stacked on top of each other with the greyscale representing the change in the material density. To represent the pelvis geometry, a mask was defined and the entire pelvic bone was highlighted in every 2D image using a greyscale threshold via the “paint with threshold” tool which specifically identified the cortical bone density. This highlighted all the pixels which were within a certain range of greyscale colour associated with cortical bone density. This produced a hollow mask of the bony geometry (Figure 2.3). Once the “paint with threshold” tool had been used and identified all of the cortical bone, there were gaps inside where the less dense cancellous bone hadn’t been highlighted. The areas inside the bone were then manually highlighted in every 2D image so that a full 3D geometry with no cavities could be generated.

Once the pelvic bone had been fully highlighted in the mask (Figure 2.3), the mask was then smoothed via a recursive Gaussian smoothing with a 1.0 x 1.0 x 1.0 pixel standard deviation which was used over the whole of the pelvic surface geometry mask. This reduced the CT scan image noise and reduced potential segmentation errors of the cortical bone. The surface geometry was then exported as an STL mesh file (Figure 2.4). The whole process was then repeated for the relevant femur and the exact same methodology was carried out and exported as a separate STL mesh file.

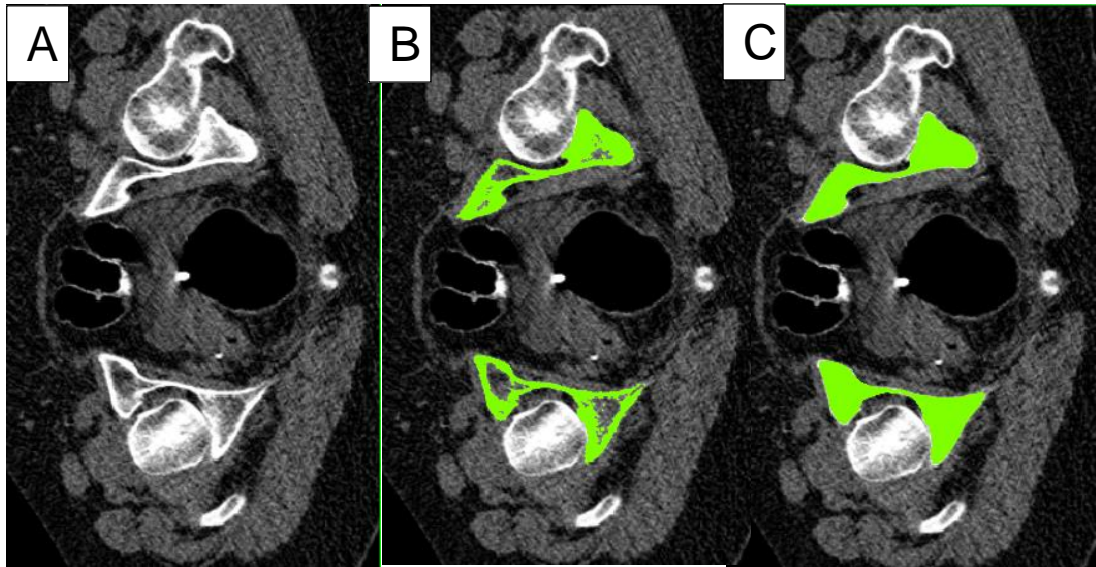


Figure 2.3 A transverse plane view of three 2D slices of the same CT scan image of one of the CT scans used in this study including all of the tissue shown as a greyscale in the Simpleware ScanIP software. A) The greyscale tissue with no highlighting. B) The same CT scan image after it has been highlighted by the greyscale range which highlighted cortical bone and demonstrates the inner cancellous bone which was not highlighted during this step. C) The same CT scan image following the manual highlighting of the cancellous bone in the pelvis.

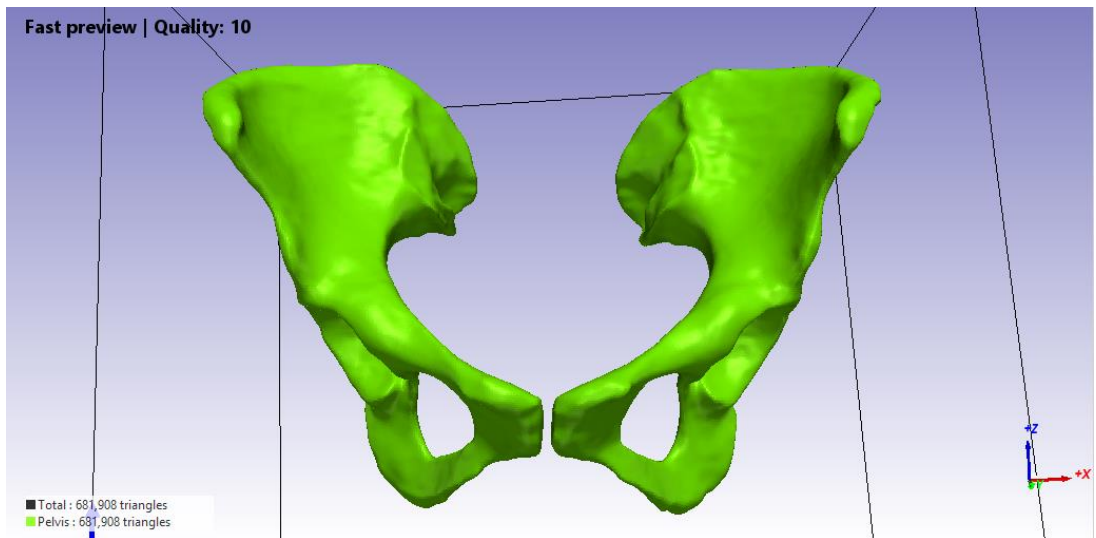


Figure 2.4 A coronal view of a full pelvis mask in the Simpleware ScanIP software following all of the steps of segmentation and smoothing ready for exporting as an STL file for one of the CT scans used in this study.

2.2.5 Conversion of surface meshes to 3D solid geometry

An STL mesh file (Figure 2.4) is a raw unstructured triangulated surface mesh which must be converted to a solid geometry for use in Solidworks (Version 2019, Dassault Systèmes, Vélizy-Villacoublay, France). Solidworks includes a tool called “Scanto3D” which creates faces and edges which fit to the mesh. There was no simplification or smoothing of the mesh once the file was loaded into Solidworks. The solid parts were automatically created from the mesh using the “scanto3D” tool. During this process, the number of faces which fit to the surface mesh could be altered on a sliding scale of low, medium or high numbers of faces. This would have had an effect on the run time of the geometric models and therefore it was desired to have a lower number of surfaces.

A sensitivity analysis was carried out to determine the effect that the change in the number of face shapes had on the topology and geometry of the models (Table 2.1). Two geometric models were processed from the same CT scan (bony geometry ID number 1) with a high number of face shapes (23548) and a medium number of face shapes (2507). The numbers of face shapes differed depending on the geometry of the bone. The two geometries were then compared by taking measurements to key bony anatomy points from the origin of the part (which was the same for both models) which included the two ASIS points, the two anterior peaks of the AIIIS and the midpoint at the pubic symphysis (Table 2.1 & Figure 2.5). The greatest difference between the two models was less than 0.42mm and therefore was deemed suitable to apply a medium number of face shapes to the geometries to reduce the computational power needed to carry out experiments with the nine geometric models.

Table 2.1 A comparison of the distance measures to bony features used to investigate the effect of the number of faces to create a 3D geometric model from a mesh between a medium and high detailed geometric model using bony geometry ID number 1. The distance measures to bony features were from the origin of the acetabulum to the bony features indicated for the medium and high detailed pelvises which were in an identical position.

		Distance to bony features (mm)		
		Medium detail	High detail	Difference
Left ASIS	Total distance	453.1334	453.0851	0.0483
	X direction	110.0833	110.0851	0.0019
	Y direction	231.0493	231.0622	0.0130
	Z direction	373.9355	373.8670	0.0685
Right ASIS	Total distance	463.3500	463.7650	0.4150
	X direction	128.5915	128.8917	0.3002
	Y direction	222.6968	222.7250	0.0282
	Z direction	385.4395	385.8219	0.3824
Left AIIS	Total distance	473.8870	473.9346	0.0476
	X direction	94.5661	94.5496	0.0164
	Y direction	208.6221	208.6345	0.0124
	Z direction	414.8530	414.9048	0.0519
Right AIIS	Total distance	484.0036	484.2148	0.2112
	X direction	114.3666	114.1468	0.2198
	Y direction	202.8666	202.9593	0.0927
	Z direction	424.2935	424.5492	0.2557
Pubic point	Total distance	535.9254	535.8498	0.0756
	X direction	10.5729	10.7316	0.1587
	Y direction	232.8921	232.8769	0.0152
	Z direction	482.5615	482.4813	0.0802

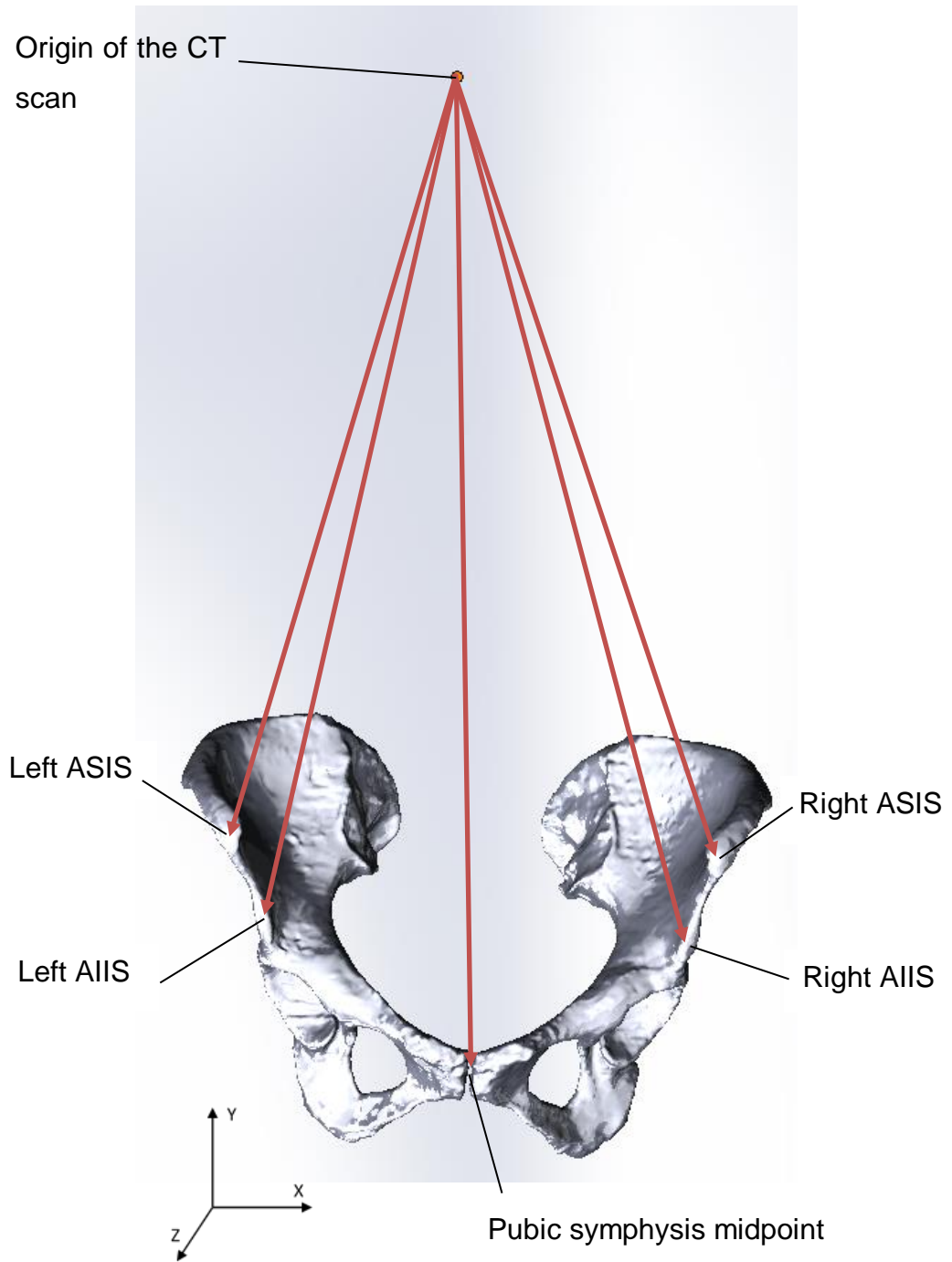


Figure 2.5 A coronal plane view of one of the geometric models in Solidworks which includes the origin from the CT scan and the five distance measures to bony features used to investigate the effect of the number of faces to create a 3D geometric model from a mesh between a medium and high detailed geometric model. Bony geometry ID number 1 was used.

2.2.6 Removal of osteophytes

Following the creation of the geometric models of the femur and pelvis, the latter were checked for osteophytes which would be removed during THR surgery. All of the pelvises were checked for protrusions of bone which extended from typical geometry by over 4mm. The osteophytes which protruded further than 4mm and needed to be removed were cut at the base of the osteophyte, perpendicular to the direction of protrusion (Figures 2.6 & 2.7). This would be standard procedure during a THR surgery. One osteophyte which protruded by more than 4mm was discovered on bony geometry ID number 5 and was therefore removed (Figures 2.6 & 2.7).

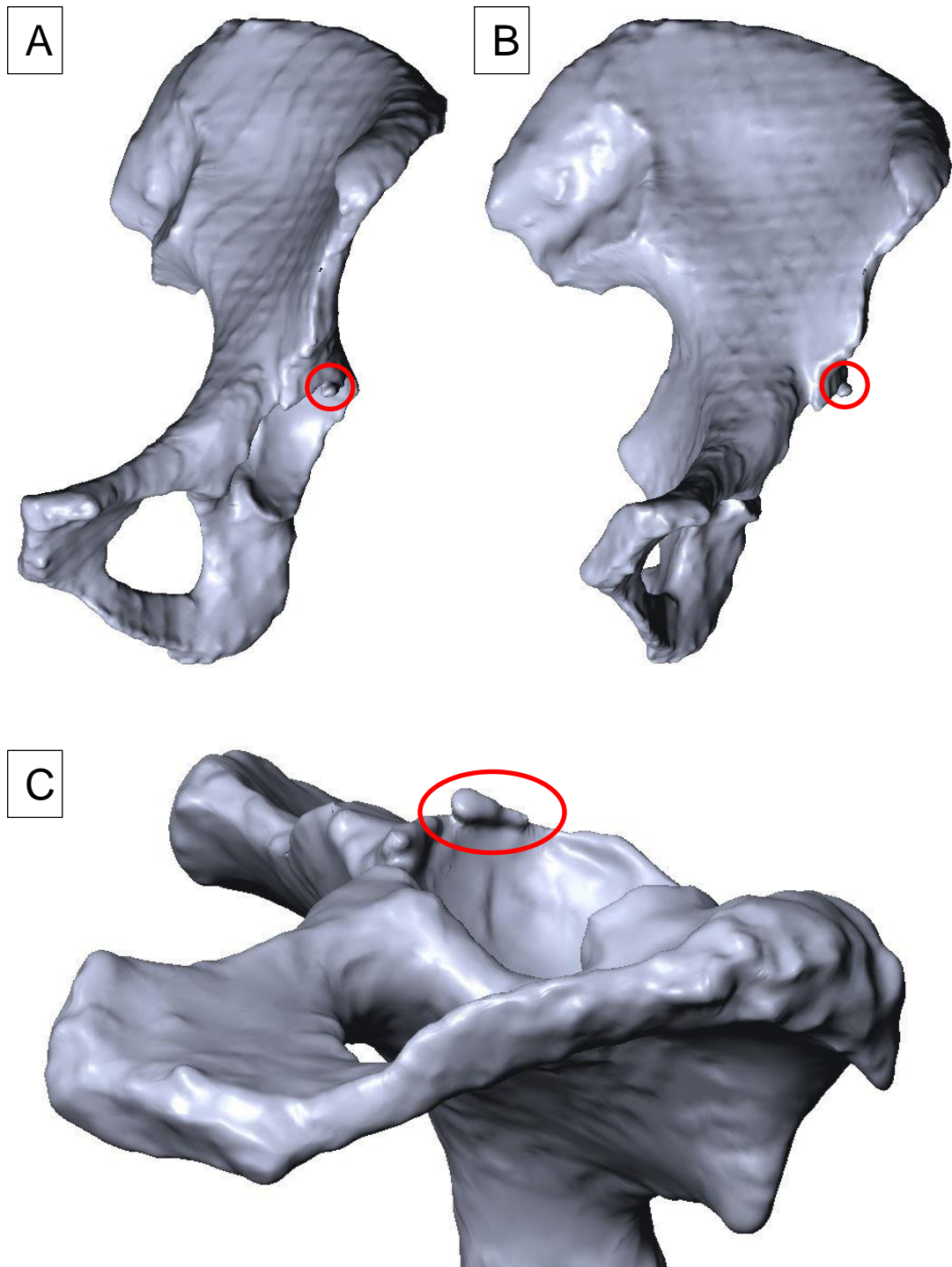


Figure 2.6 An osteophyte found on bony geometry ID number 5 for A) a coronal view B) A 45° angle to the coronal view and C) A view of the acetabulum from an inferior-superior view in line with the transverse acetabular ligament.

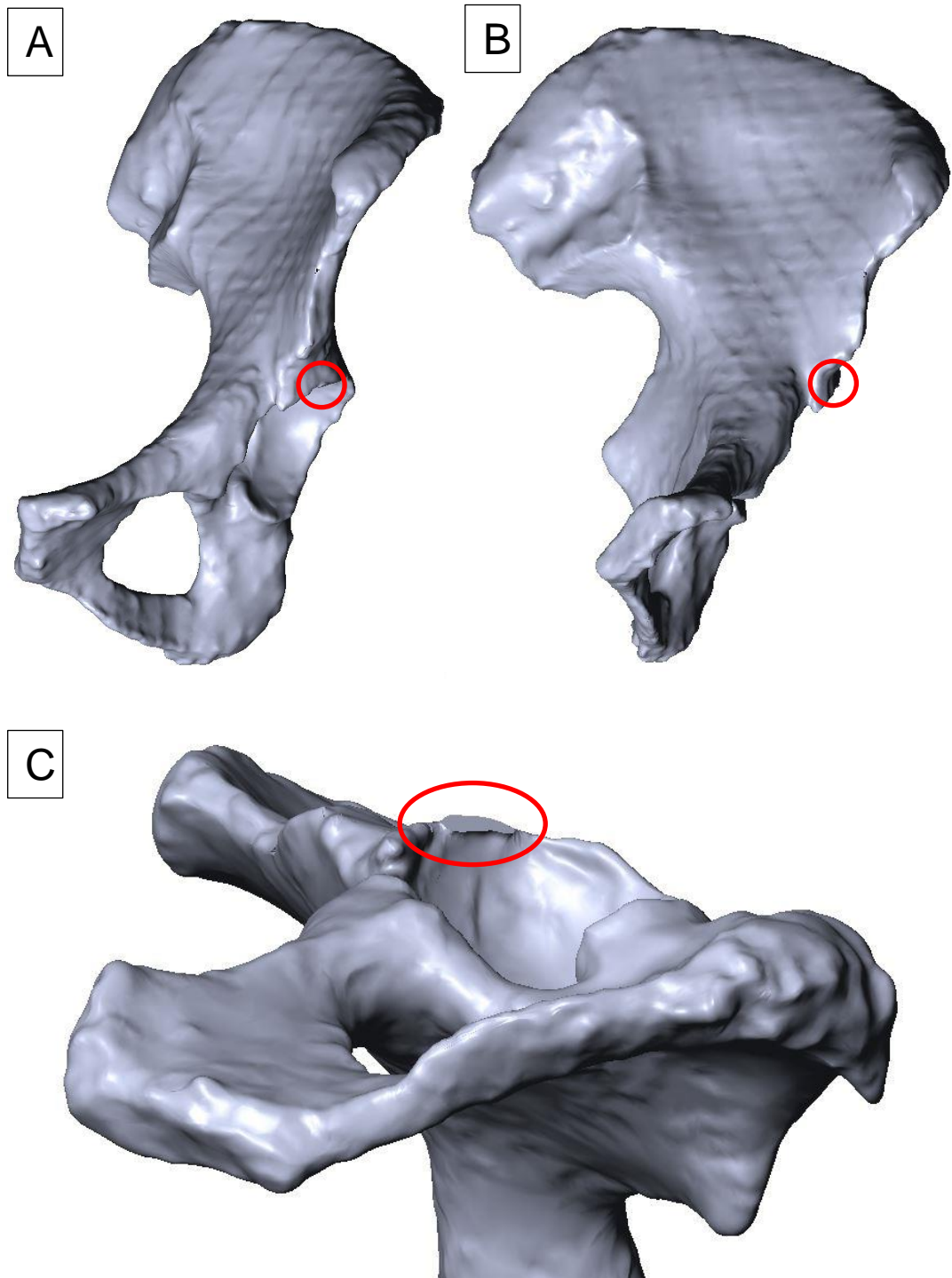


Figure 2.7 Bony geometry ID number 5 with the osteophyte removed from A) a coronal view B) A 45° angle to the coronal view and C) A view of the acetabulum from an inferior-superior view in line with the transverse acetabular ligament.

2.2.7 Defining the Centre of Rotation

To define the CoR of the femoral head, a sphere was fitted to the head in Solidworks (Figure 2.8). Due to it not being completely spherical, the head was measured for its diameter three times using the Solidworks “measure” tool. These three measurements were taken from the most superior to the most inferior point, the most lateral to the most medial point and the most anterior to the most posterior point on the femoral head. A sphere was then created using the average diameter and manually positioned to the centre of the head. The centre of the sphere was then defined as the CoR of the femoral head.

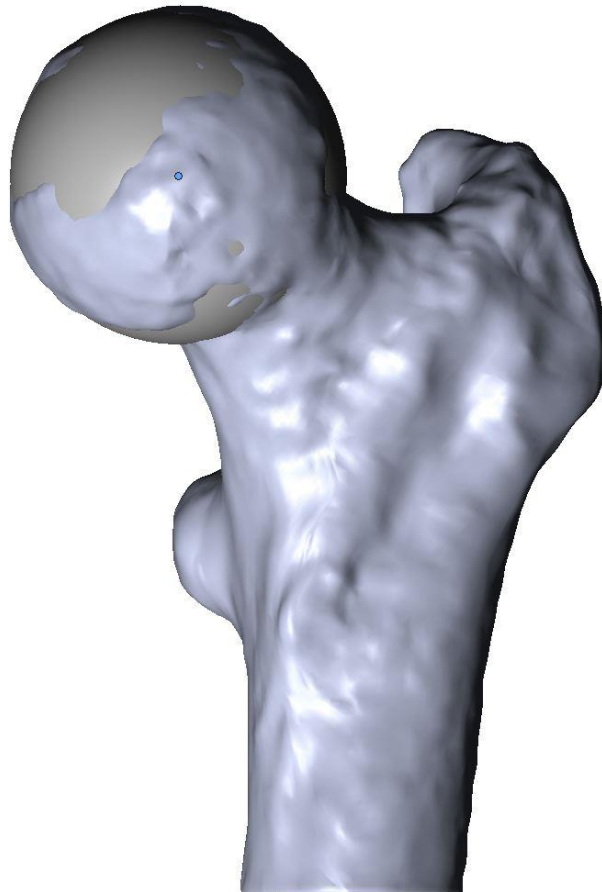


Figure 2.8 A coronal view of one of the left femurs in Solidworks with a sphere added in order to define the centre of rotation of the femur. The centre of rotation is at the centre of the sphere in blue. The femoral head was measured and an average taken to draw the size of the sphere.

To define the CoR of the acetabulum, the inside of the acetabulum was measured three times using the Solidworks “measure” tool and an average diameter was taken. The three measurements were taken from just inside the acetabular rim with the aim of measuring the diameter of the acetabulum. The three measurements were taken around the acetabulum at three equispaced intervals, not including the notch where the transverse acetabular ligament (TAL) would be. A sphere with the diameter of the mean of the three measurements was then attached to the inside of the acetabulum with the centre of the sphere defining the CoR of the acetabulum and therefore the pelvis (Figure 2.9).



Figure 2.9 A coronal view of one of the left pelvises in Solidworks with a sphere added in order to define the centre of rotation of the acetabulum. The centre of rotation is at the centre of the sphere in blue. The inside of the acetabulum was measured and an average taken to draw the size of the sphere.

2.2.8 Defining the coordinate systems

The coordinate system of the pelvis was defined using the Anterior Pelvic Plane (APP) coincident with the CoR of the acetabulum (Tannast, et al., 2005; Kubiak-Langer, et al., 2007). The APP was defined by bony landmarks on the pelvis including the two anterior superior iliac spine (RASIS and LASIS) points and a midpoint (MPS) between the two pubic symphysis points (LPS, RPS) (Figure 2.10) (Tannast, et al., 2005; Kubiak-Langer, et al., 2007). To determine the correct points for the ASIS and pubic symphysis, an iterative process was carried out to mark the most anterior points of each of the four bony landmarks. For this iterative process, a point was roughly added to each of the four bony landmarks and a midpoint created between the pubic symphysis points. A plane was then created using the RASIS, LASIS and MPS. The plane was then visually inspected for protrusion of bone through the RASIS and LASIS points. A new improved guess point was then added to the highest part of the protrusion through the plane and a new plane was added. This process was carried out iteratively until there was no protrusion of bone through the plane and hence the RASIS and LASIS were the most anterior points selected. This process was then repeated for the two pubic symphysis points. The final coordinate system was then defined using the final RASIS, LASIS and MPS points to define the APP.

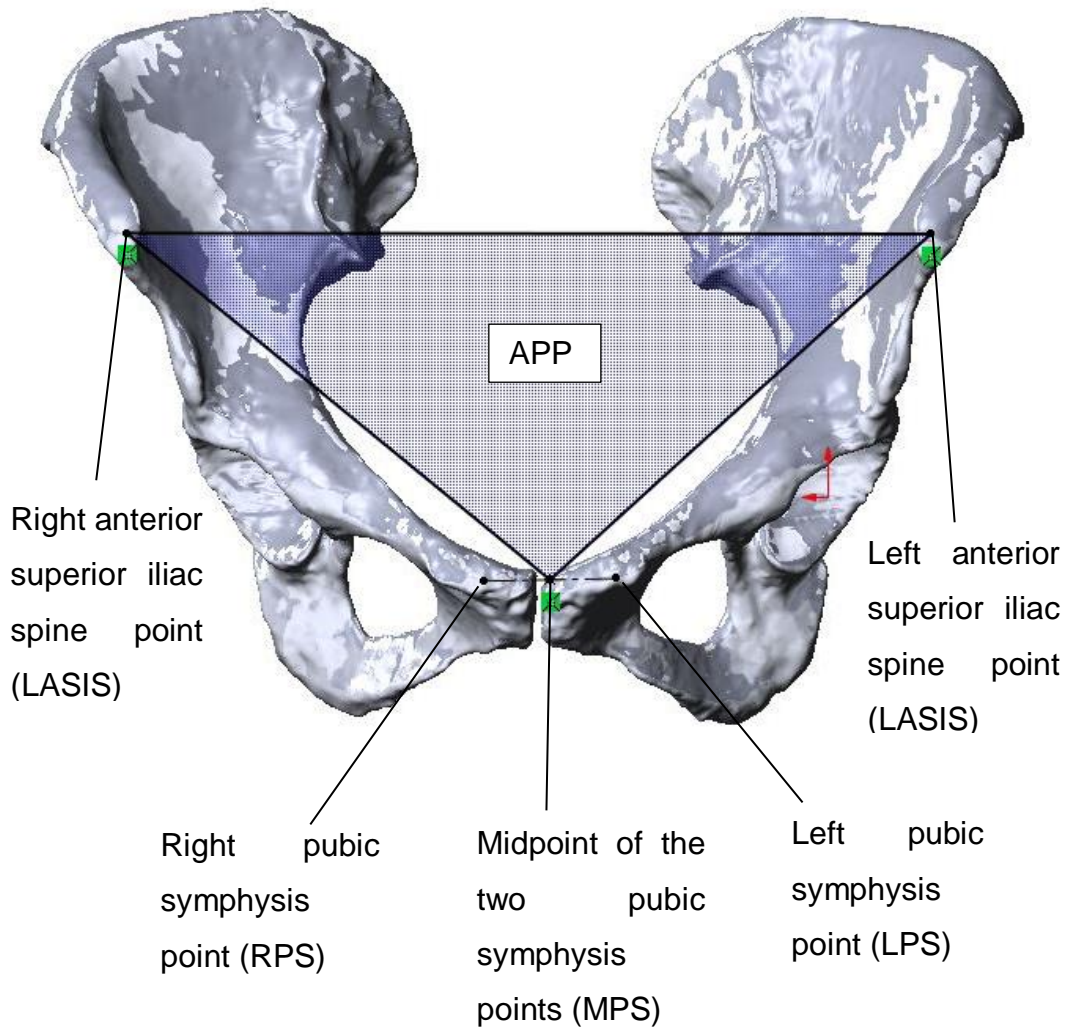


Figure 2.10 A coronal view of one of the pelvises in Solidworks including the bony landmarks used to define the anterior pelvic plane (APP). The APP was defined using the left anterior superior iliac spine point (LASIS), the right anterior superior iliac spine point (RASIS) and the midpoint of the pubic symphysis (MPS).

According to methods in the literature (Wu, et al., 2002; Kubiak-Langer, et al., 2007), the coordinate system of the femur should use the CoR of the femoral head and the posterior condyles of the knee. Due to the CT scans used in this study only capturing the top part of the femur, this was not possible. Therefore to define the coordinate system of the femur, the femurs were aligned to an existing femur where the entire femur was visible (Pryce, et al., 2022) which had used the previous methods from the literature to define the coordinate system (Wu, et al., 2002; Kubiak-Langer, et al., 2007). To achieve this, a plane

was used which was defined by the CoR of the femoral head and a line which was positioned through the centre of the shaft of the femur (Figure 2.11). To define the line, two cross sections were made along the shaft whose midpoints were used to define the line through the centre of shaft. The same method was used to define a plane in the existing femur with the defined coordinate system. The planes of the two femurs were then aligned and the CoR of the femoral heads were aligned. The lines through the centre of the shaft were made parallel so that the coordinate system could be used for the new femur. The femur was then saved as a new part which used the existing coordinate system which had been defined in the previously used femur based on the literature recommendations. This method kept the femoral coordinate systems consistent throughout the nine geometric models.

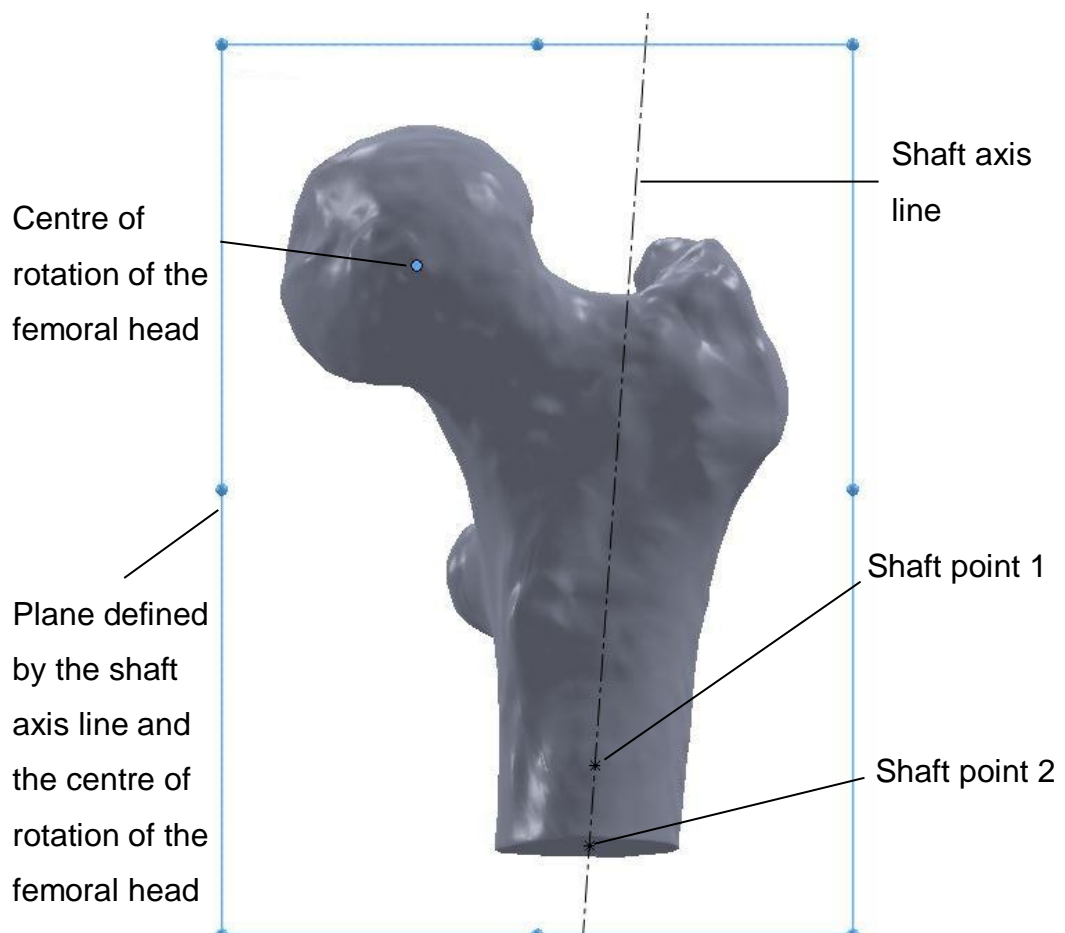


Figure 2.11 The plane and bony features used to align the femurs to an existing femur with a correct coordinate system. To align the femurs, the shaft axis and the centre of rotation of the femoral head were used.

2.2.9 Scaling of the geometric models

All nine of the CT scans were processed into solid geometries with the coordinate systems and CoR defined. The models were scaled so that the same THR components could be attached to each bony geometry model and therefore characteristics related to the implant design, such as size, did not affect the results. The size of each acetabulum was measured previously to determine the location of the CoR of the acetabulum (section 2.2.7). The acetabula were then scaled (Table 2.2) so that they were all 52mm in diameter with the intention of implanting components which appropriately fit later on in the process (described in detail in section 2.2.10). The “scale” tool in Solidworks was used to scale the pelvises and femurs by a factor determined by either the increase or decrease in the size of the pelvis and femur to allow the acetabulum to be 52mm in diameter. The pelvis and femur were scaled around the CoR which had no effect on the outcome.

Table 2.2 The acetabulum diameter before and after the scaling process including the ratio which was used to scale the models.

Bony geometry ID number	Acetabulum size before scaling (mm)	Acetabulum scaling ratio	Acetabulum size after scaling (mm)
1	45.65	1.139	52.00
2	43.17	1.205	52.00
3	46.61	1.116	52.00
4	46.29	1.123	52.00
5	45.64	1.139	52.00
6	51.88	1.002	52.00
7	53.99	0.963	52.00
8	45.16	1.151	52.00
9	47.03	1.106	52.00

2.2.10 Virtual total hip replacement

Once the solid bony geometries had a defined coordinate system, a CoR and had been scaled, a virtual THR was carried out. The components which were used for the virtual THR were all commercially available products manufactured by DePuy Synthes which were provided as component part files. These consisted of a simplified Pinnacle® 100 series shell (54mm), a simplified DePuy Marathon® neutral liner (36mm/54mm), an Articul/Eze M-spec™ metal head (36mm) and a simplified Corail® standard stem (size 12) (Table 2.3).

Table 2.3 Components used in the virtual total hip replacements of the nine geometric models. All components were commercially available products manufactured by DePuy Synthes which were provided as drawings.

Stem	Head	Shell	Liner
Corail® standard stem (Size 12)	Articul/Eze M- spec™ metal head (36mm)	Simplified Pinnacle® 100 series shell (54mm)	Simplified Marathon® neutral liner (36mmID/54mmOD)

2.2.10.1 Femoral component assembly

In order to simulate the femoral neck cut, a virtual osteotomy was performed on the femur as per the recommendations from DePuy Synthes product literature (DePuy Synthes, 2019) (Figure 2.12). To achieve this, a 45° line was added from the shaft axis up to the CoR of the femur. A plane was then defined which was perpendicular to this line and 30mm proximal to the femur where a circle of 52mm diameter was drawn (ensuring that all femoral head sizes would be inside this). This circle was then cut extruded distally into the femur so that the femoral head was no longer there and most of the femoral neck

removed in line with a standard osteotomy surgery. The osteotomy was then checked by an orthopaedic surgeon.

Once the osteotomy was carried out, the femoral head and stem were fixed into position inside the cut femur. This included constraining the stem and head to the femur to prevent relative movement between the parts. The stem and head were constrained together ensuring that the inside of the head was concentric to the stem taper. The correct offset of the head and the stem was then calculated based on DePuy Synthes literature (DePuy Synthes, 2019) and applied to the head and stem. The femoral head with stem attached was then positioned so that the centre of the femoral head component was exactly where the CoR of the natural femoral head used to be before the osteotomy. The bottom of the stem was then attached to the shaft axis so that the stem aligned in the centre of the shaft of the femur bone, therefore the relative angle of the stem to the global coordinate system was positioned based on the shaft angle of the femur. The stem was then anteverted 15° to keep consistency throughout the nine geometric models to complete the femoral setup (Dorr, et al., 2009).

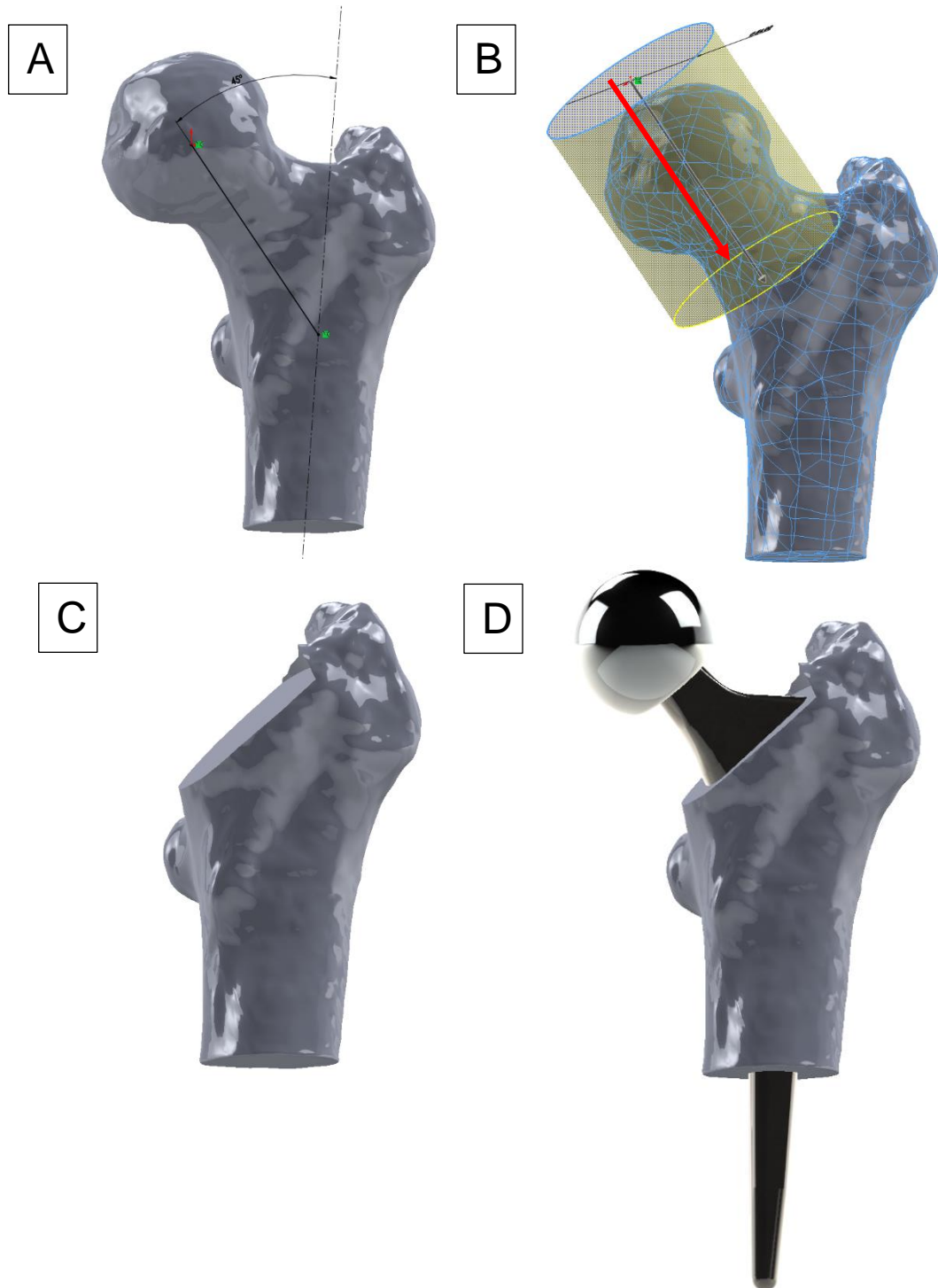


Figure 2.12 Coronal views in Solidworks of a left femur from one of the geometric models used in this study. The process used to carry out the osteotomy on the femur and the insertion of the femoral THR components is demonstrated. A) A 45° angle to the shaft axis was used for the angle of the osteotomy. B) A circle was drawn which covered the size of the femoral head and was extruded into the femoral head to remove it. C) The final femur bony geometry following the osteotomy. D) The CoR of the femoral head was then restored and the stem inserted along the shaft axis at an anteversion angle of 15°.

2.2.10.2 Acetabular component assembly

For the acetabular component insertions, the shell and liner were attached together concentrically so that the liner was positioned inside the shell and the anti-rotation locks were positioned together. To attach the acetabular components to the pelvis, a line was drawn from the CoR of the acetabulum and was inclined and anteverted to a radiographic inclination angle of 45° and a radiographic anteversion angle of 20°. If the shell and liner required medialisation, it would be along this reaming line. These angles were used for all of the nine geometric models as recommended by DePuy Synthes literature (DePuy Synthes, 2019) which occurs during the surgical reaming process. The acetabular components were then attached in line with this positional line so that the CoR of the liner was at the same place as the CoR of the acetabulum. An orthopaedic surgeon then gave guidance on the positioning and medialisation of the acetabular components on each of the nine geometric models. It was suggested that the inclination be fixed at 45° and the anteversion and medialisation adjusted on a case by case basis. These were adjusted accordingly to ensure sufficient bone coverage at the anterior side of the acetabulum, that the anteversion was in line with the transverse acetabular ligament (TAL) and that the liner was not protruding out of the socket. The nine geometric models therefore had different orientations of the acetabular components (Table 2.4).

Table 2.4 Acetabular component orientations for each of the nine geometric models including the radiographic inclination, radiographic anteversion and the amount of medialisation. The medialisation reaming line was 45° radiographic inclination and 20° radiographic anteversion.

Bony geometry ID number	Radiographic inclination	Radiographic anteversion	Medialisation
1	45°	25°	2mm along reaming line
2	45°	35°	1.5mm along reaming line
3	45°	30°	2mm along reaming line
4	45°	25°	None
5	45°	32.5°	2mm along reaming line
6	45°	20°	None
7	45°	25°	None
8	45°	25°	2mm along reaming line
9	45°	25°	None

2.2.10.3 Complete geometric model

The pelvis and femur complete with acetabular and femoral components respectively were then grouped together in an assembly where the pelvis was fixed in the global coordinate system and the CoR of the femoral head was aligned to the CoR of the liner. The femoral coordinate system was then rotated around the global coordinate system. The two coordinate systems were aligned which created the starting position for all of the testing (Figure 2.13).

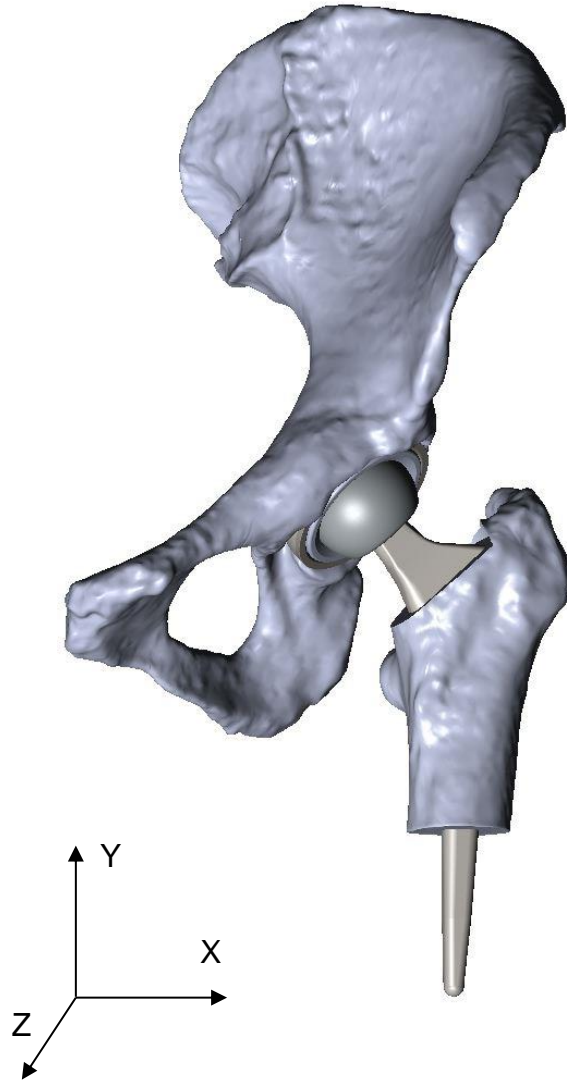


Figure 2.13 A coronal view in Solidworks of the final setup of the geometric model with bony geometry ID number 1 for a left hip including the relevant global coordinate system.

2.2.11 Bony geometry measurements

An anterior peak point of the AIIS was defined using a similar process that was used to identify the bony landmarks to define the APP plane (section 2.2.8). An initial rough estimate point was added to the AIIS and a plane was created which went through this initial rough estimate point and was parallel to the APP. The area of the AIIS was then inspected to identify any bony protrusion through the plane, where an improved guess point was added and

the plane was redefined through this new point. This was iteratively carried out until the most anterior point was selected where there was no bone protrusion through the defined plane. The final AIIIS point was then defined as this most anterior point on the AIIIS. This defined anterior peak point was used to measure the peak of the AIIIS in relation to the CoR of the THR for the anterior, superior and lateral directions in each of the geometric models (Table 2.5) in the global coordinate system. These were defined as the distance between the CoR of the THR and the anterior peak of the AIIIS in the anterior/posterior axis, inferior/superior axis and the medial/lateral axis for the anterior, superior and lateral measurements respectively (Figures 2.14-2.16). Previously the three smallest, closest to the mean and largest anterior protrusion of the AIIIS were selected to obtain a range of bony geometry measures, however following the scaling process, these rough measurements changed. The AIIIS measures were accurately taken in the nine geometric models after the scaling process and it was found that while the values were no longer three small values, three from the mean and three large values, a range of AIIIS measures still existed following the scaling and therefore no other CT scans were chosen.

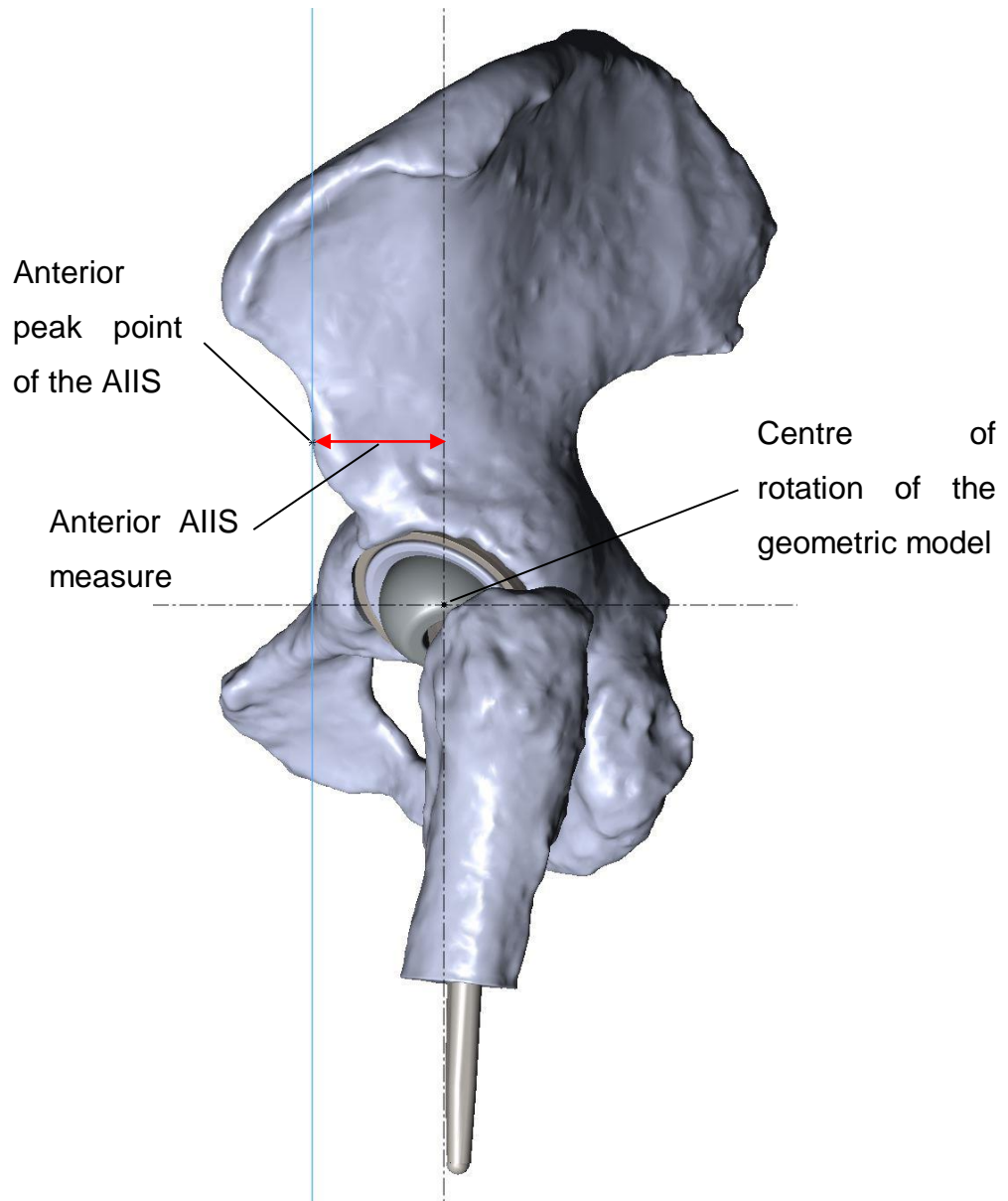


Figure 2.14 The anterior AIIIS measure demonstrated in a sagittal view of bony geometry ID number 1, of a left hip. The blue line is the plane parallel with the coronal plane and coincident with the anterior peak point of the AIIIS. The dotted black line is the inferior/superior axis which is coincident with the centre of rotation of the THR. The red arrowed line denotes the anterior measure of the AIIIS.

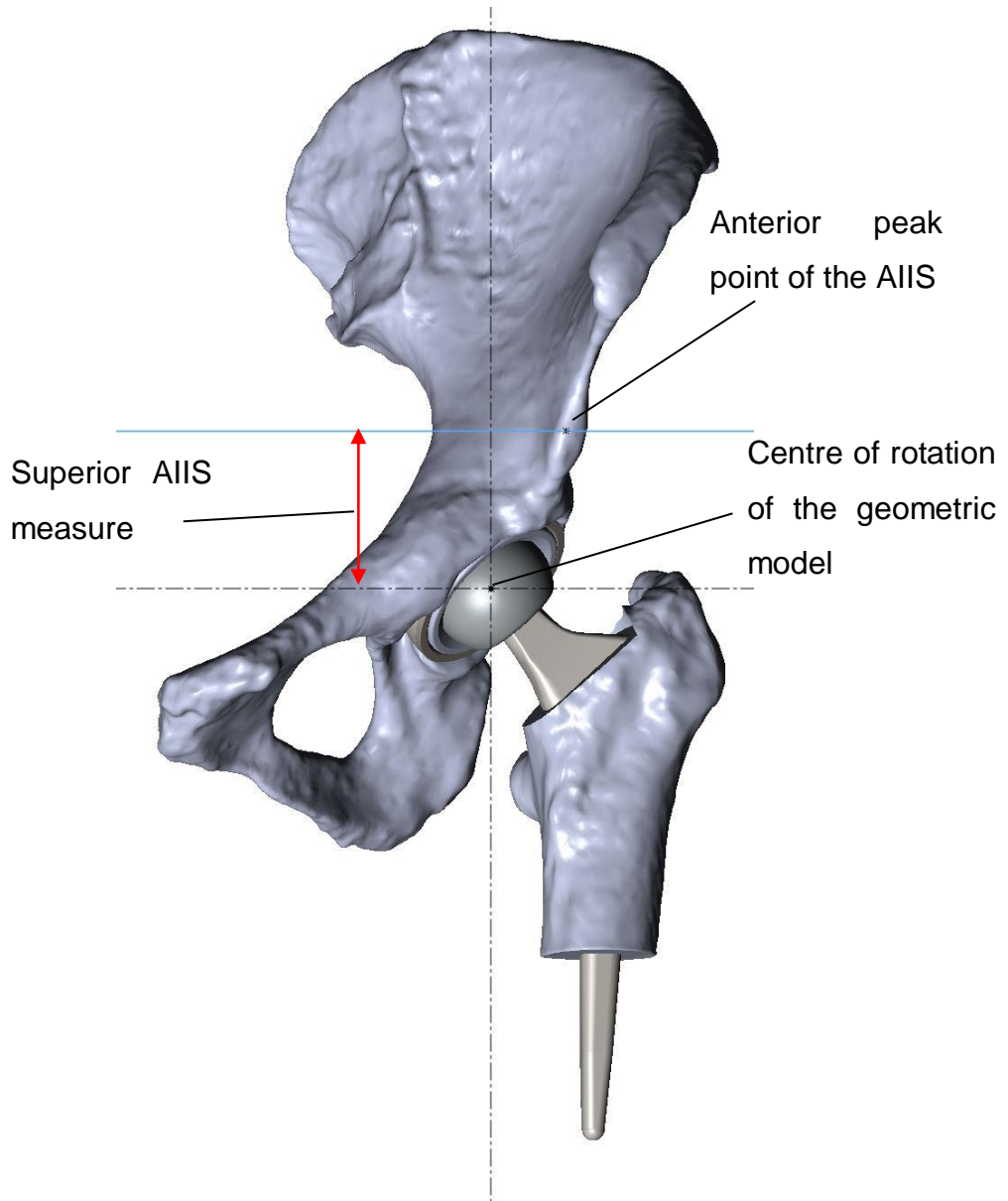


Figure 2.15 The superior AIIS measure demonstrated in a coronal view of bony geometry ID number 1, of a left hip. The blue line is the plane parallel with the transverse plane and coincident with the anterior peak point of the AIIS. The dotted black line is the medial/lateral axis which is coincident with the centre of rotation of the THR. The red arrowed line denotes the superior measure of the AIIS.

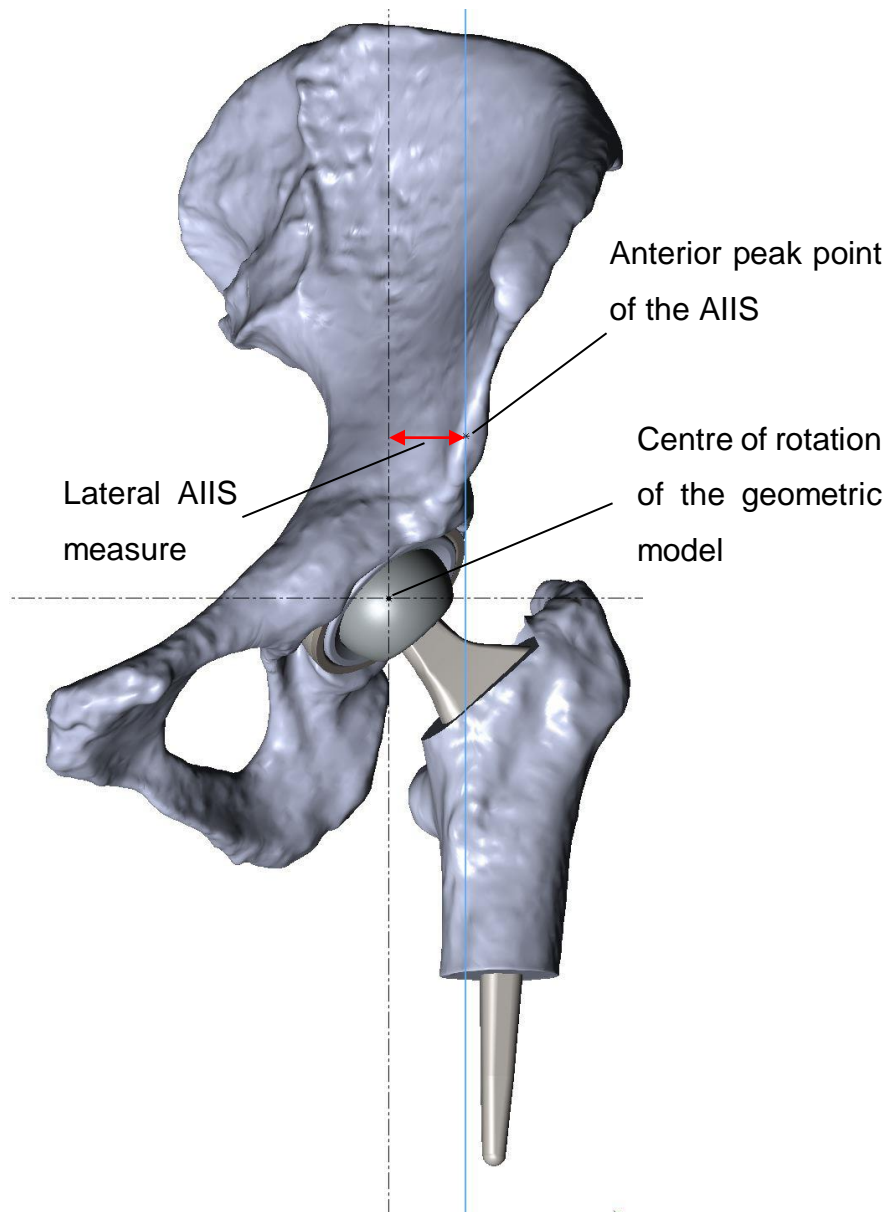


Figure 2.16 The lateral AIIIS measure demonstrated in a coronal view of bony geometry ID number 1, of a left hip. The blue line is the plane parallel with the sagittal plane and coincident with the anterior peak point of the AIIIS. The dotted black line is the inferior/superior axis which is coincident with the centre of rotation of the THR. The red arrowed line denotes the lateral measure of the AIIIS.

The anteversion angles of the natural acetabulum (Figure 2.17) were also measured in each of the nine geometric models (Table 2.5) as this would be investigated in later chapters of this thesis as potentially affecting activities prone to posterior impingement. This work was carried out previously in an ongoing project where a point cloud was defined along the edge of the rim (excluding the TAL notch). An iterative approach was then used to identify the points which were at the highest point on the rim of the acetabulum. These points were used to define a plane using a least squares fitting method across the face of the acetabulum. The anteversion angle of the natural acetabulum was defined as the angle change around the inferior-superior axis of the acetabular rim plane until the plane was perpendicular to the view. This defined the radiographic anteversion angle as previously described in the literature (Murray, 1993). These measured values were checked using a Matlab (Mathworks, Massachusetts, USA) code which used 20 3D coordinate points around the acetabular rim and a least squares fitting method for 3D coordinates to plot a plane with known coordinates that could be used in Solidworks.

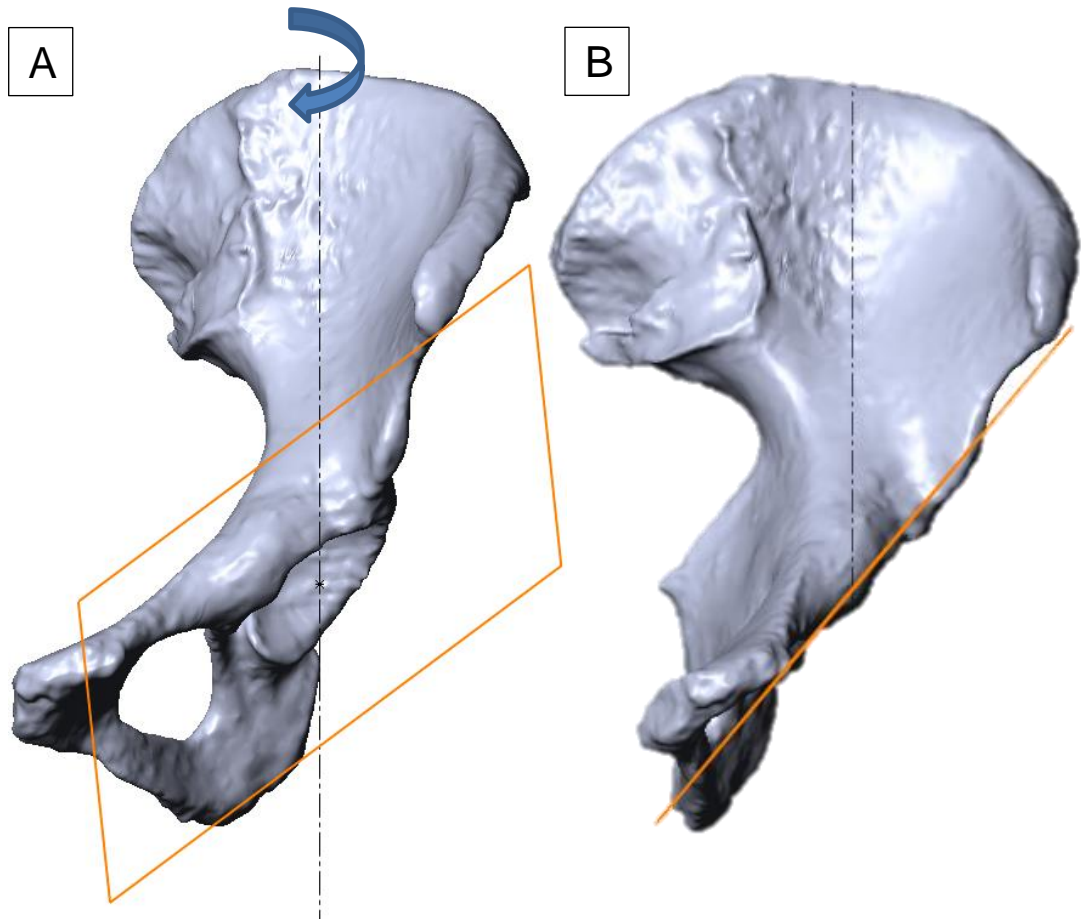


Figure 2.17 The anteverision angle measurement of the natural acetabulum. A) A coronal view of a left pelvis in Solidworks of one of the geometric models used in this study demonstrating a plane over the face of the acetabulum. B) The pelvis is rotated around the inferior-superior axis until the face of the plane is perpendicular to the view. The rotation around the inferior-superior axis is the anteverision angle of the natural acetabulum. The anteverision angle of the natural acetabulum was measured in each of the nine geometric models.

The AIIIS measures and the anteverision angles of the natural acetabulum for each geometric model are described in Table 2.5.

Table 2.5 The AIIS measures in the nine geometric models following the scaling process including the anterior, superior and lateral AIIS measures as well as the anteversion angles of the natural acetabulum.

Bony geometry ID number	Anteversion angle of the natural acetabulum (°)	Anterior measure of the peak of the AIIS (mm)	Superior measure of the peak of the AIIS (mm)	Lateral measure of the peak of the AIIS (mm)
1	21.0	33.6	33.5	8.9
2	30.2	35.9	44.5	6.0
3	20.2	36.3	42.7	8.9
4	18.8	36.5	45.3	21.4
5	23.6	37.1	42.9	5.6
6	6.3	40.4	38.3	17.0
7	13.3	41.8	39.8	9.6
8	13.0	42.8	35.7	23.5
9	17.2	44.2	40.1	11.2

2.2.12 Cardan sequences to input known rotations

To apply motions to the geometric model, the pelvis was fixed and the femur could rotate around it. To move the femur in the geometric model, two vectors were added which were attached to the femur so that they could be manipulated into rotations of the femur around the fixed pelvis (Figure 2.18). One of the two vectors added controlled the y axis of the femur and could apply flexion/extension and adduction/abduction angles. The other vector controlled the coronal plane of the femur and could apply internal/external rotations in the geometric model.

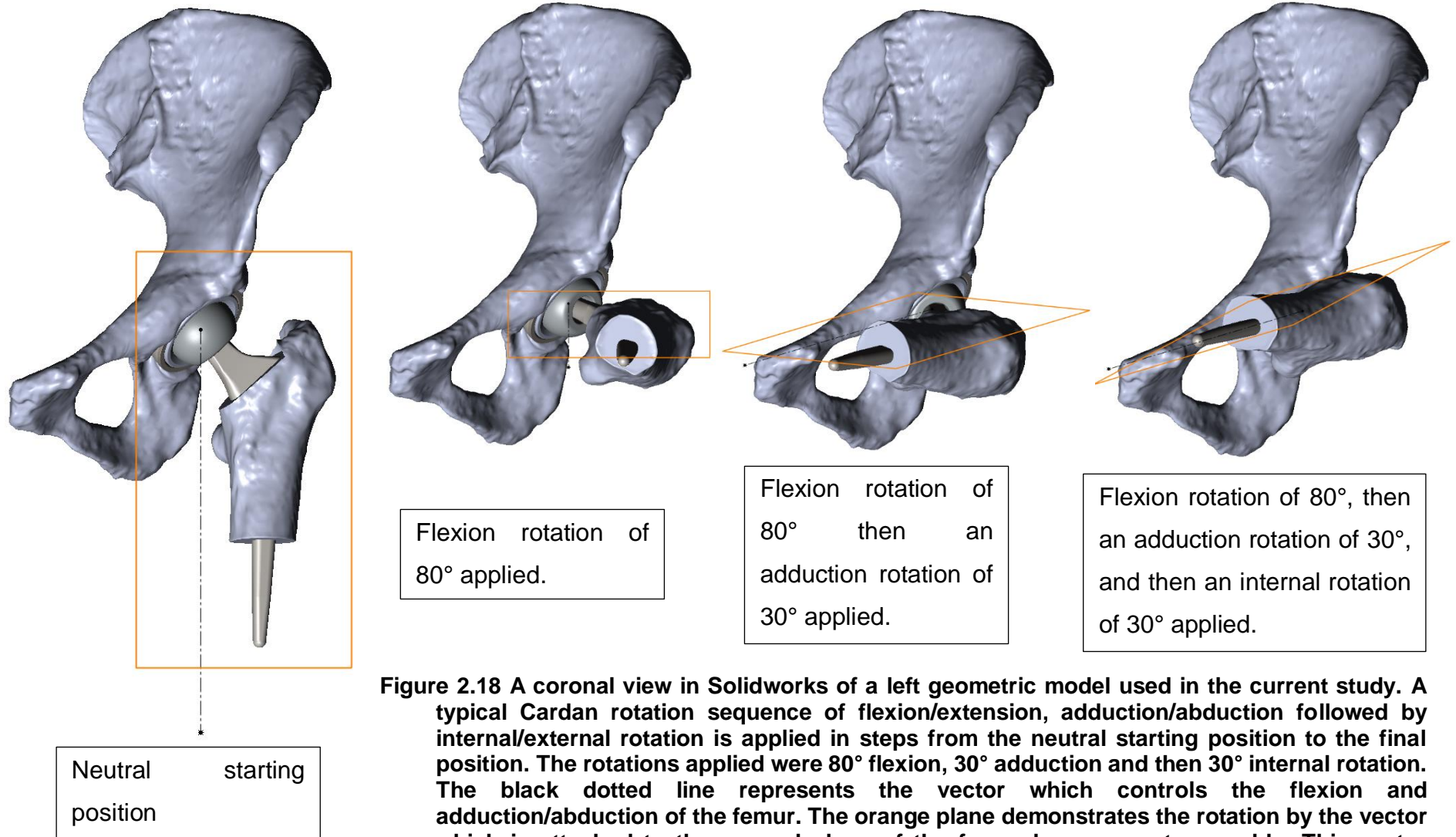


Figure 2.18 A coronal view in Solidworks of a left geometric model used in the current study. A typical Cardan rotation sequence of flexion/extension, adduction/abduction followed by internal/external rotation is applied in steps from the neutral starting position to the final position. The rotations applied were 80° flexion, 30° adduction and then 30° internal rotation. The black dotted line represents the vector which controls the flexion and adduction/abduction of the femur. The orange plane demonstrates the rotation by the vector which is attached to the coronal plane of the femoral component assembly. This vector controls the internal/external rotation.

This application of movements around the fixed pelvis allowed for the use of a cardan sequence of rotations to be applied to the geometric model. Rotational matrices were used to control the vectors and apply the correct sequence of rotations. The two vectors had a known length and therefore a rotation matrix could be applied to the vectors to rotate them in three dimensional space. This meant that kinematic activity data (Nadzadi, et al., 2003; Layton, et al., 2021) which included cardan angles could be applied to the geometric model.

Three basic rotational matrices were used to rotate the vectors by angle α around the x axis (flexion/extension), β around the y axis (internal/external rotation) and γ around the z axis (adduction/abduction). This assumes the right hand rule for the direction of the rotations. The rotational matrices for each of the three rotations are:

$$R_x(\alpha) = \begin{bmatrix} 1 & 0 & 0 \\ 0 & \cos \alpha & -\sin \alpha \\ 0 & \sin \alpha & \cos \alpha \end{bmatrix}$$

$$R_y(\beta) = \begin{bmatrix} \cos \beta & 0 & \sin \beta \\ 0 & 1 & 0 \\ -\sin \beta & 0 & \cos \beta \end{bmatrix}$$

$$R_z(\gamma) = \begin{bmatrix} \cos \gamma & -\sin \gamma & 0 \\ \sin \gamma & \cos \gamma & 0 \\ 0 & 0 & 1 \end{bmatrix}$$

The global coordinate system chosen for the geometric models was an x axis which was medial-lateral, a y axis which was inferior-superior and a z axis which was posterior-anterior. Following the right hand rule, this meant that a positive α resulted in an extension rotation, a positive β resulted in an external rotation and a positive γ resulted in an abduction rotation (Figure 2.13).

Therefore, to calculate the correct rotation matrix and apply it to the vectors which control the femur, the order of rotations in the cardan sequence must be correct. For a standard order of rotations which uses flexion/extension, adduction/abduction and then internal/external rotation, the original vector (G)

would be multiplied by the three directions of rotational matrices giving the new vector (L) as:

$$[L] = [R_y(\beta)][R_z(\gamma)][R_x(\alpha)][G]$$

The same coordinate system was used for the left and right hips, therefore the rotations were adjusted so that the rotations were positive in the correct direction.

2.2.13 Outputs of the geometric model

The output data from the geometric model included detecting impingement, the type of impingement, outputting RoM data and calculating the severity of impingement. The components and bone in the geometric models did not interact with each other when they contacted but were instead transparent and could overlap each other. Impingement could be measured via the 'interference detection' tool in Solidworks which identified any overlapping geometries which were in contact. The type of impingement (including implant-on-implant, implant-on-bone and bone-on-bone) could be recorded by noting the solid bodies which were the first to encounter contact. By using the 'measure' tool in Solidworks, the RoM at which impingement occurred could be taken. If the solid bodies in the model overlapped, the volume of overlap could be measured which could be used for a severity of impingement measure (Figure 2.19).

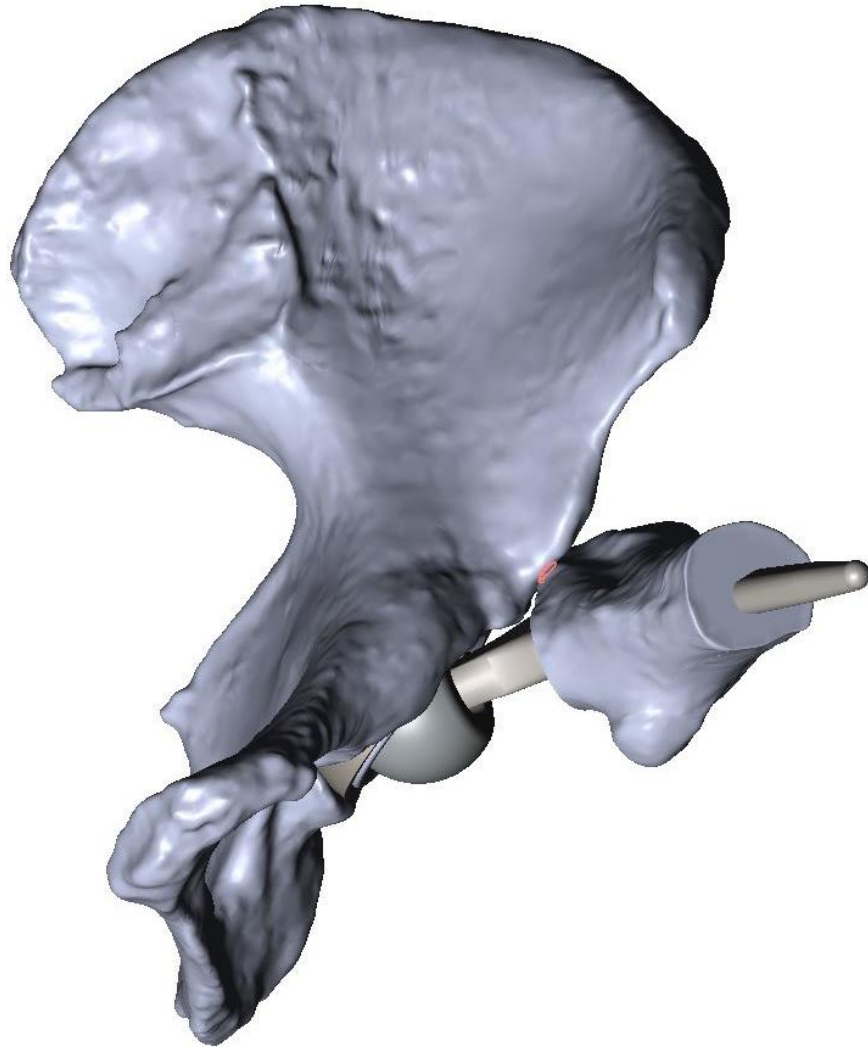


Figure 2.19 A view at a 45° angle to the coronal and sagittal plane of the left hip of one of the geometric models. The volumetric overlap (outlined in red) is demonstrated between the femur and the pelvic bone in the region of the A.I.S.

2.2.14 Verification of the geometric model

To verify that the geometric models were correctly carrying out the rotations inputted into the geometric models, a number of positions following different rotations were manually inputted into the geometric models. The ‘measure’ tool in Solidworks was used to ensure that the angles of the femur following the inputs to the vector lines which controlled the rotation of the femur were all correct. The impingement detection was also verified by inputting known rotations for impingement and using the interference detection tool.

2.3 Discussion

The aim of this method development section was to develop nine THR geometric models with different bony geometries from CT scan images which could be used to investigate impingement conditions. Nine models were produced with different bony geometries including a range of positional measures of the AIIIS and anteversion angles of the natural acetabulum. Clinically relevant THR components from DePuy Synthes were implanted in the geometric models through a virtual THR. The femur could move around the fixed pelvis through known rotations in flexion/extension, adduction/abduction and internal/external rotation. Kinematic activity data could also be applied to the models in the form of a cardan sequence using rotational matrices. There was also the ability to be able to insert different THR components and to change the orientations of the components to further investigate conditions which could contribute towards impingement in THR's. The geometric models could detect impingement, output ROM data as well as calculate the severity of impingement through the volumetric overlap of the solid bones and components in the models.

The nine geometric models developed in this section, addressed the limitations of previous THR modelling studies to investigate impingement. The majority of the FEA studies which simulated THR components and the conditions around impingement only included the THR components and did not include any bone or soft tissue (Callaghan, et al., 2002; Nadzadi, et al., 2003; Ghaffari, et al., 2012; Pedersen, et al., 2005; Saputra, et al., 2013; Ezquerro, et al., 2017). The geometric models of THR's to simulate impingement found in the literature mostly included only one bony morphology (Barsoum, et al., 2007; Kessler, et al., 2008; Pryce, et al., 2022). The development of nine different bony morphologies addressed the limitations of using only one bony geometry allowing for investigation of impingement conditions across multiple bony geometries. One study (Patel, et al., 2010) used eight individual geometric models similar to the models developed in the current study. However, the kinematic motions used were simplified and not clinically relevant. The bony geometries were also not compared and the only

output was a RoM in the general direction of each activity. The geometric models developed in this section can simulate clinically relevant kinematic activities and inputs.

2.3.1 Limitations

There were some limitations to the geometric models produced in this study. Firstly, there were no soft tissue included in the nine geometric models developed. Soft tissue has been reported to restrict the RoM in the hip (Hayashi, et al., 2012; Woerner, et al., 2017) and would therefore have an effect on RoM values reported when using these geometric models. Therefore any results from studies which use these models must be used cautiously when drawing conclusions and applying them to clinical conditions.

Secondly, the CT scan images used in the development of the geometric models were from an online colon cancer database which particularly focussed on the colon, therefore only the top portion of the femur was included. Consequently the femoral coordinate system could not be defined by the ISB recommendations (Wu, et al., 2002) which required use of the knee and was instead aligned to an existing model of a femur where the femoral coordinate system had already been defined by the ISB recommendations. This could have caused slight differences in the orientation of the neutral starting position of each femur in accordance with the ISB recommendation (Wu, et al., 2002), however the femurs were still thought to be in clinically-relevant positions and the use of the shaft angle and CoR plane that was used to align to the existing femur was an effective method of standardising the starting position for each femur.

Thirdly, the alignment of the CoR to both the femur and pelvis was done using spheres and manually aligned to the bony areas. This could have produced a small amount of error in the final position of the coordinate system and therefore the components, however this error was thought to be negligible as the size of the spheres were based on accurate measurements used by the Solidworks “measure” tool and therefore the manual alignment of the spheres to the bony areas left little scope for error.

Fourthly, the pelvis and femur were scaled so that the size of the shell fit the acetabula of the nine models. The same size stem was used for all models, however this may not have been the clinically optimal choice following the scaling process and therefore this was an assumption made to standardise the tests across the nine models.

Fifthly, due to the clearances manufactured into the component files, there was a small gap between the femoral head and the acetabular liner, meaning that the femoral head was 'floating' in the acetabular liner.

Finally, the application of movements in the models included fixing the pelvis in position and rotating the femur around the fixed pelvis. This therefore did not take into account pelvic movements or pelvic tilt and so the kinematic data which can be applied to the geometric models must have the pelvic motion already captured in the kinematic data if a clinically relevant analysis which includes spino-pelvic mobility is to be carried out.

2.4 Summary

Nine geometric models of total hip replacements which contained different bony geometries were produced which can simulate the conditions surrounding impingement, and output relevant measurable data. The geometric models were produced from nine CT scans of non-THR subjects and have a range of measurable bony features such as the anterior inferior iliac spine and the anteversion angle of the natural acetabulum. The geometric models simulated bony geometries with implanted total hip replacement components and could provide a clinically-relevant simulation of the motions of a THR. The geometric models can detect bone-on-bone, implant-on-implant and implant-on-bone impingement as well as outputting ranges of motion and severity of impingement. Therefore with the nine geometric models, factors which could be contributing to impingement can be investigated with multiple bony morphologies.

Chapter Three : Identifying anatomical bony features and their effect on patient's with THR's

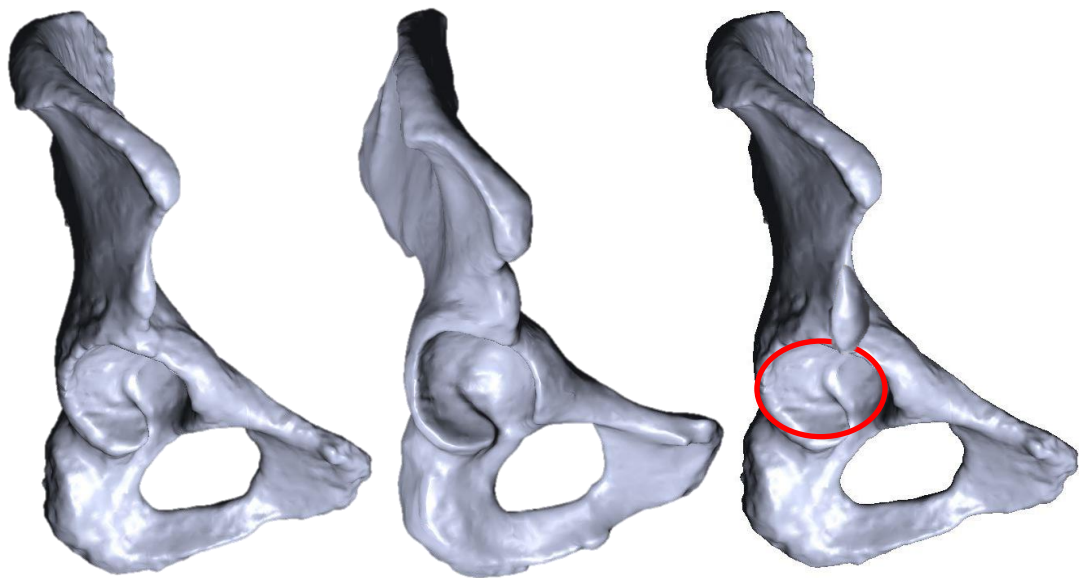
3.1 Introduction

A patient's bony morphology has been identified as being a factor which effects impingement (Kessler, et al., 2008; Shoji, et al., 2016). To reduce occurrence of dislocation, larger femoral head sizes have been shown to increase stability by increasing the jumping distance of the implant, however as the head sizes of implants increase, the limiting factor to RoM becomes bone-on-bone impingement (Burroughs, et al., 2005). This raises questions as to the effect of the geometry of the patient's bone which has been previously shown to affect the outcomes of impingement (Shoji, et al., 2016; Tabata, et al., 2019).

The anterior inferior iliac spine (AIIS) (Figure 3.1) is a bony feature on the pelvis, superior to the acetabulum and can vary in size and location of the peak (Hetsroni, et al., 2013). The size and location of the peak of the AIIS differs between patients. During high flexion movements, bone-on-bone impingement can occur at the AIIS of the pelvis (Patel, et al., 2010; Shoji, et al., 2016). It occurs when the anterior side of the greater trochanter of the femur contacts the AIIS (Davidovitch, et al., 2015). Therefore the location of the peak of the AIIS could have an effect on the RoM of the implant. The anterior peak of the AIIS and its effect on RoM has been previously investigated in patients who had dysplastic hips, a correlation between the anterior measure of the AIIS and a reduction in the RoM of the implant was observed (Shoji, et al., 2013). It has also been found that patients who had an increased lateral measure of their AIIS had a reduced RoM (Shoji, et al., 2016).

A classification system has previously been produced to categorise a patient's AIIS morphology into three variants to help identify problematic AIIS bony geometries in the natural hip (Hetsroni, et al., 2013). Type 1 has a smooth part of ilium wall between the acetabular rim and the AIIS; Type 2 has the base of

the AIIS start at the acetabular rim with no ilium wall in between; and in Type 3, the AIIS extends distally below the rim of the acetabulum (Figure 3.1). The patient's hips which had an AIIS which were either type 2 or 3 have been shown to have a reduction in the RoM (Hetsroni, et al., 2013). There have been cohort studies which have identified the number of prominent AIIS types (type 2 and type 3) as 11.5% of a population of 400 young patients who had been admitted to hospital for trauma (note these were not THR patients) (Klasan, et al., 2019).



A) Type 1 AIIS – Type 1 has a smooth part of ilium wall between the acetabular rim and the AIIS.

B) Type 2 AIIS - Type 2 has the base of the AIIS start at the acetabular rim with no ilium wall in between.

C) Type 3 AIIS – the AIIS extends distally below the rim of the acetabulum.

Figure 3.1 The three previously defined types of AIIS (Hetsroni, et al., 2013) demonstrated on a hemi-pelvis of different geometric models from this study. A) Type 1 AIIS – Bony geometry ID number 4 at 45° to the coronal plane (bony geometry ID number 4 is a left hip however it has been mirrored in this figure for comparison purposes). B) Type 2 AIIS – Bony geometry ID number 1 at 45° to the coronal plane. C) Type 3 AIIS – An edited version of bony geometry ID number 1 with the AIIS artificially extended to demonstrate a type 3 AIIS at 45° to the coronal plane.

The aim of this study was to investigate how the location of the peak of the anterior inferior iliac spine (AIIS) on the pelvis affected the RoM before impingement in a series of THR geometric models. The location of the anterior peak of the AIIS was defined by three measures along the anatomical axes (anterior/posterior, inferior/superior and medial/lateral) in relation to the CoR of the hip. The differences in type of AIIS were also investigated as part of the study using a previously defined method of classifying the AIIS (Hetsroni, et al., 2013) and comparing the different types for their effect on RoM.

3.2 Method

3.2.1 Overview of method

To investigate the effect of the location of the peak of the AIIS on the RoM, a series of nine geometric models previously described in Chapter Two (Section 2.2) were used where the anterior peak of the AIIS was measured in each of the models. The RoM was measured in each geometric model to understand the effect of the AIIS measures. These AIIS measurements were also combined to investigate the effects of different directional location measures of the AIIS on the RoM. This was carried out by using Pythagoras theorem to calculate the overall distance in the combinations of AIIS measurements. The type of AIIS was also recorded according to a previous classification (Hetsroni, et al., 2013), as well as the type of impingement which restricted the RoM.

3.2.2 Classification analysis (Hetsroni, et al., 2013)

The classification of the types of AIIS on the pelvis geometries as previously defined in a study (Hetsroni, et al., 2013) was carried out by one user (the author) and followed the same methodology as reported in the study. If there was any bony area between the base of the AIIS and the acetabulum, then the AIIS was classified as a Type 1 AIIS. If the base of the AIIS started at the acetabulum with no bony area between them, then the AIIS was classified as being a Type 2 AIIS. If the AIIS extended distally and protruded over the acetabulum, then the AIIS was classified as being a Type 3 AIIS. Classifying

the AIIS on the pelvic geometries was subjective, based on the authors assessment in relation to these definitions provided. There was only Type 1 (6/9 of the hips from the series of geometric models) and Type 2 (3/9 of the hips from the series of geometric models) AIIS's found in the series of the geometric models (Table 3.1). None of the geometric models contained a Type 3 AIIS.

Table 3.1 Anterior, superior and lateral measures of the peak of the most anterior point on the anterior inferior iliac spine. The classification was also determined using a previously defined system (Hetsroni, et al., 2013).

Bony geometry ID number	Anterior measure of the peak of the AIIS (mm)	Superior measure of the peak of the AIIS (mm)	Lateral measure of the peak of the AIIS (mm)	Hetsroni classification
1	33.6	33.5	8.9	Type 2
2	35.9	44.5	6.0	Type 1
3	36.3	42.7	8.9	Type 2
4	36.5	45.3	21.4	Type 1
5	37.1	42.9	5.6	Type 1
6	40.4	38.3	17.0	Type 1
7	41.8	39.8	9.6	Type 1
8	42.8	35.7	23.5	Type 2
9	44.2	40.1	11.2	Type 1

3.2.3 Assessing range of motion

To assess the RoM of the geometric models, the femur was rotated around the fixed pelvis until any type of impingement occurred. The femur was rotated through internal rotation at varying degrees of fixed high flexion (90°, 100° and 110°). This method was used to simulate activities of daily living which had a high flexion angle and has been used previously in computational RoM studies (Shoji, et al., 2013; Shoji, et al., 2016; Tabata, et al., 2019). These fixed high flexion angles were typical ranges of motion for a kinematic dataset from the

literature (Nadzadi, et al., 2003). The order of motions were applied by rotating the femur through the fixed angle of flexion and then the internal rotation was applied until impingement. The internal rotation was rotated in 1° increments until impingement was found. The internal rotation required to reach impingement was then recorded along with the type of impingement which occurred. The interference detection software in Solidworks was used which detected the overlap of solid bodies in the geometric model so that the type and occurrence of impingement could be found.

To achieve the desired cardan angles and rotations of the femur to be able to measure the RoM, rotational matrices for three dimensional space were used (described in section 2.2.12). The flexion/extension angle was first applied to the femur, followed by the internal/external rotation. To calculate the correct femoral rotations, rotational matrices were used to move the reference lines on the femoral sub-assembly to achieve the desired rotation of the femur.

3.2.4 Statistical analysis

The statistical methods used in the current study were applied using SPSS v26.0.0 (IBM, Armonk, New York). To analyse the correlation between the AIIIS measurements and the internal rotation to impingement at fixed flexion angles, the Pearson's chi-squared test was used, with a p value of <0.05 considered to be a statistical significance.

3.3 Results

3.3.1 Overview of results

The RoM prior to impingement differed for each of the THR geometric models suggesting that the difference in bony geometry for each model affected the RoM. There was a significant correlation between the lateral measure of the AIIS and the internal rotation to impingement at fixed flexion angles of 90° and 100°. There were no significant correlations between the anterior or superior measures of the AIIS and the internal rotation to impingement at any fixed high flexion angle. When bone-on-bone impingement occurred, the AIIS was the location of impingement in every occurrence. There were no combinations of AIIS measurements which resulted in a significant correlation with the internal rotation to impingement. There was general agreement with the change in RoM and the type of AIIS as defined by a previous classification (Hetsroni, et al., 2013), however no statistical significance was found.

3.3.2 The effect of the location of the peak of the AIIS on the range of motion

The lateral measure of the AIIS had a significant correlation with the RoM of the geometric models at fixed flexion angles of 90° and 100° (Figure 3.2). For the fixed flexion of 90°, there was typically a reduction in internal rotation of 0.9° for every millimetre the AIIS peak was located laterally. For the fixed flexion angle of 100°, there was typically a reduction in internal rotation of 1.1° for every millimetre the AIIS peak was located laterally. For the fixed flexion angle of 110°, there was found to be no significant correlation between the lateral measure of the AIIS and the RoM of the geometric model. The p values of the t tests for the correlations were 0.021 at 90° flexion, 0.047 at 100° flexion and 0.052 at 110° flexion.

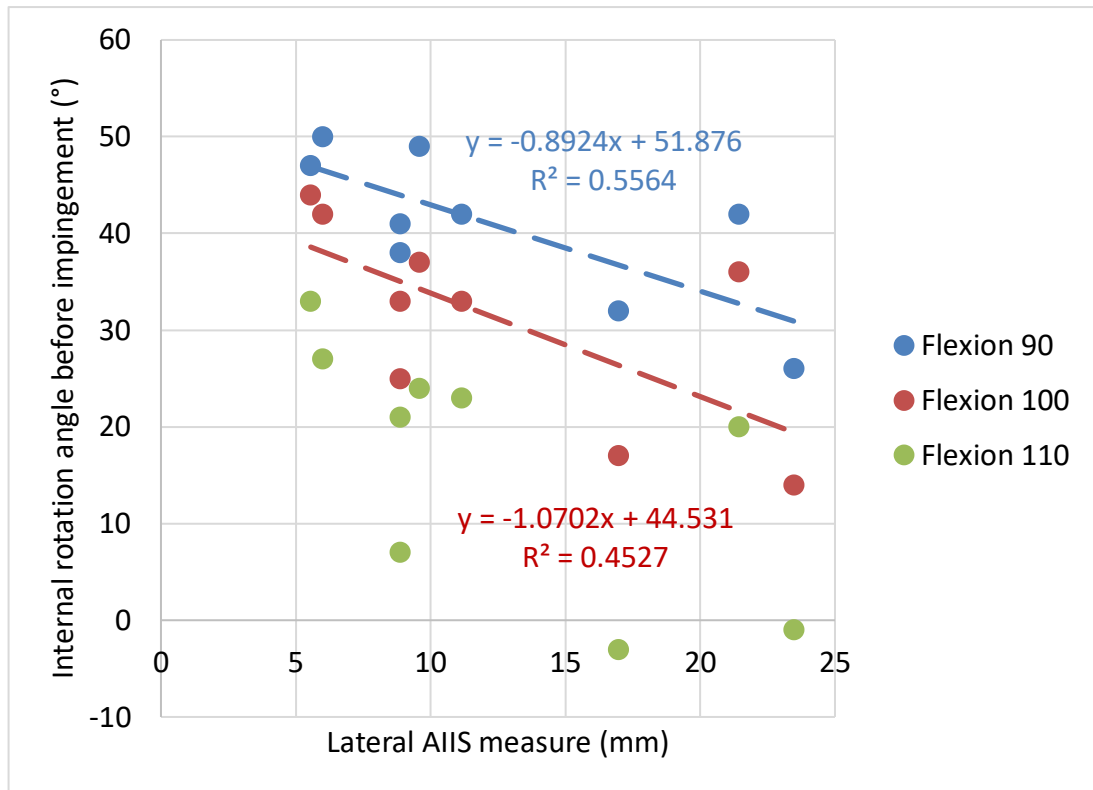


Figure 3.2 The effect of the lateral measure of the anterior inferior iliac spine on the internal rotation angle before impingement at varying degrees of fixed high flexion. Each point represents one of the nine geometric models at each fixed flexion angle. Only the correlation lines that were significant have been added.

There were no significant correlations for any of the fixed angles of flexion between the anterior measure of the AIIS and the internal rotation of the geometric models (Figure 3.3). There were also no significant correlations between the superior measure of the AIIS and the RoM of the geometric models. The p values of the correlations between all of the AIIS measures and the RoM of the geometric models are described in Table 3.2.

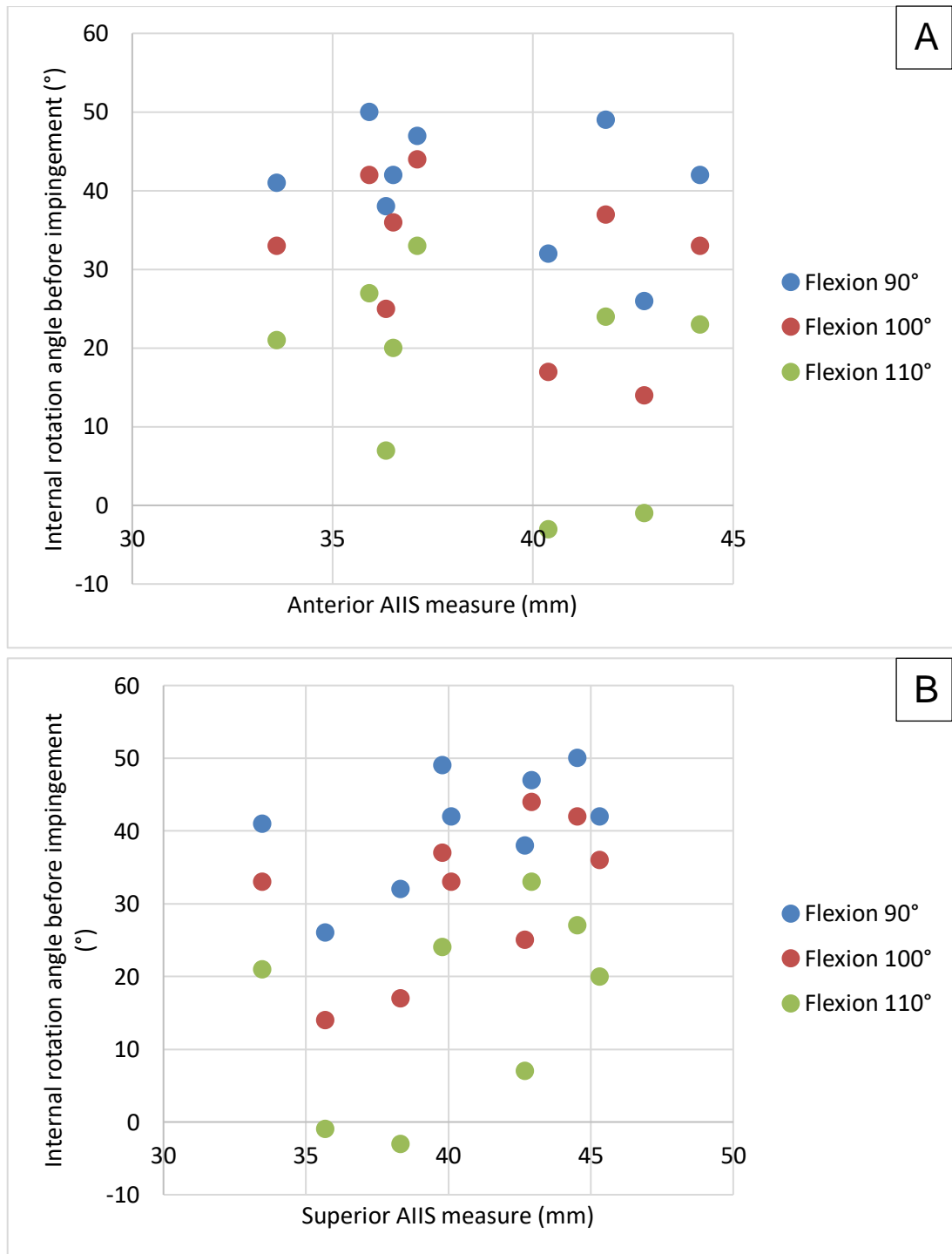


Figure 3.3 A) The effect of the superior measure of the anterior inferior iliac spine on the internal rotation angle before impingement at varying degrees of fixed flexion. B) The effect of the anterior measure of the anterior inferior iliac spine on internal rotation angle before impingement at varying degrees of fixed flexion. Each point represents one of the nine geometric models at each fixed flexion angle. No significant correlations were found.

Table 3.2 The internal rotation angle in the hip before impingement in a series of THR geometric models at different fixed angles of flexion and comparing across the three location measures of the AIIIS. The statistical test was a Pearson's chi-squared test for correlation.

	Range of internal rotation at a fixed angle of 90°	Range of internal rotation at a fixed angle of 100°	Range of internal rotation at a fixed angle of 110°
Anterior measure of the AIIIS	0.387	0.0288	0.441
Superior measure of the AIIIS	0.139	0.135	0.274
Lateral measure of the AIIIS	0.021*	0.047*	0.052

3.3.3 Impingement locations

The type of impingement (bone-on-bone, implant-on-bone or implant-on-implant) differed during the RoM testing of the geometric models (Table 3.3). For the instances of bone-on-bone impingement, RoM was restricted by contact between the AIIIS and the anterior portion of the greater trochanter, close to the osteotomy cut. For the instances of implant-on-bone impingement, RoM was restricted by the roof of the acetabulum (superior to the acetabulum) and the femoral neck of the stem component. There were no occurrences of implant-on-implant impingement during the RoM testing.

Table 3.3 The ranges of internal rotation at each of the fixed flexion angles for the entire series of geometric models. The colours denote the type of impingement found during the range of motion testing. Yellow is when the range of motion was restricted by bone-on-bone impingement. Blue is when the range of motion was restricted by implant-on-bone impingement.

Bony geometry ID number	Internal rotation before impingement for a fixed flexion angle of 90°	Internal rotation before impingement for a fixed flexion angle of 100°	Internal rotation before impingement for a fixed flexion angle of 110°
1	41	33	21
2	50	42	27
3	38	25	7
4	42	36	20
5	47	44	33
6	32	17	-3
7	49	37	24
8	26	14	-1
9	42	33	23

3.3.4 Amount of difference in range of motion across the geometric models

There was a relatively large difference in the internal rotation angle before impingement between the total hip replacements at each of the fixed flexion angles (Figures 3.4A, 3.4B & 3.4C). For the fixed flexion angle of 90°, the smallest internal rotation before impingement was 26° in bony geometry ID number 8 and the largest was 50° in bony geometry ID number 2. For the fixed flexion angle of 100°, the smallest internal rotation angle before impingement was 14° in bony geometry ID number 8 and the largest was 44° in bony geometry ID number 5. For the fixed flexion angle of 110°, the smallest internal rotation angle before impingement was -3° in bony geometry ID number 6 and the largest was 33° in bony geometry ID number 5.

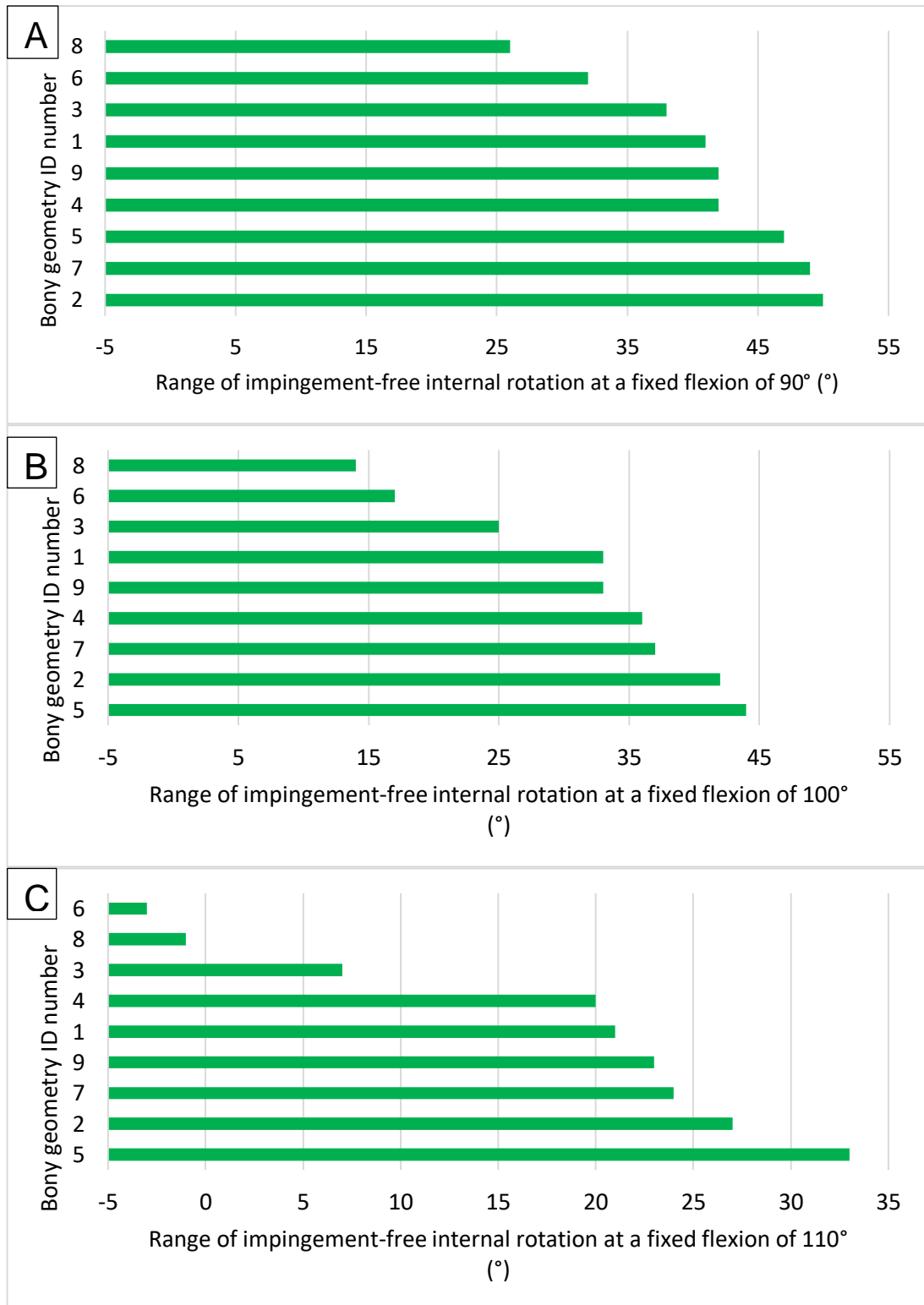


Figure 3.4 A) The internal rotation angle before impingement at a fixed flexion of 90° for all of the nine geometric models in descending order of range of motion. 3.4 B) The internal rotation angle before impingement at a fixed flexion of 100° for all of the nine geometric models in descending order of range of motion. 3.4 C) The internal rotation angle before impingement at a fixed flexion of 110° for all of the nine geometric models in descending order of range of motion.

3.3.5 AIIIS combination measures

The three AIIIS measures were combined to further analyse whether there were combinations of AIIIS measures which would be deemed as having a significant effect on the ROM of the total hip replacement. There was found to be no combinations of AIIIS measures which caused a significant correlation with the internal rotation angle before impingement of the total hip replacement for any of the fixed flexion angles (Table 3.4).

Table 3.4 The p values of the Pearson's chi-squared test for correlation comparing the combinations of AIIIS location measures and the RoM across the series of nine geometric models at varying degrees of fixed high flexion.

	Range of internal rotation at a fixed angle of 90°	Range of internal rotation at a fixed angle of 100°	Range of internal rotation at a fixed angle of 110°
Anterior and superior combination measure of the AIIIS	0.625	0.707	0.767
Anterior and lateral combination measure of the AIIIS	0.104	0.100	0.168
Superior and lateral combination measure of the AIIIS	0.844	0.730	0.955
Anterior, superior and lateral combination measure of the AIIIS	0.727	0.731	0.688

3.3.6 Classification analysis (Hetsroni, et al., 2013)

The AIIIS bony feature on the pelvic geometries were categorised into three classes based on previous literature (Hetsroni, et al., 2013). Type 1 has a smooth part of ilium wall between the acetabular rim and the AIIIS; Type 2 has the base of the AIIIS start at the acetabular rim with no ilium wall in between; and in Type 3, the AIIIS extends distally below the rim of the acetabulum (Figure 3.1). There were only type 1 and type 2 AIIIS morphologies found in the geometric models. When comparing the mean internal rotations before impingement for type 1 against the type 2 AIIIS geometric models, it was found generally that type 1 had a larger ROM than type 2 (Figure 3.5). Statistical testing was not deemed appropriate due to the low numbers of each type of AIIIS in the study.

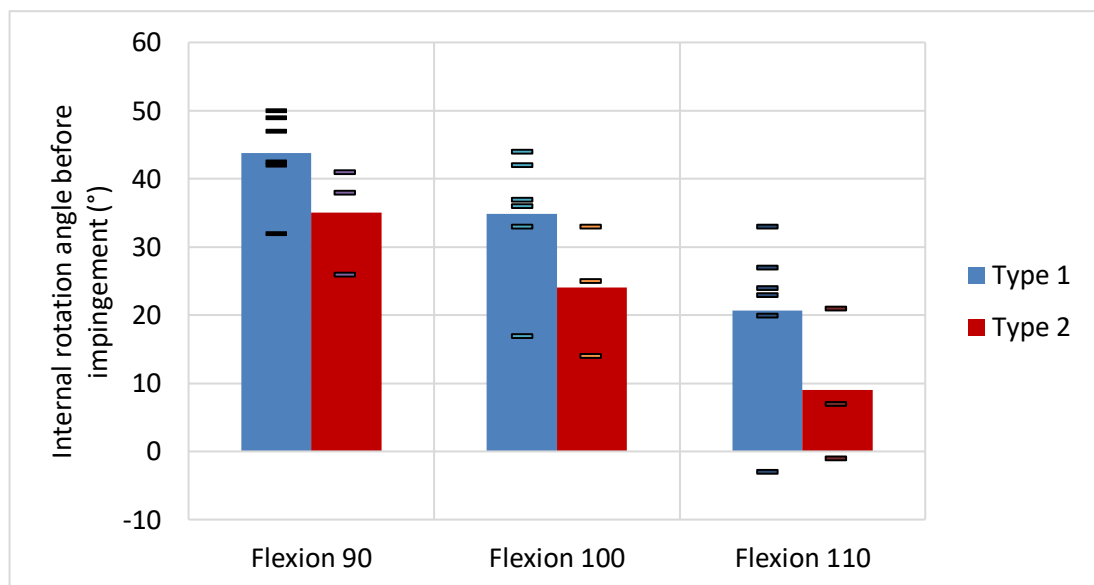


Figure 3.5 A comparison of internal rotation angle before impingement between the two different types of AIIIS found in the series of geometric models at varying degrees of fixed high flexion. The black lines represent the range of motion for each individual model.

3.4 Discussion

This study aimed to analyse the effect that bony geometries have on the RoM in a series of THR geometric models. The difference in bony geometries was measured by the location of the anterior peak of the AIIIS on the pelvis which has been previously shown to be a location of impingement at high ranges of flexion in computational modelling studies. The RoM was defined by measuring the internal rotation angle to impingement at varying degrees of fixed high flexion. This study aimed to analyse whether the location of the AIIIS had an effect on the internal rotation to impingement in a series of THR geometric models. There was a significant correlation between the lateral measure of the AIIIS and the internal rotation to impingement in the geometric models at fixed flexion angles of 90° and 100°. The anterior and superior measures of the AIIIS resulted in no significant correlations with the internal rotation to impingement. This suggested that the lateral protrusion of the AIIIS could be a predictor for bone-on-bone impingement.

3.4.1 The effect of the location of the peak of the AIIIS on the range of motion of the geometric models

The lateral measure of the AIIIS had a significant correlation ($p < 0.05$) with the internal rotation angle to impingement of the geometric models during the fixed flexion angles of 90° and 100°. As the AIIIS was located increasingly laterally, it protruded further over the femoral coordinate system and therefore impeded the motion of the femur, reducing the internal rotation angle needed for impingement to occur during high flexion rotations. This agreed with a previous study that also found that patients with a laterally large AIIIS significantly reduced the internal rotation to impingement at 90° flexion (Shoji, et al., 2016). The study included 85 THR patient's CT scans which were used to measure the AIIIS and RoM. The size of the component bearings used for the components were 32mm, however the implant sizes were selected on a patient-specific basis and therefore differed across the 85 patients which could have affected the results of the study. It was also not clear whether there was any medialisation of the components to determine the centre of rotation which

could have affected the biomechanics. Different implant sizes would have different offset lengths which have been previously demonstrated to affect the RoM in THR's (Matsushita, et al., 2009). To address this limitation, the current study investigated the RoM by scaling the geometric models so that the same component size and design could be used for each hip and thereby reduced the bias of these parameters. The use of the same components across the geometric models also resulted in a significant correlation between the lateral measure of the AIIIS and the internal rotation to impingement at a fixed high flexion angle.

The study (Shoji, et al., 2016) also found that the anterior and superior AIIIS measures had a significant correlation with the internal rotation to impingement at 90° flexion. Another study of 63 patient's CT scans also found a significant correlation between the anterior AIIIS measures and the internal rotation to impingement at 90° flexion (Shoji, et al., 2013). The current study concluded that neither the anterior nor the superior measures of the AIIIS resulted in a significant correlation with the internal rotation to impingement at any fixed flexion angles which disagreed with the two studies (Shoji, et al., 2013; Shoji, et al., 2016). This difference in agreement could have been because the differences in the AIIIS measures from the geometric models in the current study were subtle and not sufficient enough to achieve a statistical significance. There was a difference in components, component sizing and geometric model setup between the studies which could have caused slight differences in the results. The method of finding the CoR was not described in detail and the differences in method could have resulted in a difference in the biomechanics of the test.

There could be other bony measurements of the AIIIS not measured in the current study which could have contributed to the outcomes of the RoM. While the anterior peak of the AIIIS was a good indicator of the location of the AIIIS in relation to the CoR, the impingement site was typically occurring at the base of the AIIIS on the lateral side. Bony measurements such as the width and steepness from the base could have contributed to the effect on the RoM. The width of the AIIIS measured in the medial-lateral axis would have increased

the lateral protrusion of the bony feature which may not have been captured in the lateral AIIIS measure used in the current study and could explain some of the variation in the data. The steepness of the AIIIS could have protruded the base of the AIIIS further out which was not captured in the current study. The morphology of the femurs in the geometric models could also have been a contributing factor to a difference in the RoM to impingement and could also explain some of the variation in the data.

In the literature, there have been some case studies of femoroacetabular impingement where there has been a resection of the AIIIS to improve ROM in the natural hip (Larson, et al., 2011; Davidovitch, et al., 2015). In extreme cases, for patients with laterally large AIIIS measures, the AIIIS could be resected which could help in reducing AIIIS related impingement and improve outcomes of ROM. This method could also be translated for use in total hip replacement impingement for extreme cases of AIIIS impingement.

3.4.2 Location and type of impingement

Analysis of the impingement locations resulted in contact between the AIIIS (typically on the lateral side) and the anterior portion of the greater trochanter close to the location of the osteotomy cut on the femur in every occurrence of bone-on-bone impingement. This agreed with a study (Shoji, et al., 2016) which recorded that when bone-on-bone impingement occurred in 85 CT scan models of THR's, the impingement location was between the anteroinferior edge of the AIIIS and the anterior side of the greater trochanter of the femur. The current study found that the contact on the AIIIS was typically on the lateral side which differed with the previous study where there were more instances which contacted the anteroinferior edge of the AIIIS. This was thought to be because the RoM recorded in the current study involved measuring the angle of internal rotation at varying degrees of fixed high flexion, whereas the previous study (Shoji, et al., 2016) included pure flexion as well as internal rotation at 90° fixed flexion which would therefore see more impingement cases towards the middle of the AIIIS as opposed to the lateral side of the AIIIS.

There were two types of impingement which occurred during the RoM testing for the series of THR geometric models; implant-on-bone and bone-on-bone impingement. The occurrences of implant-on-bone impingement typically occurred between the femoral stem neck and the roof of the acetabulum. Therefore the AIIIS measures would have had no effect on the outcomes of those RoM tests. This was a limitation to the current study and should be considered when interpreting the results. There were no occurrences of implant-on-implant impingement which was thought to be because of the use of a larger femoral head (36mm) as well as the acetabular cup being in a well-positioned orientation for each geometric model (45° radiographic inclination and between 20°-35° radiographic anteversion).

3.4.3 Range of motion difference across the geometric models

There was a relatively large difference in the internal rotation before impingement at fixed flexion angles when comparing the geometric models (Figure 3.4). There were some geometric models which had a reduced RoM due to the location of the AIIIS which suggests that these specific bony geometries may be indicators of an increased risk of bone-on-bone impingement. This data suggests that there is a need for patient-specific THR preoperative planning.

3.4.4 AIIIS combination measures

The measures of the AIIIS were combined in different ways to analyse whether there would be significant correlations in multiple directions of the location of the AIIIS. There were found to be no significant correlations between combinations of the measures of the AIIIS and the RoM. One study (Shoji, et al., 2016) suggested that taller subjects had a laterally larger and more anteriorly protruded AIIIS suggesting that the two measures in combination could be used as a useful measure to infer correlations and conclusions about the AIIIS and its effect on the RoM of a particular subject. The current study found no combination measurements which had a significant effect on the RoM of the geometric models. This could have been due to the difference in

components used which may have changed the biomechanics between the studies. The measures in the current study could also have been subtle and not enough to result in a statistical significance.

3.4.5 Hetsroni classification analysis

The geometric models were categorised into the different types of AIIIS morphologies based on a previously defined classification (Hetsroni, et al., 2013). There were only type 1 and type 2 AIIIS morphologies in the current study with no type 3's found. The average RoM of type 1 AIIIS's was greater than the average RoM of type 2 AIIIS's which agreed with the original classification study (Hetsroni, et al., 2013). One study (Tabata, et al., 2019) analysed 14 THR CT scan models which included AIIIS morphologies that were classified as type 1, type 2 and type 3 to analyse the differences in RoM. It was found that there were no statistical differences between the three types of AIIIS when it came to RoM difference which agreed with the trends in the current study, however the differences could have been subtle and not enough to generate a statistical significance. Another study (Shoji, et al., 2016) found that there were significant differences between the ROM in Type 3 AIIIS morphologies when compared to type's 1 and 2 when analysing the RoM in 85 CT scan models. Due to the lack of type 3 AIIIS morphologies found in the current study this result could not be directly compared.

Based on the findings from the current study, the type of AIIIS defined by the classification system (Hetsroni, et al., 2013) should not be used solely as a judgement for potential impingement. This also agrees with a previous study which found that a high percentage of problematic AIIIS morphologies (type 2 and type 3) have been found to be asymptomatic in natural hips and that the classification system should not be solely used as a judgement of potential impingement and therefore it is expected that the same could be said of AIIIS morphologies in THRs (Balazs, et al., 2017). Therefore it is suggested that the location measures used in the geometric model analysis in the current study as well as the previous classification (Hetsroni, et al., 2013) may allow for a

more comprehensive analysis for RoM and potential bone-on-bone impingement.

3.4.6 Limitations

The geometric models used in this study were the same as those developed in Chapter Two and therefore the same limitations applied which were described in Section 2.3.1. The motions used to measure RoM consisted of an internal rotation angle after a fixed flexion rotation. Other methods of measuring RoM could have resulted in different conclusions and outcomes than those presented in this chapter.

3.5 Summary

The aim of this chapter was to investigate how the location of the anterior inferior iliac spine (AIIS) on the pelvis affected the RoM before impingement in a series of geometric models of the hip joint with an implanted total hip replacement. The location of the anterior peak of the AIIS was defined by three measures along the anatomical axes (anterior/posterior, inferior/superior and medial/lateral) in relation to the CoR of the hip. The differences in type of AIIS were also investigated as part of the study using a previously defined method of classifying the AIIS and comparing the different types for their effect on the RoM.

The results from this study demonstrated a statistically significant correlation between the lateral measure of the AIIS and the internal rotation to impingement at fixed high flexion angles. The lateral measure of the AIIS could therefore be used as a predictor for bone-on-bone impingement in total hip replacements. There was insufficient evidence to support the anterior and superior measures of the AIIS being an indicator for impingement likelihood which is what had been reported previously.

As THR's are being used in increasingly younger patients who demand higher ranges of motion from their implant, preoperative planning in total hip replacements must be aware of the location of the AIIS and its effect on impingement likelihood. The results from this study have shown that the lateral

measure of the AIIIS could be a predictor for bone-on-bone impingement. To build confidence, a wider study of AIIIS location variation is needed. It is recommended that activities of daily living, particularly related to impingement and dislocation, should be tested with the geometric models to simulate impingement conditions and further investigate the AIIIS bony feature presented in this chapter.

Chapter Four : Effect of bony geometry on impingement in Total Hip Replacement during dislocation-prone activities

4.1 Introduction

A number of factors contribute to the likelihood of impingement occurring in total hip replacement (THR) patients. These include factors related to the implant design, surgical practice, patient anatomy and biomechanics (Malik, et al., 2007). The bony morphology of the patient's hip has been identified as being a factor which affects impingement (Kessler, et al., 2008; Patel, et al., 2010; Shoji, et al., 2016). In particular, the bony morphology of the anterior inferior iliac spine (AIIS) has been previously shown to influence the range of motion before impingement in total hip replacements (Patel, et al., 2010; Davidovitch, et al., 2015; Weber, et al., 2016; Shoji, et al., 2016; Tabata, et al., 2019) and in the natural hip (Larson, et al., 2011; Hetsroni, et al., 2013; Hamada, et al., 2018). Previous work in this thesis has also agreed with the effect of the AIIS on RoM to impingement (Chapter Three). It is unclear however, whether the bony morphology of a patient's AIIS would have an effect on the occurrence of impingement during clinically relevant positions such as during activities of daily living and the eventual severity of that impingement. The anteversion angle of the natural acetabulum has also been identified in the literature as affecting the range of motion in the natural hip (Nakahara, et al., 2011; Morris, et al., 2018), however this has not been investigated previously in relation to THRs. In this study, the AIIS and the anteversion angle of the natural acetabulum were investigated for their effect on the impingement occurrence and severity during dislocation-prone activities.

The most commonly used femoral head component sizes in THR's have increased in recent years from 28mm to >32mm across England, Wales and Northern Ireland (National Joint Registry, 2020). This trend in increasing head size has largely been because of the improved stability through wider ranges of motion and larger jumping distances (the amount of lateral translation of the

femoral head centre needed for dislocation to occur). Larger head sizes can reduce the implant-on-implant impingement through the wider ranges of motion however this can result in the restricting factor of range of motion to impingement changing from implant-on-implant impingement to bone-on-bone impingement (Burroughs, et al., 2005).

A published kinematic dataset including 10 individuals (note these were not THR patients) performing dislocation-prone activities of daily living was identified in the literature (Nadzadi, et al., 2003). This dataset included seven activities of daily living. It consisted of two anterior dislocation-prone activities which were prone to posterior impingement (“anterior dislocation-prone activities”) including rolling over in bed (ROLL) and a pivot of one foot through external rotation (PIVOT). Additionally, there were five posterior dislocation-prone activities which were prone to anterior impingement (“posterior impingement-prone activities”) including standing up from a low seated chair (SSL), standing up from a normal heighted chair (SSN), crossing one leg over the other from a seated position (XLG), picking up an object from the floor (STOOP) and tying the subjects own shoes from a seated position (TIE). One subject was chosen for each activity to represent the median of the 10 individuals. Other datasets which included activities of daily living were identified in the literature, however the raw data was not published (Hemmerich, et al., 2006; Sugano, et al., 2012). With no raw data published, the kinematic activities could not be extracted and then used in the geometric models for this study, hence one of the previous kinematic datasets (Nadzadi, et al., 2003) was a favoured source of information.

Dislocation-prone activities of daily living have been used across several computational studies for investigation into impingement in total hip replacements for a clinically relevant assessment (Nadzadi, et al., 2003; Pedersen, et al., 2005; Patel, et al., 2010; Ghaffari, et al., 2012; Elkins, et al., 2012; Saputra, et al., 2013; Pryce, et al., 2022). Many of these studies have used finite element analysis (FEA) (Nadzadi, et al., 2003; Pedersen, et al., 2005; Ghaffari, et al., 2012; Saputra, et al., 2013), however due to the complexity and run time of modelling bone, only one study included a bony

geometry (Elkins, et al., 2012). There have been studies which investigated impingement using geometric modelling to simulate the THR which included bony geometries (Patel, et al., 2010; Pryce, et al., 2022), however only one study used different bony geometries (Patel, et al., 2010) to investigate impingement. This study only used simplified versions of the kinematic data to find the RoM at specific angles related to the activities and there was no analysis about the difference between the bony geometries tested. The outcomes of the geometric model studies to date have focussed on the RoM and the occurrence of impingement, and there has been a lack of analysis in terms of the severity of the impingement reported as well as any analysis into the effects of different bony geometries.

The aim of this study was to investigate the effect of different bony geometries on the occurrence, severity, and type of impingement (bone-on-bone impingement, implant-on-bone impingement, or implant-on-implant), during dislocation-prone activities of daily living (Nadzadi, et al., 2003) in a series of nine THR geometric models (developed in chapter Two (Section 2.2)). Bony features involved in bone-on-bone impingement during these dislocation-prone activities of daily living were further investigated along with their link to the severity of bone-on-bone impingement. These features included the bony morphology of the AHS, specifically the location of the anterior peak in relation to the CoR of the pelvis and the anteversion angle of the natural acetabulum.

4.2 Method

4.2.1 Overview of method

To investigate the effect of different bony geometries on impingement, seven dislocation-prone activities of daily living published in the literature (Nadzadi, et al., 2003) were applied to nine geometric models (developed in chapter Two (section 2.2)) and the occurrence, type and severity of impingement was recorded for each activity and each model. For the severity of impingement analysis, only bone-on-bone impingement was investigated so that this study could focus on the effect of different bony geometries. The severity of bone-

on-bone impingement during the anterior dislocation-prone activities, including how the natural angle of the acetabulum affected the severity of bone-on-bone impingement was compared across the models. The severity of bone-on-bone impingement for the posterior dislocation-prone activities were then compared including analysis of how the AIIIS positional measures in the three anatomical axes affected the severity of bone-on-bone impingement.

4.2.2 Geometric models and the dislocation-prone activities of daily living (Nadzadi, et al., 2003)

The nine geometric models developed in Chapter Two were used to investigate the effect of using different bony geometries on impingement during dislocation-prone activities. The components and the implantation positions of the components were the same as described in Chapter Two (section 2.2.10). The kinematic dataset used in the study was a previously published dataset (Nadzadi, et al., 2003) which included seven dislocation-prone activities (Section 1.3.2.1). The data consisted of a number of discrete positions that together simulated each activity. Each of these positions consisted of three angles of rotation to be used as a Cardan sequence, which simulated the positions for the femur around the pelvis, which was fixed. The sequence was to be applied to the model as the flexion/extension angle, followed by the adduction/abduction angle followed by the internal/external rotation angle. These positions, simulating each activity, were applied to the nine THR geometric models allowing the impingement occurrence, type and severity to be measured using the interference detection tool in Solidworks.

4.2.3 Bony features for comparison

For the posterior dislocation-prone activities, the anterior peak of the AIIIS, measured in each model in chapter three (Section 2.2.11) was used as a bony feature for analysis of its effect on impingement. The three measures of the location of the peak of the AIIIS in relation to the CoR were as follows: [1] anterior measure of the AIIIS peak from the CoR in the anterior-posterior axis, [2] the superior measure of the AIIIS peak from the CoR in the inferior-superior

axis and [3] the lateral measure of the AIIIS peak from the CoR in the medial-lateral axis. These three measures were compared for their effect on the severity of impingement which was measured as follows: [1] by the volumetric overlapping of the bones in the models and [2] the difference in angle at the initial impingement contact and maximum rotation of the activity. The angles were flexion for the posterior dislocation-prone activities (“flexion angle past the point of impingement”) and external rotation for the anterior dislocation-prone activities (“external rotation angle past the point of impingement”). For the anterior dislocation-prone activities, the anteversion of the natural acetabulum was used as a bony feature for analysis on its effect on impingement. These values were also compared for their effect on the severity of impingement using the same two methods.

4.2.4 Outcome measures of impingement

The outcome measures of the geometric model were the occurrence, type and severity of impingement. The occurrence and severity of impingement were measured via the ‘interference detection’ tool in Solidworks that identified which solid bodies in the assembly were overlapping, and the volume of the overlap (described in more detail in section 2.2.14). The type of impingement was then measured by noting the solid bodies in the model which were in contact during the first impingement occurrence of the activity.

The severity of impingement measures during each activity were defined as: [1] the greatest amount of volumetric overlap measured during the activity between the two solid bodies that first came into contact and [2] the difference in angle at the initial impingement contact and maximum rotation of the activity. The angles were flexion for the posterior dislocation-prone activities (“flexion angle past the point of impingement”) and external rotation for the anterior dislocation-prone activities (“external rotation angle past the point of impingement”). The interference detection tool was used to output the volume of overlapping geometries. To measure the difference in angle past the point of impingement, the RoM in either flexion or external rotation was recorded when impingement first occurred and that value was subtracted from the maximum angle (either flexion or external rotation) during the activity.

Comparison of the severity of impingement as measured by the volumetric overlap of solid bodies in the model between a bone-on-bone impingement occurrence and an implant-on-implant impingement occurrence, could not be appropriately carried out as the possible volumetric overlaps would be different due to the different shapes involved. A low volume of overlap of geometry would be expected for an implant-on-implant impingement occurrence compared with that of bone-on-bone as the bony geometry is much larger than that of the implant.

4.2.5 Statistical analysis

The statistical methods used in the current study were applied using SPSS v26.0.0 (IBM, Armonk, New York). The statistical tests to analyse the correlations between the severity of impingement measures and the bony features was a Pearson's chi-squared test. A P-value of <0.05 was considered significant.

4.3 Results

4.3.1 Overview of results

The bony geometry had an effect on the occurrence, type and severity of impingement during the dislocation-prone activities of daily living. The anteversion angle of the natural acetabulum had a significant effect on the severity of impingement during the anterior dislocation-prone activities. The lateral measure of the AIIIS had an effect on the severity of impingement during the STOOP activity, however this was only a significant result for the volumetric overlap and not the difference in flexion angle past the point of impingement. The other AIIIS measures had no effect on the severity of impingement. Other than the STOOP activity, there were relatively low levels of impingement during the posterior dislocation-prone activities.

4.3.2 Occurrence and types of impingement across different bony geometries

The occurrence and type of impingement encountered during each activity differed across the nine geometric models (Figure 4.1). Across the nine geometric models and seven activities considered, there were 28/63 (44%) occurrences of impingement. Of the 28 impingement occurrences, 21 were bone-on-bone impingement (75%), 3 were implant-on-implant (11%) and 4 were implant-on-bone impingement (14%). This data suggested that the bony geometry had an effect on the occurrence and type of impingement that would occur.

For the anterior dislocation-prone activities, the ROLL activity produced the greatest amount of bone-on-bone impingement occurrences (8/9 geometric models). The PIVOT activity also resulted in a great amount of bone-on-bone impingement occurrences (6/9 of the geometric models).

For the posterior dislocation-prone activities, the STOOP activity produced a great amount of impingement occurrences (7/9 of the geometric models including 4/9 bone-on-bone impingement and 3/9 implant-on-bone impingement). There were not many impingement occurrences across the other posterior dislocation-prone activities. The XLG and SSL activities recorded no occurrences of impingement.

Activities applied to the geometric model		Bony geometry ID number								
		Model 1	Model 2	Model 3	Model 4	Model 5	Model 6	Model 7	Model 8	Model 9
Anterior dislocation-prone activities	PIVOT	Yellow	Yellow	Yellow	Yellow	Yellow	Green	Red	Yellow	Red
	ROLL	Yellow	Yellow	Yellow	Yellow	Yellow	Yellow	Yellow	Green	Yellow
Posterior dislocation-prone activities	STOOP	Yellow	Green	Blue	Blue	Green	Yellow	Blue	Yellow	Yellow
	XLG	Green	Green	Green	Green	Green	Green	Green	Green	Green
	TIE	Green	Green	Green	Green	Green	Red	Green	Yellow	Green
	SSL	Green	Green	Green	Green	Green	Green	Green	Green	Green
	SSN	Green	Green	Blue	Green	Green	Yellow	Green	Yellow	Green

Figure 4.1 Occurrence and type of impingement found in the series of nine geometric models during the seven dislocation-prone activities of daily living. The type of impingement was defined as the solid bodies which were first to impinge in the model during the activity.

4.3.3 Severity of bone-on-bone impingement for the anterior dislocation-prone activities

The majority of impingement occurrences during the anterior dislocation-prone activities resulted in bone-on-bone impingement. So that appropriate analysis could be done to investigate the effect of different bony geometries, only the severity of bone-on-bone impingement was investigated.

4.3.3.1 The effect of different bony geometries

The severity of impingement measured by volumetric overlap differed across the nine geometric models during the anterior dislocation-prone activities (Figure 4.2). This data suggested that the bony geometries of the models affected the severity of impingement during the activities. The ROLL activity resulted in greater severities of bone-on-bone impingement when compared to the PIVOT activity. To demonstrate the range in the volume of overlapping bones, the greatest volume of impingement was 5746mm³ for the ROLL activity in bony geometry ID number 2 compared with bony geometry ID number 8 which didn't result in any impingement. The greatest volume of

impingement for the PIVOT activity was 3019mm³ in bony geometry ID number 2 compared with bony geometry ID number 6 which didn't result in any impingement. Such relatively large differences in the volume of impingement between geometric models with different bony geometries demonstrated how much the bony geometry could affect the likelihood and severity of impingement.

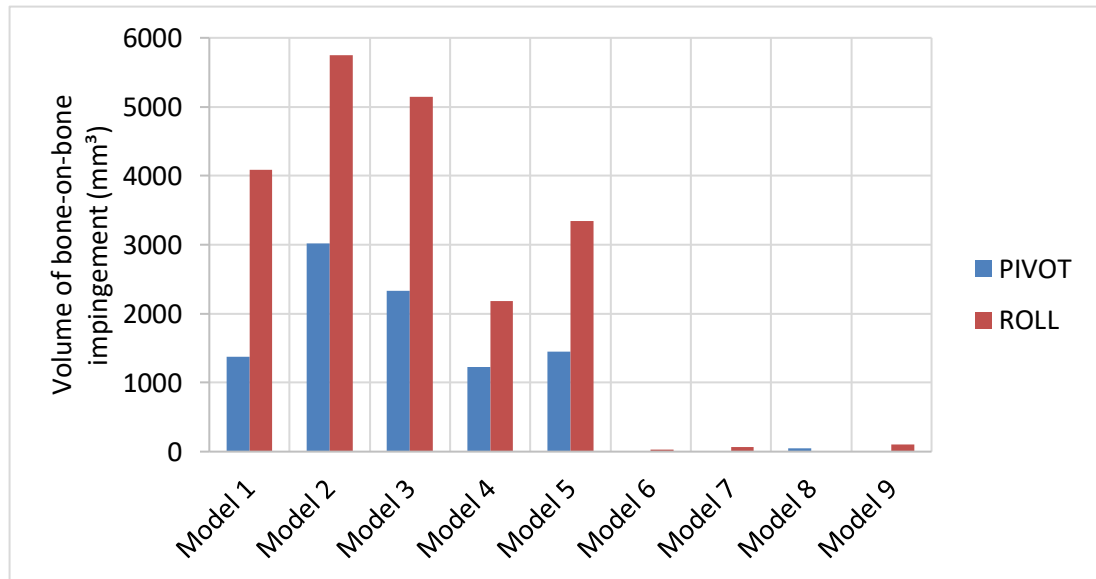


Figure 4.2 The severity of bone-on-bone impingement as measured by the volume of overlapping bones found for each of the nine geometric models of a THR during anterior dislocation-prone activities (PIVOT and ROLL). The severity of impingement was defined by measuring the volumetric overlap of the pelvic bones and femur at the greatest volume of impingement. Only severity of bone-on-bone impingement has been assessed this way (and not other types of impingement).

The severity of impingement measured by the difference in external rotation past the point of impingement also differed across the nine geometric models (Figure 4.3). This data further suggested that the bony geometries affected the RoM and severity of impingement during the activities. The PIVOT activity resulted in greater differences in the external rotation angle past the point of impingement than the ROLL activity. To demonstrate the range in the external rotation past the point of impingement in the models, the greatest angle was 27.7° for the PIVOT activity in bony geometry ID number 2 compared with bony geometry ID number 8 which didn't result in any impingement. The

greatest angle for the ROLL activity was 17.2° for bony geometry ID number 2 compared with bony geometry ID number 6 which didn't result in any impingement. Such variation in the differences in the external rotation angle past the point of impingement between geometric models with different bony geometries demonstrated how much the bony geometry could affect the likelihood and severity of impingement.

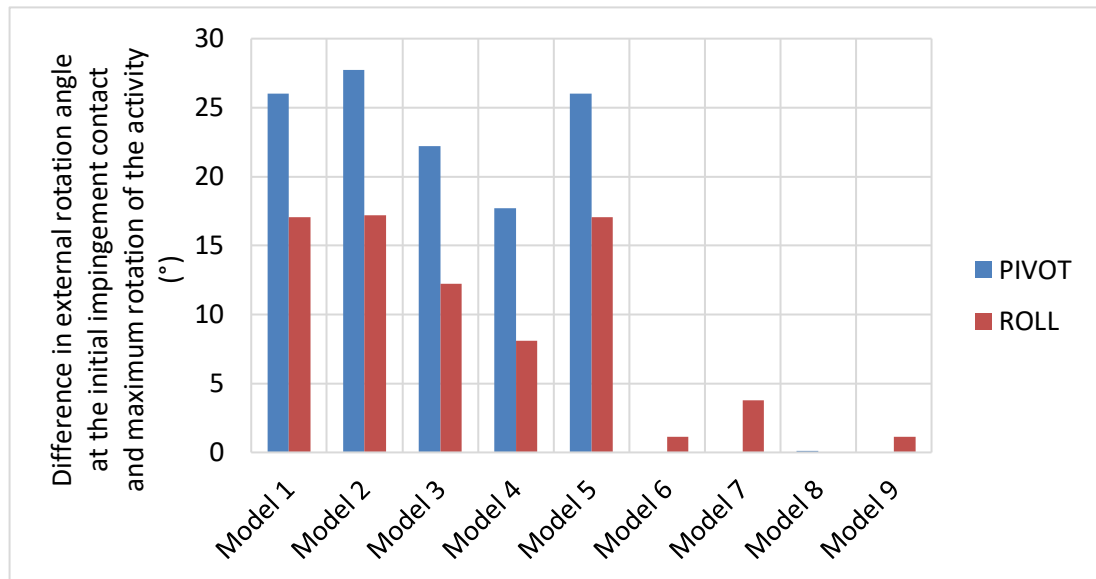


Figure 4.3 The difference in external rotation angle at the initial bone-on-bone impingement contact and maximum rotation of the activity in each of the nine geometric models of a THR during the anterior dislocation-prone activities (PIVOT and ROLL). Only severity of bone-on-bone impingement has been assessed this way (and not other types of impingement).

When comparing the severity of bone-on-bone impingement across the nine geometric models during the anterior dislocation-prone activities both in terms of the volumetric overlap and the difference in external rotation angle past the point of impingement, it was concluded that the morphology of the bony geometry had an effect on the severity of impingement.

4.3.3.2 The effect of the anteversion angle of the natural acetabulum

There was a significant ($p < 0.05$) correlation between the anteversion angle of the natural acetabulum and the severity of bone-on-bone impingement as measured by the volume of overlapping bones during both the PIVOT and ROLL activities (Figure 4.4). An increase in anteversion angle of 1° of the natural acetabulum typically resulted in an increase of 158mm^3 of volume of bone-on-bone impingement during the PIVOT activity and 277mm^3 of volume of bone-on-bone impingement during the ROLL activity. This could indicate that an increased anteversion angle of a patient's natural acetabulum could lead to an increased likelihood and severity of bone-on-bone impingement and potential subluxation/dislocation in THR patients.

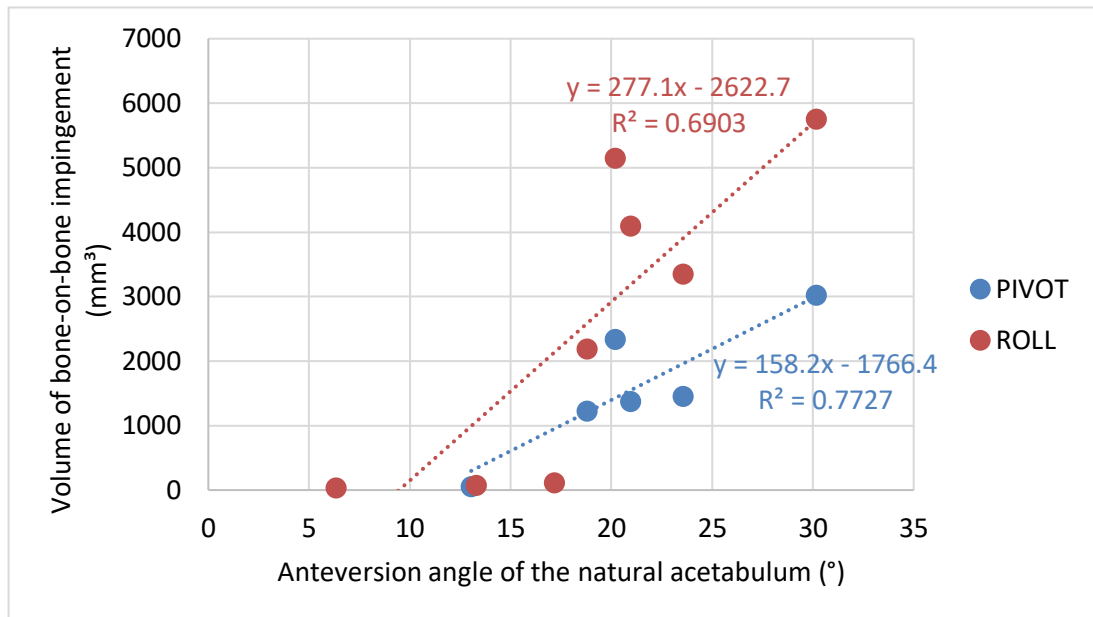


Figure 4.4 Effect of the anteversion angle of the natural acetabulum on the severity of bone-on-bone impingement during the PIVOT and ROLL activities. Each point represents one of the series of nine geometric models of a THR which encountered bone-on-bone impingement (i.e. six models as shown for the PIVOT activity (blue) in Figure 4.4).

There was a significant correlation ($p < 0.05$) between the anteversion angle of the natural acetabulum and the difference in external rotation angle past the point of impingement during the PIVOT and ROLL activities (Figure 4.5). An increase of 1° of anteversion of the natural acetabulum typically resulted in an increase of 1.6° external rotation angle past the point of impingement during the PIVOT activity and 0.8° external rotation angle past the point of impingement during the ROLL activity. This data further suggested that an increased anteversion angle of a patient's natural acetabulum could lead to an increased likelihood of bone-on-bone impingement and potential subluxation/dislocation in a patient's THR. This measure also gave an indication as to the angle that the femoral head could lever out during a potential impingement event, therefore increasing the likelihood of a potential dislocation.

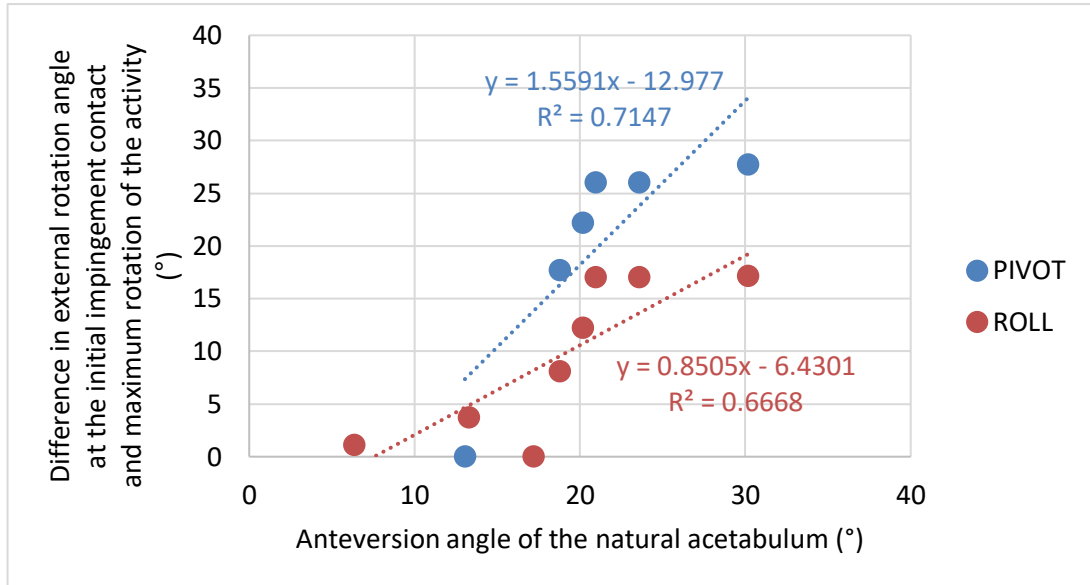


Figure 4.5 Effect of the anteversion angle of the natural acetabulum on the difference in external rotation angle at the initial bone-on-bone impingement contact and maximum rotation of the PIVOT and ROLL activities. Each point represents one of the series of nine geometric models of a THR which encountered bone-on-bone impingement (i.e. six models as shown for the PIVOT activity (blue) in Figure 4.5).

The ROLL activity had a steeper increase in volumetric overlap per degree of anteversion angle of the natural acetabulum when compared to the PIVOT activity. The difference in angle of the external rotation angle past the point of impingement increased more steeply for the PIVOT activity when compared to the ROLL activity.

4.3.4 Severity of bone-on-bone impingement for the posterior dislocation-prone activities

The majority of impingement occurrences during the posterior dislocation-prone activities resulted in bone-on-bone impingement. So that appropriate analysis could be done to investigate the effect of different bony geometries, only the severity of bone-on-bone impingement was investigated.

4.3.4.1 The effect of bony geometries

The posterior dislocation-prone activity which resulted in the greatest number of occurrences of impingement was the STOOP activity (7/9 geometric models) (Figure 4.1). Four out of seven of these occurrences resulted in bone-on-bone impingement and the volume of overlapping bones differed in each of these models during the STOOP activity (Figure 4.6). There were no occurrences of impingement during the XLG and SSL activities in any of the nine geometric models (Figure 4.1). There were some instances of impingement during the TIE (2/9 of the geometric models) and SSN (3/9 of the geometric models) activities.

To demonstrate the range in the volume of overlapping bones during the STOOP activity, the greatest volume of overlapping bones was 2388mm³ for bony geometry ID number 8 compared with the bony geometries which didn't result in any impingement (Figure 4.6). Such relatively large differences in the volume of impingement between geometric models during the same activity demonstrated the extent that the bony geometry could affect the likelihood and severity of impingement.

The geometric models that impinged during the TIE and SSN activities also had the greatest severity of impingement (as measured by the volume of overlapping bones) during the STOOP activity (bony geometry ID numbers 6 and 8). This suggested that these bony geometries had an increased likelihood of impingement during high flexion activities and if impingement were to occur would have a higher severity of impingement.

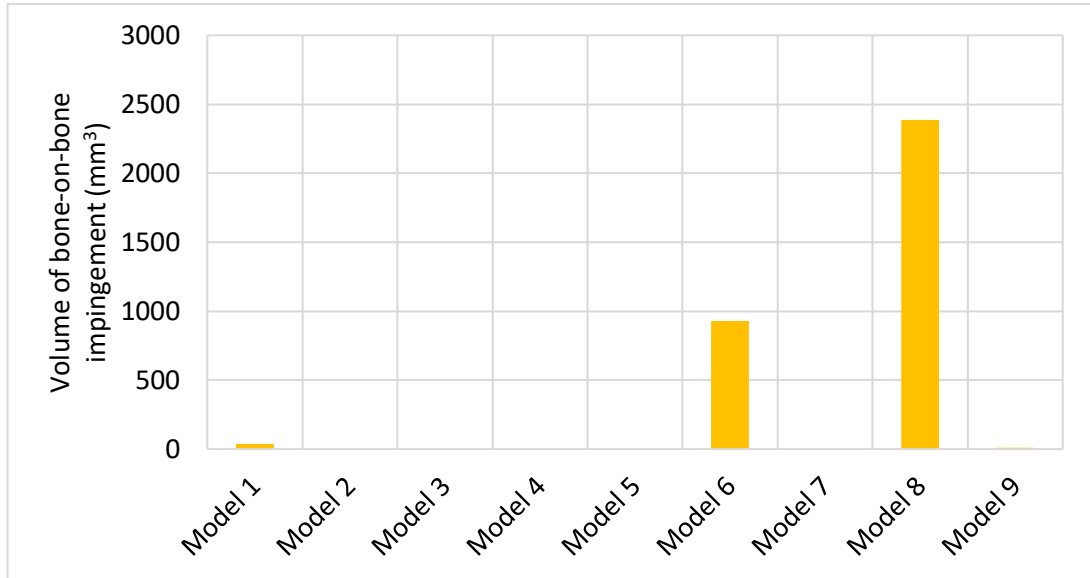


Figure 4.6 Volume of bone-on-bone impingement for each of the nine geometric models of a THR during the SToop activity. The impingement is recorded as zero if bone-on-bone impingement wasn't the first type of impingement encountered.

The difference in flexion angle past the point of impingement was also measured in each of the nine geometric models for the SToop activity (Figure 4.7). To demonstrate the range in angle of flexion past the point of impingement for the SToop activity, the greatest angle was 13.7° for bony geometry ID number 8 compared with the bony geometries which didn't result in any impingement (Figure 4.7). Such relatively large differences in the angle of flexion past the point of impingement between geometric models during the same activity demonstrated how much the bony geometry could affect the likelihood and severity of impingement.

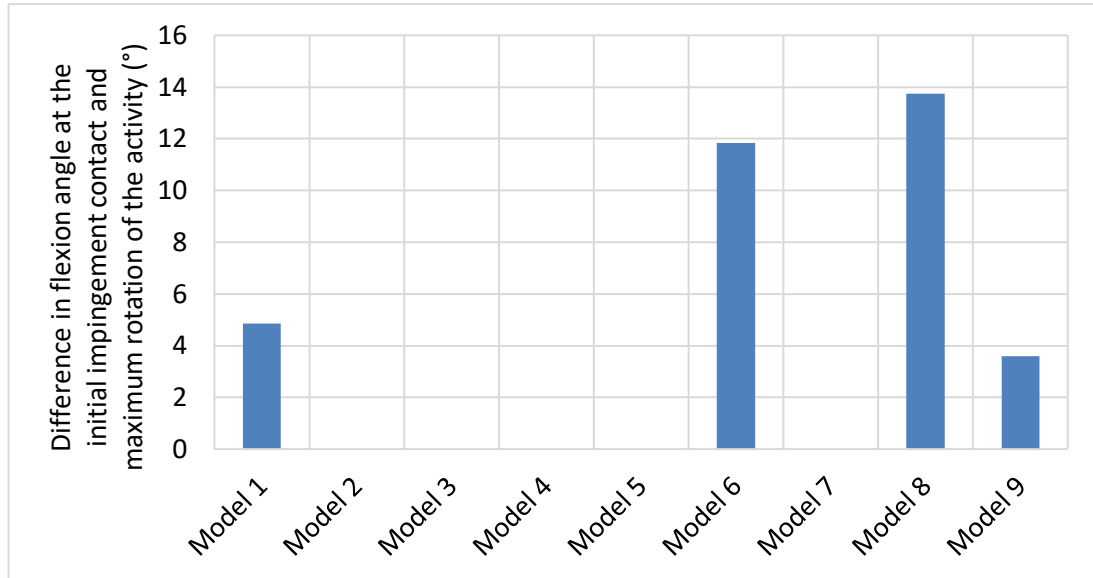


Figure 4.7 The difference in flexion angle at the initial bone-on-bone impingement contact and maximum rotation of the STOOP activity for each of the series of nine geometric models of a THR. Only the geometric models which encountered bone-on-bone impingement as the first impingement contact during the STOOP activity are displayed here.

When comparing the severity of bone-on-bone impingement across the geometric models during the posterior dislocation-prone activities, both in terms of the volumetric overlap and the difference in flexion angle past the point of impingement, the data suggested that the morphology of the bony geometry could have had an effect on the severity of impingement.

4.3.4.2 The effect of the location of the anterior inferior iliac spine

Of the posterior dislocation-prone activities, only the STOOP activity was assessed for a correlation with the AIIS location due to the limited occurrences of bone-on-bone impingement for the other activities. There were only four occurrences of bone-on-bone impingement out of the nine geometric models, therefore no correlation statistics were carried out.

There was generally a strong trend between the lateral AIIS location measure and the severity of bone-on-bone impingement as measured by the volume of overlapping bones during the STOOP activity (Figure 4.8). There was also generally a strong trend between the lateral AIIS location measure and the severity of bone-on-bone impingement as measured by the difference in

flexion angle past the point of impingement for the STOOP activity (Figure 4.9). This could indicate that an increase in the lateral location measure of the AHS could mean an increase in the likelihood and severity of impingement and potential subluxation/dislocation in a patient's THR.

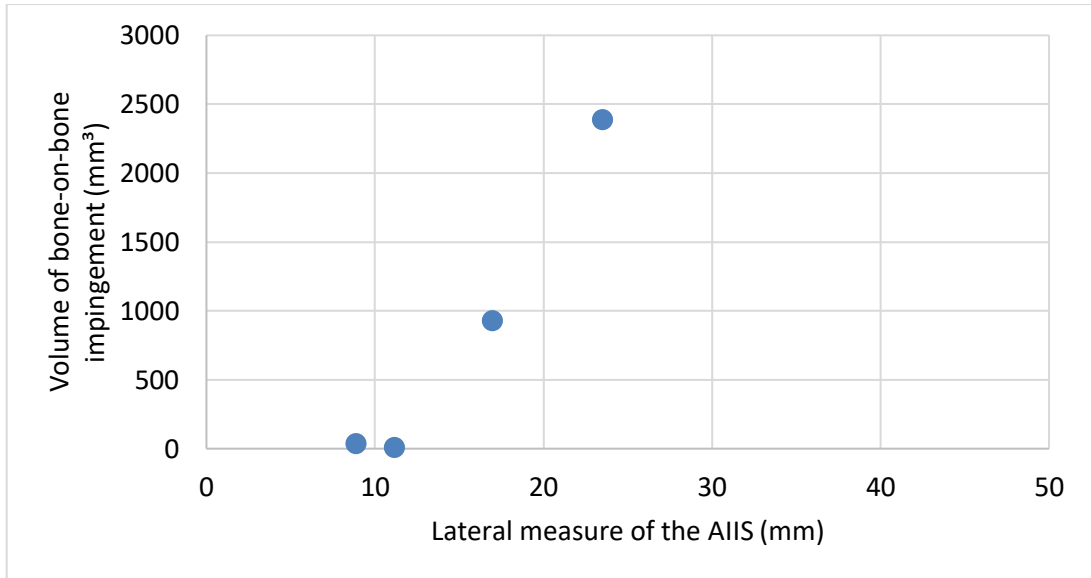


Figure 4.8 Effect of the lateral measure of the AIIS on the severity of bone-on-bone impingement as measured by the volume of overlapping bones during the STOOP activity. Each point represents one of the series of nine geometric models of a THR that encountered bone-on-bone impingement (i.e. four models as shown in Figure 4.8) (note; five of the geometric models did not show impingement).

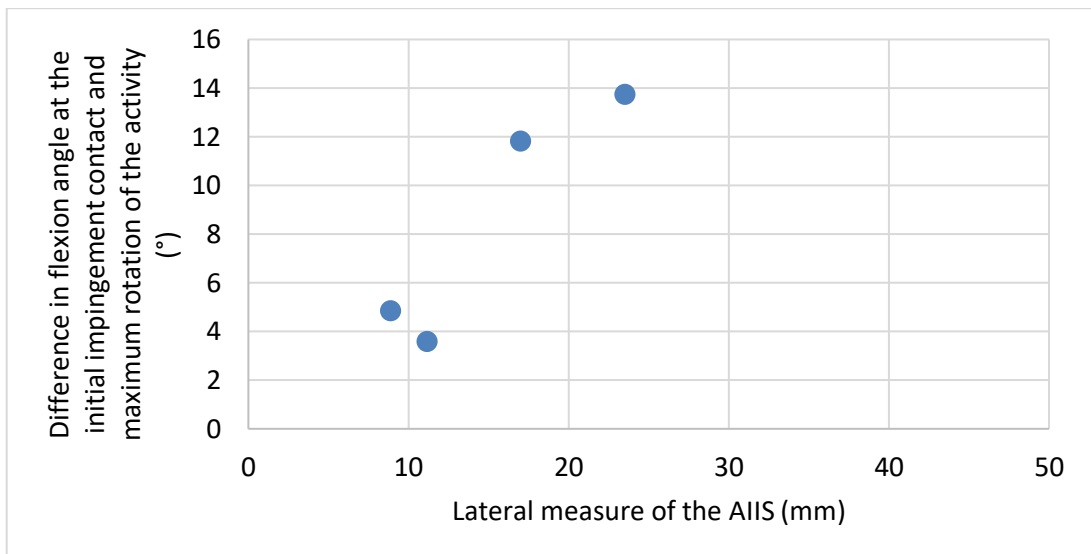


Figure 4.9 Effect of the lateral measure of the AIIS on the severity of bone-on-bone impingement as measured by the difference in flexion angle at the initial bone-on-bone impingement contact and maximum rotation of the STOOP activity. Each point represents one of the series of nine geometric models of a THR that encountered bone-on-bone impingement (i.e. four models as shown in Figure 4.9). (note; five of the geometric models did not show impingement).

The anterior measure of the peak of the AIIIS was compared with both measures of the severity of impingement during the STOOP activity. There was no observable trend between the anterior AIIIS location measure and the severity of bone-on-bone impingement as measured by the volume of overlapping bones during the STOOP activity (Figure 4.10). There was also no observable trend between the anterior measure of the AIIIS and the difference in flexion angle past the point of impingement (Figure 4.11). Therefore it was unlikely that the anterior measure of the AIIIS had any effect on the likelihood of impingement.

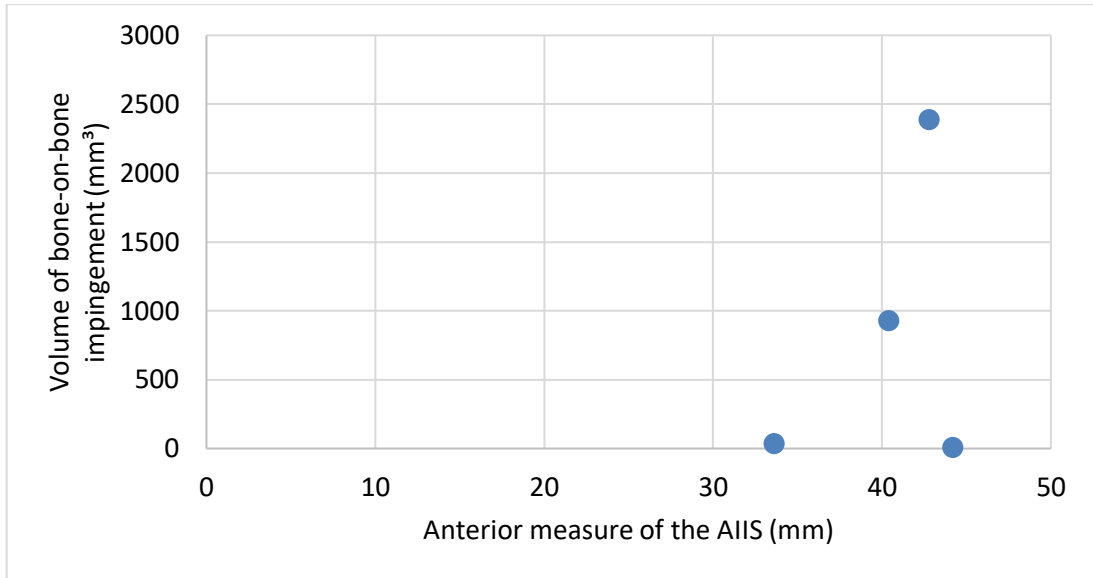


Figure 4.10 The effect of the anterior measure of the AIIS on the severity of bone-on-bone impingement as measured by the volume of overlapping bones during the STOOP activity. Each point represents one of the series of nine geometric models of a THR which encountered bone-on-bone impingement (i.e. four models as shown in Figure 4.10). (note; five of the geometric models did not show impingement).

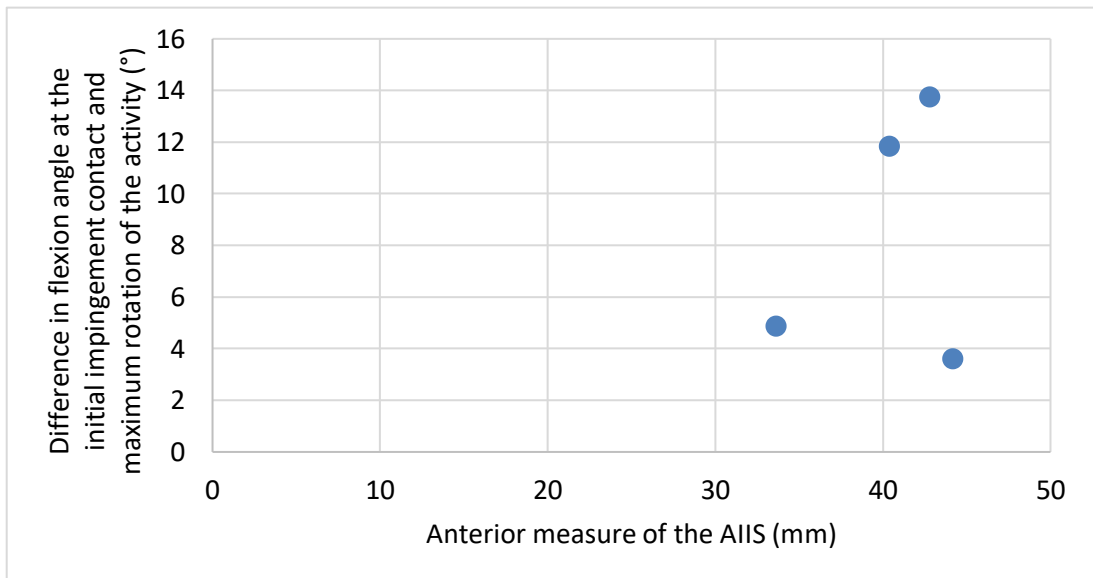


Figure 4.11 The effect of the anterior measure of the AIIS on the severity of bone-on-bone impingement as measured by the difference in flexion angle at the initial impingement contact and maximum rotation of the STOOP activity. Each point represents one of the series of nine geometric models of a THR which encountered bone-on-bone impingement (i.e. four models as shown in Figure 4.11). (note; five of the geometric models did not show impingement).

The superior measure of the peak of the AIIIS was compared with both measures of the severity of impingement during the STOOP activity. There was no observable trend between the superior AIIIS location measure and the severity of bone-on-bone impingement as measured by the volume of overlapping bones during the STOOP activity (Figure 4.12). There was also no observable trend between the superior measure of the AIIIS and the difference in flexion angle past the point of impingement (Figure 4.13). Therefore it was unlikely that the superior measure of the AIIIS had any effect on the likelihood of impingement.

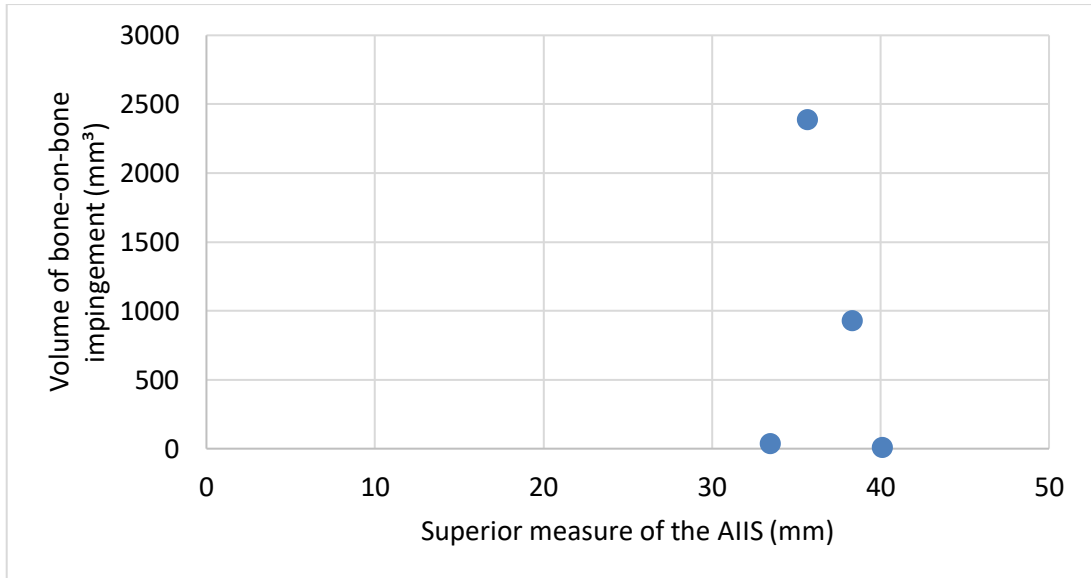


Figure 4.12 The effect of the superior measure of the AIIS on the severity of bone-on-bone impingement as measured by the volume of overlapping bones during the STOOP activity. Each point represents one of the series of nine geometric models which encountered bone-on-bone impingement (i.e. four models as shown in Figure 4.12). (note; five of the geometric models did not show impingement).

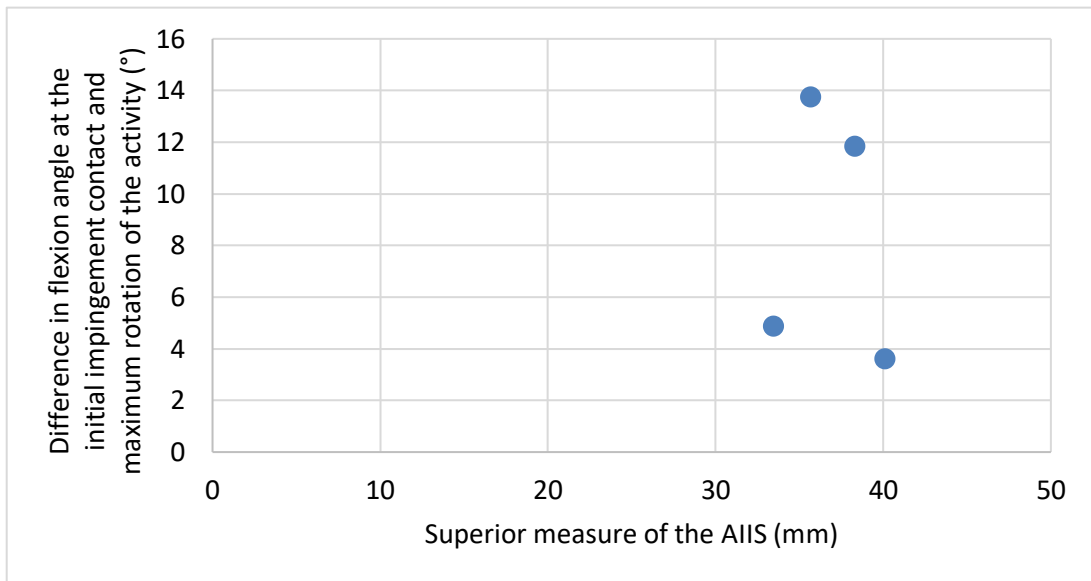


Figure 4.13 The effect of the superior measure of the AIIS on the severity of bone-on-bone impingement as measured by the difference in flexion angle at the initial impingement contact and maximum rotation of the STOOP activity. Each point represents one of the series of nine geometric models which encountered bone-on-bone impingement. (i.e. four models as shown in Figure 4.13). (note; five of the geometric models did not show impingement).

4.3.5 Bone-on-bone impingement sites

During the anterior dislocation-prone activities, the bone-on-bone impingement site was between the ischium and either the lesser trochanter or the intertrochanteric crest of the femur. The location of the bone-on-bone impingement was different depending on the activity. During the PIVOT activity, the impingement site was always between the lesser trochanter and the ischium (Figure 4.14A). This was because the PIVOT activity included a small amount of extension rotation and thus the closest impingement site through external rotation was between the lesser trochanter and the ischium. During the ROLL activity, the impingement site was always between the intertrochanteric crest of the femur and the ischium (Figure 4.14B). This was because there was no extension rotation during the activity, which was present in the PIVOT activity, and so the angle between the intertrochanteric crest of the femur and the ischium was the smallest as the femur externally rotated. During the posterior dislocation-prone activities, when bone-on-bone impingement occurred, the site was always between the AIIS and the anterior side of the femur (Figure 4.15).

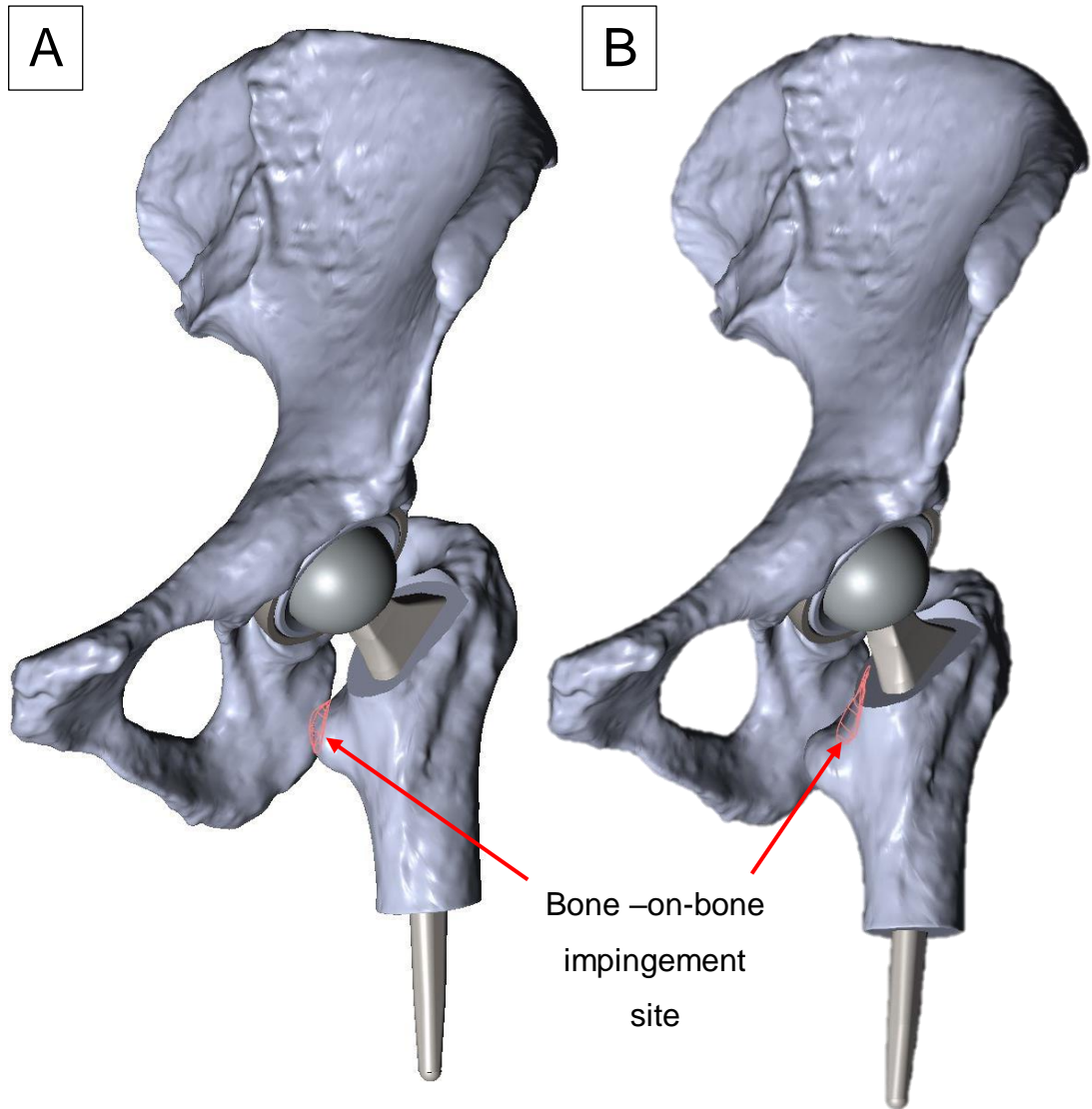


Figure 4.14 A coronal view of the same left hip geometric model demonstrating typical bone-on-bone impingement sites for the PIVOT and ROLL activities. (A) Bone-on-bone impingement at the posterior side of the hip between the ischium and the lesser trochanter for bony geometry ID number 1 during the PIVOT activity. The impingement site included the lesser trochanter. (B) Bone-on-bone impingement at the posterior side of the hip between the ischium and the intertrochanteric crest of the femur for bony geometry ID number 1 during the ROLL activity.

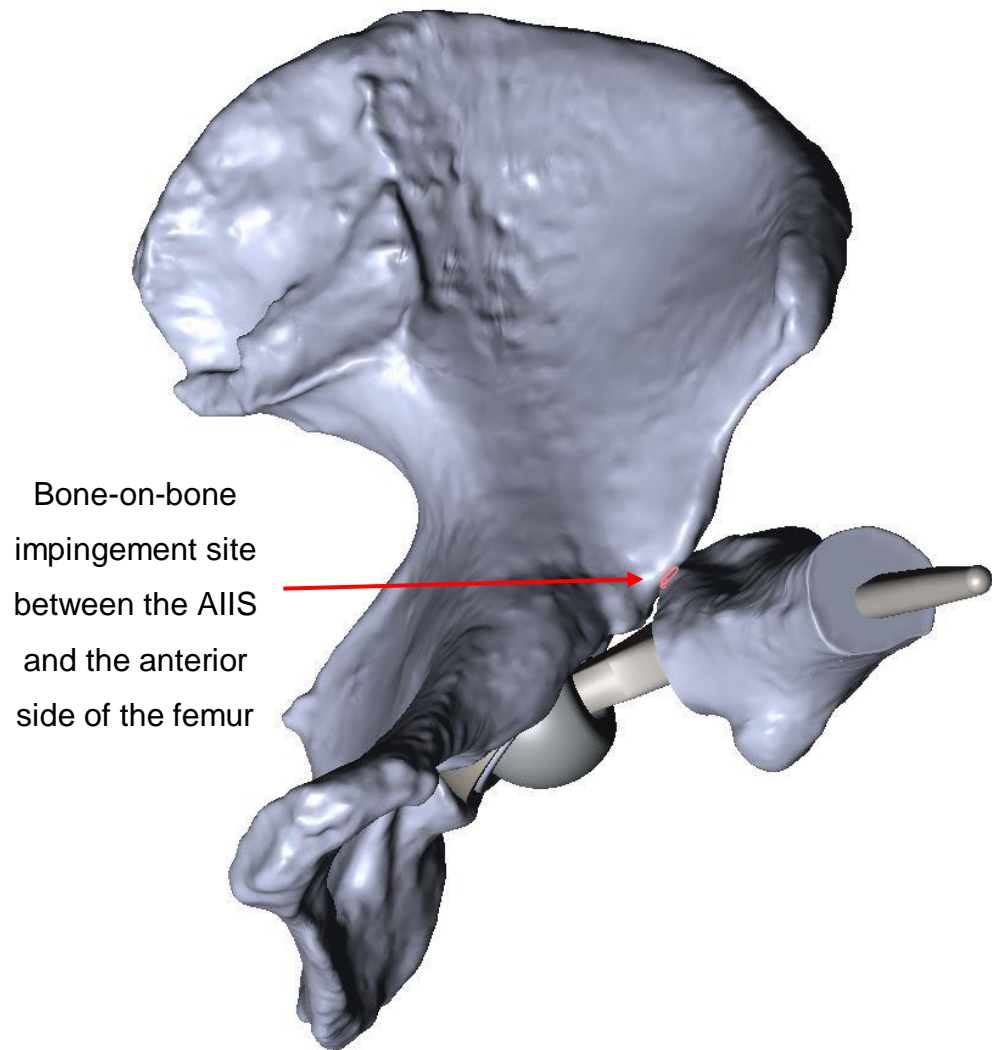


Figure 4.15 A view at a 45° angle to the coronal and sagittal plane of the left hip of the bony geometry ID number 1 during the STOOP activity. Typical bone-on-bone impingement site demonstrating the volumetric overlap (outlined in red) between the femur and the pelvic bone in the region of the AIIIS.

4.4 Discussion

Clinically-relevant dislocation-prone activities of daily living were applied to a series of nine THR geometric models and were compared for analysis into the change in type, occurrence and severity of impingement. The results suggested that the bony geometry had an effect on the type, occurrence and severity of impingement. This could mean that the geometry of a patient's bone affected the outcomes of impingement clinically; in particular that the location of the peak of the AHS and the anteversion angle of the natural acetabulum could be predictors for bone-on-bone impingement. The volume of overlapping bones and the difference in angle past the point of impingement could be used to indicate the severity of impingement and potential risk of dislocation in geometric models. Bony geometry should be assessed preoperatively to identify potentially high severity impingement-risk patients, and components should be chosen and positioned to minimise the potential risks of impingement.

4.4.1 Occurrence and types of impingement across differing bony geometries

The occurrences and types of impingement differed across the nine geometric models with most of the impingement occurrences being bone-on-bone impingement. This is thought to be because of the use of a large femoral head (36mm) and a well-orientated cup position in each model. It has been demonstrated previously that increasing the size of the femoral head has led to an increase in the RoM and a shift in the restricting factor from implant-on-implant impingement to bone-on-bone impingement (Burroughs, et al., 2005).

While there have not been any studies which have investigated the effect of a change in bony geometries during dislocation-prone activities, the RoM has been used to compare them which would give an indication as to the difference in impingement likelihood (Patel, et al., 2010; Shoji, et al., 2013). The results from these studies as well as Chapter Three of this thesis (Section 3.3.2) found that the RoM differed across different bony geometries, agreeing with the results from the current study. The change in type and occurrence for

the different bony geometries indicated that clinically, the geometry of a patient's bone could affect the likelihood of impingement in their THR as well as the damage which could occur as a result of this impingement.

4.4.2 Effect of the anteversion angle of the natural acetabulum on the severity of impingement

The anteversion angle of the natural acetabulum in each geometric model had a significant effect on the severity of impingement as measured by the volumetric overlap of bones in the geometric models and the difference in external rotation angle past the point of impingement, during the anterior dislocation-prone activities. An increase in the anteversion angle typically resulted in an increase in the severity of impingement, suggesting that the anteversion angle of the natural acetabulum could be used as a predictor for bone-on-bone impingement and potential severity of the impingement.

There have been no studies which investigated the effect of the anteversion angle of the natural acetabulum on impingement, however there have been studies which investigated the RoM in the natural hip and how this was affected by the anteversion angle of the natural acetabulum (Nakahara, et al., 2011; Morris, et al., 2018). These studies were in agreement that an increase in the anteversion angle of the natural acetabulum resulted in a decreased RoM both in a cadaveric study of 206 natural hips (Morris, et al., 2018) and a computational study using CT scans of 106 natural hips (Nakahara, et al., 2011). A lower RoM could result in an increased likelihood and severity of impingement in THR patients, therefore it could be concluded that the current study agreed with the previous RoM studies.

An increased anteversion of the natural acetabulum could suggest a wider bony geometry of the pelvis where the ischium is positioned further forwards resulting in the angle between the ischium and the intertrochanteric crest or the lesser trochanter of the femur being reduced, with increasing anteversion of the natural acetabulum leading to an increased likelihood of impingement.

4.4.3 Effect of the location of the AIIIS on the severity of impingement

There was a strong trend between the lateral measure of the AIIIS in each geometric model and the severity of bone-on-bone impingement as measured by the volume of overlapping bones during the STOOP activity. This indicated that the lateral measure of a patient's AIIIS on their pelvis could be used as a predictor for bone-on-bone impingement during high flexion activities.

One study (Shoji, et al., 2016) concluded that the lateral measure of the AIIIS had a significant effect on the flexion RoM with an increased lateral measure resulting in reduced flexion. The previous work in this thesis in chapter three also concluded that the RoM was significantly reduced by the lateral measure of the AIIIS. This reduction in RoM because of the lateral measure of the AIIIS would have also meant that the severity of impingement would increase under kinematic data of known ranges of motion, therefore agreeing with the current study's conclusions. The same study also found the flexion RoM had significant correlations with other AIIIS measures including the anterior and superior measure of the AIIIS, however a trend was not found in the current study. The differences in the anterior and superior measures in the current study could have been subtle and not sufficient so as to generate a significant result. There was also a difference in components, component sizing and geometric model setup between the studies which could have caused slight differences in the results. The method of finding the CoR was not described in detail and the differences in method could have resulted in a difference in the biomechanics of the test.

There were only four occurrences of bone-on-bone impingement during the STOOP activity and therefore no correlation statistics were carried out due to this low number. There were some studies whose computational models resulted in bone-on-bone impingement of the AIIIS during high flexion activities (Patel, et al., 2010; Shoji, et al., 2016), however neither of these studies investigated the AIIIS itself and its effect on the likelihood or severity of impingement. Some of the studies identified the Hetsroni classification type of

the AIIIS and related this to the RoM, however the location of the AIIIS peak was not investigated (Tabata, et al., 2019).

4.4.4 Effect of different activities on the severity of impingement

Comparing the seven dislocation-prone activities of daily living; the activities which recorded the greatest number of occurrences of impingement in the nine geometric models as well as the greatest severity of impingement were the two anterior dislocation-prone activities (PIVOT and ROLL). One geometric model study (Pryce, et al., 2022) which used one bony geometry found that the ROLL activity also resulted in the greatest number of impingement occurrences when the cup orientation was varied, however there were reduced amounts of impingement during the PIVOT activity. One of the geometric models in the current study (bony geometry ID number 6) also resulted in impingement during the ROLL activity but no impingement during the PIVOT activity which could mean that the bony geometry used in this study (Pryce, et al., 2022) could have had similar bony features to bony geometry ID number 6. The offset and difference in component size could also have affected this with an increased offset expected to reduce impingement. A finite element analysis study (Pedersen, et al., 2005) also investigated cup orientation using these activities, however the study did not include any bony geometry and therefore, with the ROLL and PIVOT activities mostly resulting in bone-on-bone impingement in the current study, the finite element analysis study resulted in minimal impingement for these activities. This highlighted the importance of including bony geometries in computational studies of THRs. One FEA study (Elkins, et al., 2012) which included bony geometry, investigated these activities with a 42mm liner and femoral head and found no occurrences of impingement for any of the activities, disagreeing with the current and previous studies. The size of the femoral head used as well as the shape of the bony geometry used could most likely have been the reasons for this lack of impingement.

The posterior dislocation-prone activity which resulted in the greatest number of occurrences and greatest severity of impingement was the STOOP activity.

One geometric model study (Pryce, et al., 2022) which included one bony geometry also found that the STOOP activity had the greatest number of impingement occurrences when the cup orientation was varied. The majority of well-positioned cup orientations however resulted in implant-on-implant impingement instead of the mostly bone-on-bone and implant-on-bone impingement found in the current study. The reason for this could be because the 36mm THR components used in the current study were larger than the 32mm THR components used in this study (Pryce, et al., 2022) and therefore it would be expected that the current study would result in an increased number of occurrences of bone-on-bone impingement at the same cup positions. A RoM study (Patel, et al., 2010) which replicated the rotations from the activities in the current study found that the STOOP activity allowed the lowest RoM out of all of the posterior dislocation-prone activities, agreeing with the current study. Some finite element analysis studies (Pedersen, et al., 2005; Ghaffari, et al., 2012) used simplified geometries to test various component features using the activities from the current study. Both of these studies also concluded that the STOOP activity was the most severe activity as measured by the greatest number of impingement occurrences when the cup orientation was varied (Pedersen, et al., 2005) and the angular margin to impingement measured throughout the activity (Ghaffari, et al., 2012). Neither of the two FEA studies included any bone and therefore the impingement occurrences encountered were all implant-on-implant impingement.

Clinicians advise against the use of low heighted chairs to avoid dislocation post-THR surgery, however the current study found that the SSN (sit to stand from a normal heighted chair) activity resulted in more impingement occurrences than the SSL (sit to stand from a low heighted chair) activity. This agreed with previous studies (Pedersen, et al., 2005; Pryce, et al., 2022) and is thought to be because of the increased internal rotation associated with the SSN activity which reduced the angle of flexion to impingement during high flexion activities. The kinematic dataset used in these studies including the current study consisted of a single subject representing a cohort of 10 non-THR subjects and therefore this difference in the SSN and SSL activities may

only exist when comparing these two particular subject's activities. It is not known whether this difference in kinematics of the SSN and SSL activities would exist in a wider population.

The SSL and XLG activities resulted in no occurrences of impingement for any of the nine geometric models and were deemed the safest activities of the seven. One study (Pryce, et al., 2022) had similar results, the SSL and XLG activities resulted in the least number of impingement occurrences out of a range of cup orientations. Another study (Patel, et al., 2010) also found that the simplified XLG and SSL activity rotations allowed the largest RoM out of the activities, further agreeing with the relative safety of these two activities. Two finite element analysis studies (Pedersen, et al., 2005; Ghaffari, et al., 2012) were in agreement that the XLG activity was one of the safest activities as measured by the lowest number of cup orientations which impinged and the largest angular margin to impingement respectively. All of these studies used the same activity dataset however and it is not clear whether these activities would be considered safe when carried out by different subjects.

4.4.5 Bone-on-bone impingement sites

When bone-on-bone impingement occurred during the posterior dislocation-prone activities, the impingement site was between the AIIIS and the anterior side of the femur. Other geometric model studies also found that the AIIIS and anterior side of the femur was the bone-on-bone impingement site during high flexion positions (Patel, et al., 2010; Hetsroni, et al., 2013; Shoji, et al., 2016; Tabata, et al., 2019). The FEA studies which have investigated impingement using dislocation-prone activities did not include any bone and therefore could not be compared (Pedersen, et al., 2005; Ghaffari, et al., 2012). One study (Kessler, et al., 2008) investigated RoM in a THR geometric model and found that the RoM was limited by impingement occurring between the anterior side of the femur and the superior rim of the acetabulum during pure flexion. This difference in impingement site could have been attributed to the geometry of the patient's bone used in the model as the study only included one bony geometry. The study also only used pure flexion to investigate high flexion positions which were different biomechanics to the dislocation-prone activities

investigated in the current study, potentially explaining the differences between the impingement sites. The lateral measure of the AIIIS was an effective measure to identify potentially problematic bony geometries for impingement at the anterior of the hip during the STOOP activity.

When bone-on-bone impingement occurred during the anterior dislocation-prone activities, the impingement site was between the ischium and the lesser trochanter during the PIVOT activity and between the ischium and the intertrochanteric crest of the femur during the ROLL activity. The PIVOT activity consisted of external rotation with a small amount of extension of the femur meaning that the lesser trochanter was rotated more posteriorly than a simple external rotation and therefore resulted in impingement on the lesser trochanter. The ROLL activity was also mostly external rotation however did not contain the added extension which was in the PIVOT activity, and also had a small increase in adduction which is why the ROLL activity avoided the lesser trochanter impinging and instead the intertrochanteric crest of the femur impinged on the ischium.

During the RoM studies, pure external rotation was used which closely resembled the movements of PIVOT and ROLL. Some of the studies found bone-on-bone impingement between the posterior side of the femur (intertrochanteric crest) and the ischium when investigating pure external rotation (Kessler, et al., 2008; Shoji, et al., 2017) and some studies found bone-on-bone impingement between the lesser trochanter and the ischium when investigating pure external rotation (Patel, et al., 2010; Shoji, et al., 2016) which agreed with the two bone impingement sites in the current study. The difference in impingement site between studies could have been attributed to the components used, the positioning of the components or the geometry of the bones used in each study. The anteversion angle of the natural acetabulum was an effective measure to identify potentially problematic bony geometries for impingement at the posterior of the hip during the anterior dislocation-prone activities. The geometry of the lesser trochanter could also be investigated in future work to improve understanding of impingement risks.

4.4.6 The severity of impingement measures

The volume of impingement overlap used in the geometric models demonstrated how much volume would be displaced during an impingement event. When impingement did occur, the volume of impingement could be used as an indicator for potential subluxation and dislocation due to the levering out mechanism of impingement (Brown, et al., 2014). An increased amount of subluxation could also mean an increased amount of applied stress to the bearing surface of the liner following a subluxation event as well as the potential for edge loading. If implant-on-implant impingement were to occur, an increased volumetric overlap in the model could lead to increased damage with greater severities of volumetric overlap resulting in greater forces at the liner rim.

The method of measuring the severity of impingement presented in the current study used the volume of overlapping bones and the difference in angle past the point of impingement during clinically-relevant dislocation-prone activities. This method provided a way of interpreting severity of impingement for comparison across activities and bony geometries. Computational model studies on impingement have concentrated on the RoM of geometric models (Barsoum, et al., 2007; Kessler, et al., 2008; Ji, et al., 2010; Ezquerra, et al., 2017) and the occurrence of impingement during activities of daily living (Pedersen, et al., 2005; Patel, et al., 2010; Ghaffari, et al., 2012; Pryce, et al., 2022), however there was a lack of analysis into the severity of the reported occurrences of impingement. Some of these studies varied the acetabular cup orientation and used the number of cup orientations which resulted in impingement as a form of severity measure (Pedersen, et al., 2005; Pryce, et al., 2022). Some studies (Turley, et al., 2013; Palit, et al., 2017) have measured the RoM in patient's CT scan data and compared it with an "expected" RoM which was defined by previous activity data. The severity measure included the RoM of the CT scan which was greater than the "expected" RoM which would denote impingement, with a larger RoM area of impingement representing a more severe impingement clinically. This method had only limited relevance however, as the output was calculated using an

expected RoM calculated from different sources and would not be the same for every patient, therefore could have given incorrect indications about possible impingement. A RoM “area” also made the data difficult to interpret. The RoM was also in all directions some of which were not clinically relevant for the function of a THR. The current study generated a more clinically-relevant method for comparing the severity of impingement with different geometric model conditions.

When comparing the two severity of impingement measures; volumetric overlap of bones and the difference in external rotation angle past the point of impingement for the PIVOT and ROLL activities, a higher difference in angle did not result in a higher volume of severity for the majority of geometric models (Figures 4.2. 4.3. 4.4 & 4.5). This difference was due to the change in impingement site for the PIVOT and ROLL activities. The lesser trochanter is a smaller bony feature and therefore would produce a limited amount of volumetric overlap when the difference in the angle of the external rotation past the point of impingement was increased. All of the posterior dislocation-prone activities of daily living impinged on the AIIIS, therefore the results for the volume of overlapping bones were comparable across activities due to the same impingement site. Therefore, both measures of severity should be used to gain a full analysis of the conditions surrounding the impingement of the geometric models when there are different impingement sites.

4.4.7 Clinical significance

The use of larger heads in total hip replacement has become more prevalent due to the favourable range of motion and reported reduction in impingement/dislocation (Cuckler, et al., 2004; Jameson, et al., 2011; Stroh, et al., 2013; Waddell, et al., 2018). This means that the restriction of RoM in THRs shifts from implant-on-implant impingement to bone-on-bone impingement. The variation in the bony geometries across the series of geometric models in this study demonstrated the effect that a patient’s bony geometry could have on the occurrence, type and severity of bone-on-bone impingement. The bony features outlined in this study could be used as predictors for bone-on-bone impingement preoperatively and care should be

taken to maximise the RoM when selecting and implanting components in patients who have a laterally large AIIS or a large anteversion angle of the natural acetabulum. The variation in the RoM of different patient's bony anatomy could affect the way in which impingement damage and potential subluxation/dislocation could occur due to the change in impingement mechanics and loading across different patients and their kinematic activities of daily living.

When bone-on-bone impingement is the limiting factor to RoM, factors such as increasing the component offset, which has been previously demonstrated to reduce impingement (Matsushita, et al., 2009; Shoji, et al., 2016; Jinno, et al., 2017), can be used to maximise RoM. The use of resection of the AIIS has been demonstrated clinically (Davidovitch, et al., 2015) and could be an option to reduce impingement on the AIIS in extreme cases intraoperatively.

The dislocation-prone activities used in this study demonstrated that impingement occurred even in models with well-positioned components and large femoral heads, and therefore care should be taken when advising on the use of these high RoM activities after THR surgery, in particular the STOOP, PIVOT and ROLL activities which resulted in the greatest number of occurrences of impingement in the geometric models.

4.4.8 Limitations of the study

There were limitations to this study. Firstly, the geometric models used in this study were developed in Chapter Two and therefore the same limitations applied, which were described in Section 2.3.1.

Secondly, the method of data collection for the previously published (Nadzadi, et al., 2003) kinematic dataset of dislocation-prone activities included measuring the activities of 10 subjects (note these were not THR patients) and selecting one of those subjects at the median, to represent the 10 subjects for each activity. There was variability between the subject selected and the rest of the cohort for each activity, therefore the results from the current study may not have been the same if the kinematic data of the other subjects were

used. It is also not known whether the kinematic data of the subjects were typical of a population, therefore the results and conclusions from this study should be used with caution when applied to a whole population. It is also not known whether the subjects were blinded to the study or whether they knew that this was a study analysing dislocation, which could have affected the manner in which the subjects carried out their set of activities.

Thirdly, the kinematic dataset consisted of femoral rotations in relation to a fixed pelvis. The method of data collection used by the previous study (Nadzadi, et al., 2003) for the kinematic dataset, meant that the pelvic movement of the subjects during the activities was included in the data. Therefore each activity included an unknown amount of pelvic movement depending on which subject was selected to represent the cohort for each activity and how much their pelvis moved during the activity. The pelvic rotations of individual subjects has been previously shown to differ (Pierrepont, et al., 2017), therefore any analysis of patient-specific pelvic movements could not be investigated with these models and this kinematic data.

Finally, the series of nine geometric models were modelled from an online CT scan repository (Johnson, et al., 2008) and the kinematic activities of daily living were from a previously published dataset (Nadzadi, et al., 2003). Therefore the combination of two different sources for the geometric models and kinematic data could mean that the subjects from the CT scan repository who had the individual bony geometries could produce different results and conclusions, if their kinematic data was available for testing.

4.5 Summary

The aim of this chapter was to investigate the effect of bony morphology on the type, occurrence and severity of impingement during seven dislocation-prone activities of daily living in a series of nine geometric models of total hip replacements. All of the activities were applied to all of the geometric models. Bony features involved in typical bone-on-bone impingement sites during

these dislocation-prone activities of daily living were investigated for their effect on the bone-on-bone impingement. These bony features included the location of the anterior inferior iliac spine (AIIS) on the pelvis during the posterior dislocation-prone activities (prone to anterior impingement) and the anteversion of the natural acetabulum during the anterior dislocation-prone activities (prone to posterior impingement).

It was concluded that the geometry of the bone had an effect on the type, occurrence and severity of impingement during clinically-relevant dislocation-prone activities. For the anterior dislocation-prone activities, the anteversion angle of the natural acetabulum had a significant effect on the severity of bone-on-bone impingement as measured by the volume of overlapping bones and the angle past the point of impingement. For the posterior dislocation-prone activities, there was a strong trend between the lateral measure of the peak of the AIIS and the severity of bone-on-bone impingement as measured by the volume of overlapping bones. These bony features could be used as predictors for bone-on-bone impingement. This study demonstrated the need for multiple geometries of bone to be considered in computational modelling studies when investigating impingement conditions.

This chapter demonstrated that some bony features significantly affected the severity of impingement in total hip replacements during dislocation-prone activities including which dislocation-prone activities of daily living were more likely to result in impingement. The results presented in this chapter used single subject kinematic data for each activity, therefore the results and conclusions made about the severity of impingement would apply if the subject used in the data was being analysed, however other subject's activity data may not result in the same conclusions. Therefore it is recommended that individual subject-specific kinematic data be used to further analyse the conditions of impingement during dislocation-prone activities of daily living.

Chapter Five : Subject-specific kinematic activities of daily living and their effect on impingement in THR's

5.1 Introduction

Variation is observed between subject kinematics when carrying out activities of daily living. Therefore there could be variation between THR patients in terms of the likelihood of impingement when carrying out specific activities. Kinematic datasets of activities of daily living which were potentially prone to impingement have been collected in previous studies (Nadzadi, et al., 2003; Sugano, et al., 2012; Layton, et al., 2021) and have been used in computational studies to investigate different parameters associated with impingement in THRs (Nadzadi, et al., 2003; Pedersen, et al., 2005; Hemmerich, et al., 2006; Patel, et al., 2010; Ghaffari, et al., 2012; Saputra, et al., 2013).

One of the kinematic activity datasets represented a mean of multiple subjects carrying out the same activities and analysed the joint angles of the activities (Sugano, et al., 2012), another dataset used a chosen subject from a cohort to represent the median movements of the cohort for each activity (Nadzadi, et al., 2003). These studies therefore included no subject variation and could not be analysed on a subject-specific basis. One kinematic dataset (Layton, et al., 2021) included thirteen activities of daily living, most of which were considered to be impingement-prone, carried out by eighteen subjects and included the subject variation for each activity. This dataset had not been used in any investigations into impingement in THRs. This kinematic dataset (Layton, et al., 2021) was therefore used with one of the geometric models to investigate the effect of subject variation in kinematics on impingement in THRs.

The effect of the orientation of the acetabular cup on impingement and dislocation has been investigated previously in the literature. A previously defined safe zone has been reported as an area of cup orientation which produced a reduced number of dislocation occurrences (Lewinnek, et al.,

1978). This safe zone was defined as between 30°-50° radiographic inclination and 5°-25° radiographic anteversion and is still widely used clinically as a guide for acetabular cup placement. This safe zone has been disputed however (Minoda, et al., 2006; Abdel, et al., 2016; Danoff, et al., 2016) including one study which produced their own “safe zone” based on retrospective dislocations at a different institution (Danoff, et al., 2016). Clinically, acetabular cup orientations have been found to be positioned between 18-80° inclination and (-)17-48° anteversion (Minoda, et al., 2006; Danoff, et al., 2016) in studies of THR populations. There have been a number of computational studies which have concluded that the orientation of the acetabular cup can influence impingement and potential dislocation during impingement-prone activities (Pedersen, et al., 2005; Ghaffari, et al., 2012; Pryce, et al., 2022), however they have all used the same kinematic dataset of one subject’s activity (Nadzadi, et al., 2003). Therefore investigating the effect of cup orientation on impingement for a subject with the same bony anatomy, but different subject-specific activity data would add new understanding in this area.

The kinematic dataset collected previously (Layton, et al., 2021) included eighteen subjects (not THR patients) between the ages of 20 and 70 years (mean of 44.2 years). Each subject carried out five trials of thirteen activities. These activities were walking, walk and turn, incline walk, decline walk, stand to sit, sit to stand, cross legs, squat, stand reach, kneel reach, lunge, golf swing and cycling. The gathered data consisted of the relative movements between the femur and pelvis, therefore spinopelvic movements were included in the data.

The aim of this study was to investigate acetabular cup orientation and its effect on impingement in THR’s using kinematic data of different subjects to understand not only the effect of the cup orientation on impingement but also the effect of the kinematic data itself. One of the series of nine geometric models (i.e. a single bony geometry) was used to investigate the type, occurrence and severity of impingement at different acetabular cup orientations.

5.2 Method

5.2.1 Overview of study design

Eight impingement-prone activities were applied to one of the geometric models from the series of nine geometric models developed in Chapter Two (section 2.2). One bony geometry was chosen so that the focus of this study could be on the cup orientation and kinematic data with subject variation and not the effect of the bony anatomy. The severity of impingement was assessed in the squat activity of the different subjects when the acetabular cup was malpositioned. The effect of a range of acetabular cup orientations was then investigated for all activities. The acetabular cup was varied between 30°-50° radiographic inclination and 0°-30° radiographic anteversion (5° increments). A grid for each activity which included all 35 of the acetabular cup orientations was produced which demonstrated the impingement occurrences at each cup orientation. A grid for each subject was then produced including all 35 of the acetabular cup orientations and the impingement occurrences at each cup orientation.

5.2.2 Individual kinematic activity data (Layton, et al., 2021)

The individual kinematic activity dataset consisted of 18 subjects carrying out 13 common activities of daily living. The data also consisted of five trials of each activity for each subject. Therefore there were five individual attempts of the same activity for each of the subjects. Due to issues with data collection in the original study, there was not a complete set of 18 subjects for each of the 13 activities, however there were at least 8/18 subjects for each activity. The individual femoral movements in relation to the pelvis were recorded for each of the subjects during each trial of each activity, therefore the spino-pelvic movement was included in the data. The kinematic data for each trial consisted of a number of discrete positions which made up the dynamic activity. The positions consisted of a flexion/extension angle, an adduction/abduction angle and an internal/external rotation. The activities were applied in a Cardan angle sequence of flexion/extension, adduction/abduction and then internal/external rotation. Due to the amount of

individual kinematic activity data, the number of trials and activities were reduced for a focussed analysis (Figure 5.1).

Firstly, only the activities which were considered to be impingement-prone were included, therefore the 13 activities were reduced to eight activities (“impingement-prone activities”). This was carried out by testing the activity data in the geometric model with a malpositioned cup (30° radiographic inclination and 0° radiographic anteversion) and using only the activities which resulted in more than two impingement events. The individual kinematic activity data for the eight activities consisted of two anterior dislocation prone activities which were prone to posterior impingement (“posterior impingement-prone activities”) including a golf swing, and walking followed by a turn. There were also six posterior dislocation-prone activities which were prone to anterior impingement (“anterior impingement-prone activities”) including reaching forward from a kneeling position to simulate gardening, lunge, sitting crossed legged, squat, reaching forward whilst standing and sitting down from a standing position.

Secondly, there were exclusions to reduce the five trials for each subject down to one trial per subject in the dataset. Only the trial which yielded the highest RoM for each subject’s activity was included in the analysis as this would be the trial which would result in the greatest likelihood of impingement. This reduction in the number of trials accounted for some subjects who may have needed a couple of attempts to get used to the movement and therefore reach a more natural range of motion during the activity. This resulted in up to 18 subjects carrying out eight impingement-prone activities (one trial each) which allowed for the subsequent impingement analysis.

Finally, for part of the testing, only the subjects whose activity data included all eight activities was required to analyse the impingement on a subject-specific basis. A further reduction was carried out for this particular testing resulting in six subjects whose data included all eight impingement-prone activities (one trial each) to analyse the effect of kinematic subject variation on impingement. Only the subjects whose data included all eight of the

activities were selected for the subject-specific analysis as the comparisons would not be appropriate if some subjects had missing activity data.

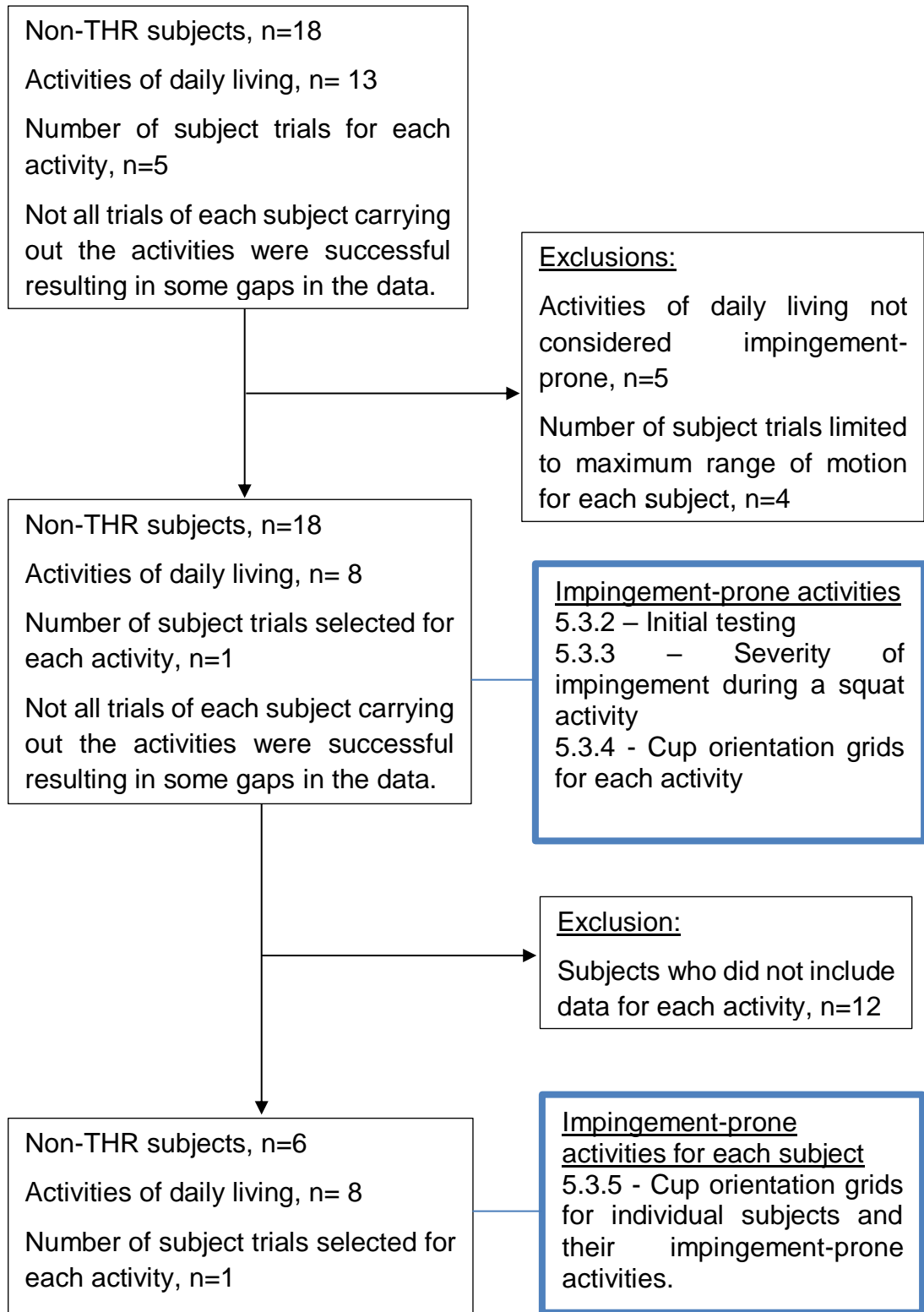


Figure 5.1 Consort diagram of how the individual kinematic activity data (Layton, et al., 2021) was focussed for each study section and analysed. The blue boxes label the results section of the study which the data was used in.

5.2.3 Initial testing

The impingement-prone activities were applied to bony geometry ID number 8 which was chosen because it was the geometric model which had the lowest RoM across the nine geometric models from the results of Chapters Three and Four (Sections 3.3 and 4.3). One bony geometry was chosen so that the focus of this study could be on the cup orientation and kinematic data with subject variation and not the effect of the bony anatomy. The components in the geometric model were also changed from 36mm components to 28mm components as the smaller femoral head size would allow for reduced range of motion and therefore increased occurrences of impingement for analysis which has been highlighted in the literature (Section 1.3.1.1).

The series of nine geometric models developed in Chapter Two (Section 2.2) included THR components produced by DePuy Synthes which were a simplified Pinnacle® 100 series shell (54mm), a simplified DePuy Pinnacle® neutral liner (36mm/54mm), an Articul/Eze M-spec™ metal head (36mm) and a Corail® standard stem (size 12). The femoral head, acetabular liner and acetabular shell were replaced with smaller components which consisted of a Pinnacle® 100 series shell (50mm), a DePuy Pinnacle® neutral liner (28mm/50mm), an Articul/Eze M-spec™ metal head (28mm) and the stem remained the same which was a Corail® standard stem (size 12) (Table 5.1). The outer shell used in the original series of nine geometric models had a 54mm diameter, and the smaller outer shell in the current study had a 50mm diameter. Therefore the geometric model needed to be adapted so that instead of the acetabulum being the correct size for a 54mm diameter outer shell, the models needed to fit a 50mm diameter outer shell. To apply this change in the geometric model, the bony morphology was scaled using the same method as described in Chapter Two (Section 2.2.9). The scaling factor used for the geometric model was 0.926 (50/54) which was carried out using the origin at the CoR. The components were then attached via a virtual THR using the same method as described in chapter two (Section 2.2.10). The impingement-prone activities were then applied to the 28mm geometric model with bony geometry ID number 8, to analyse the incidences of impingement

in the smaller component model. The radiographic inclination of the geometric model was 45° radiographic inclination and 25° radiographic anteversion. The smaller component model of bony geometry ID number 8 was used for all testing in Chapter Five.

Table 5.1 Components used in the virtual THR of the one bony geometry used in Chapter Five. All components were commercially available products manufactured by DePuy Synthes which were provided as drawings.

Stem	Head	Shell	Liner
Corail® standard stem (Size 12)	Articul/Eze M- spec™ metal head (28mm (+1.5mm))	Simplified Pinnacle® 100 series shell (50mm)	Simplified Marathon® neutral liner (28mmID/50mmOD)

To further analyse the impingement occurrences during the impingement-prone activities, the acetabular cup orientation was temporarily adjusted into a malposition (30° radiographic inclination and 0° radiographic anteversion) and all of the available activities of the different subjects were applied to the geometric model.

5.2.4 Severity of impingement during a squat activity

To analyse the severity of impingement in the activities of different subjects, the acetabular cup orientation was adjusted into a malposition (30° radiographic inclination and 0° radiographic anteversion) and all of the available squat activities of the different subjects were applied to the geometric model. The squat activity was chosen to focus the analysis for the severity of impingement as this activity resulted in one of the greatest number of impingement occurrences out of the impingement-prone activities. The squat activity resulted in 7/11 (63.6%) occurrences of impingement in the malpositioned model, compared with stand to sit which had 5/8 (62.5%) and

kneel reach which had 8/13 (61.5%) (these results are described in more detail in section 5.2.2.2). The severity of impingement was measured by the volumetric overlap of solid geometries in the model which is a method that has been developed in chapter two (method described in section 2.2.14). The maximum flexion angle in each subject's kinematic squat activity was then analysed for correlation with the maximum severity of impingement encountered during the activity.

The cup orientation selected was a radiographic inclination of 30° and a radiographic anteversion angle of 0°. This was selected as it was just outside of a previously defined (Lewinnek, et al., 1978) safe zone and was therefore deemed malpositioned but according to recent population studies, was still a clinically relevant cup position (Minoda, et al., 2006; Danoff, et al., 2016). To investigate the effect of the kinematic data of different subjects on the severity of impingement, the squat activity of the different subjects were positioned at the greatest overlapping volume of impingement in the geometric model and recorded for comparison.

5.2.5 Cup orientation grids for each activity

To investigate the number of occurrences of impingement for each activity, the impingement-prone activities were applied to the geometric model, when the cup was positioned at various acetabular cup orientations. The acetabular cup orientations were varied between a radiographic inclination angle of 30°-50° in 5° increments and a radiographic anteversion of 0°-30° in 5° increments, which provided a total of 35 individual cup orientations. When the activity data was applied to the geometric model, if impingement, including either implant or bone, occurred at any point during the activity, the test was recorded as an occurrence of impingement. If there was no contact between either the bone or the implant then the test was recorded as no occurrence of impingement. The results for each activity were then collated into impingement grid tables representing the impingement occurrences across all of the subjects for each activity at various acetabular cup orientations. Due to there being different numbers of subject data for each activity, the cup

orientation grids included a total number of possible occurrences of impingement which was different for each activity.

5.2.6 Cup orientation grids for each subject

Only the subjects which had all eight activities registered in their individual kinematic activity data were included for this analysis and therefore the number of subjects was reduced from 18 subjects down to six subjects (Figure 5.1). The individual kinematic activity data for each of the six subjects (“subject-specific impingement-prone activities”) was applied to the geometric model at various acetabular cup orientations. The acetabular cup orientations were varied between a radiographic inclination angle of 30°-50° in 5° increments and a radiographic anteversion of 0°-30° in 5° increments for a total of 35 individual cup orientations. If impingement, including either implant or bone, occurred at any point during the activity, the test was recorded as an occurrence of impingement. If there was no contact between either the bone or the implant then the test was recorded as no occurrence of impingement. The results of each subject was then collated into impingement grid tables which represented the number of occurrences of impingement at each of the acetabular cup orientations.

5.2.7 Statistical analysis

The statistical methods used in the current study were applied using SPSS v26.0.0 (IBM, Armonk, New York). The statistical test to analyse the correlation between the volumetric overlap of implant-on-implant impingement and the size of the flexion angle reached in the squat activity of the different subjects was a Pearson’s chi-squared test. A P-value of <0.05 was considered significant.

5.3 Results

5.3.1 Overview of results

The initial testing of the well-positioned 28mm diameter components with the impingement-prone activities resulted in a small number of impingement occurrences. The squat activity of the different subjects when the liner was malpositioned resulted in different severities of impingement measured by the volume of overlapping components. The severity of impingement was significantly affected by the maximum flexion of each subject's squat activity. Eight acetabular cup orientation grids were produced which contained the number of impingement occurrences at each acetabular cup orientation for each of the eight activities. There were high numbers of impingement occurrences at low inclination and anteversion angles. There were also some impingement occurrences at high anteversion angles which occurred during the posterior impingement-prone activities. Six acetabular cup orientation grids were also produced which contained the number of impingement occurrences at each acetabular cup orientation for each of the six subjects whose data included all eight impingement-prone activities. The number of impingement occurrences was different for each subject including the area on the grid which registered little or no impingement. Therefore, this data suggests that a clinically validated subject-specific approach would be the best way to reduce impingement and potential dislocations in THR's.

5.3.2 Initial testing

5.3.2.1 28mm THR components

The impingement-prone activities were applied to the geometric model containing the 28mm components to analyse the number of impingement occurrences with a previously published kinematic dataset (Layton, et al., 2021). There were found to be limited numbers of impingement occurrences (Figure 5.2). The relatively small amount of impingement was found to be bone-on-bone impingement which occurred during either the lunge activity or the golf swing activity. There were no occurrences of implant-on-bone or implant-on-implant impingement for any of the activities. The activity which

resulted in the most amount of bone-on-bone impingement was the golf swing activity.

Type of impingement	Colour
No impingement	Green
Implant impingement	Red
Bone impingement	Yellow
No data available	Black

Activities applied to the geometric model		Kinematic Subject ID																	
		A	B	C	D	E	F	G	H	I	J	K	L	M	N	O	P	Q	R
Posterior impingement-prone activities	Golf swing	Yellow	Green	Black	Green	Green	Green	Green	Green	Green	Green	Green	Green	Green	Green	Green	Green	Green	Green
	Walk turn	Green	Green	Green	Green	Green	Green	Green	Green	Green	Green	Green	Green	Green	Green	Green	Green	Green	Green
Anterior impingement-prone activities	Sit crossed legged	Green	Green	Black	Green	Green	Green	Green	Black	Green	Green	Green	Green	Green	Green	Green	Green	Green	Green
	Stand to sit	Green	Green	Green	Green	Green	Green	Green	Green	Green	Green	Green	Green	Green	Green	Green	Green	Green	Green
	Squat	Green	Green	Green	Black	Green	Green	Green	Green	Green	Green	Green	Green	Green	Green	Green	Green	Green	Green
	Kneel reach	Green	Green	Green	Green	Green	Green	Green	Green	Green	Green	Green	Green	Green	Green	Green	Green	Green	Green
	Stand reach	Green	Green	Green	Black	Green	Green	Green	Green	Green	Green	Green	Green	Green	Green	Green	Green	Green	Green
	Lunge	Green	Green	Black	Green	Green	Green	Green	Yellow	Green	Green	Green	Green	Green	Green	Green	Green	Green	Green

Figure 5.2 The occurrences and types of impingement during the eight impingement-prone activities for the eighteen subjects in geometric model with bony geometry ID number 8 with the 28mm sized THR components. The impingement type was recorded as the first contact to occur between solid bodies in the geometric model. The component orientation of the cup was 45° radiographic inclination and 25° radiographic anteversion.

5.3.2.2 Impingement occurrences in a malpositioned acetabular cup

The impingement-prone activities were applied to the geometric model with a “malpositioned” acetabular liner (Figure 5.3). Across all of the activities and all of the subjects, the number of occurrences of impingement increased from 5/106 (5%) in a well-positioned cup to 40/106 (38%) in a malpositioned cup. There was a relatively large increase in the amount of implant-on-implant impingement across the impingement-prone activities. These implant-on-implant impingement occurrences typically occurred at low inclination and low anteversion angles. With six of the eight activities being anterior impingement-prone, the acetabular cup rim would be rotated further towards the stem during high flexion movements causing an increase in the occurrences of implant-

on-implant impingement. The instances of bone-on-bone impingement found during the testing on well-positioned components were the same as those found in the malpositioned geometric model, however the lunge activity for subject G changed from a bone-on-bone impingement occurrence in the well-positioned cup to an implant-on-implant impingement occurrence in the malpositioned cup. This was because the acetabular cup was orientated so that the stem contact on the rim of the liner preceded bone-on-bone impingement for this particular subject's lunge activity.

Activities applied to the geometric model		Kinematic Subject ID																	
		A	B	C	D	E	F	G	H	I	J	K	L	M	N	O	P	Q	R
Posterior impingement-prone activities	Golf swing	Yellow	Green	Black	Green	Green	Green	Green	Green	Green	Green	Green	Green	Green	Green	Green	Green	Green	Green
	Walk turn	Green	Green	Green	Green	Green	Green	Green	Green	Green	Green	Green	Green	Green	Green	Green	Green	Green	Green
Anterior impingement-prone activities	Sit crossed legged	Green	Red	Black	Red	Green	Green	Green	Green	Green	Green	Green	Green	Green	Green	Green	Green	Green	Green
	Stand to sit	Red	Red	Black	Green	Green	Green	Green	Green	Green	Green	Green	Green	Green	Green	Green	Green	Green	Green
	Squat	Red	Red	Black	Red	Green	Green	Green	Green	Green	Green	Green	Green	Green	Green	Green	Green	Green	Green
	Kneel reach	Red	Red	Black	Red	Green	Green	Green	Green	Green	Green	Green	Green	Green	Green	Green	Green	Green	Green
	Stand reach	Green	Red	Green	Black	Green	Green	Green	Green	Green	Green	Green	Green	Green	Green	Green	Green	Green	Green
Lunge	Red	Red	Black	Green	Green	Green	Green	Green	Green	Green	Green	Green	Green	Green	Green	Green	Green	Green	

Type of impingement	Colour
No impingement	Green
Implant impingement	Red
Bone impingement	Yellow
No data available	Black

Figure 5.3 The occurrences and types of impingement found during the eight impingement-prone activities for the eighteen subjects in bony geometry ID number 8 with malpositioned 28mm sized THR components. The malposition was 30° radiographic inclination and 0° radiographic anteversion. The impingement type was recorded as the first contact to occur between solid bodies in the geometric model.

5.3.3 Severity of impingement during a squat activity

The severity of impingement as measured by the volumetric overlap of solid geometries in the model was measured during the squat activity of the different subjects when the acetabular cup orientation was malpositioned. All of the impingement occurrences during the subject's squat activity was implant-on-implant impingement, therefore the volumetric overlap of the stem and liner was measured and compared. There were different severities of impingement when comparing the squat activity from each subject (Figure

5.4). This data suggests that the kinematic data of some subjects may be more susceptible to impingement damage and potential dislocation than others under these conditions.

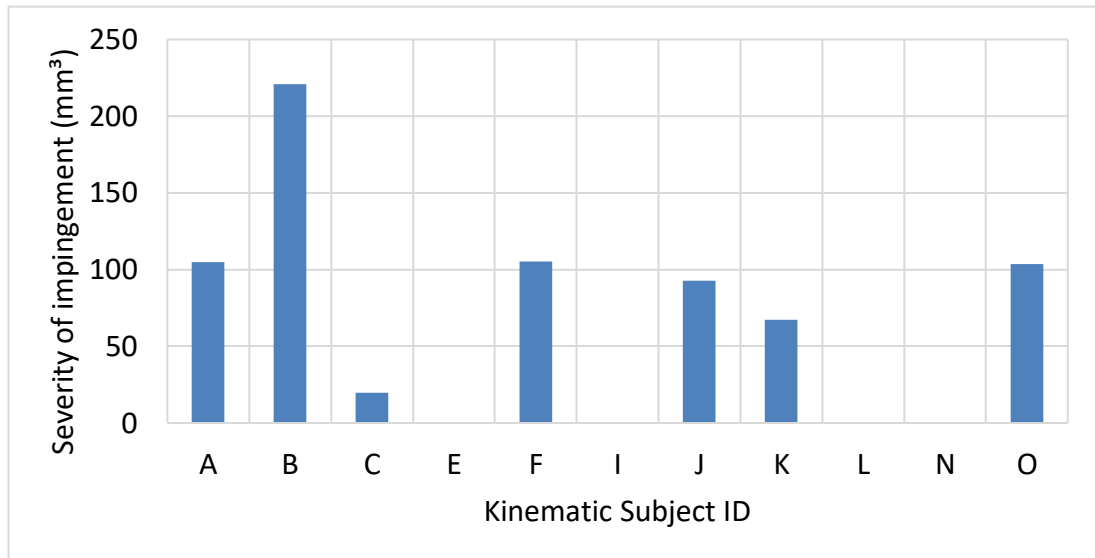


Figure 5.4 The change in severity of impingement as measured by the volume of overlap of the stem and liner in the THR geometric model for each of the available squat activities of the different subjects. The subject's which did not register a squat activity are not included in the figure.

The magnitude of the flexion angle during each subject's squat activity at the greatest point of the activity was also compared between each subject to investigate its effect on the severity of impingement as measured by the volumetric overlap in the geometric model (Figure 5.5). The maximum flexion angle during each subject's squat activity was found to have a significant effect ($P < 0.05$) on the severity of impingement as measured by the volumetric overlap of components when the acetabular cup was malpositioned. An increase of 1° in the maximum flexion angle typically resulted in an increase of 4mm^3 in volumetric overlap of the stem on the liner. Variation was expected in the correlation analysis because the internal rotation and adduction angle would have had a small effect on the severity of impingement, however a significant effect with the flexion angle was found as the squat activity mainly consisted of a flexion angle.

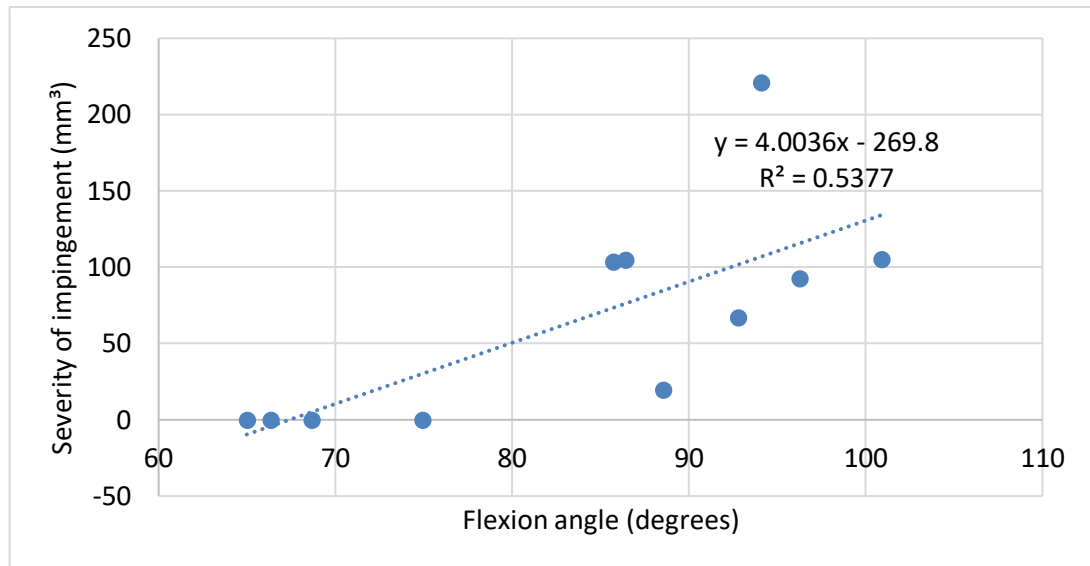


Figure 5.5 The greatest registered flexion angle during a squat activity compared to the severity of impingement as measured by the volume of overlap of the stem and liner in the geometric THR model. Each marker represents an individual kinematic squat activity by a different subject.

5.3.4 Cup orientation grids for each activity

The impingement-prone activities were applied to the geometric model at a range of different acetabular cup orientations. The number of impingement occurrences were then displayed in cup orientation grids separated by activity so that the number of impingement occurrences for each activity could be analysed (Figure 5.6). The number of subjects which had available data for each activity was displayed on each individual activity grid. The grids were colour coded to represent the type of impingement (implant-on-implant or bone-on-bone). There were no occurrences of implant-on-bone impingement for any of the cup orientations or kinematic data of the different subjects. Most of the impingement-prone activities analysed in this study were anterior impingement-prone activities involving high flexion positions (6/8 activities) which should be noted when interpreting the cup orientation grids for each activity.

5.3.4.1 Occurrence and type of impingement during the anterior impingement-prone activities

For the anterior impingement-prone activities, there was an increased amount of impingement occurrences at low inclination and anteversion angles. This was because at low inclination and anteversion angles, the acetabular liner rim was orientated so that the rim was rotated further towards the direction of the stem during high flexion positions causing an increased amount of impingement occurrences. The types of impingement found were mostly implant-on-implant impingement, however there was one incidence of bone-on-bone impingement which occurred during one of the subject's lunge activity. This instance of bone-on-bone impingement occurred because the flexion angle was relatively high which resulted in the anterior side of the femur impinging on the AHS before implant-on-implant impingement could take place.

5.3.4.2 Occurrence and type of impingement during the posterior impingement-prone activities

For the posterior impingement-prone activities, there was an increased amount of implant-on-implant impingement occurrences at high anteversion angles. The inclination angle of the acetabular cup didn't seem to have as much of an effect as the anteversion angle on the incidences of impingement. This was because the posterior impingement-prone activities mainly consisted of an external rotation, therefore the inclination angle, which would rotate almost perpendicular to an external rotation, would have minimal effect on the occurrences of impingement whereas the anteversion would rotate in the direction of the external rotation and would therefore have a greater effect. The type of impingement found for the posterior impingement-prone activities was mostly bone-on-bone impingement which did not change for any of the acetabular cup orientations.

5.3.4.3 Number of occurrences of impingement for each activity to demonstrate severity

The most severe activities as measured by the greatest amount of impingement occurrences at any one cup orientation as a fraction of the number of subjects who were tested based on available data were the kneel reach (8/13), squat (7/11), golf swing (7/14) and lunge (7/17). The kneel reach, squat and lunge activities all consisted of a high flexion range of motion alongside small amounts of adduction or internal rotation which rotated the stem close to the rim of the liner resulting in greater occurrences of impingement. The golf swing activity consisted of a relatively high external rotation angle which rotated the femur posteriorly resulting in impingement for some subjects when the cup was orientated at high inclination and anteversion angles as well as some other subjects resulting in bone-on-bone impingement. The greatest number of impingement occurrences at any one cup orientation for the rest of the activities were the sit crossed legged (6/14), the stand to sit (5/8), the stand reach (3/11) and the walk turn (2/18).



Figure 5.6 Cup orientation grids for each activity. This includes the THR geometric model results for all of the impingement-prone activities of the available subject's data at each acetabular cup orientation. Each individual box represents the number of impingement occurrences at each respective acetabular cup orientation. The number of subjects included for each activity is displayed in the top left corner of each activity cup orientation grid. The cup orientation boxes are individually coloured based on the type of impingement found as well as the total number of impingement occurrences. Walk turn and Golf swing were prone to posterior impingement, all other activities were prone to anterior impingement.

5.3.5 Cup orientation grids for individual subjects and their subject-specific impingement-prone activities

To analyse the impingement occurrences on a subject-specific basis and to make comparisons between subjects possible, the eight impingement-prone activities for the six subjects who had a complete set of activity data was applied to the geometric model at a range of different acetabular cup orientations. Cup orientation grids were produced which outlined the number of impingement occurrences at each acetabular cup orientation for each individual subject (Figure 5.7). The grids were colour coded to represent the type of impingement (implant-on-implant or bone-on-bone). Most of the impingement-prone activities analysed in this study were anterior impingement-prone activities involving high flexion positions (6/8 activities) which should be noted when interpreting the cup orientation grids for each subject.

5.3.5.1 Impingement occurrences across subjects

Each individual subject had a different number of impingement occurrences at each acetabular cup orientation, therefore the impingement-prone activities of each subject had an effect on the likelihood of impingement. This may be interpreted to mean that the movement of individual THR patients could affect the likelihood and severity of impingement in their THR.

The cup orientation grids identified some areas where there were little to no impingement occurrences for each subject. This area of little to no impingement differed for each subject. This may be interpreted to mean that the movement of individual THR patients could dictate the ideal cup orientation implantation targets for their THR surgery. Half of the subjects did not have an area where there were no occurrences of impingement, instead bone-on-bone impingement restricted the activities where there was no implant-on-implant impingement. The acetabular cup orientation would not change this bone-on-bone impingement as the impingement contact was between the bony geometries of the femur and pelvis where a change in cup orientation would not have any effect. Therefore other surgical techniques

would have to be used to reduce the bone-on-bone impingement in these cases such as increasing the offset.

5.3.5.2 Analysis of the cup orientation grids of the different subjects

The subject which recorded the greatest number of impingement occurrences was subject B where 6/8 of the activities resulted in an impingement event at one acetabular cup orientation. All six of the impingement occurrences for subject B were during the anterior impingement-prone activities. There was an increased amount of impingement at a low anteversion and low inclination angle which was to be expected. However the numbers of occurrences of impingement were higher than the other five subjects. There were 18/35 cup orientations which resulted in no impingement occurrences. There was no bone-on-bone impingement recorded and also no impingement found at higher anteversion and inclination angles. This suggested that the kinematics of this subject may be more susceptible to impingement occurrences during anterior impingement-prone activities. This subject had the greatest number of impingement occurrences at any one cup orientation and also only comprised implant-on-implant impingement which highlighted the importance of a well-positioned acetabular cup for this subject.

Subject N had the least number of impingement occurrences which was a maximum of one impingement occurrence at any one acetabular cup orientation. There were 27/35 acetabular cup orientations which resulted in no impingement for any of the eight activities. The few impingement occurrences that did occur were all implant-on-implant impingement and they occurred during the golf swing activity. There was no bone-on-bone impingement found for this subject. The cup orientation grids for this subject suggested that they were at low risk of impingement. There was a large range of cup orientations which would likely result in no impingement occurrences.

Subject J registered the most amount of bone-on-bone impingement with both the walk turn and golf swing resulting in bone-on-bone impingement across all of the acetabular cup positions assessed. Thus indicating that this subject was susceptible to impingement occurrences when carrying out posterior

impingement-prone activities due to the high external rotation exhibited when carrying out these activities. There was also a number of impingement occurrences during the anterior impingement activities which occurred for low anteversion and low inclination angles of the acetabular cup. There were no acetabular cup positions which resulted in no impingement. Therefore for Subject J, the acetabular cup position may only reduce the impingement up to a point as there would be bone-on-bone impingement during the posterior activities regardless for these particular components. Other surgical techniques would need to be used to reduce this bone-on-bone impingement.

Subject E had one of the lowest numbers of impingement occurrences in their cup orientation grid. The maximum impingement found at one acetabular cup orientation was two out of the eight activities. This subject impinged during the walk turn activity which resulted in bone-on-bone impingement which was not affected by acetabular cup orientation. Apart from this there was only one other instance of impingement which was implant-on-implant impingement which resulted from the golf swing activity when the acetabular cup was positioned at a high inclination and high anteversion angle. Therefore this subject was also one of the subjects which seemed to have a high external rotation during the posterior impingement-prone activities. There were no impingement occurrences during any of the anterior impingement-prone activities.

Subject A had a relatively high number of implant-on-implant impingement occurrences. This subject also impinged via bone-on-bone impingement during the golf swing activity which was not affected by the cup orientation. There was a maximum of five out of the eight activities impinging at any one acetabular cup orientation. There were no cup orientations which resulted in no impingement. Due to the amount of implant-on-implant impingement at a number of different cup orientations, this subject would have a narrower window for the cup orientation implantation target to avoid impingement. An accurate acetabular cup orientation would be needed for this subject who would be susceptible to impingement at a higher number of cup orientations.

Subject F had a relatively high number of impingement occurrences however these were all at a low cup orientations and therefore there were a lot of cup orientations (25/35) which resulted in no impingement for any of the activities. There was no bone-on-bone impingement recorded for subject F including no impingement during any of the posterior impingement-prone activities. There were sharp increases in impingement when comparing cup orientations for Subject F (i.e. no impingement occurrences at 40° inclination and 10° anteversion and four impingement occurrences at 40° inclination and 5° anteversion) suggesting that the range of motion of the activities which did result in impingement occurred at a similar range of motion.

Kinematic Subject A		Inclination angle (°)				
		30	35	40	45	50
Anteversion angle (°)	0	5	4	4	4	4
	5	4	4	4	4	4
	10	3	3	2	2	2
	15	2	2	2	1	1
	20	2	1	1	1	1
	25	1	1	1	1	1
	30	1	1	1	1	1

Kinematic Subject B		Inclination angle (°)				
		30	35	40	45	50
Anteversion angle (°)	0	6	6	6	4	4
	5	6	5	4	4	2
	10	5	3	2	1	0
	15	3	1	0	0	0
	20	1	0	0	0	0
	25	0	0	0	0	0
	30	0	0	0	0	0

Kinematic Subject E		Inclination angle (°)				
		30	35	40	45	50
Anteversion angle (°)	0	1	1	1	1	1
	5	1	1	1	1	1
	10	1	1	1	1	1
	15	1	1	1	1	1
	20	1	1	1	1	1
	25	1	1	1	1	1
	30	1	1	1	1	2

Kinematic Subject F		Inclination angle (°)				
		30	35	40	45	50
Anteversion angle (°)	0	4	4	4	4	2
	5	4	4	4	1	0
	10	4	0	0	0	0
	15	0	0	0	0	0
	20	0	0	0	0	0
	25	0	0	0	0	0
	30	0	0	0	0	0

Total number of impingement events	Cup orientation grid colour		
	Implant impingement only	Bone impingement only	Implant and bone impingement
0	0	0	0
1	1	1	N/A
2	2	2	2
3	3	3	3
4	4	4	4
5	5	5	5
6	6	6	6
7	7	7	7
8	8	8	8

Kinematic Subject J		Inclination angle (°)				
		30	35	40	45	50
Anteversion angle (°)	0	5	5	4	3	3
	5	3	3	3	2	2
	10	3	2	2	2	2
	15	2	2	2	2	2
	20	2	2	2	2	2
	25	2	2	2	2	2
	30	2	2	2	2	2

Kinematic Subject N		Inclination angle (°)				
		30	35	40	45	50
Anteversion angle (°)	0	0	0	0	0	0
	5	0	0	0	0	0
	10	0	0	0	0	0
	15	0	0	0	0	0
	20	0	0	0	0	0
	25	1	1	1	0	0
	30	1	1	1	1	1

Figure 5.7 Cup orientation grids for each subject. The THR geometric model results for the eight impingement-prone activities of the six subjects at each acetabular cup orientation. Each individual box represents the number of impingement occurrences at each respective acetabular cup orientation. The cup orientation grids for all of the six subjects included all eight of their activities at each cup orientation and the number of impingement occurrences at each of the acetabular cup orientations. The cup orientation boxes are individually coloured based on the type of impingement found as well as the total number of impingement occurrences.

5.3.5.3 Comparison of the subjects with the greatest and smallest number of occurrences of impingement

The cup orientation grids of all six subjects demonstrated the difference in the impingement occurrences caused by the variation in impingement-prone activities for different subjects (Figure 5.7). This suggested the dependence of a patient's kinematics and cup orientation to influence the likelihood of impingement in THR's. The subject which registered the greatest number of impingement occurrences for their eight activities at any one acetabular cup orientation was subject B and the subject which had the lowest number of impingement occurrences was Subject N. The kinematics of the impingement-prone activities of the two subjects were compared to understand the differences in the number of impingement occurrences when carrying out the same activities (Figure 5.8). The flexion angles in every anterior impingement-prone activity was higher in subject B than in subject N which could explain the differences in the number of impingement occurrences. This suggested that if subject B had a THR, they would be more susceptible to impingement than Subject N based on the kinematics of their impingement-prone activities.

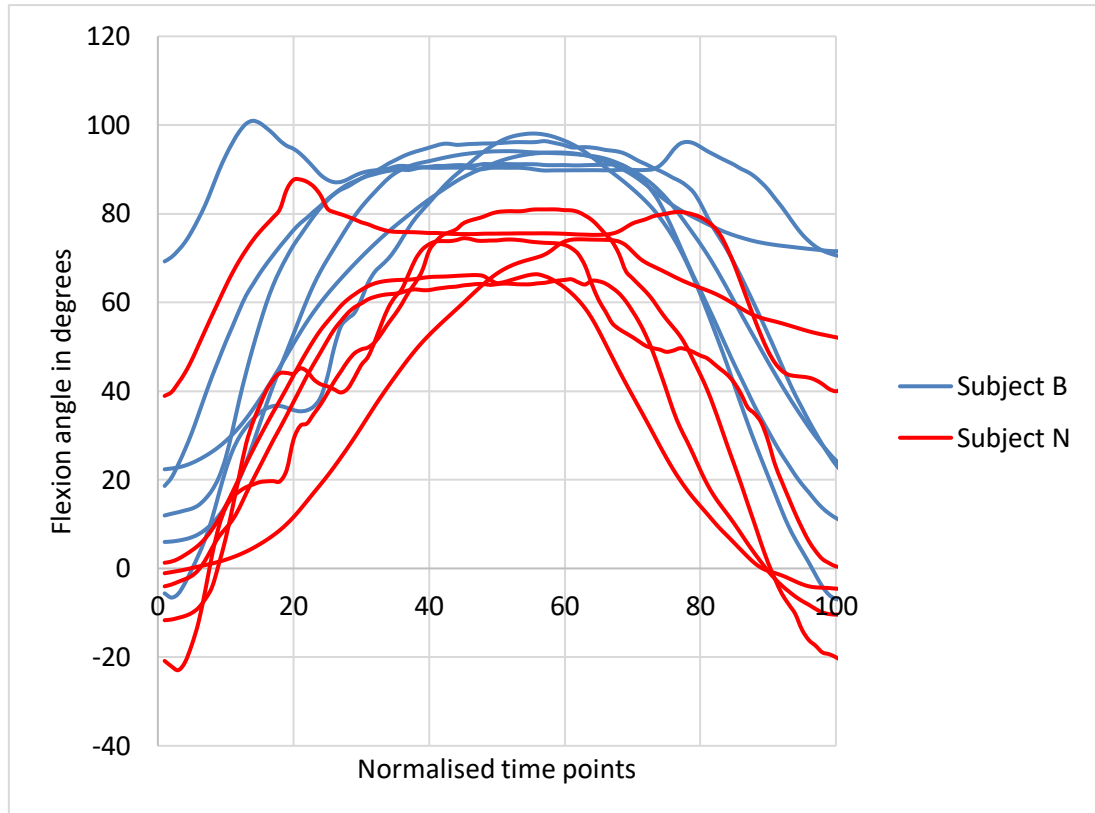


Figure 5.8 A comparison of the six anterior impingement-prone activities for Subject B and Subject N demonstrating the difference in the flexion for their activities.

Subject N had an increased number of occurrences of impingement at a high anteversion angle which would suggest an increased external rotation angle during their posterior impingement-prone activities, however this was compared between the two subjects and they were found to be similar (Figure 5.9). The flexion angles of the two subjects however showed that the femur would have been rotated through extension to be closer to the ischium, reducing the external rotation angle needed for impingement for Subject N, due to the extension angle at the time of impingement (towards the end of the activity due to the timing of the external rotation). The flexion angle in subject B therefore sufficiently rotated the femur away from the ischium to avoid impingement. Subject N was mostly in extension during the activity and therefore the femur was rotated towards the posterior of the hip before the external rotation resulted in impingement at high cup anteversion angles.

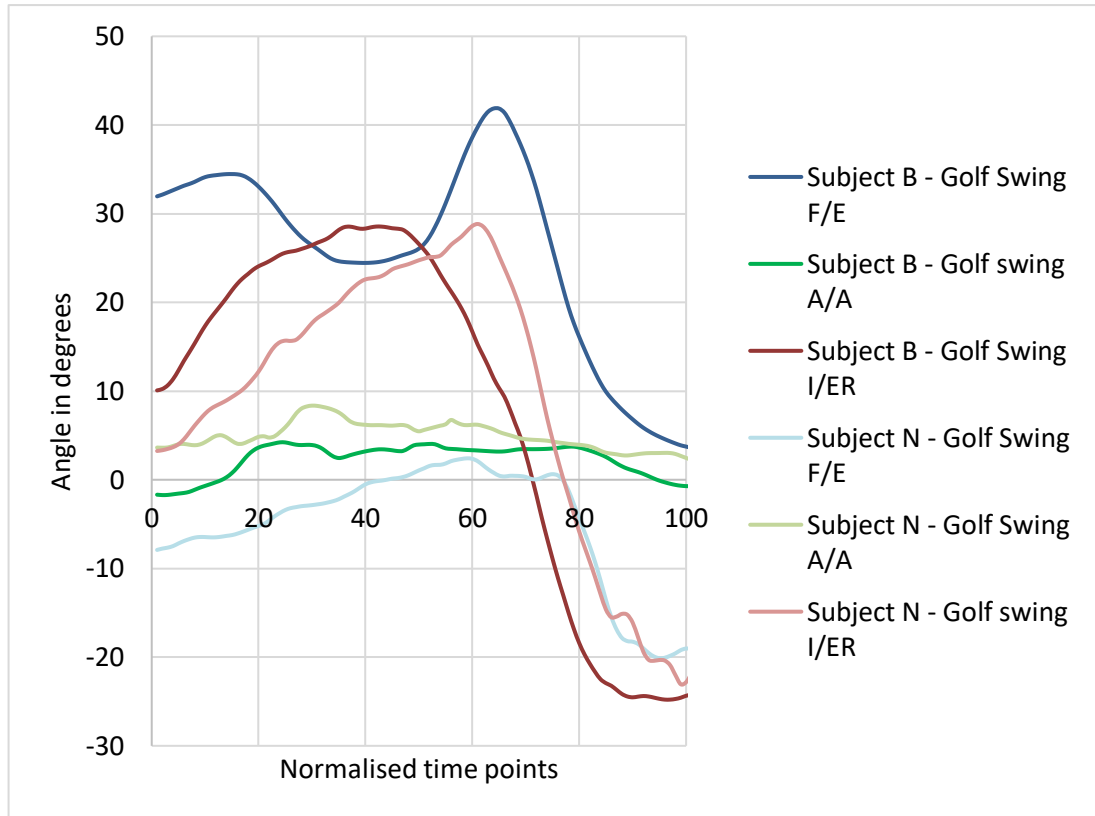


Figure 5.9 A comparison of the golf swing activity (posterior impingement-prone activity) from the impingement-prone activity data for Subject B and Subject N demonstrating the difference in the rotations for their respective golf swings. This included the three rotations (flexion/extension, adduction/abduction and internal/external rotation) that were followed for the activity.

5.4 Discussion

Impingement-prone activities were applied to a THR geometric model to investigate the effect of a change in acetabular cup orientation on impingement as well as the effect of subject variation in the kinematics of impingement-prone activities. Cup orientation grids were produced for each activity and six individual subjects which resulted in high occurrences of impingement at low anteversion and inclination angles. There were also an increased number of impingement occurrences at high anteversion angles. The grids of the six different subjects resulted in different areas of impingement occurrences because of the individual kinematic data. The area on the grid which registered little or no impingement was different amongst the subjects, suggesting that the area of implantation target for each subject may be different. This data therefore suggested that a clinically validated subject-specific preoperative planning approach would be the best way to reduce impingement and potential dislocations in THR's.

5.4.1 Comparison of the impingement-prone activities (Layton, et al., 2021) with the literature

The ranges of motion in the impingement-prone activities from the current study's dataset (Layton, et al., 2021) were smaller than the dislocation-prone activities from another previously used kinematic dataset (Nadzadi, et al., 2003). It is not known which of these kinematic datasets of activities is more representative of the wider population. There have been a number of other studies which have measured the ranges of motion including the maximum flexion of various kinematic activities in both THR and non-THR subjects (Ko & Yoon, 2008; Koyanagi, et al., 2011; Sugano, et al., 2012). One study (Ko & Yoon, 2008) measured the flexion angle in ten non-THR subjects with a mean age of 27 and found averages of 105.4°, 109.6° and 100.3° during a sit to stand activity, squat activity and sit crossed legged activity respectively. These angles of flexion were similar to those found in a previous kinematic dataset (Nadzadi, et al., 2003) which also used non-THR subjects for their analysis. On the other hand, another study measured the maximum flexion in post-THR

patients finding an average of 86°, 76°, 62° and 80° during a picking up an object off the floor whilst sitting activity, sit to stand activity, stand to sit activity and a squat activity respectively (Sugano, et al., 2012). Another post-THR study (Koyanagi, et al., 2011) measured the ROM in patients and found an average of 86.2° during squat activities in 15 patients. These post-THR ranges of motion were more similar to the flexion angles in the kinematic dataset used in the current study (Layton, et al., 2021). The lower ranges of motion for the post-THR patients are most likely because patients would be more cautious of carrying out high range of motion activities. The current study has demonstrated that even with the kinematics similar to that of a post-THR patient who may carry out activities more cautiously, there was still found to be occurrences of impingement at clinically-relevant acetabular cup orientations.

There is a need for the relevancy of the kinematic activities measured in the literature in previous datasets to be captured. The frequency that these activities in the datasets are carried out by patients on a day to day basis is not known and future work should focus on improving the relevancy of these activities which is most likely patient-specific.

5.4.2 Effect of the impingement-prone activities

Comparing the eight impingement-prone activities in this group of subjects; kneel reach, squat, golf swing and lunge resulted in the greatest number of impingement occurrences, suggesting that these activities would be the most severe and more likely to cause impingement and potential dislocation in THR patients. This study indicated that care should be taken when these activities are undertaken post-surgery due to the number of impingement occurrences found at relatively safe cup orientations. These activities were those which would require a large range of motion including activities needed for sport and gardening, compared to safer everyday household activities such as stand to sit, walk turn and sitting crossed legged. This disagreed with a previous kinematic dataset (Nadzadi, et al., 2003) which found a large RoM in everyday household activities such as the STOOP and ROLL activities

(investigated in chapter four). These differences could be because these were different individual subjects carrying out the activities with no indication as to the athletic ability of either group.

While these activities have not been investigated previously in any computational modelling studies, they were similar to the high flexion activities in another previous kinematic dataset (Nadzadi, et al., 2003) and therefore the conclusions on the low inclination and anteversion orientation of the cup resulting in high occurrences of impingement were the same for the high flexion activities (Pedersen, et al., 2005; Pryce, et al., 2022). The conclusions of the cup orientation at high inclination and anteversion angles resulting in high occurrences of impingement were also the same for the high external rotation activities (Pedersen, et al., 2005; Pryce, et al., 2022).

The stand reach and walk turn activities were the “safest” activities out of the eight as measured by the number of impingement occurrences across the cup orientations in this group of subjects. These were activities that simulated reaching forward whilst standing and a turn in direction during walking, both of which would not generally be expected to have a high range of motion. The walk turn mainly consisted of an external rotation which was similar to the PIVOT activity from a previous kinematic dataset (Nadzadi, et al., 2003), however the external rotation was not as large as the PIVOT activity. In general, the motion of the stand reach activity did not result in a high enough RoM to cause high numbers of impingement.

The sit crossed legged activity had the highest flexion angle of the eight activities in this group of subjects, however it did not result in the greatest numbers of impingement across the different cup orientations due to the relatively high external rotation angle required to carry out the activity. Data reported in Chapter Four (Section 4.3.2) also demonstrated this, with the XLG activity from a previous kinematic dataset (Nadzadi, et al., 2003) where there were no instances of impingement during the XLG activity for any of the bony geometries. Other modelling studies (Pedersen, et al., 2005; Pryce, et al., 2022) which had investigated the XLG activity from a previous kinematic

dataset (Nadzadi, et al., 2003) also agreed with this finding with the XLG activity resulting in one of the lowest numbers of impingement occurrences out of the activities tested in both studies.

5.4.3 Cup orientation and its effect on impingement

When initially testing the impingement-prone activities of the different subjects in the geometric model when the acetabular cup was well-positioned, there were few (5/106) impingement occurrences. These impingement occurrences were all bone-on-bone impingement which indicated that a well-positioned component orientation for the geometric model was sufficient as to avoid implant-on-implant impingement for all of the activities in a previous kinematic dataset (Layton, et al., 2021).

There were increased occurrences of implant-on-implant impingement at low inclination and anteversion angles. This was due to the anterior impingement-prone activities which mainly consist of a high flexion angle. These results agreed with the literature (Pedersen, et al., 2005; Pryce, et al., 2022) where it was also found that low inclination and anteversion angles resulted in increased implant-on-implant occurrences during high flexion activities. There was a small increase in the occurrences of implant-on-implant impingement at high inclination and anteversion angles. This was due to the posterior impingement-prone activities which mainly consisted of an external rotation. This increase in implant-on-implant impingement with high cup anteversion angles agreed with the literature (Pedersen, et al., 2005; Pryce, et al., 2022). These results demonstrated the importance of acetabular cup orientation as there were relatively large changes in the number of impingement occurrences at different acetabular cup orientations for each activity.

While these results demonstrated impingement occurrences at different cup orientation angles, it is important to note that other factors affect the function of the THR including edge loading. The use of higher cup inclination angles may avoid the increased occurrences of impingement at lower inclination and anteversion angles, however it may result in edge loading (Fisher, 2011; Leng,

et al., 2017). Therefore there is a compromise with different factors to consider for the overall function of the THR.

The cup orientation grids for each activity demonstrated that there were relatively high numbers of impingement occurrences at orientations which were inside a previously defined 'safe zone', which recommended cup orientation in order to reduce dislocation (Lewinnek, et al., 1978). The safe zone was defined as between 30°-50° radiographic inclination and 5°-25° radiographic anteversion. A retrospective study (Abdel, et al., 2016) found 206/9784 dislocations in one institution, 58% of which were inside the previously defined (Lewinnek, et al., 1978) safe zone. Another retrospective study (Minoda, et al., 2006) found 28/806 dislocations in a different institution, 68% of which were inside the previously defined (Lewinnek, et al., 1978) safe zone. One retrospective study (Danoff, et al., 2016) redefined the safe zone based on data of 1289 THR's from one institution where it was found that there were 44 dislocations and 47.6% of them were inside the previously defined (Lewinnek, et al., 1978) safe zone. A new safe zone was suggested which included an inclination angle of 30°-50° and an anteversion angle of between 10°-25° which reduced the percentage of THR dislocations to 23.8%. The current study resulted in impingement occurrences inside the previously defined (Lewinnek, et al., 1978) safe zone as well as this newly defined safe zone (Danoff, et al., 2016). While the data from the current study cannot make conclusions around the occurrence of dislocations at these acetabular cup orientations, the importance of correct acetabular cup orientation for the prevention of impingement was demonstrated. This data suggests that ultimately a clinically validated subject-specific preoperative approach would be the best way to reduce impingement and potential dislocations in THR's.

5.4.4 The effect of range of motion on impingement occurrence during the impingement-prone activities for different subjects

When comparing the subject variation during the impingement-prone activities, a higher range of motion generally resulted in an increased number of impingement occurrences. An increase in the maximum flexion angle of the squat activities for the different subjects significantly increased the volumetric overlap of components.

Comparing the cup orientation grids for each subject; the subject who recorded the greatest number of impingement occurrences (subject B) and the lowest number of impingement occurrences (subject F), had a clear difference in the range of motion of their respective activities. This suggested that the maximum flexion angle of a THR patient's anterior impingement-prone activities, in particular the squat activity, could be used as a predictor for an increased likelihood and potential severity of impingement. Patients who demand a higher range of motion from their implant during impingement-prone activities may be at an increased risk of impingement in their THR.

The use of the flexion angle as a predictor for likelihood of impingement may not be as straightforward for more complex activities such as the golf swing and sitting crossed legged where likelihood of impingement depended on more than one rotation of the activity. It is important to also consider the adduction/abduction and internal/external rotation when analysing potential impingement for more complex activities.

5.4.5 The effect of the subject variation on impingement occurrence during the impingement-prone activities

When the acetabular cup was malpositioned in the geometric model, there was an increase in the number of implant-on-implant impingement occurrences. There were some subjects however which, despite the malpositioned cup, did not register any impingement for their kinematic activities. This difference in the number of impingement occurrences for the

same bony geometry and cup position demonstrated the effect that different kinematics of subjects had on impingement occurrences in THRs. This data suggested that some patients may be more susceptible to impingement than others because of the kinematics of their activities of daily living.

Comparing the cup orientation grids for each subject; there were different numbers of impingement occurrences at each acetabular cup orientation. This suggested that the kinematics of a patient carrying out a set of activities could affect the likelihood and potential severity of impingement in their THR. The area on the grid which registered little or no impingement was different amongst the subjects and may suggest a difference in the ideal cup orientation for each subject. This data suggested that a clinically validated subject-specific preoperative planning approach would be the best way to reduce impingement and potential dislocations in THR's.

5.4.6 Dynamic assessment and THR surgical preoperative planning potential

Current preoperative planning techniques in THR include analysing radiographs of the patient's pelvis and femur to decide on component design, component size, leg length and offset. In some cases 3D modelling would be used to carry out a more detailed preoperative planning, however the activity data of patients is not included in any preoperative planning. The use of activity data in a dynamic assessment of a 3D geometric model could be a useful tool in THR surgical preoperative planning. However, there may be limitations to the collection of the kinematic data from THR patients who are in pain. In the current study, the cup orientation grids for each of the six subjects included areas where there was little to no impingement occurrences which differed for each subject. This may suggest that there is a difference in the ideal cup orientation for each subject. Therefore this data suggested that a clinically validated subject-specific preoperative planning approach would be the best way to reduce impingement and potential dislocations in THR's. As THR's are implanted in younger and more active patients who may demand higher ranges of motion from their implant (Sechriest, et al., 2007;

Cherian, et al., 2015), the need for correct acetabular cup orientation to avoid impingement is of increased importance.

5.4.7 Limitations

There were limitations to this study. Firstly, the geometric models used in this study were developed in Chapter Two and therefore the same limitations applied which were described in Section 2.3.1.

Secondly, the method used in this study used one geometric model of a THR and then used a different group of subjects for the kinematic activity data to apply the motions to the geometric model. The occurrences of impingement may have been different if a different bony geometry was used. Clinically, the subjects which resulted in bone-on-bone impingement could have had a different shaped bony geometry which may not have resulted in bone-on-bone impingement. The data was not available to use the same bony geometry and kinematic activity data from one subject.

Thirdly, the impingement-prone activities used in the current study were specific to this group and therefore the impingement occurrences found may differ when using the kinematic data of other subjects. There was also no data on the activity level or athletic ability of the group of subjects which carried out the activities, therefore some of the activities including golf swing, squat and lunge should be approached with caution as the activity may not have been carried out correctly, depending on the experience of the subjects who carried out the activity. Other more experienced subjects could have carried out the activities with better form and therefore have had potentially higher/lower ranges of motion which could have led to a difference in the impingement occurrences reported here.

Fourthly, the impingement-prone activities dataset was incomplete due to errors in data collection from the original study (Layton, et al., 2021). Therefore comparisons across activities were limited due to the bias of some subjects being included and some not. During the testing, it was evident that there were some subjects who impinged more than other subjects across all activities. Therefore it mattered which subject was missing in the data as this could have

affected the overall numbers of impingement occurrences for each activity and therefore the interpretation of the results. The results of the cup orientation grids for each activity should therefore be interpreted with this in mind.

Finally, in the cup orientation grids for each subject, each of the eight dislocation-prone activities are equally weighed in terms of impingement occurrence, however it is not known how often these activities are carried out by individual subjects (i.e. once a day or 100 times a day). The cup orientation grids should therefore be interpreted with this in mind.

5.5 Summary

The aim of this chapter was to investigate the effect of subject variation of individual kinematic activity data on the occurrences of impingement as well as the effect of varying the acetabular cup orientation in a single bony geometry. Eight impingement-prone activities were applied to a single geometric model of a total hip replacement while the cup orientation was varied between 30°-50° radiographic inclination and 0°-30° radiographic anteversion. The number of impingement occurrences at each cup orientation was recorded and grids were produced for each activity to demonstrate the impingement occurrences at each acetabular cup orientation. Grids were also produced for individual subjects demonstrating the impingement occurrences at each acetabular cup orientation.

The cup orientation grids for each individual subject had varying occurrences of impingement at each orientation which suggested that a patient's kinematic data may have an effect on the likelihood and severity of impingement. The data indicated that patients who demand a higher RoM from their total hip replacement may potentially be at an increased risk for impingement. The areas on the grid which registered little or no impingement was different amongst the subjects and therefore this data suggested that a clinically validated subject-specific approach to preoperative planning would be the best way to reduce impingement and potential dislocations in total hip replacements. The number of occurrences of impingement at each cup

orientation angle varied among the different activities, with the kneel reach, squat, lunge and golf swing activities registering the greatest numbers of impingement. These were all considered to be high range of motion activities and therefore this study indicated that care should be taken when these activities are suggested to be undertaken post-surgery.

The outputs of the geometric models investigating impingement have so far been volumetric overlaps of impingement to demonstrate the severity of impingement. There is a need to characterise the damage and find the *in vitro* consequences of the impingement detected in the geometric model.

Chapter Six : *In vitro* consequences of impingement in total hip replacements during clinically-relevant motions

6.1 Introduction

As well as potentially leading to dislocation (Malik, et al., 2007), implant-on-implant impingement has been found to cause damage to the acetabular rim of polyethylene liners in THRs (Birman, et al., 2005; Shon, et al., 2005; Usrey, et al., 2006; Marchetti, et al., 2011; Waddell, et al., 2018). This damage to the rim can lead to an increase in wear particulate debris which can lead to osteolysis (Shon, et al., 2005; Malik, et al., 2007). The abnormal forces at the rim through impingement and potential subluxation of the head could also lead to loosening of the components (Murray, 1993; Shon, et al., 2005; Malik, et al., 2007). In some cases, fatigue damage such as cracking due to repetitive impingement has also been found on retrieved polyethylene liners (Birman, et al., 2005).

There have been a limited number of *in vitro* studies which have investigated impingement damage during cyclic loading in a hip simulator (Holley, et al., 2005; Pryce, 2019). A standard for impingement testing (ASTM F2582, 2020) also exists in the literature which outlines a standard test method for dynamic impingement. These tests have included different setups, loading, methods of output measurement, kinematics and number of cycles. One study (Holley, et al., 2005) applied “orbital motion” to hip components using a peak 2kN load applied as a walking gait profile and was run for five million cycles. The method of measurement was gravimetric wear testing which was possible due to the number of cycles. There is limited data on the number of times patients carry out high RoM activities in the lifetime of an implant however five million was thought to be excessive. The gravimetric wear testing would only be likely to be effective over a high number of cycles as a low number would be unlikely to generate detectable levels of gravimetric loss. It would also be difficult to determine whether the weight loss was from bearing wear or impingement damage. The standard for impingement testing (ASTM F2582, 2020) aims to

apply a simple wave profile under constant impingement at a high abduction angle under a constant 600N load for one million cycles. To measure impingement, the liners are analysed under a microscope and inspected for fatigue damage. This is not a clinically-relevant setup for impingement, nor are the motions or loads under constant impingement. The other study (Pryce, 2019) applied one kinematic activity which was simplified to THR components under a peak load of 800N for 40k cycles. The study assessed the ML displacement to measure the subluxation, however did not capture the AP displacement to gain a full understanding of the subluxation during the impingement event. This study only used one activity which was simplified. To measure the impingement damage to the rim, the liners were geometrically measured using a coordinate measuring machine (CMM). These impingement tests were discussed in more depth in Section 1.6.

The THR geometric models used in Chapters 3, 4, and 5 of this thesis provided an output in regard to the severity of impingement measure during impingement events. This was the volumetric overlap of solid geometries in the geometric models. However, this gave no indication as to the damage or effect that this would have on THR components *in vitro*. This chapter details the experimental application of impingement conditions, observed in the geometric model, to THR components in a physical, cyclic simulator.

The aims of this study were: to develop a method to apply clinically-relevant motion and force profiles in a hip simulator which replicated the kinematics of three subjects carrying out a squat activity; to generate and measure subsequent impingement damage to the acetabular liner rims; and to assess whether the computational volumetric overlap measure can be used for effective impingement damage prediction.

6.2 Method

6.2.1 Overview of method

To simulate clinically-relevant motions in a hip simulator and analyse the damage, three squat activities from a previous kinematic dataset (Layton, et al., 2021) were selected and cyclically applied to clinically-available THR components in a hip simulator under load. The three squat activities which were previously applied to the geometric model (detailed in chapter five), were predicted to result in varying severities of impingement. The THR components were orientated and cemented to fixtures and mounted in the hip simulator so that there would be an impingement event in the three squat activities but was ensured that the RoM wasn't so high as to cause a dislocation event which would cause damage to the simulator. Geometric measures were taken using a CMM of penetration depth (mm) and circumferential location of damage on the liner rims. Displacement measures in the medial-lateral and anterior-posterior directions were also taken during the impingement event and subsequent subluxation. The results were compared to each other to analyse the difference in damage for different subject's activity data. The results were also compared with the geometric model predictions for the three relevant squat activities.

6.2.2 THR components

All of the THR components which were supplied by DePuy Synthes (Table 6.1) are the same components which were used in Chapter Five. The components were Marathon® polyethylene neutral liners (28mm/50mm), Articul/Eze M-spec™ metal heads (28mm (+1.5mm)), Pinnacle® 100 series shells (50mm) and Corail® standard offset stems (size 12).

Table 6.1 Product names and sizes of the total hip replacement components (DePuy Synthes, Leeds, UK) used in the hip simulator study.

Stem	Head	Shell	Liner
Corail® standard stem (Size 12)	Articul/Eze M- spec™ metal head (28mm (+1.5mm))	Simplified Pinnacle® 100 series shell (50mm)	Simplified Marathon® neutral liner (28mmID/50mmOD)

6.2.3 Development of *in vitro* impingement test inputs

6.2.3.1 Selection of the three squat kinematics

The squat activities from the previous kinematic dataset (Layton, et al., 2021) consisted of 101 discrete femoral positions in relation to the pelvis, described by three anatomical rotations (flexion/extension, adduction/abduction, internal/external rotation). These discrete data points formed the squat activity and were defined as relative hip angles between the femur and pelvis in 3D space. Therefore any pelvic rotation was contained in the relative hip angles between the pelvis and femur.

Previous work in this thesis investigated impingement in a number of squat activity's from the kinematic dataset (Layton, et al., 2021) in a malpositioned cup. Of the 11 subject's squat activity, seven resulted in impingement (described in more detail in section 5.3.2.2).

Three squat activities were chosen out of the group of seven subject's squat activity which impinged. The seven squat activities were compared for their three anatomical rotations (flexion/extension, adduction/abduction and internal/external rotation) and the squat activities which had the greatest magnitude of RoM for each of the rotations was chosen (Figure 6.1). This was so that a range of different kinematics could be applied in the hip simulator. Subject F registered the highest flexion angle, subject A registered the highest adduction angle and subject B registered the highest internal rotation angle.

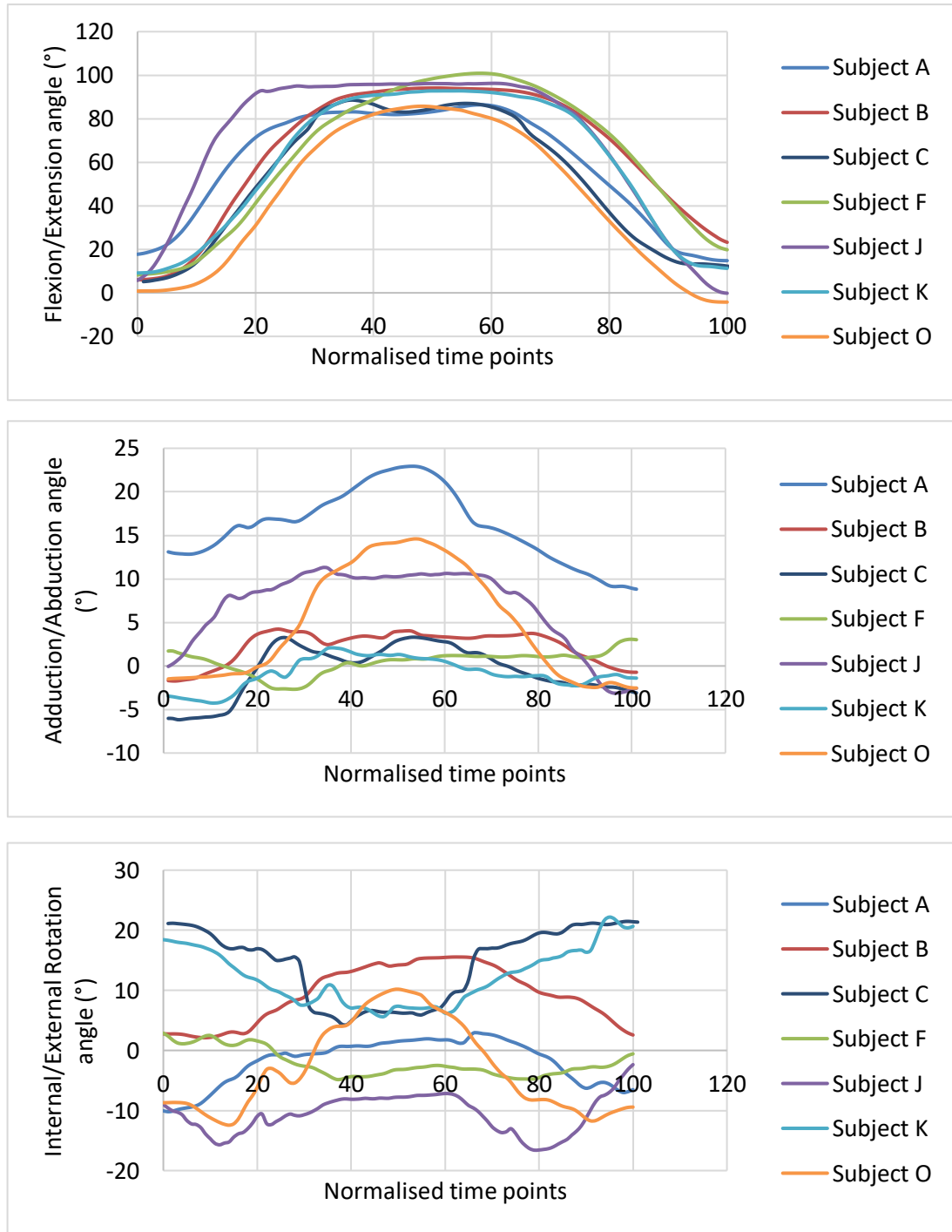


Figure 6.1 All of the raw kinematic squat data from the previous kinematic dataset (Layton, et al., 2021) for the subjects which resulted in impingement in the malpositioned geometric model used in Chapter Five (Section 5.3.2.2). The subjects which were chosen were all the maximums of each individual rotation. Subject F had the highest flexion angle, subject A had the highest adduction angle and subject B had the highest internal rotation angle.

6.2.3.2 Component orientation

The orientation of the components were selected for the study to ensure that there would be impingement in all three squat activities but not so high as to cause a dislocation event in the simulator. The orientations of the THR components were also desired to be in as clinically relevant orientations as possible. One stem fixture existed in the laboratory which would position the stem at 0° anteversion and 10° adduction and could be adapted to be the correct height for the CoR in the simulator which satisfied the need of this study (described in more detail in section 6.2.4.3). This orientation of the stem was chosen, which meant that the orientation of the acetabular cup needed to be chosen to allow for impingement in each case but avoiding dislocation in the simulator.

The three squat activities were applied to the geometric model with the acetabular cup positioned in varying degrees of orientation and the impingement volumes of overlapping components as well as the angle past the point of impingement were calculated for each of the three squat activities. Based on these results, the acetabular cup orientation was chosen to be 45° radiographic inclination and 10° radiographic anteversion. This component orientation allowed for impingement in all subjects however was not predicted to be high enough to cause dislocation. This orientation selection was regarded as clinically relevant based on previous studies (Minoda, et al., 2006; Danoff, et al., 2016) and was also inside previously defined “safe zones” for cup implantation targets (Lewinnek, et al., 1978; Danoff, et al., 2016).

6.2.3.3 Using the incorrect sequence of rotations in the simulator

The joint angles used from the gait lab study in the previous dataset (Layton, et al., 2021) were derived using a Cardan sequence in the specific order of FE-AA-IE. The nesting of the rotating carriages in the experimental simulator machine design dictated a rotation sequence of AA-FE-IE. The original angles from the previous kinematic dataset (Layton, et al., 2021) were applied unchanged to the simulator, meaning that the resulting joint orientation was

different to that originally recorded in the gait lab study (Figure 6.2). Therefore this issue needed to be mitigated.

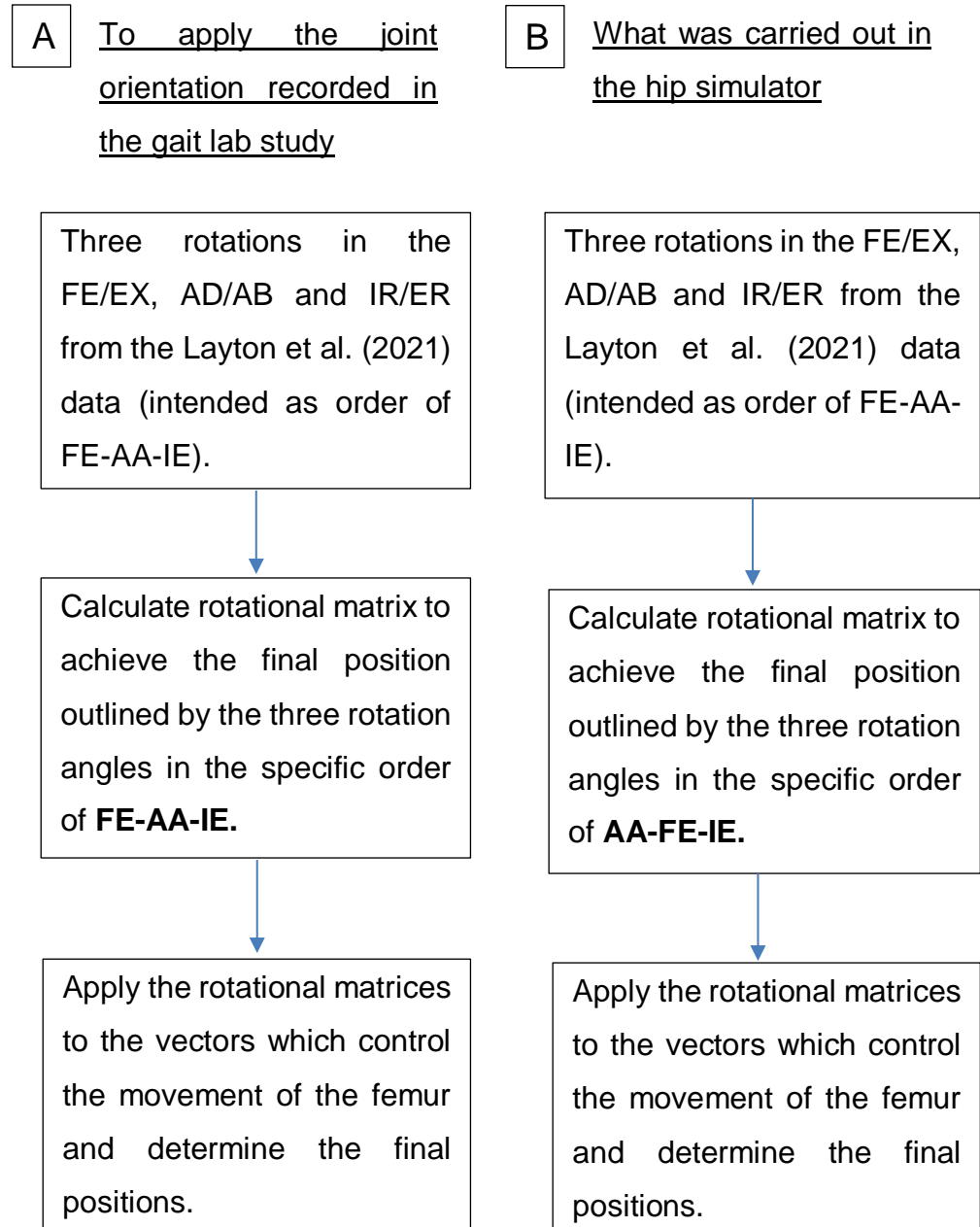


Figure 6.2 A consort diagram demonstrating the process used to calculate a rotational matrices from a set of three rotations and move the femur component in relation to the fixed acetabular component. A) to achieve the joint orientation positions which were recorded in the gait lab study (Layton, et al., 2021). This was the process used for the geometric model in Chapters Three, Four and Five. B) The process which was carried out in the hip simulator where the incorrect order of rotations was applied.

6.2.3.3.1 Mitigations taken for using the incorrect order of rotations in the hip simulator

The first mitigation was to verify that the simulator tests were consistent with the model predictions, therefore the geometric model settings were adjusted to match those used in the hip simulator testing. Namely, the use of the hip joint angles in the previous kinematic dataset (Layton, et al., 2021), along with the simulator rotation sequence of AA-FE-IE. This step brings the modelling conditions in line with the simulator conditions and allows the isolation of differences caused by either model or experimental limitations alone. Therefore the geometric model predictions in this study all used the order AA-FE-IE to align with the application of rotations in the simulator.

The second mitigation aimed to assess whether the orientations achieved in the simulator were within the envelope of possible orientations in the wider dataset (Layton, et al., 2021). This was done by comparing the hip joint angles from the wider set of subjects in the dataset to an equivalent set of angles representing what happened in the hip simulator. These equivalent angles were calculated (Figure 6.3) by taking the three original angles used, then calculating the rotational matrices in the AA-FE-IE order and then working backwards to calculate what equivalent rotation angles would result in the same rotational matrices in the FE-AA-IE sequence. This provided three rotational angles at each point in the activity cycle which are comparable to what was carried out in the hip simulator.

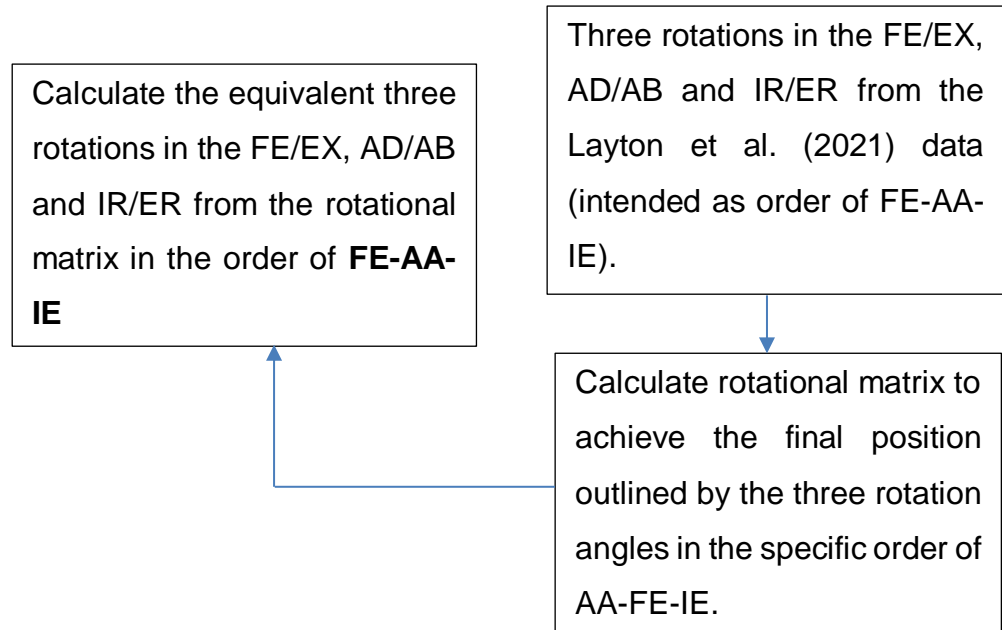


Figure 6.3 The process used to calculate the equivalent FE-AA-IE rotational angles for what was carried out in the hip simulator study.

6.2.3.3.2 Comparisons of the equivalent rotations of the simulator inputs with the previous kinematic dataset (Layton, et al., 2021)

The three equivalent rotational angles calculated in the FE-AA-IE order of rotations at each point in the activity cycle for the three squat activities were inside the population of possible orientations from the previous kinematic dataset (Layton, et al., 2021) (Figure 6.4).

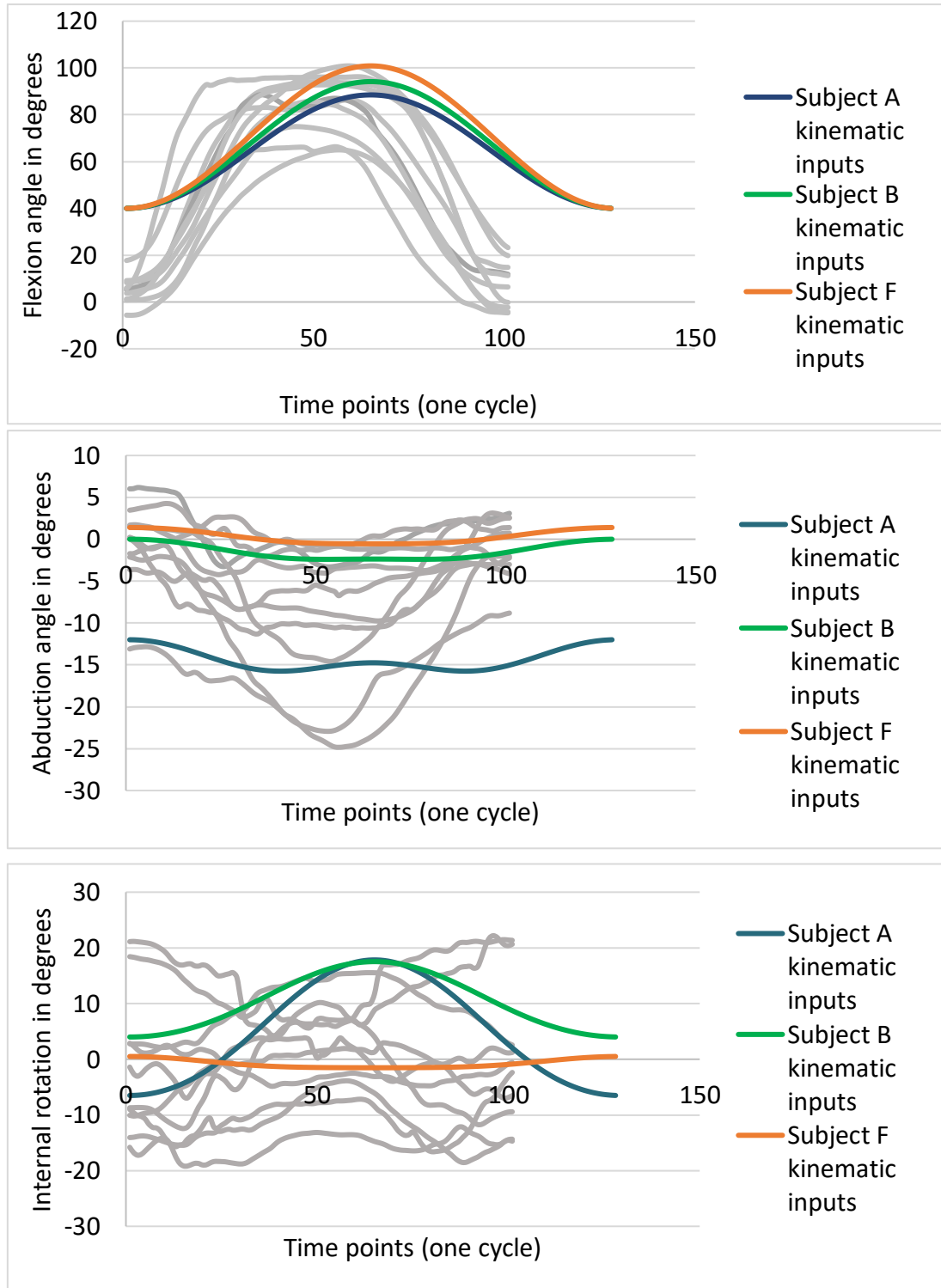


Figure 6.4 The three rotational angles for the three squat activities which were applied in the simulator in an equivalent FE-AA-IE order of rotations when compared to the Layton et al. (2021) dataset of squat activities. The grey lines represent the squat activities in the previous kinematic dataset (Layton, et al., 2021). The raw data consisted of 101 discrete time points, however the simulator software required 128 discrete time points hence the difference in time points between the raw data and simulator inputs.

6.2.3.4 Development of kinematic simulator inputs

For the kinematics to be applied in the simulator, there needed to be no vibration in the simulator which meant that the noise in the raw data needed to be reduced. The raw kinematic data for each squat activity also consisted of 101 discrete positions, however the data needed to be made up of 128 discrete positions for use in the simulator.

In the raw data, the greatest RoM of the activity would generally occur halfway through the squat activity, therefore a simplified sinusoidal wave was produced for each of the three rotations that made up each of the three squat activities (Figure 6.5). The sinusoidal waves consisted of 128 discrete positions and had a peak at the centre of the cycle. The magnitude of the peak was chosen as the exact same femoral position as the greatest RoM during each squat activity which also caused the greatest impingement based on geometric model measurements. The lower trough of the sinusoidal wave matched the starting point in the raw data so that the sinusoidal wave tracked the raw data as well as possible for a smooth input. The wave profiles also started in the first 5% of the cycle and ended in the last 5% of the cycle so that the cyclic motion in the simulator would run smoothly between cycles. Due to the simulator setup, the flexion rotation inputs started at 40° (the reason for this is described in detail in section 6.2.4.2).

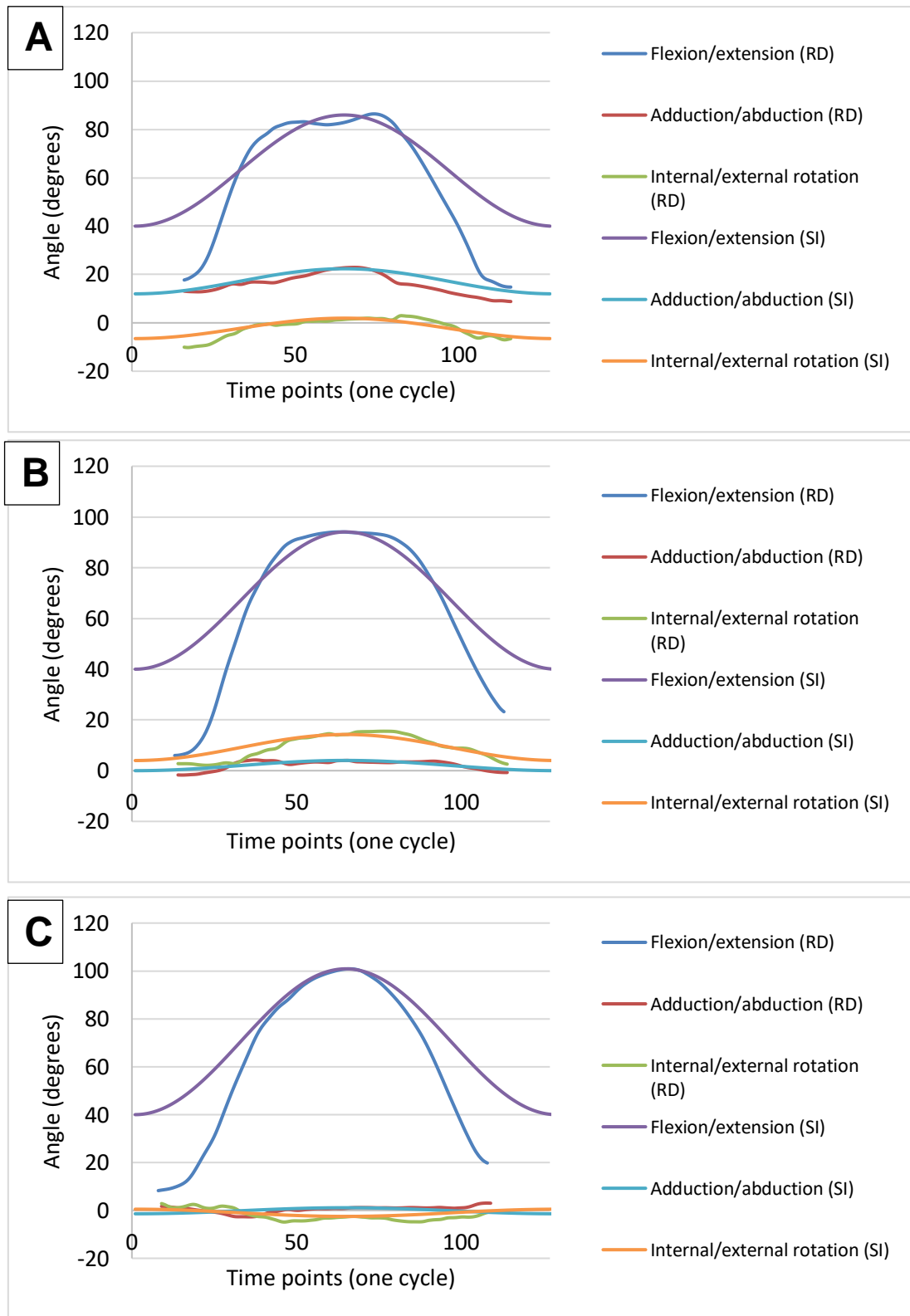


Figure 6.5 The final kinematic simulator inputs for subjects A) A, B) B and C) F with the raw data overlaid for comparison. SI=smoothed simulator input; RD=raw data. The simulator inputs for flexion started at 40° due to the setup of the simulator which is described in detail in section 6.2.4.2.

6.2.3.5 Effect of smoothing on the impingement event

To understand the effect that the smoothing of the raw data for use in the simulator had on the impingement event, the raw data and the smoothed simulator inputs were applied to the geometric model and compared for the three squat activities (Figure 6.6). The features of the impingement event such as the volumetric overlap of impingement at the greatest RoM of the activity, the duration of the impingement event and the time point in the activity of greatest volume of impingement overlap were compared. Both the raw data and the smoothed simulator inputs were expressed in the Cardan angle sequence of AA-FE-IE.

The features of the impingement event for the smoothed simulator inputs differed slightly to the raw data for the three squat activities. The volumetric overlap of components at the highest RoM of the activity was the same in the raw data as it was for the smoothed simulator inputs for Subject's A and F, but was slightly different for Subject B. The reason for this was that the simulator inputs were derived from the original FE-AA-IE rotation order and this difference in mismatched sequence of rotations led to the maximum overlap of impingement occurring at a different femoral position with different rotations for Subject B. The length of time of the impingement event was different for Subject's B and F including a longer impingement event for subject F and a shorter impingement event for subject B, potentially resulting in slightly different damage outcomes than the kinematics of the raw data would result in. The peak of the volume of impingement was at different places during the impingement event for all subjects. While there were slight differences in the characteristics of the impingement events between the raw data and the smoothed simulator inputs, there was a close resemblance in the overall volume of the impingement event and the severities of the three subject's impingement events were distinguishable.

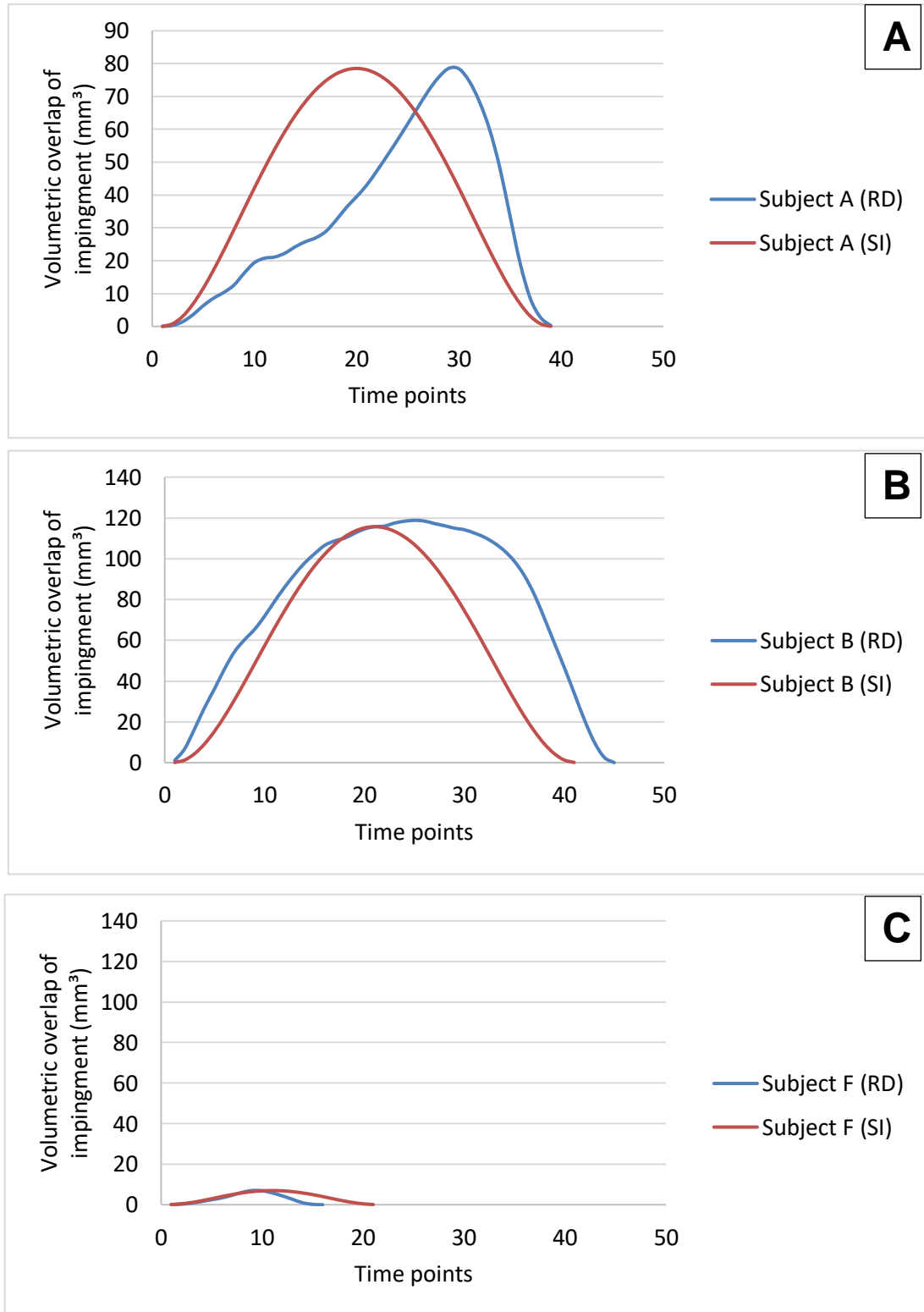


Figure 6.6 The volumetric overlap of impingement measured from the geometric model for the impingement event in the raw data compared with the smoothed kinematic squat activities of A) subject A, B) subject B and C) subject F. SI=simplified simulator input; RD=raw data . The order of rotations for the geometric model was AA-FE-IE.

6.2.3.6 Angular sliding distance during impingement

The angular sliding distance during the impingement activity was analysed in the raw data and compared with the smoothed simulator inputs using the geometric model. The location on the liner rim at the start of the impingement event was captured and then compared with the location at the end of the impingement event (Figure 6.7). To measure the angular sliding distance, the angle between the centre of the location of impingement at the start of the impingement event and at the end of the impingement event was measured. The angular sliding distances around the rim of the liner were 3.3° for subject A, 3.4° for subject B and 1.1° for subject F. While the angular sliding distance for the raw data of the kinematics of the three squat activities was relatively low, the smoothed simulator inputs had zero sliding distance, which was a limitation to this study.

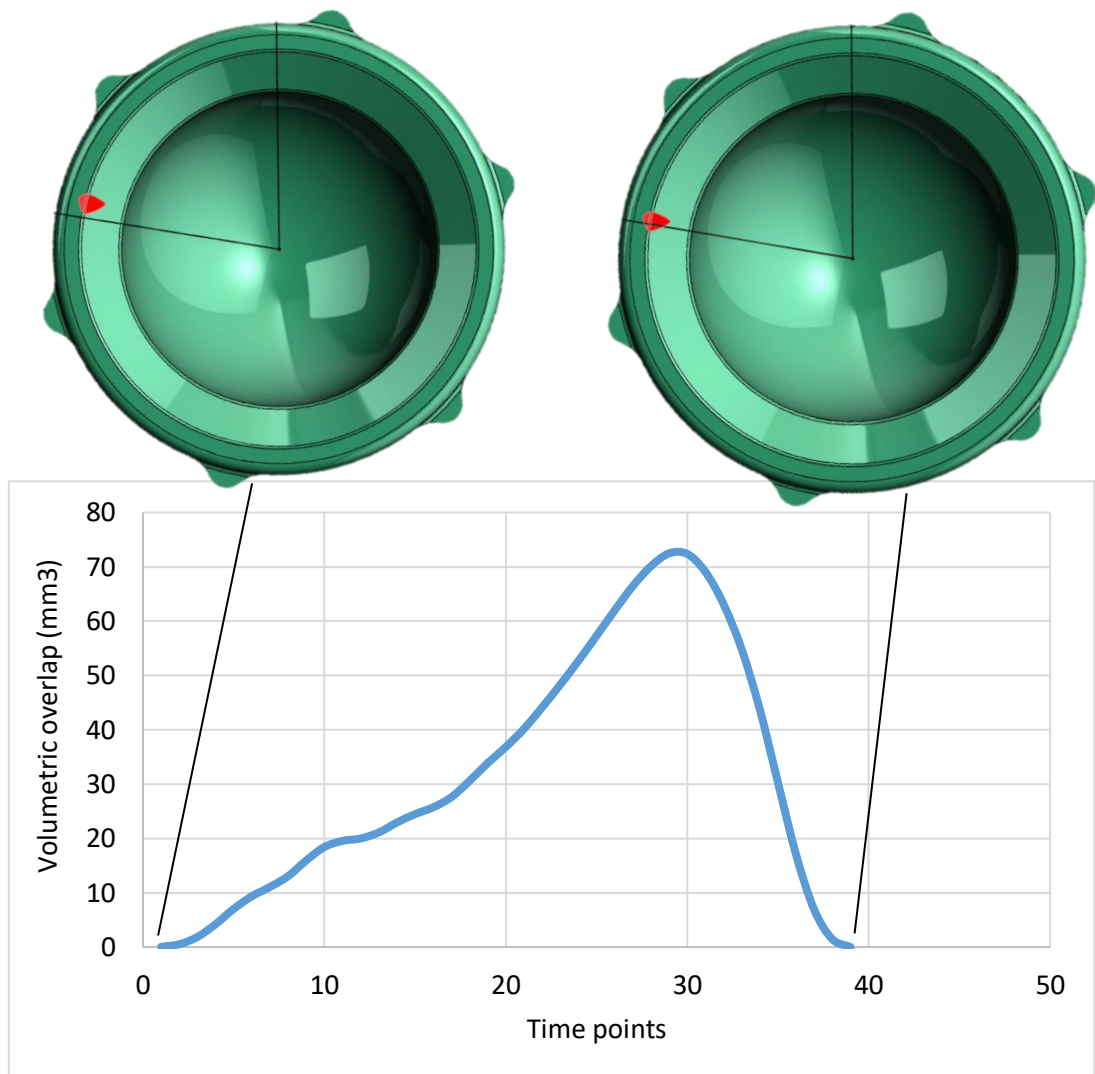


Figure 6.7 The sliding distance for the impingement event during the raw data of the squat activity of Subject A. The green liner on the left is demonstrating the location of impingement at the initial impingement contact. The green liner on the right is demonstrating the impingement contact at the end of the impingement event. The graph demonstrates the volumetric overlap of impinging solids in the geometric model over the impingement event.

6.2.3.7 Simulator force input

The kinematic dataset (Layton, et al., 2021) included force data for some of the subject's squat activities, including two of the squat activities which were selected for this study (subject's B and F). The axial force for the two squat activities consisted of a peak of over 3400N of axial load (Figure 6.8). The magnitude of these forces would have presented a risk to the simulator as the femoral head would be at the edge of the liner during the high peak load, presenting a high risk of dislocation. Therefore it was decided to use a smaller force that would be a safer way of carrying out the test whilst still inflicting relevant impingement damage to the components.

There was a common trend for the profile of the axial force during the squat activities, which included a gradual raise to a sharp peak (Figure 6.8). Therefore a simple sinusoidal wave was defined which would represent the same axial force profile for all three of the subject's squat activity's (Figure 6.9). The current study focussed on the kinematics of the three squat activities, therefore the same force profile was used for all three subject's activities. The profile created for the force input was defined by an initial input of 300N which rose to a peak of 800N. The duration of the force application was determined by the duration of the force data from the previous dataset (Layton, et al., 2021). The peak of the force profile was centred in the middle of the cycle at the same time point as the peak range of motion of the kinematic data. These force values were selected based on a previous *in vitro* impingement test development study (Pryce, 2019). A medial-lateral force was also defined which included a constant force of 200N which was applied with the aim of keeping the femoral head inside the acetabular liner during the testing to prevent dislocation (Figure 6.9).

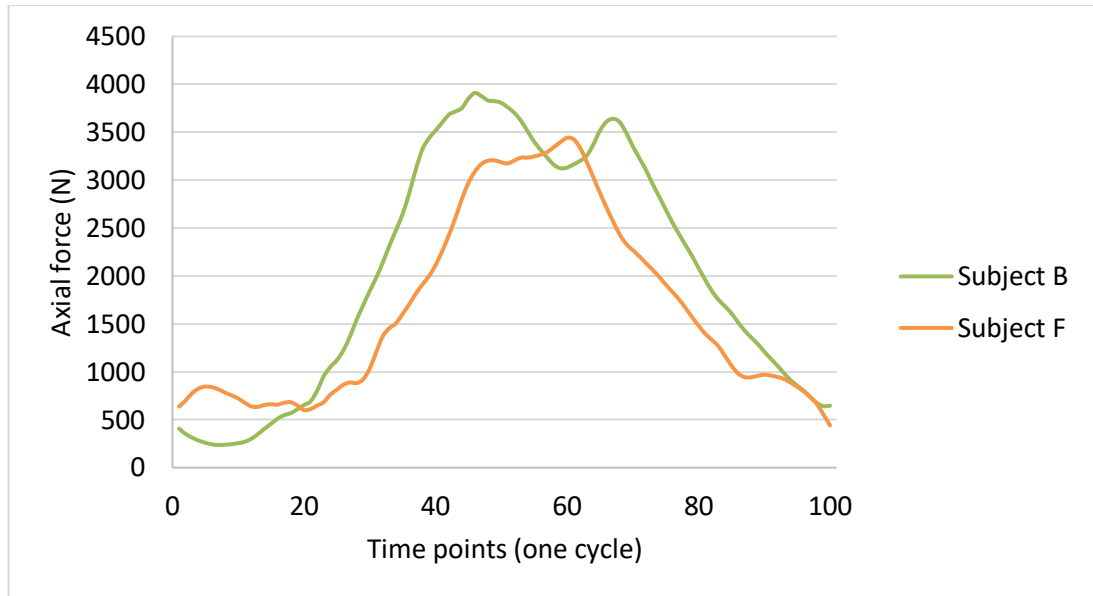


Figure 6.8 The axial force data measured in the previous kinematic dataset (Layton, et al., 2021) for Subject's B and F (Subject A's data was not registered in the study).

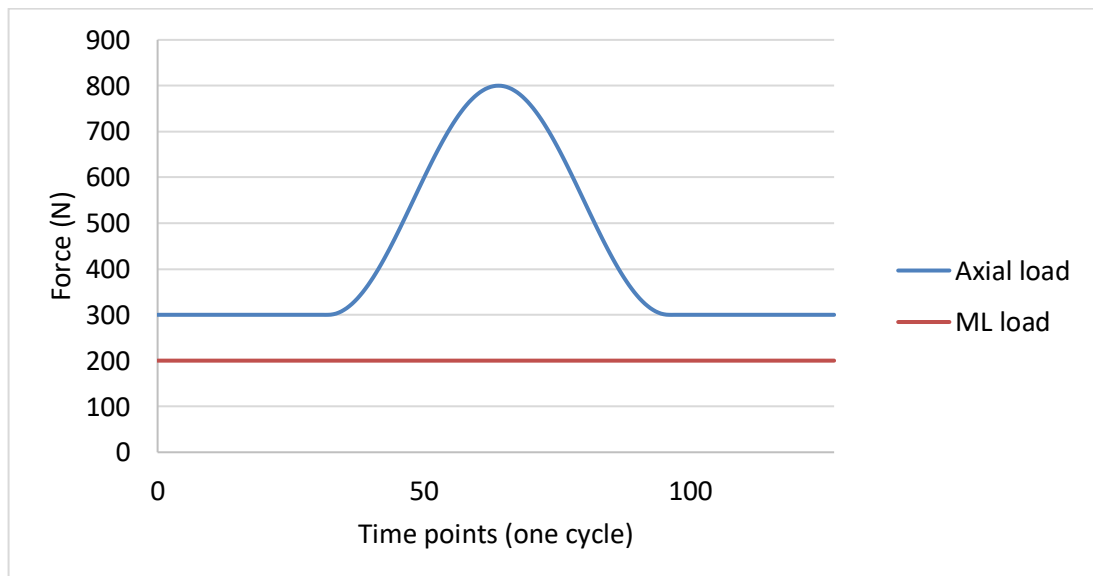


Figure 6.9 The loading profile used in the hip simulator for the impingement testing for both the axial load and the medial-lateral load. The peak of the force was positioned so that this was the point in the kinematics where the greatest range of motion was.

6.2.4 Test Setup

6.2.4.1 Simulator details and capabilities

A Simsol (Stockport, UK) Prosim Six axis single station anatomical hip simulator (AHS) was selected (Figure 6.10), which was electromechanically driven and could apply dynamic force in the three anatomical axes and dynamic motion to the three anatomical planes of rotation. The motions and forces were applied through motors which could be controlled to ensure the simulator provided the correct input profiles. The loads were applied to the top fixture of the simulator and the motions applied to the bottom fixture of the simulator (Table 6.2). In this study, the stem and head were affixed to the top of the simulator and the acetabular cup was affixed to the bottom of the simulator, therefore the femoral stem was loaded and the motions were applied to the acetabular cup.

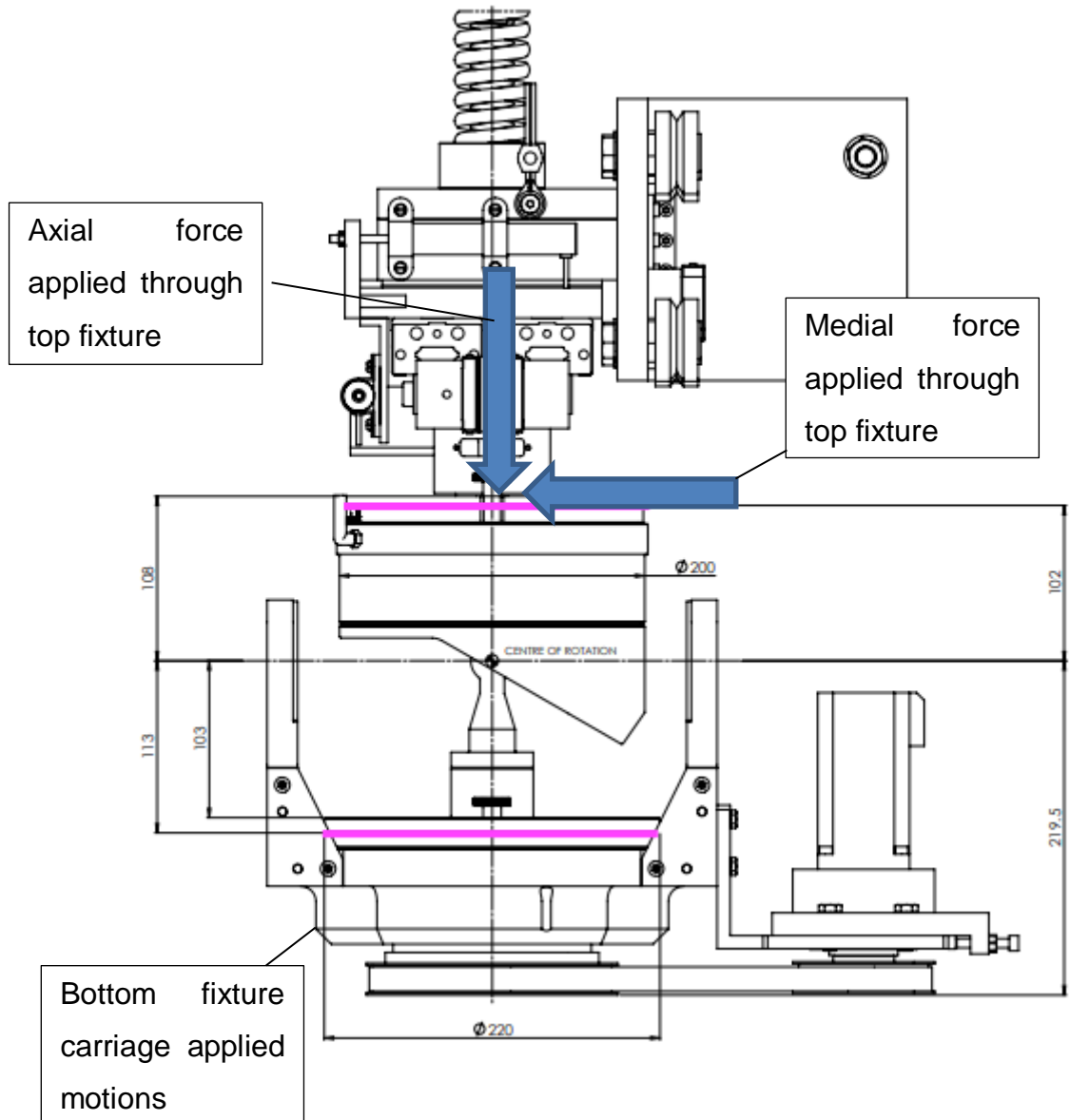


Figure 6.10 Simsol Prosim six axis hip simulator (AHS) schematic drawing of the working area and height of the centre of rotation. The pink lines indicate the size of the working space in the simulator and the height needed for the design of the fixtures to achieve the correct centre of rotation. Note: the components in this diagram are test dummy components and were not used in the current study. In the current study, the femoral stem and head were fixed to the top of the simulator and the acetabular cup attached to the bottom of the simulator.

Table 6.2 The motion and load specifications of the Simsol Prosim six axis, single station anatomical hip simulator.

Axis	Load/Motion	Applied to top/bottom fixture	Details
1	Load – Axial force	Top fixture	Up to 5kN applied to the top fixture through the combination of a motor and a tension/compression spring which can be either force or displacement controlled.
2	Load – Medial/lateral force	Top fixture	Up to 1.5kN applied to the top fixture through the combination of a motor and a tension/compression spring which can be either force or displacement controlled.
3	Load – Anterior/posterior force	Top Fixture	Up to 1.5kN applied to the top fixture through the combination of a motor and a tension/compression spring which can be either force or displacement controlled.
4	Motion – Flexion/extension	Bottom fixture	Up to +10/-25° of motion applied to the bottom fixture via displacement control.
5	Motion – Adduction/abduction	Bottom fixture	Up to ±61° of motion applied to the bottom fixture via displacement control.
6	Motion – Internal/external rotation	Bottom fixture	Up to ±45° of motion applied to the bottom fixture via displacement control.

6.2.4.2 Simulator setup

The simulator applied axial load to the top fixture which could not rotate, therefore any component loaded into the top fixture must remain fixed relative to the direction of the load. Whereas the component loaded into the bottom fixture could rotate relative to the load direction. The force direction during high flexion activities of daily living pushed the femoral head towards the posterior of the hip while the acetabular components rotated relative to the force direction (Nadzadi, et al., 2003). Therefore the components were setup in an inverted orientation compared to their anatomical position with the stem fixed to the top fixture and the acetabular components fixed to the bottom fixture. With the axial force pressing down from the top of the simulator and pressing the femoral head onto the liner and the kinematic motion moving the acetabular cup on the bottom fixture relative to the direction of the force, the force direction would be in a clinically-relevant direction throughout the squat activity.

The capabilities of the anatomical hip simulator meant that the flexion/extension could be a maximum of $\pm 61^\circ$, however one of the squat activities needed a flexion angle up to 100.9° . Therefore, a cup fixture was produced so that the starting neutral position of the hip joint was at a relative pre-flexed 40° position by rotating the cup the appropriate inclination and anteversion angle which was associated with a 40° flexion rotation (Table 6.3). Fixtures were produced which fixed the acetabular cup in the correct pre-flexed orientation (Figure 6.11) (fixtures described in more detail in section 6.2.4.3). This provided a relative maximum flexion capability of the hip components of up to 101° . The capabilities of the simulator also meant that the maximum abduction/adduction angle was $+25^\circ/-15^\circ$, however one of the squat activities needed an adduction angle of $(-)21.2^\circ$. Therefore to achieve the higher adduction rotations, the fixtures were rotated 180° around the superior/inferior axis so that there was a maximum abduction/adduction capability of $+15^\circ/-25^\circ$. With this rotation, all of the relevant forces and rotations were reversed so that the setup rotated in the correct directions.

Table 6.3 The acetabular cup orientation in the geometric model in terms of the radiographic inclination and anteversion. The values include the orientation of the acetabular cup in the femoral coordinate system at the starting position in the geometric model and the orientation of the acetabular cup in the femoral coordinate system after the femur has been flexed 40°. The pre-flexed 40° cup orientation is the orientation of the cup used for the simulator setup.

Orientation of the acetabular cup	Radiographic inclination	Radiographic anteversion
Original orientation	45°	10°
Pre-flexed 40° orientation	49.83°	-14.31°

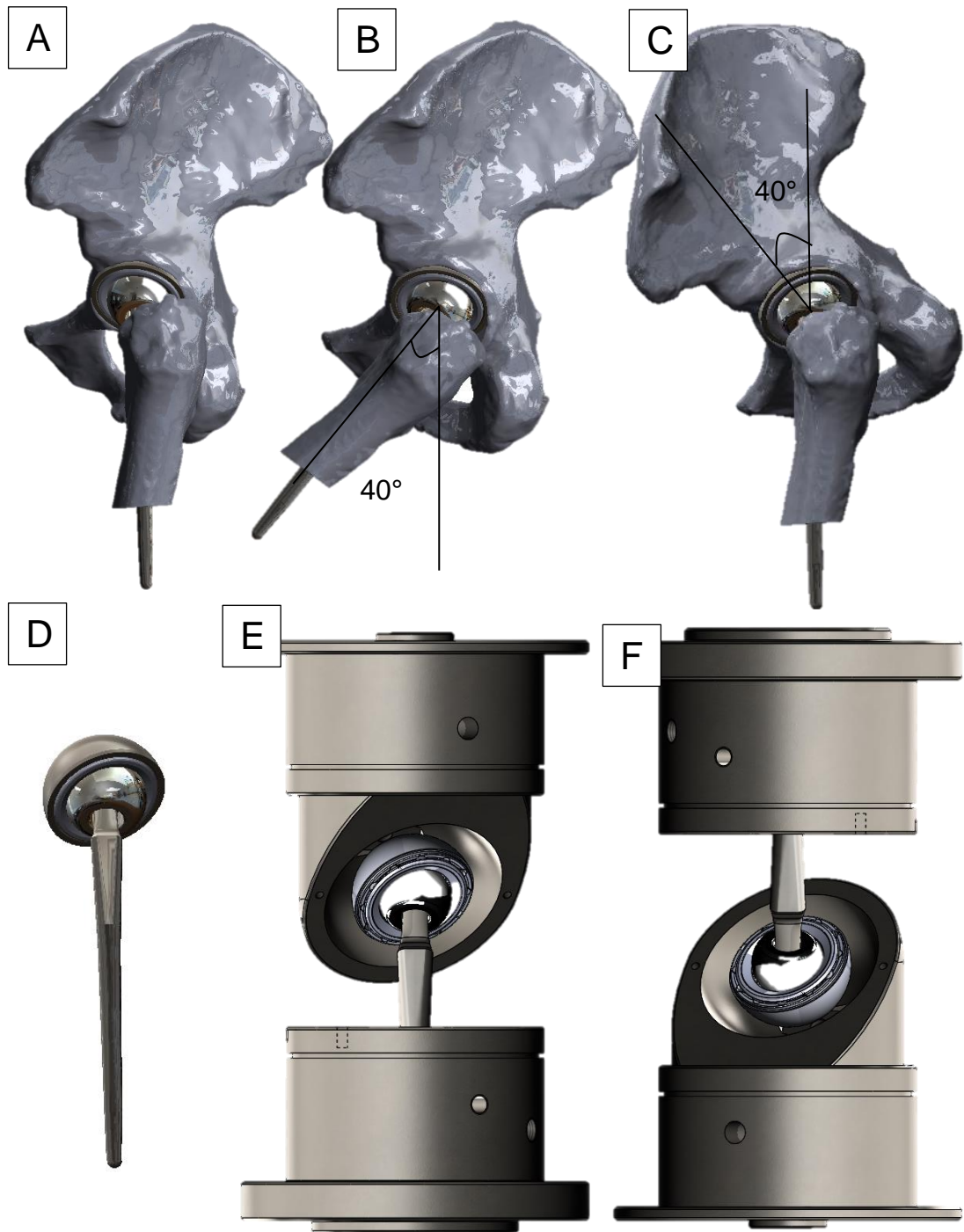


Figure 6.11 Geometric models demonstrating the process of pre-flexing the femur 40° and the mounting of the components into the fixtures. Followed by the components being flipped upside down so that the force direction is correct during the impingement testing. A) A sagittal view of the original setup of the bony geometries and components. B) The femur is flexed 40°. C) The relative position of the femur and pelvis is rotated so that the femur is in its original position. D) The bony geometries are removed leaving just the stem, liner and head. E) The components are mounted in fixtures. F) The fixtures are rotated 180° resulting in the final setup in the hip simulator.

6.2.4.3 Fixtures and mounting of components

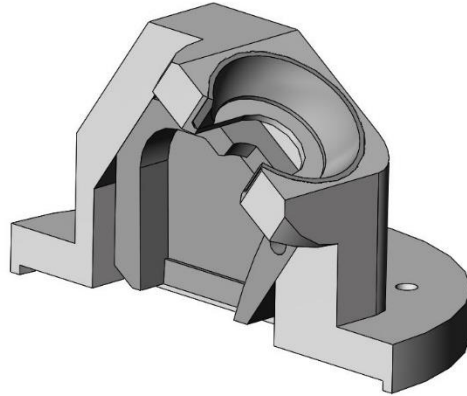
To achieve the correct component positions and height of the CoR in the simulator, the components were attached to fixtures. Some fixtures already existed in the laboratory which satisfied the need of the current study (Pryce, 2019) (Figure 6.12). This included a stem holder which housed the cemented stem in a clinically-relevant orientation and a stem cementing jig which held the stem in the correct position during the cementing process. The stem holder was designed for a different simulator (Prosim Single-Station Deep Flexion Electromechanical Hip Simulator - "SSHS") and therefore would position the stem at an incorrect height for the CoR of the AHS. To adapt the existing stem holder to allow for the stem and head to have the correct CoR and to fix to the AHS, a plate was produced which allowed fixation of the stem holder to the AHS to achieve the correct height for the CoR.

A new acetabular cup fixture was designed and manufactured to provide the correct anteversion and inclination angles needed for this study. The acetabular cup fixture was intentionally designed for the SSHS and a plate adaptor was also produced as a risk aversion measure in case of any problems with the AHS, the study could be adapted for use on the SSHS. The two plate adaptors and the acetabular cup fixture were manufactured from Stainless Steel 303 and the engineering drawings for these three parts have been added to the appendices (Appendix A). To ensure the loads were applied to the fixtures at the correct height in the simulator, a load spacer was produced so that the spring loading of the axial force was in direct contact with the fixtures. The load spacer was produced so that the fixtures and the load spacer combined would have a height of 2150mm which was the height of the working area in the AHS (Figure 6.10). The load spacer was made to be 71mm and was produced out of Delrin (polyoxymethylene).

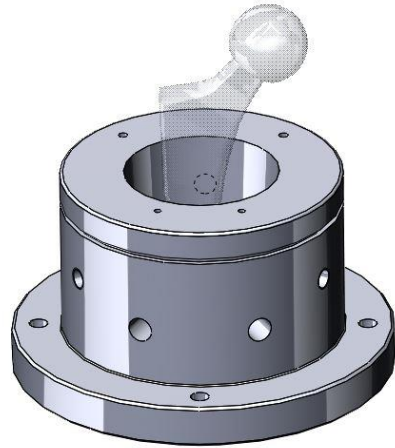
The THR components were cemented to the fixtures using poly (methyl methacrylate) (PMMA) cement. To ensure that the orientation and the CoR of the acetabular liner was correct in the fixtures, a cementing jig was designed and produced so that the shell could be cemented inside the fixture at the

correct position to ensure that the liner would fit inside the shell at the correct height for the CoR of the simulator. The cup cementing jig was produced out of Delrin and could temporarily attach to the cup holder for cementing. The engineering drawing for this part has also been added to the appendices (Appendix A). For the stem, the existing stem cementing jig was used which could already attach to the stem holder.

Existing fixtures

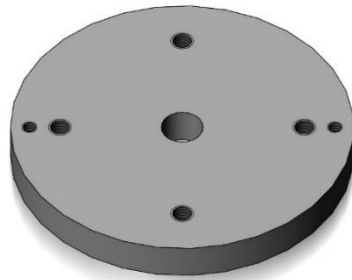


Stem cementing jig (Delrin)

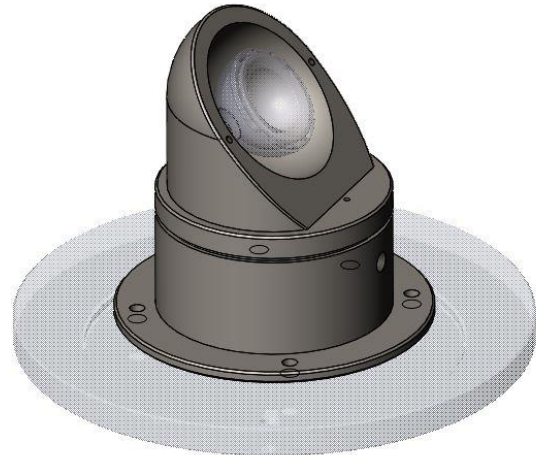


Stem holder (Stainless Steel 303)

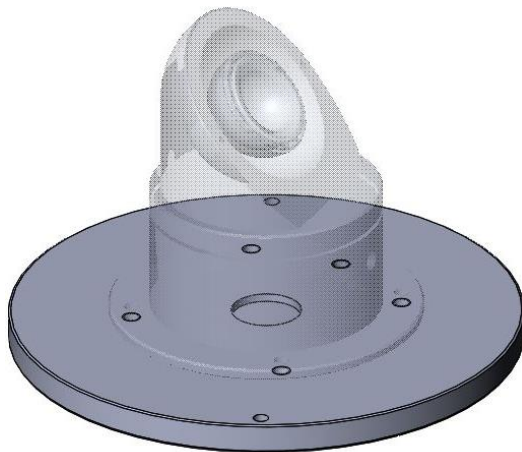
New fixtures



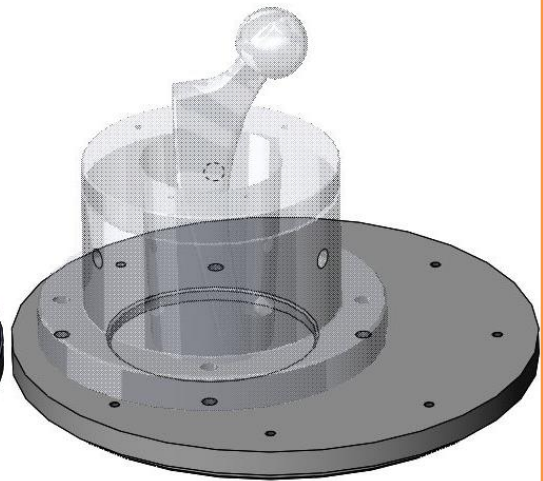
Cup cementing jig (Delrin)



Cup holder (Stainless Steel 303)



Acetabular plate adaptor
(Stainless Steel 303)



Femoral plate adaptor
(Stainless Steel 303)

Figure 6.12 The fixtures which were used in the current study including those that already existed and those that needed to be developed.

6.2.4.4 Sensitivity analysis for cementing process

The aim of the cementing process was to fix the components in place with a specific CoR and orientation for both the acetabular cup and femoral stem and head. To understand the effects of minor changes of up to $\pm 5^\circ$ to the orientation of the components due to potential errors in the cementing process, the geometric model was used with a setup of the THR components and a sensitivity analysis was carried out on the femoral stem orientation (Figure 6.13). The stem position was modified by $\pm 5^\circ$; inaccuracies in the cementing process were not expected to be greater than $\pm 5^\circ$. The stem was rotated in anteversion and adduction/abduction and the resulting volume of impingement was measured in the geometric model.

The volume of impingement overlap was effected by the anteversion and the adduction of the femoral stem. This meant that slight inaccuracies in the cementing process could have effected the severity of the impingement damage. However, the order of impingement severity for the three subjects remained consistent, no matter the orientation of the femoral stem. It was clear that slight changes of up to $\pm 5^\circ$ in the resulting orientation after the cementing process could effect the amount of damage expected and this demonstrated that the expected volumes of impingement were sensitive to changes in component orientation.

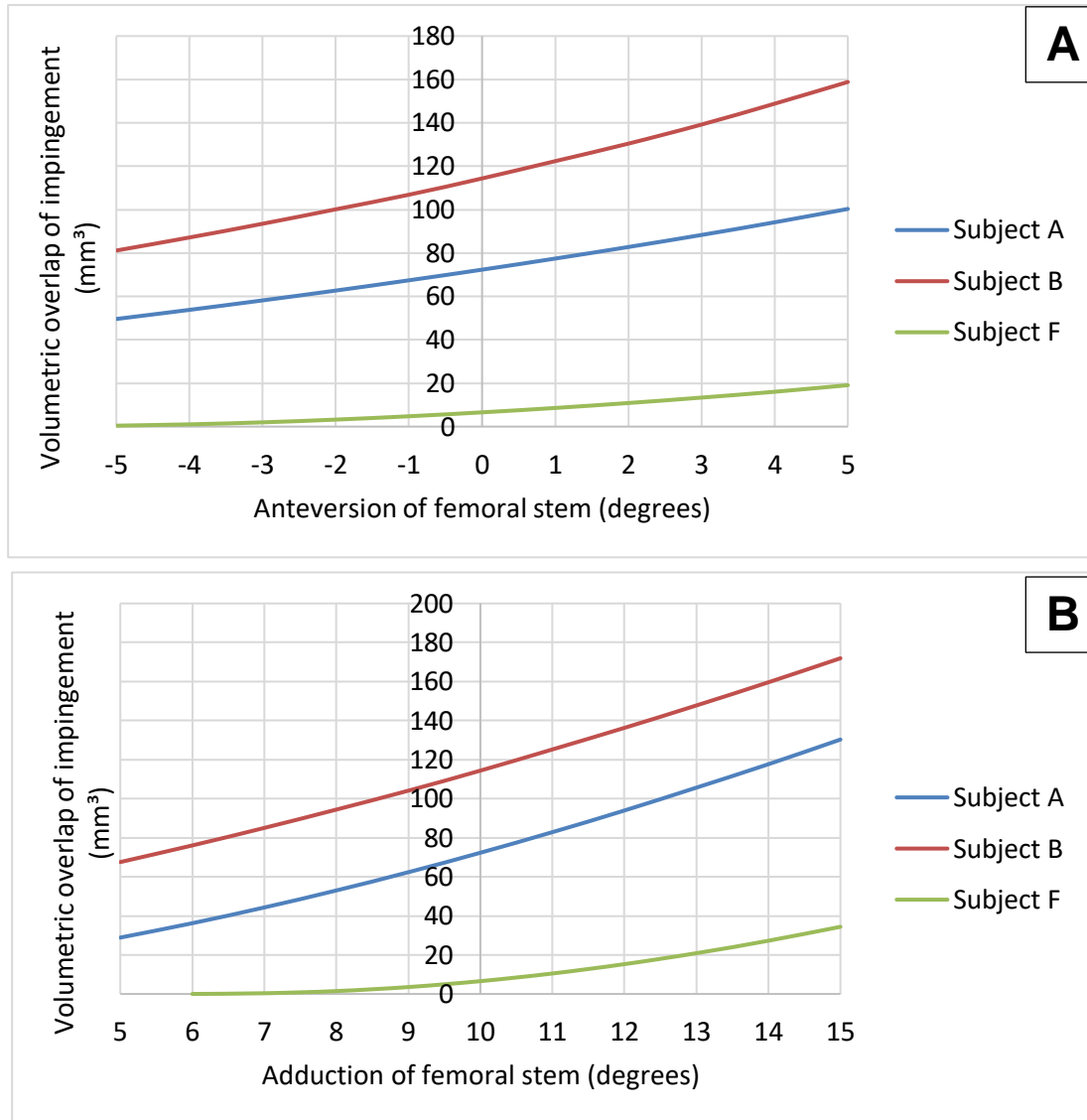


Figure 6.13 A sensitivity analysis for the cementing process measured in the geometric model including A) the effect on the volumetric overlap of impingement between components when the anteversion of the stem was varied and B) the effect on the volumetric overlap of impingement between components when the adduction of the stem was varied. The original orientation of the femoral stem was 0° anteversion and 10° adduction (at the y axes).

6.2.4.5 Lubrication of components

To lubricate the THR components during the testing, a lubricant which consisted of 25% new born calf serum, 0.04% sodium azide to prevent bacterial growth, and sterile water was used. A gaiter which held the serum was attached to the fixtures so that the joint was fully submerged in the lubricant throughout the test.

6.2.4.6 Calibrations

The simulator was calibrated before the start of the test following a local standard operating procedure. Externally calibrated load cells were used to calibrate the forces and torques in the simulator. Slip gauges were used to calibrate the anterior-posterior displacement and the medial-lateral displacement. There was also a zeroing fixture which ensured the correct zero positions for all motor positions and displacement sensors.

The Legex coordinate measuring machine (CMM) (Legex 322, Mitutoyo, Halifax, UK) was calibrated before each measurement using a ceramic sphere supplied by the manufacturer. Values of deviation from the sphere below 1µm were accepted.

6.2.5 Test Outputs

6.2.5.1 Pre-testing CMM measurements

All of the liners tested in the hip simulator study were scanned using a coordinate measuring machine (CMM) (Legex 322, Mitutoyo, Halifax, UK) before testing for comparison with their damaged form after testing. The liners were all kept at the same temperature in the laboratory 24 hours before testing to allow for any changes to the geometry of the liner due to temperature change. From the CMM process, a coordinate system was defined by taking point measurements on the pole, bearing surface, rim and two of the anti-rotation devices on the outside of the liner. The CMM process then consisted of scanning the bearing surface and rim as a set of coordinate points in 3D space, which described the liner articular surface and rim. The 1mm CMM probe collected 40 coordinate points across the top edge of the bearing

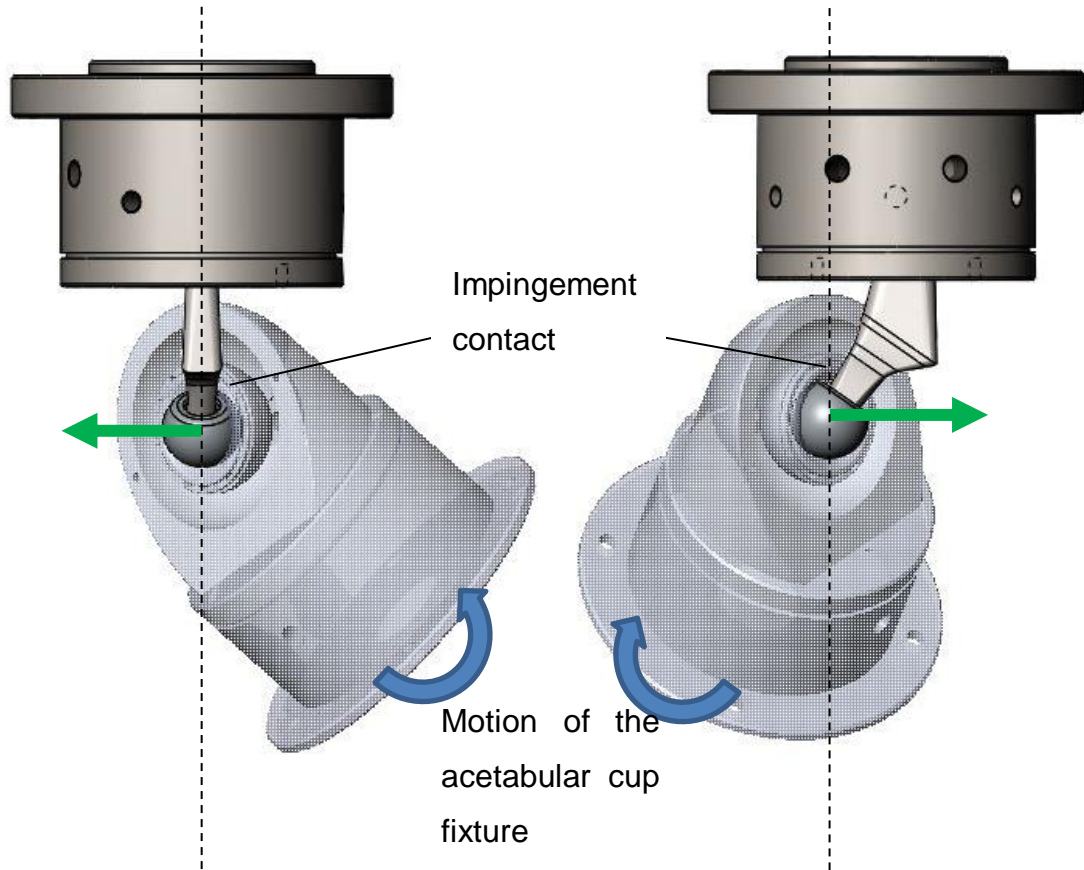
surface, over the chamfer and over the rim at 1° intervals around the liner for a liner rim analysis. The probe also analysed the bearing surface of each liner and relayed 124 coordinate points across the bearing surface at 5° intervals. The bearing surface was not measured in 1° intervals as the main focus of the analysis was the liner rim damage from impingement, with the bearing surface analysis checking for potential edge loading during the test and therefore did not need a higher detailed analysis.

6.2.5.2 Processing of CMM data

A Matlab script was used to process the CMM data (Pryce, 2019). The raw data was inputted into the script which separated the individual traces and aligned the pre-test raw data with the post-test raw data by aligning the coordinate system which was defined at the start of each test using features of the liner. The pre-test and post-test data was then compared and a plot was generated which demonstrated where the deviation from the original liner was, which represented the impingement damage. A colour coded plot was produced to visualise the impingement damage areas on the liner rim which corresponded to what the penetration depth was at the impingement site.

6.2.5.3 Displacement of the CoR in the ML and AP directions

Throughout the simulator test, the displacement of the femoral head away from the CoR of the simulator during the impingement event was measured in the medial-lateral and anterior-posterior directions (Figure 6.14) to measure potential subluxation. The anterior-posterior and medial-lateral displacement values were collected from the simulator at intervals of one cycle every 1000 cycles between the 10,000th cycle and the 40,000th cycle. An average of the 30 measurements were then carried out followed by an average of the three repeat measurement averages. This provided an average displacement of the femoral head away from the CoR including data from all of the repeats and across multiple cycles. The medial-lateral displacement and the anterior-posterior displacement were also combined to measure a resultant displacement from the CoR. This was carried out by using Pythagoras theorem.



Displacement measurement of the femoral head in the anterior-posterior axis due to the impingement contact

Displacement measurement of the femoral head in the medial-lateral axis due to the impingement contact

Figure 6.14 The displacement measurements of the femoral head away from the CoR of the simulator in the A) anterior-posterior view and B) medial-lateral view. The acetabular cup would rotate and make impingement contact on the femoral stem, pushing the femoral head away from the CoR of the simulator. Figure includes the impingement test setup demonstrating the rotation of the acetabular fixture, location of impingement contact and the direction of the measurement of the displacement of the femoral head after impingement contact.

6.2.5.4 Frequency of data collection from the simulator

The outputs from the hip simulator included the applied force and kinematic data as well as the displacement values in the anterior-posterior and medial-lateral directions. The applied force and kinematic data values were collected as 5 cycles taken every 200 cycles. The anterior-posterior and medial-lateral displacement values were collected from the simulator at intervals of one cycle every 1000 cycles between the 10,000th cycle and the 40,000th cycle.

6.2.6 Predictions from the geometric model

6.2.6.1 Volumetric overlap of impingement

Since the only order of rotation which can be applied in the simulator was AA-FE-IE, it was important to understand any effect that changing the order might have. The volumetric overlap predictions from the geometric model using the FE-AA-IE and AA-FE-IE rotation orders are demonstrated in Table 6.4.

The order of rotations made a difference to the volumetric overlap prediction of severity of impingement. With the FE-AA-IE order of rotations, subject A was predicted to result in the greatest amount of damage in the simulator, whereas in the AA-FE-IE rotation order, subject B was predicted to result in the greatest amount of damage in the simulator. This is an important distinction and should be noted when interpreting the results. The expected results of the severity of damage to the THR components in the simulator would be the AA-FE-IE rotation order predictions.

Table 6.4 The geometric model predictions of the volumetric overlap of impingement for subjects A, B and F. Two orders of rotations were included in the predictions including the original FE-AA-IE order and the hip simulator order of AA-FE-IE. These were measured by rotating the femur into the greatest range of motion during the activity and measuring the volumetric overlap of components giving an indication to the severity of impingement. The expected order of severity of impingement is the AA-FE-IE rotation order which was carried out in the simulator.

	Peak volumetric overlap in the geometric model for subject A	Peak volumetric overlap in the geometric model for subject B	Peak volumetric overlap in the geometric model for subject F
FE-AA-IE rotation order	72.36mm ³	50.20mm ³	13.15mm ³
AA-FE-IE rotation order (expected results in the hip simulator test)	78.52mm ³	115.71mm ³	6.98mm ³

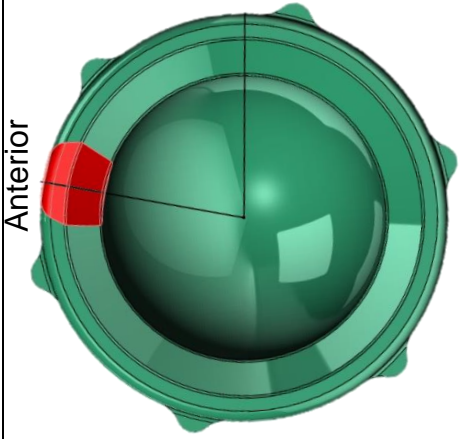
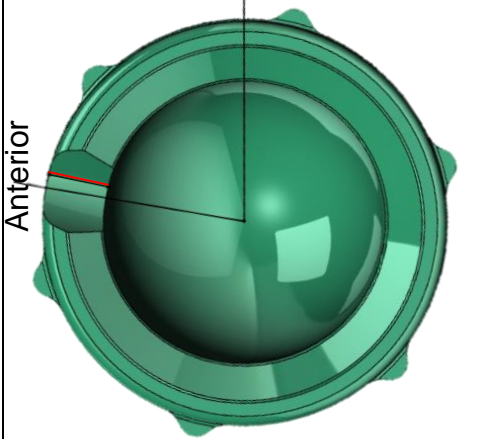
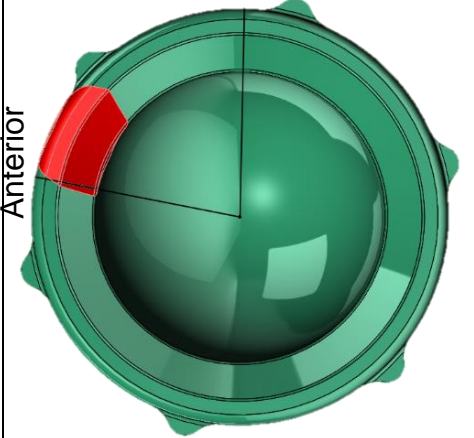
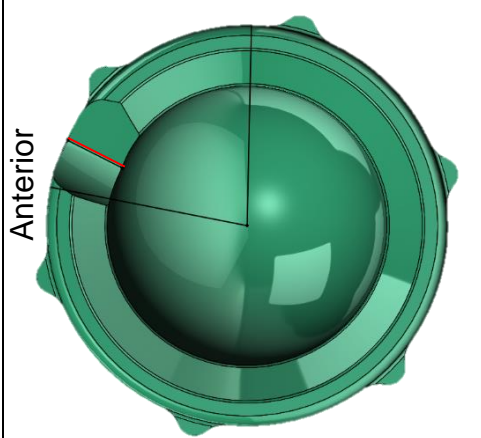
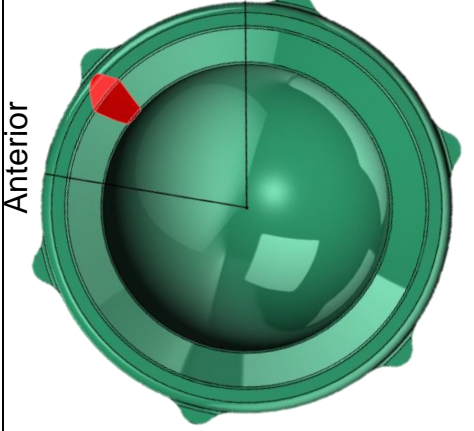
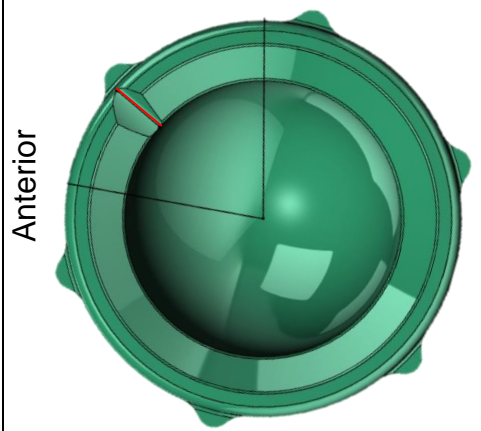
6.2.6.2 Location of impingement damage around the liner rim

The location of expected impingement damage around the liner rim could be measured with the geometric model (Tables 6.5 and 6.6). The kinematic simulator inputs were applied to the geometric model and the location around the liner rim during the most severe volumetric overlap of the activity was measured. This had its limitations however as it was not known whether the exact location of the expected damage location would be at the location of the first contact of impingement or the location of the deepest overlap of impingement. This analysis used the assumption that the deepest overlap of impingement was the location of the most severe impingement point around the rim.

Table 6.5 The geometric model predictions of the location of impingement around the liner rim. These were measured by rotating the femur into the greatest range of motion during the activity and measuring the angle of rotation at the deepest point of impingement from the anterior axis on the liner. This was carried out in the AA-FE-IE rotation order.

	Expected location of impingement as an angle clockwise from the anterior axis
Subject A	4.2
Subject B	14.2°
Subject F	31.2°

Table 6.6 The predicted location of impingement for the three kinematic squat activities which highlight the area of volumetric overlap as well as the location of the deepest part of the impingement.

	The volumetric overlap of impingement from above the acetabular liner (highlighted in red)	Highlighting the location of the deepest part of the volumetric overlap
Subject A	<p style="text-align: center;">Superior</p>  <p style="text-align: center;">Anterior</p>	<p style="text-align: center;">Superior</p>  <p style="text-align: center;">Anterior</p>
Subject B	<p style="text-align: center;">Superior</p>  <p style="text-align: center;">Anterior</p>	<p style="text-align: center;">Superior</p>  <p style="text-align: center;">Anterior</p>
Subject F	<p style="text-align: center;">Superior</p>  <p style="text-align: center;">Anterior</p>	<p style="text-align: center;">Superior</p>  <p style="text-align: center;">Anterior</p>

6.3 Results

6.3.1 Overview of results

The kinematics of three subject's squat activities were developed for use in a hip simulator to cyclically apply impingement damage of varying levels of severity to THR components. There was found to be a difference in the penetration depth of impingement damage to the liner rims when comparing the three subject's squat activities. The order of the severity of impingement damage on the liner rims was consistent with the geometric modelling predictions as well as the prediction of the location of the impingement damage on the liner rims. One of the subject's kinematic data did not result in any impingement. The resultant displacement of the femoral head away from the CoR during the impingement events was similar for the subjects which encountered impingement. There was found to be no geometric changes to the bearing surface and no evidence of any edge loading.

6.3.2 Damage to the acetabular liner rim

There was a significant difference in the penetration depth of the impingement damage on the liner rims when comparing the three different squat activities (Figure 6.15). The subject B input conditions had the greatest resultant penetration of the liner with a mean value of 0.28mm which was almost double that of subject A which had a mean value of 0.15mm. The subject F input conditions resulted in no impingement.

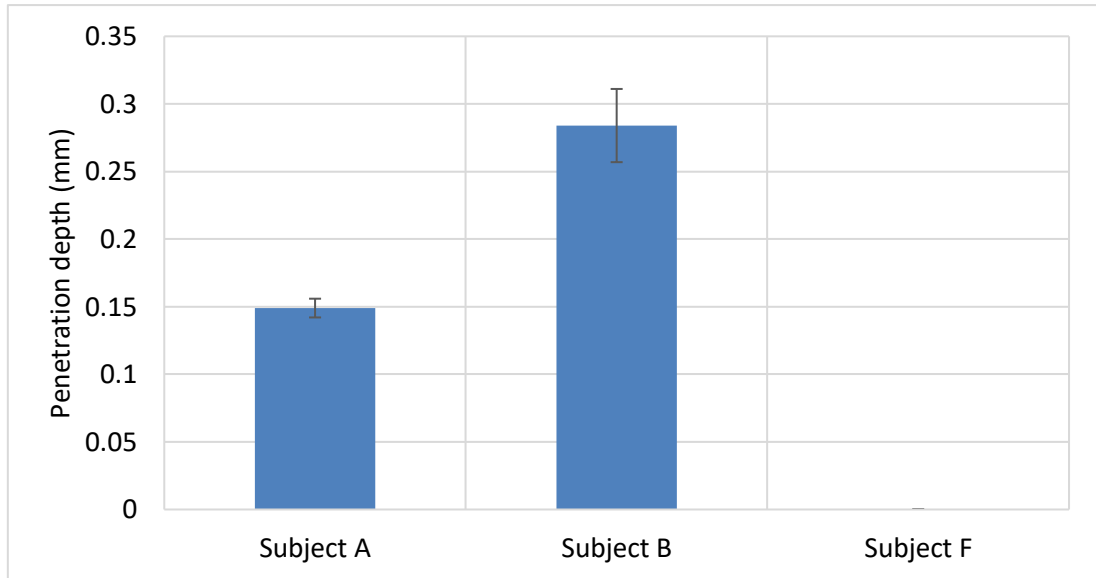


Figure 6.15 The mean penetration depth of the three squat activities. The penetration depth was recorded as the greatest deviation from the unworn liners. There were three repeats for each subject and the error bars demonstrate the standard deviation of the three repeats.

A small burr on the polyethylene liner rim was generated from the impingement testing. This was observed by physical inspection as well as in the CMM data (Figure 6.16). The small area in dark red to the right side of the impingement damage demonstrated where material had been pushed upwards and protruded from the liner rim. The impingement damage caused the protrusion of the small amount of material from the liner rim following testing using the data input from subjects A and B.

6.3.3 Location of impingement

For the input conditions from the kinematics of subject A, the mean angle of the greatest penetration depth observed on the acetabular liner rim, as measured by the CMM, was 6.3° clockwise from the anterior axis (Figure 6.16). For the kinematics of subject B, the mean angle of the greatest penetration depth observed on the acetabular liner rim was 16.7° clockwise from the anterior axis. For the kinematics of subject F, there was no impingement damage to the acetabular liner rims (for any of the repeats).

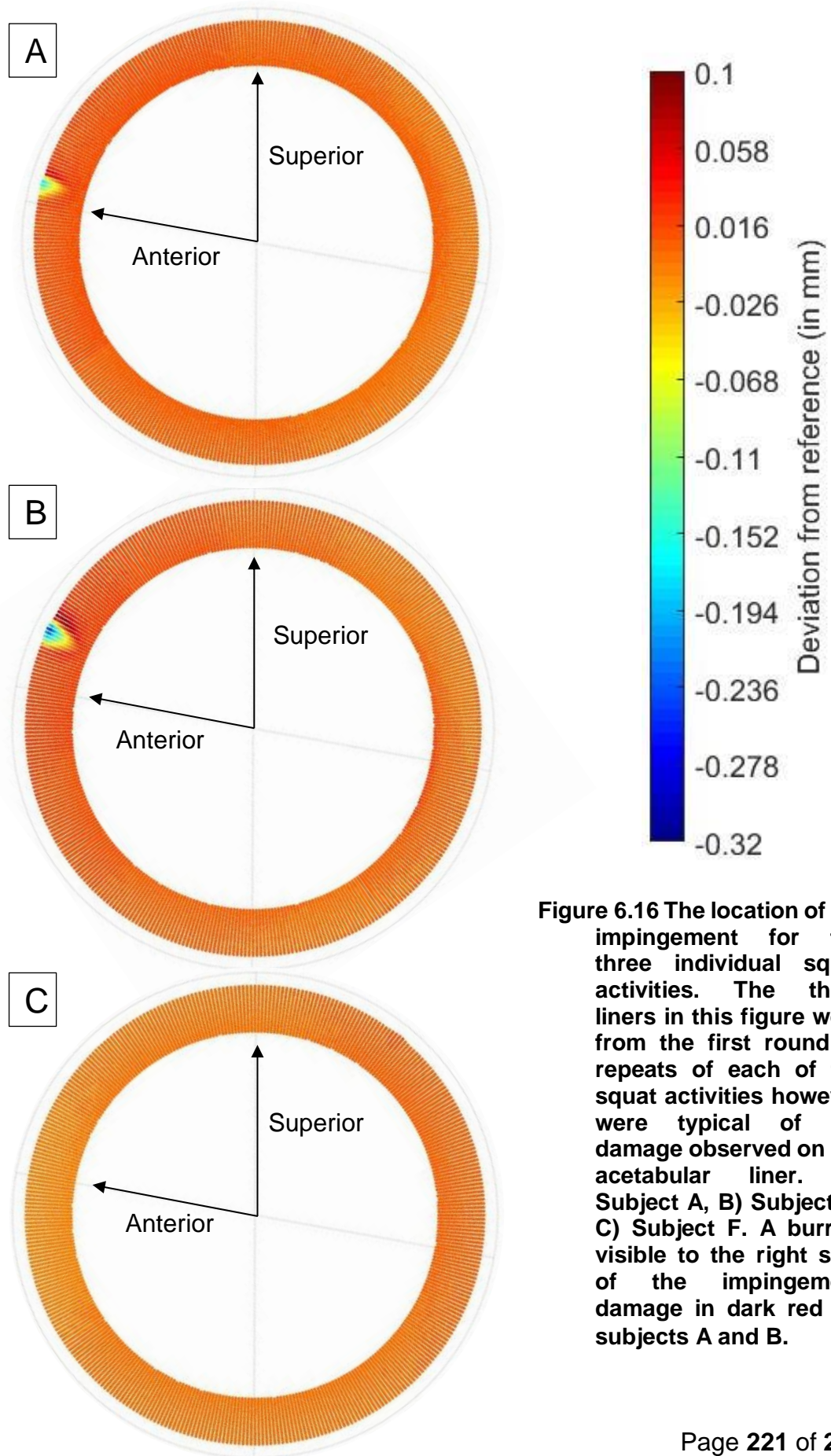


Figure 6.16 The location of the impingement for the three individual squat activities. The three liners in this figure were from the first round of repeats of each of the squat activities however were typical of the damage observed on the acetabular liner. A) Subject A, B) Subject B, C) Subject F. A burr is visible to the right side of the impingement damage in dark red for subjects A and B.

6.3.4 Displacement of the femoral head away from the CoR of the simulator in the ML and AP directions

The displacement of the femoral head away from the CoR of the simulator was measured to record any potential subluxation during the impingement events. The average displacement of the femoral head from the CoR of the simulator in the medial-lateral direction for the kinematics of Subject A was 1.73mm, for Subject B was 1.60mm and for Subject F was 0.23mm (Figure 6.17). The displacement of the femoral head away from the CoR of the simulator in the medial-lateral direction was slightly higher in subject A than in subject B. There was a slight movement of the femoral head away from the CoR of the simulator in the M-L direction for Subject F which was thought to be because of the clearance of the THR components where the acetabular cup would roll the femoral head around the bearing surface causing a slight change in the CoR of the femoral head in the ML direction. The clearance between the femoral head and acetabular liner was 0.5mm.

The average displacement of the femoral head away from the CoR of the simulator in the anterior-posterior direction for the squat activity by Subject A was 0.24mm, for Subject B was 0.66mm and for Subject F was 0.01mm (Figure 6.18). The displacement of the femoral head away from the CoR of the simulator in the anterior-posterior direction was relatively higher in subject B than in subject A. There was a negligible change in the displacement of the femoral head away from the CoR of the simulator in the anterior-posterior direction for subject F.

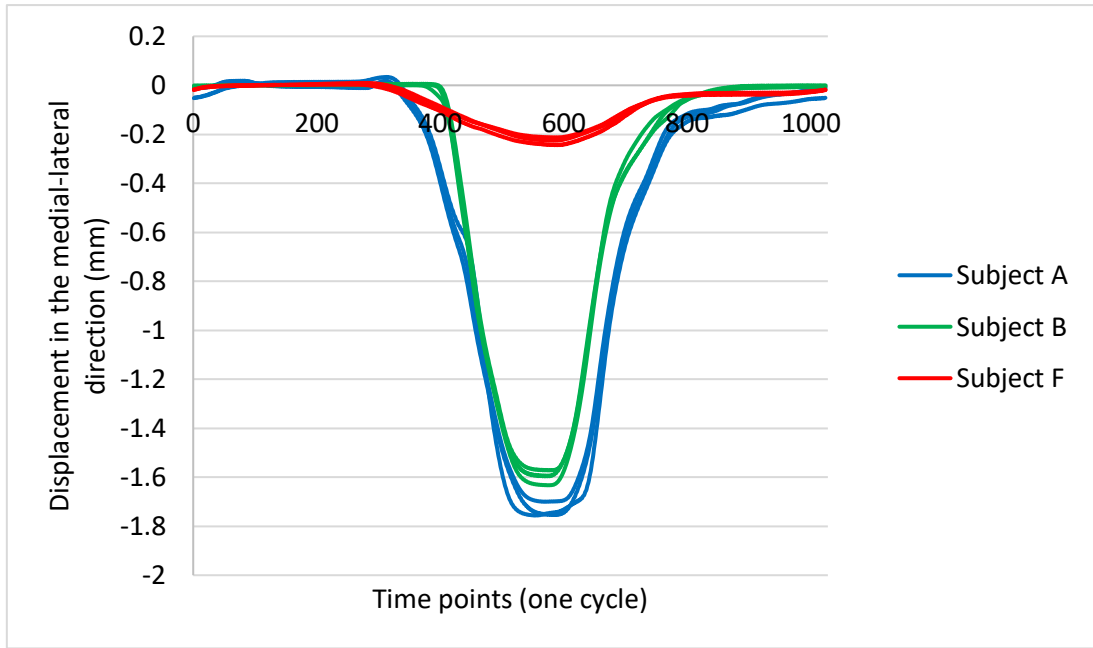


Figure 6.17 The displacement of the femoral head away from the centre of rotation in the medial-lateral direction for all of the subjects and all of the repeats. The values were taken every 1k cycles between 10k and 40k cycles

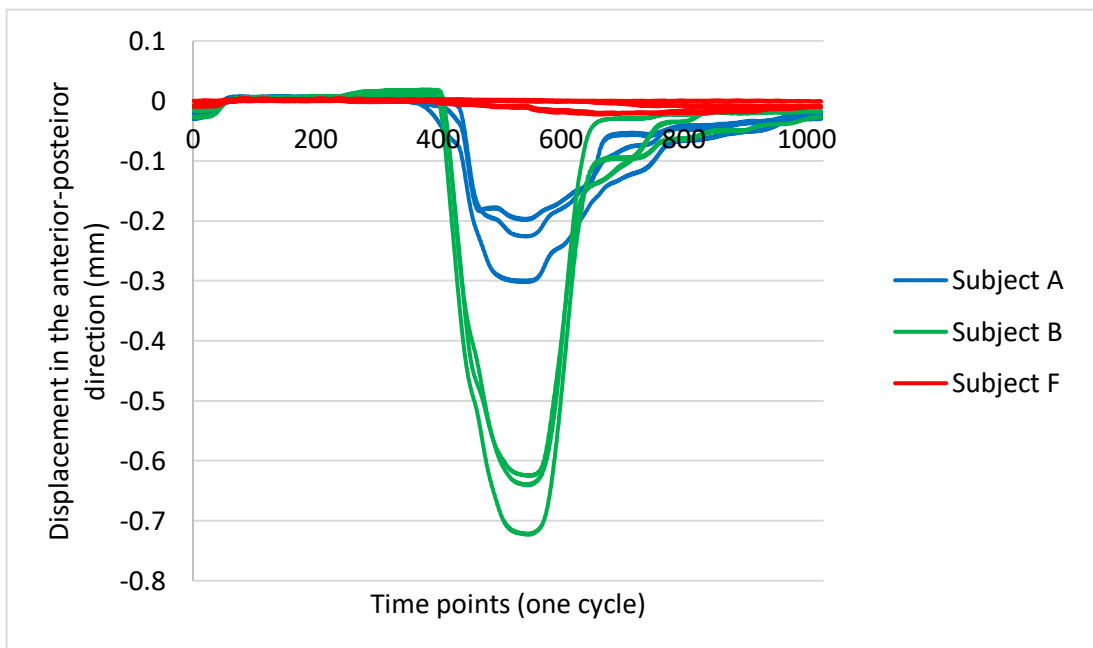


Figure 6.18 The displacement of the femoral head away from the centre of rotation in the anterior-posterior direction for all of the subjects and all of the repeats. The values were taken every 1k cycles between 10k and 40k cycles.

By combining the displacements of the femoral head away from the CoR of the simulator in both the anterior-posterior axis and medial-lateral axis, the resultant displacement was measured (Figure 6.19). The resultant change in the CoR of the femoral head during the impingement event was similar for subjects A and B. Subject F had a small change in the displacement of the femoral head, however this was thought to be because of the clearance manufactured into the acetabular liner, which would roll the femoral head slightly away from the CoR.

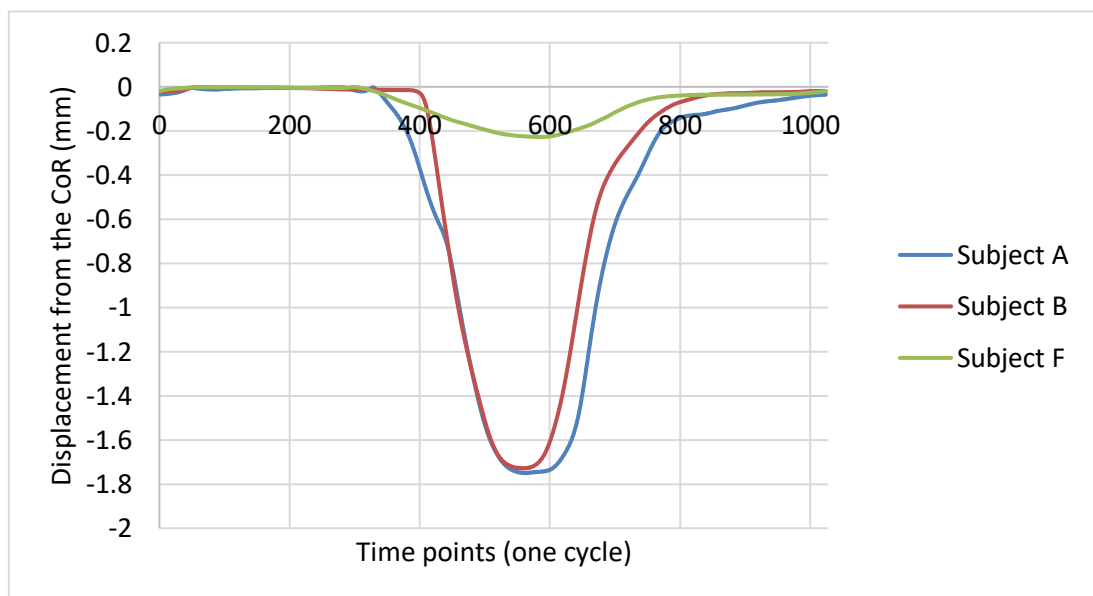


Figure 6.19 The average displacement of the femoral head away from the centre of rotation of the simulator in a resultant direction of the anterior-posterior and medial-lateral direction. The values were averages of the three repeat tests taken every 1k cycles between 10k and 40k cycles.

6.3.5 Forces acting in the simulator comparing the kinematics of subjects A and B

A 200N medial force was applied in the simulator to keep the femoral head inside the liner and prevent a dislocation event. The simulator had difficulty following the 200N constant medial force applied to the head due to the impingement and following subluxation causing a jump in the medial force. The controls on the force motors were adjusted to attempt to keep the force at a constant 200N however this was not possible for subjects A and B. Therefore there was some variation in the amount of medial force applied to the femoral head (Figure 6.20). The AP force which was an output acting on the femoral head was also measured throughout the testing. The forces acting on the femoral head in the AP direction for subject B were much higher than subject A (Figure 6.21). There was a peak in the AP force which demonstrated where the impingement event occurred. By combining these forces in the two directions, it was clear that a greater force was being applied in subject B than subject A. It is worth noting that the ML force was an input and the AP force was a measured output.

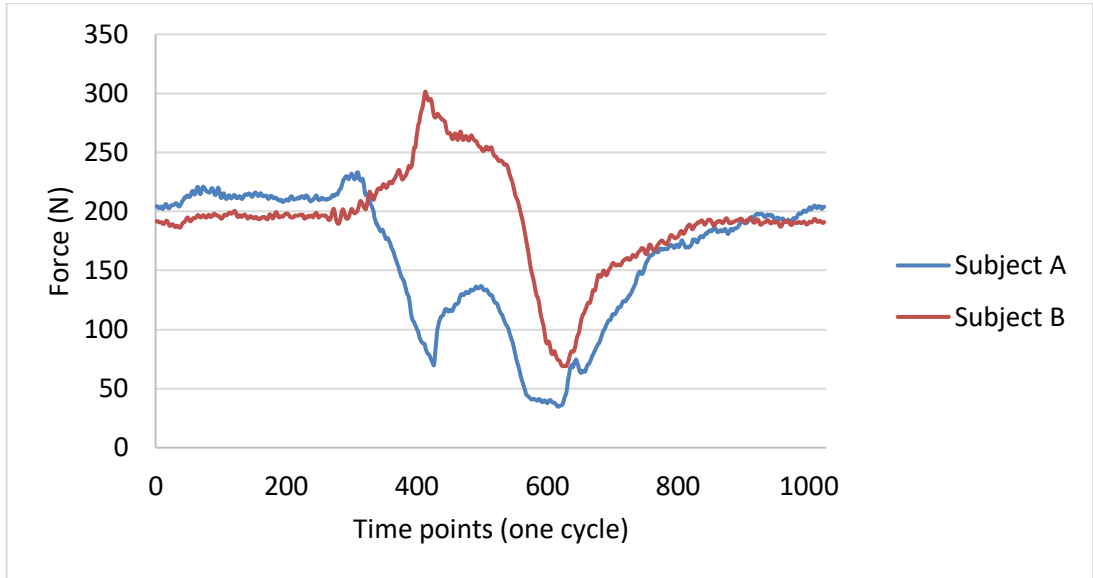


Figure 6.20 An average of the medial force applied to the femoral head by the simulator during one cycle. The average was taken from the three repeats between cycles 10k-40k (at 1k intervals).

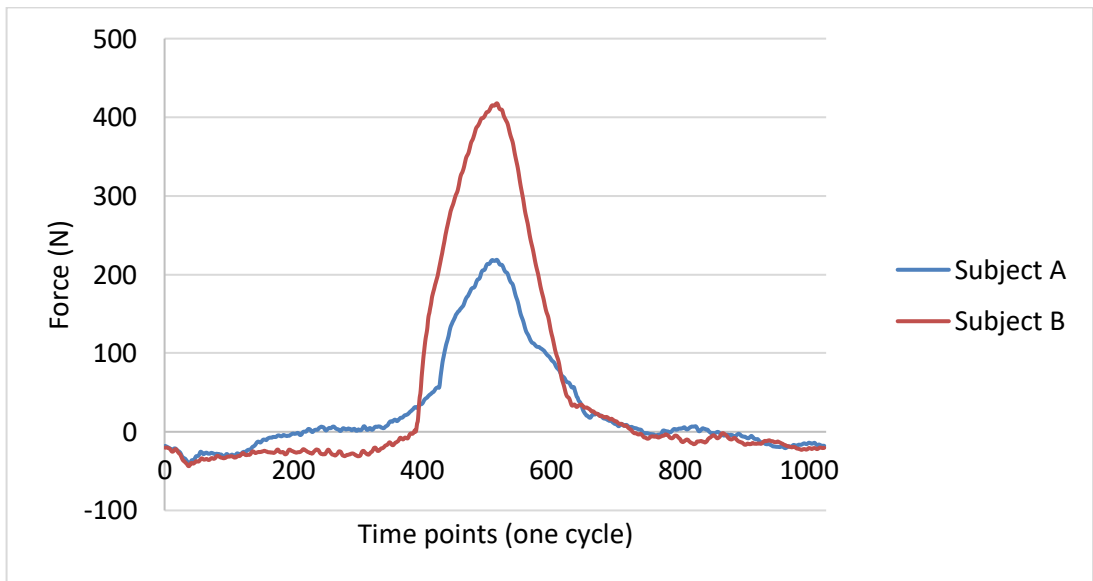


Figure 6.21 An average of the anterior-posterior force applied to the femoral head by the impingement event during one cycle. The average was taken from the three repeats between cycles 10k-40k (at 1k intervals).

6.3.6 Analysis of the bearing surface

The bearing surface was analysed using the CMM to investigate whether there was any bearing wear or edge loading during the impingement test. There was found to be negligible bearing wear to the surface and no evidence of any damage or edge loading for any of the three subject's kinematic data in any of the three repeats (Figure 6.22). The 40k cycles and load inputs were not sufficient to create any damage to the surface of the bearing.

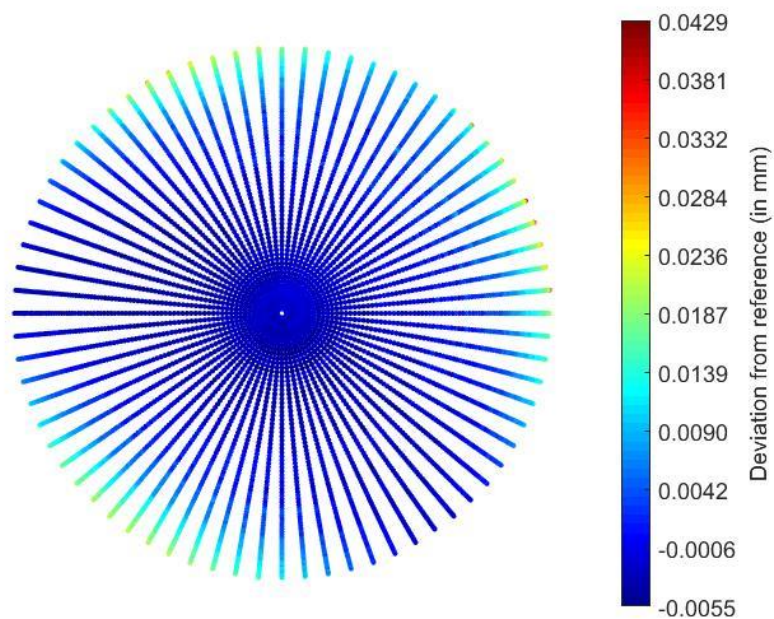


Figure 6.22 The bearing surface of a liner after the impingement test of the kinematics of Subject A (Repeat 1) as measured by the CMM, demonstrating the low levels of wear encountered to the bearing surface. This measurement was representative of all three repeats of all three subject kinematic data.

6.3.7 Comparison with geometric model predictions

The predictions from the geometric model were compared with the outputs from the simulator study. This included a comparison of the location of predicted impingement as well as the severity of impingement predicted.

6.3.7.1 Location of impingement

The geometric model could predict the location of impingement to within 3.8° when compared to the CMM measurements on the liner rims from the simulator test (Table 6.7, Figure 6.23). The geometric model predictions were on average 2.3° different to the CMM measurements when taking the mean of the repeats for subjects A and B. The CMM results did not detect any impingement on the liner rim of subject F and therefore could not be compared to the other measurements.

Table 6.7 The location of impingement measurements taken from the predictions of the geometric model and the results from the CMM measurements of the simulator study. A comparison was made between the prediction of the geometric model and the outcomes of the simulator tests.

	Degrees clockwise from anterior axis to impingement (geometric model predictions)	Degrees clockwise from anterior axis to impingement (CMM results from simulator study)	Difference from simulator results to geometric model predictions
Subject A (repeat 1)	4.2°	6°	1.8°
Subject A (repeat 2)		5°	0.8°
Subject A (repeat 3)		8°	3.8°
Subject B (repeat 1)	14.2°	16°	1.8°
Subject B (repeat 2)		16°	1.8°
Subject B (repeat 3)		18°	3.8°
Subject F (repeat 1)	31.2°	N/A	N/A
Subject F (repeat 2)		N/A	N/A
Subject F (repeat 3)		N/A	N/A

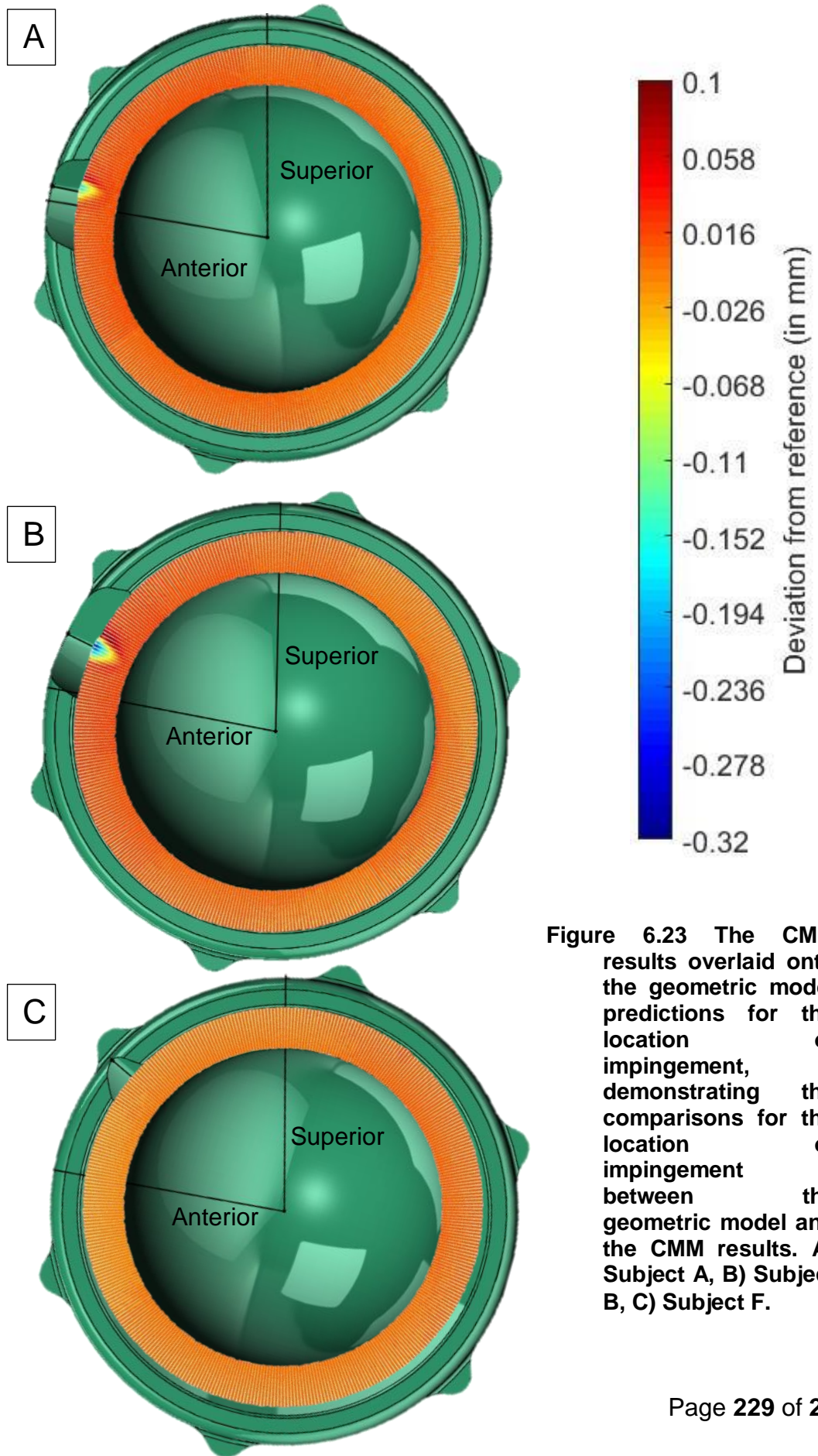


Figure 6.23 The CMM results overlaid onto the geometric model predictions for the location of impingement, demonstrating the comparisons for the location of impingement between the geometric model and the CMM results. A) Subject A, B) Subject B, C) Subject F.

6.3.7.2 Severity of impingement

One of the outputs of the geometric model predictions was the severity of impingement as measured by the volumetric overlap at the greatest volume of impingement during the activity. The outputs of the simulator were the linear penetration depth to the liner rim as measured by the CMM at the deepest part of the damage cavity. While these cannot be directly compared as they are different measures (volume and linear distance measure), they can be compared by the orders of severity. The geometric model predicted that the kinematics of subject B would have the greatest volumetric overlap and therefore would be expected to have the greatest amount of damage to the liner rim (Figure 6.24). The second greatest predicted damage was subject A followed by a low amount of impingement for subject F.

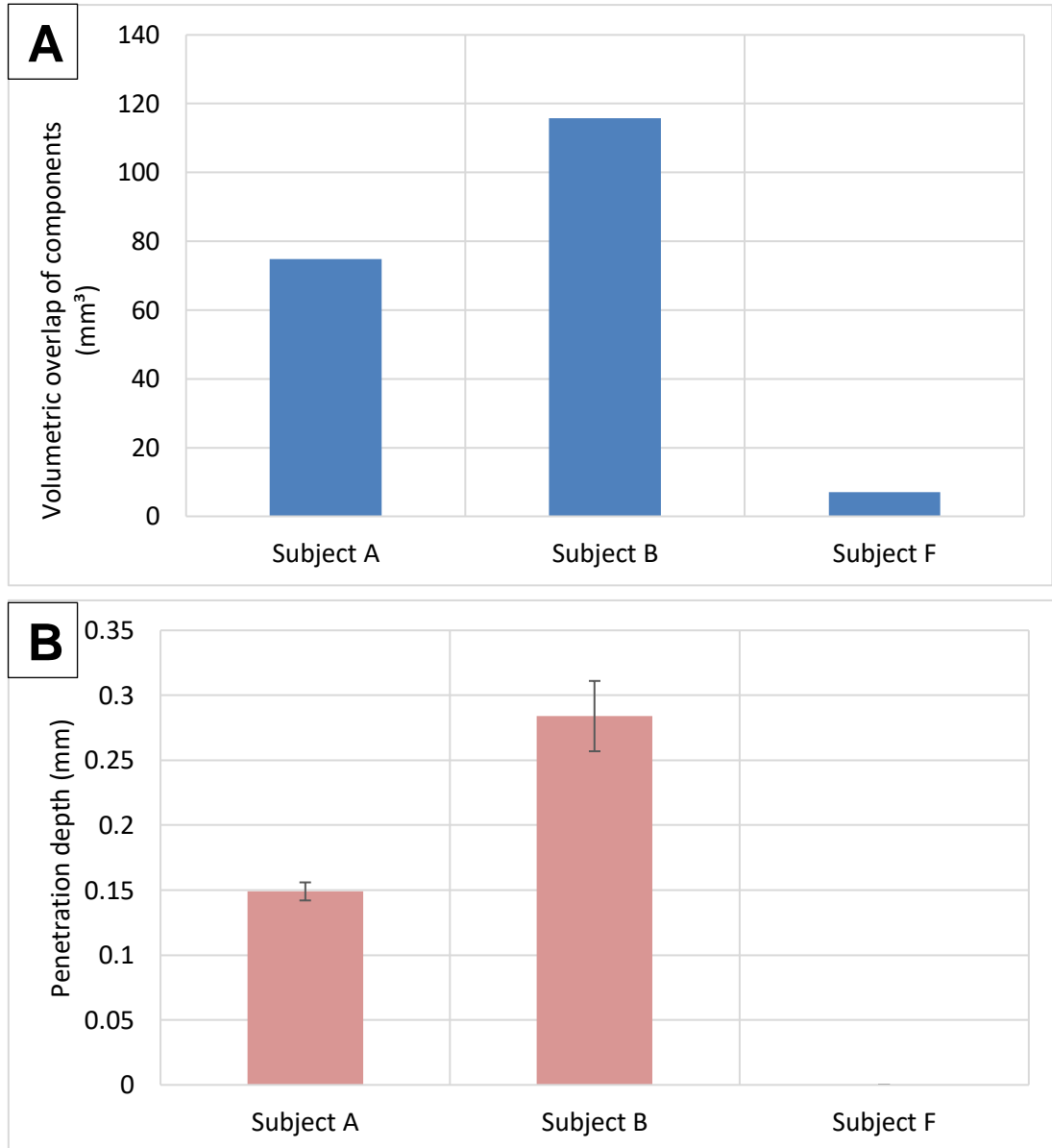


Figure 6.24 A) The predicted volumetric overlap of impingement from the geometric model demonstrating the expected order of severities of impingement. B) The penetration depths as measured by the CMM from the damaged liner rims following the simulator study.

6.4 Discussion

A method was developed to apply the clinically-relevant kinematic data of three subjects carrying out a squat activity (Layton, et al., 2021) in a hip simulator to apply impingement damage to THR components. This impingement test applied impingement damage cyclically during clinically-relevant motions and loads. The impingement damage was measured and compared across the three subjects where it was demonstrated that the kinematics of the three subject's squat activity had an effect on the severity of the impingement damage. These results were compared with the geometric model which was effective at predicting the order of severity of impingement damage for the three squat activities as well as the location of the impingement damage to the acetabular liner rims.

6.4.1 Development of *in vitro* impingement test inputs

The raw kinematic data of three subject's carrying out a squat activity was effectively developed into clinically-relevant impingement conditions which were able to be consistently replicated in the hip simulator. Force data was also used with the kinematic inputs to allow for investigation into impingement damage using clinically-relevant inputs. The smoothed sinusoidal waves closely replicated the original raw data with reduced noise and simplification of the motion, whilst still being clinically relevant by capturing the greatest RoM position of the activity and returning to the starting position, tracking the original raw data effectively. This simplification did slightly affect the impingement event in terms of the sliding distance and expected volume of impingement over time, however the impingement at the greatest point in the activity and therefore the point at which the maximum damage was thought to occur was effectively replicated.

The components were setup and orientated in the simulator to achieve a clinically-relevant impingement test. The orientation of the components were in the range of clinical-relevance (Minoda, et al., 2006; Danoff, et al., 2016). Other cup orientations would have resulted in different outcomes and the cup orientations were purposely chosen to simulate impingement. The

components were cemented in this position using jigs, which could have slightly effected the relative positions of the cup and stem if there were slight cementing errors.

6.4.1.1 Effect of the order of rotations

The order of rotations made a difference to the relative final position of the femoral and acetabular components. The International Society of Biomechanics (ISB) (Wu, et al., 2002) recommends the order of rotations as FE-AA-IE and this has been used throughout this thesis in the geometric modelling work. This was also the intended rotation order for the raw data in the previous kinematic dataset (Layton, et al., 2021), however the hip simulator used in the current study did not apply the rotations in this order and instead applied them in the order AA-FE-IE due to the nesting of the rotating carriages. This meant that the relative positions of the femoral and acetabular components were slightly different than the desired positions derived from the original raw data. The FE-AA-IE order equivalent rotations of the positions simulated in the test were calculated and this remained clinically-relevant and within the population of the dataset.

This change in the order of rotations meant that the original predictions using the geometric model in the FE-AA-IE needed to be changed so that the final positions carried out by the simulator in the AA-FE-IE order were predicted in the geometric model. Therefore all of the modelling predictions for this study were carried out using the AA-FE-IE order of rotations, meaning that the predictions were valid for comparison with the simulator work.

6.4.1.2 Effect of the size of the forces on the impingement damage

The aim for the test was to maintain a constant 200N force in the medial direction to keep the femoral head inside the acetabular cup during the impingement event and prevent dislocation. However, this was difficult to maintain as there was a sharp increase in the force when impingement and the subsequent subluxation occurred. Work was carried out on the force control for the motors to try and match the constant 200N force however this

was not possible with the time constraints of the study. Therefore the ML force was slightly varied for subjects A and B (subject F did not encounter impingement and therefore could maintain a 200N constant force). This resulted in subject A having around 135N at the time of the greatest range of motion and subject B having around 250N at the time of the greatest range of motion. This difference in medial force was not thought to have had a large effect on the damage. A previous study concluded that when the medial force was doubled during a high RoM test (from 100N to 200N), the damage increase to the acetabular liner was small at high flexion angles (Pryce, 2019). There was a measured output resultant force acting on the femoral head in the anterior-posterior direction. This AP force was the force reaction of the acetabular liner acting on the femoral head and was indicative of the force at the liner rim in the AP direction. This demonstrated the effect of the kinematics on the force being transferred in the AP direction as it was a reaction force. This data suggested that the kinematics of subject B caused this additional damage in the AP direction and therefore the kinematics of subject B generated the increased damage to the liner rims.

6.4.1.3 Force inputs in comparison to a previous dataset (Layton, et al., 2021)

The force inputs for the current study included a sinusoidal wave which had a peak of 800N at the midpoint of the cycle which was at the highest range of motion for the three squat activities. When comparing this to the force data from the previous dataset (Layton, et al., 2021), the 800N force in the current study was smaller than what was measured during the original study. The original force data in the previous dataset (Layton, et al., 2021) could not be used because of the lack of soft tissue to stabilise the joint in the simulator and not cause dislocation. The only force that attempted to keep the head inside the liner was the constant 200N ML load. Therefore clinically, there would be an increased force acting through the THR components and therefore the damage recorded in this study would be less than what would be expected in a THR patient if the same conditions described were used.

6.4.2 Measurable damage outputs

6.4.2.1 Penetration damage to the liner rims for the three squat activities

The kinematics of the three squat activities made a difference to the severity of the impingement damage to the THR components in the hip simulator as measured by the penetration depth of the liner rims. Another simulator study (Pryce, 2019) used the kinematics of the STOOP activity from a previous dataset (Nadzadi, et al., 2003) to simulate damage to THR components. However, the study did not replicate the most severe part of the activity, but instead adapted the activity until impingement occurred and then smoothed the data to replicate the activity at controlled amounts of impingement angles. The study also found that additional range of motion in the activity data resulted in greater impingement damage, which agreed with the current study.

For subjects A and B, due to the impingement damage to the acetabular rim, there was a build-up of material at the edge of the impingement site in the form of a burr which protruded outwards. This damage mode could create large wear particles and potentially be the cause of further complications to the THR such as osteolysis and aseptic loosening.

6.4.2.2 The displacement of the femoral head away from the CoR and its association with the damage to the acetabular liner rim

The displacement of the femoral head away from the CoR of the simulator was measured to record any potential subluxation during the impingement event. The resultant displacement (in the ML and AP axes) from the CoR during the impingement event was similar for both subjects A and B, despite the kinematics of subject B resulting in almost double the penetration depth of damage to the acetabular liner rim. The displacement in the AP direction was relatively greater in subject B when compared with subject A. The displacement in the ML direction was similar for both subjects. There was a small amount of ML displacement for subject F, however the kinematics of this subject resulted in no impingement damage to the liner rim. This small increase in the ML displacement of the femoral head was due to the clearance

manufactured for the acetabular liner and the femoral head which caused a slight change in the CoR of the femoral head as the acetabular cup rotated to high ranges of motion, rolling the head around the articular liner surface. This could be one reason for the increased resultant displacement of the femoral head for subject A compared with subject B. The displacement in the ML direction because of the actual impingement event could have been smaller and therefore resulted in a smaller displacement for subject A.

Previous work (Pryce, 2019) investigated the ML displacement of the femoral head away from the CoR at varying degrees of flexion. It was found that an increase in the impingement damage severity resulted in an increased displacement of the femoral head in the ML direction. The AP displacement was not measured in the study however, and it is not known how this would have been affected by the inputs. It is suggested that the AP displacement be measured when comparing damage with dislocation-prone activities in a hip simulator as it could give additional information as to the severity of the impingement event and size of the subluxation.

6.4.2.3 Bearing surface changes

There were limited changes to the bearing surface after 40k cycles for all repeats of the three squat kinematics. This was measured by the CMM after the impingement test which demonstrated the deviation of surface changes from the unworn pre-test. There was a negligible change in the surface deviation when compared with the original pre-tested liner measurements for all repeats. Typical wear tests in hip simulator studies which analyse bearing surface wear use gravimetric wear testing methods which are done after millions of cycles (Leslie, et al., 2009; Al-Hajjar, et al., 2013a). It was demonstrated that 40k cycles were not sufficient as to cause any damage to the bearing surface even under the extreme testing conditions. This disagreed with a similar study (Pryce, 2019) which found that after 40k cycles, there was some evidence of edge loading. The reason for this difference could have been the variation in simulator, components, component orientation and the

different kinematics applied to the components which could have resulted in slight differences to the mechanics of the tests.

6.4.3 Geometric model predictions with the given kinematic inputs

The order of the severity of impingement damage to the acetabular liner rims for the three squat activities were effectively predicted by the geometric model. When impingement did occur, the geometric model also effectively predicted the location of the impingement damage at an accuracy of up to 3.8°. The reason for these slight differences between model and simulator outcomes could be because the geometric model was setup with a precise CoR for both components which did not change, no friction, no cementing errors, and various other parameters which could not be absolutely consistent between the geometric model and the hip simulator conditions.

The predictions made about the location of impingement around the liner rim by the geometric model also made the assumption that the volumetric overlap at the greatest penetration depth would be the location of the greatest penetration depth of impingement damage from the simulator results which could have resulted in slightly different location comparisons. Therefore considering the desirable conditions in the geometric model, a difference of 3.8° was considered to be an accurate prediction from the geometric model. These results were an indication that the geometric model was valid as an effective tool to use for predicting impingement damage to THR components given these particular inputs.

All of the locations of the impingement occurrences around the liner rim were in the anterior and superior direction (closer to the anterior) which was expected with high flexion positions. This agreed with a study (Pryce, 2019) where the impingement damage during a simplified and reduced RoM STOOP activity from a previous dataset (Nadzadi, et al., 2003) was also in the anterior and superior direction (closer to the anterior) on the acetabular liner rim. The STOOP activity was used in that case which was a high flexion activity and

therefore the damage was expected to be in the same area as the current study's results.

The geometric model predicted impingement to occur for the kinematics of the three squat activities, however following the hip simulator testing, damage to the acetabular liner rims was only measured in two of the three squat activities. The kinematics of subject F was predicted to result in a small amount of impingement in the geometric model however no impingement was measured or observed following the hip simulator testing. The reasons for this could be that the geometric model was setup under ideal conditions which were not present in the simulator and therefore there was a slight difference between the prediction and the simulator results.

6.4.4 Comparison with current impingement test methods and standards

The impingement test developed in the current study effectively applied clinically-relevant kinematic activities to THR components in a hip simulator to measure impingement damage. This application of high flexion kinematic activities was improved on other *in vitro* impingement tests which simulated orbital motion or simple kinematics under constant impingement, neither of which were clinically-relevant (Holley, et al., 2005; ASTM F2582, 2020).

The application of force data which resembled the measured force data in the previous dataset (Layton, et al., 2021) was improved on previous applications of force which included constant impingement (ASTM F2582, 2020). While it was not as high as those found in the dataset or other *in vitro* tests (Holley, et al., 2005), the application of force to the liner rim was relevant and created impingement damage. This reduction in force was necessary to prevent dislocation in the simulator. The components in the current study were also setup in a clinical way with the correct loading directions for high flexion activities. This clinical setup of components was an improvement on other *in vitro* impingement tests who simulated impingement either using non clinical components (Holley, et al., 2005) or would position the components into impingement which would not occur clinically (ASTM F2582, 2020).

The method of assessing damage in the current study was a quantitative geometric measurement which effectively recorded the severity of the damage inflicted on the liner rims. The standard for impingement testing (ASTM F2582, 2020) assesses damage by visually inspecting the liners for failure modes which is not a quantitative method of measuring impingement. Another study (Holley, et al., 2005) ran for five million cycles and therefore could use gravimetric wear testing of the liners, however this method could not distinguish between bearing wear and impingement wear. The five million cycles was also thought to be excessive and therefore would not be an effective method of measuring rim damage over a reduced number of cycles.

The measuring of the AP and ML displacement allowed for an effective analysis into the subluxation which occurred during the impingement event of the different kinematics applied in the simulator. This was not measured in any of the other *in vitro* impingement tests (Holley, et al., 2005; Pryce, 2019; ASTM F2582, 2020) and was an improvement in the analysis of the impingement tests.

6.4.5 Clinical significance

Retrieval studies have demonstrated the severity and frequency of impingement damage to polyethylene liner rims clinically (Birman, et al., 2005; Shon, et al., 2005; Usrey, et al., 2006; Marchetti, et al., 2011; Waddell, et al., 2018), which has included fatigue damage and the cracking of liners (Birman, et al., 2005) as well as deformation of the liner rim including notches along the surface (Shon, et al., 2005; Usrey, et al., 2006; Marchetti, et al., 2011; Waddell, et al., 2018). The *in vitro* impingement test developed in this thesis applied clinically-relevant load and motion data which could generate deformation of the polyethylene liner rim which included a notch in the acetabular liner rim surface similar to what has been found clinically in retrievals (Shon, et al., 2005; Usrey, et al., 2006; Marchetti, et al., 2011; Waddell, et al., 2018). The notches observed clinically in the literature have included deformation which spanned a large area around the rim (Usrey, et al., 2006; Marchetti, et al., 2011; Waddell, et al., 2018) due to multiple motions

and activities applying damage clinically, however the current impingement test only applied one motion at a time, hence the concentration of damage. It would be a useful development of the current study to apply more activities and motions to cause impingement damage around the rim to create a more clinically-relevant testing method that more closely resembled the impingement damage seen in retrievals.

The standard for impingement testing (ASTM F2582, 2020) aims to apply impingement damage to acetabular liner rims as a tool to evaluate impingement in THR components. However, the standard does not use clinically-relevant motions and the THR components are not positioned in a clinically relevant manner. There are questions around the standard in regards to testing across multiple liner designs and sizes, as the standard appears to only test fatigue damage in the material and not clinical function of the liner. In contrast, the current study developed an impingement test which applied clinically-relevant activity and force data to generate impingement damage to acetabular liners using a clinical setup of the components and therefore tested the clinical function of acetabular liners. As the impingement test in the current study did not test for fatigue damage, it is suggested that *in vitro* testing for impingement could use a combination of the standard for impingement testing (ASTM F2582, 2020) and a developed impingement test from the current study to provide comprehensive impingement testing methods that can be used in the development process of new THR materials and designs.

A larger head size is often considered to be advantageous clinically (Cuckler, et al., 2004; Burroughs, et al., 2005; Jameson, et al., 2011; Stroh, et al., 2013). However, for smaller sized patients who have a smaller acetabulum, space for the associated shell and liner is limited. Therefore, the acetabular liner rim becomes thinner to accommodate the larger head. There are questions around how thin such liner designs can be; due to the thinner material at the rim, the liners are at an increased risk of wear and fatigue-like damage (cracking or fracturing) (Blom, et al., 2006; Tower, et al., 2007). Therefore there are questions as to whether there is a threshold of impingement damage than can be applied to polyethylene liners until they experience fatigue-like

damage and there is a need to quantify this threshold in the development of new THR designs. Therefore an *in vitro* testing method developed from the current study along with the standard for impingement testing (ASTM F2582, 2020) would be effective tests in the development and testing of these thinner liners.

The geometric model was effectively used in predicting impingement damage to the acetabular liner rim. The geometric model could be an effective tool in future experimental test planning for *in vitro* impingement tests. Future work should focus on quantifying the severity of impingement measures into predictable data of deformation damage to provide increased understanding to the outputs of the geometric model.

6.4.6 Limitations

There were some limitations to the simulator study. Firstly, the kinematics used in the simulator were simplified versions of the original raw data and were therefore a representation of the raw data. This was thought to have minimal effect on the outcomes of the impingement damage as the volumetric overlap at the greatest volume of impingement during the activity was the same across both the raw data and the simplified kinematics used in the simulator.

Secondly, the force input data was a simple wave profile with a peak of 800N. The actual forces which occurred in the hip as measured by the raw data were much higher and could have resulted in a larger amount of damage had the raw data been used. This reduction in force was necessary due to the constraints of the simulator setup and the possible dislocation which could occur.

Finally, the geometric model made predictions based on desirable conditions including a precise CoR for components, no friction, no cementing errors, matching CoR between the femoral head and liner and various other parameters which could not be absolutely consistent between the geometric model and simulator test. There was also no deformation during any of the impingement events in the geometric model, therefore what happened after

the impingement event could not be predicted. Due to the clearance between the femoral head and the liner, there were expected to be some errors in the results.

6.5 Summary

A method was developed to apply three squat activities from a clinically-relevant kinematic dataset (Layton, et al., 2021) to total hip replacement components under load in a Simsol Prosim six axis hip simulator. The activities were chosen so that there would be varying severities of impingement damage as measured by a geometric model. The impingement damage from the simulator was measured using a coordinate measuring machine to detect the penetration depth at the liner rim. The results from the simulator were then compared to the predictions from the geometric model to investigate the consequences of the impingement found in the model.

The kinematics of the squat activities resulted in different amounts of impingement damage as measured by the penetration depth of the liner rim suggesting that the kinematics of a patient could affect the likelihood and severity of impingement to their total hip replacement. The order of the predictions of the severity of impingement from the geometric model for the three squat activities agreed with the severity of damage found from the simulator results. When impingement occurred, the geometric model could also accurately predict the location of impingement around the liner rim. There were no notable changes to the bearing surface after 40k cycles for any of the kinematic squat activities including no evidence of any edge loading.

The results in this study demonstrated that the geometric model could effectively predict the order of the severity of impingement across different kinematic activities including the location of the impingement damage around the liner rim. The impingement test developed in this study could be used to aid in testing product designs of new implants. This work also provided context to the geometric model work in this thesis.

Chapter Seven : Discussion and future work

7.1 Introduction

There were 95,677 total hip replacements in 2019 across England, Wales and Northern Ireland and this number has been increasing each year (National Joint Registry, 2020) (2019 results here as the COVID-19 pandemic reduced this number). One of the most common reasons for failure in THR's is dislocation secondary to impingement (Malik, et al., 2007; Brown, et al., 2014; National Joint Registry, 2020). Implant-on-implant impingement can also lead to an increase in wear which can cause other failure modes such as aseptic loosening (Fisher, 2011; Brown, et al., 2014). Impingement has been reported in retrieved hip replacements, occurring in 25% to 77% of liners including those which had not been retrieved for impingement related failure (Birman, et al., 2005; Shon, et al., 2005; Usrey, et al., 2006; Marchetti, et al., 2011; Lee, et al., 2011; Waddell, et al., 2018).

To improve stability in THR's there has been an increase in the use of larger femoral heads (>32mm). While this allows for a greater RoM for the implant, the restricting factor for the RoM of the hip becomes bone-on-bone impingement (Burroughs, et al., 2005; Malik, et al., 2007). Bony features including the AIIS and the anteversion angle of the natural acetabulum have been reported to reduce the RoM in both the natural hip and THR's (Patel, et al., 2010; Larson, et al., 2011; Nakahara, et al., 2011; Hetsroni, et al., 2013; Davidovitch, et al., 2015; Weber, et al., 2016; Hamada, et al., 2018; Shoji, et al., 2016; Morris, et al., 2018; Tabata, et al., 2019). However, these bony features have not been investigated for their effect on the likelihood or severity of impingement during dislocation-prone activities.

High RoM activities of daily living have resulted in THR patients dislocating their implant through impingement (Smith, et al., 2012). Kinematic datasets of activities of daily living exist in the literature (Nadzadi, et al., 2003; Saputra, et al., 2013; Zhou, et al., 2013; Layton, et al., 2021) and some have been used with computational models to assess conditions of impingement (Nadzadi, et

al., 2003; Pedersen, et al., 2005; Patel, et al., 2010; Ghaffari, et al., 2012; Saputra, et al., 2013; Pryce, et al., 2022). However, the majority of these studies only included one bony geometry and therefore their results were limited to that particular subject's bony geometry. These studies also all used the same kinematic dataset which contained seven activities of daily living carried out by one subject to represent the median of 10 subjects and therefore has no kinematic variation intra and inter-subject (Nadzadi, et al., 2003). This would also limit the results of the studies to the kinematic data of the one subject that represented each activity.

The most common form of surgical preoperative planning of a THR includes the use of 2D radiographs of the pelvis and femur to carry out templating to make decisions such as the size of the components, offset, inclination angle of the acetabular cup and limb length (Bono, 2004; Flecher, et al., 2016; Lakstein, et al., 2016; Colombi, et al., 2019). While 2D templating is a good method for predicting component size, limb length and offset (Valle, et al., 2005; Gamble, et al., 2010; Efe, et al., 2011; Montiel, et al., 2020; Kristoffersson, et al., 2021), it relies on the quality of the 2D radiograph which has been reported to contain inaccuracies as the 2D measurement depends on the orientation of the patient (Davies, et al., 2007; Schiffner, et al., 2018; Colombi, et al., 2019; Holzer, et al., 2019). The 2D radiographs are typically carried out with the patient in a supine position (Holliday & Steward, 2021; Kristoffersson, et al., 2021) and therefore the preoperative planning decisions are made without the consideration of the hip being functionally loaded which could result in inaccurate component placement. This method is also limited in allowing any decisions to be made with regards to the radiographic anteversion of the acetabular cup. The use of 3D templating is currently mainly used for patients whose THR may be complicated such as those who are at risk of instability, however the use of 3D templating with a CT scan has been reported to have increased accuracy in templating measurements when compared to 2D templating (Lecerf, et al., 2009; Sariali, et al., 2009; Schiffner, et al., 2018). Unlike 2D it allows additional decisions to be made such as the anteversion angle of the acetabular cup.

7.1.1 Project aim

The aim of this thesis was to analyse factors (such as patient bony anatomy, patient activity and acetabular cup orientation) effecting the likelihood and severity of impingement in order to inform on the conditions of impingement and reduction of impingement related failure rates in total hip replacements.

7.2 Bony features which have an effect on impingement in total hip replacements

7.2.1 Anterior inferior iliac spine

The geometric models developed in this thesis which included pelvic and femur geometries from nine different CT scans, resulted in different ranges of motion because of the geometry of the bones (Chapter 3). In this study, a bony feature (anterior inferior iliac spine – “AIIS”) was shown to restrict the RoM during internal rotation at varying degrees of high flexion, particularly the lateral measure of the peak of the AIIS. This was also the finding from the literature with laterally large AIIS patients resulting in significantly reduced RoM (Shoji, et al., 2016). The same bony feature (AIIS) was also shown as the site of impingement during activities of daily living which were prone to posterior dislocation (Nadzadi, et al., 2003), which resulted in bone-on-bone impingement and significantly affected the severity of impingement (Chapter 4). This agreed with the literature as the AIIS was also found to be an impingement site during a number of computational model investigations into the conditions of impingement during posterior dislocation-prone activities (Patel, et al., 2010; Hetsroni, et al., 2013; Shoji, et al., 2016; Tabata, et al., 2019; Pryce, et al., 2022). The AIIS could be used as a potential identifier for patients who are at risk of bone-on-bone impingement during posterior dislocation-prone activities which are susceptible to anterior impingement. Therefore additional care should be taken when deciding on the design, size and orientation of the THR components in patients who have the peak of their AIIS positioned at an increased distance in the lateral direction.

7.2.2 Anteverision angle of the natural acetabulum

The anteverision angle of the natural acetabulum had a significant effect on the severity of impingement during anterior dislocation-prone activities which were susceptible to posterior impingement (Chapter 4). The impingement site during these activities was between the ischium and either the lesser trochanter or the intertrochanteric crest of the femur. The locations of impingement agreed with those found in the literature which used computational models to investigate the conditions of impingement during anterior dislocation-prone activities (Kessler, et al., 2008; Patel, et al., 2010; Shoji, et al., 2016; Pryce, et al., 2022). The increased anteverision angle of the natural acetabulum appeared to indicate that the pelvis was wider and therefore the ischium was positioned more anteriorly, reducing the external rotation angle prior to impingement between the femur and the ischium. The anteverision angle of the natural acetabulum could be used as an indicator that a patient is at an increased risk of bone-on-bone impingement during anterior dislocation-prone activities which are susceptible to posterior impingement. Therefore additional care should be taken when deciding on the design, size and orientation of the THR components in patients who have a high anteverision angle of their natural acetabulum.

7.3 The kinematic activities of patients can affect impingement

The individual kinematic data of activities of daily living in different subjects had an effect on the likelihood and severity of impingement (Chapter 5). Different subjects carrying out the same set of eight activities resulted in a change in the number of occurrences of impingement at different cup orientations. This data suggested that the individual kinematic activities of each subject, affected the likelihood of impingement. This also suggested that the recommendation of cup orientation targets for each patient should be patient-specific depending on their kinematic data. There were areas in the cup orientation grids of each subject which had minimal impingement for each

subject. These areas of little to no impingement were different for each subject which suggested that a well-positioned acetabular cup could avoid implant-on-implant impingement during high RoM activities and that these cup orientations which can avoid implant-on-implant differ between subjects.

Comparing the kinematic datasets from the literature, the average value of the greatest RoM data point for all of the high flexion activities in a previous kinematic dataset (Nadzadi, et al., 2003) (mean of 106.3°) was typical of other non-THR subject data with high RoM flexion activities (mean of 98.3°) (Ko & Yoon, 2008), however the reduced average RoM of another kinematic dataset (Layton, et al., 2021) (mean of 86.0°) were typical of other data collected from patients post-THR (mean of 86.2° and 74.8°) (Koyanagi, et al., 2011; Sugano, et al., 2012) (described in more detail in section 5.4.1). The reduced RoM for the post-THR patients could be because post-THR patients were more cautious of carrying out high range of motion activities. The previous kinematic dataset (Layton, et al., 2021) which had kinematics similar to that of a post-THR patient who may carry out activities more cautiously was still found to result in occurrences of impingement at clinically-relevant acetabular cup orientations (Chapter 5).

The frequency that high RoM activities of daily living occur in daily life is not known and there is a need to better understand the frequency of these activities to improve the relevancy of the kinematic datasets for future impingement testing. The squat activities replicated in the hip simulator were applied to the components for 40k cycles (Chapter 6) which was thought to be less impingement than expected during the lifetime of the implant. As a reference if a patient carries out 20 of the activities of daily living such as standing up, sitting down or tying their shoes in a day, then that would be less than six years of THR impingement damage. The 800N axial load applied during the simulator study was also less than expected *in vivo*, with standard gait tests usually applying axial force of up to 3kN (Leslie, et al., 2009; Al-Hajjar, et al., 2013a). These conditions however still produced damage at a lower number of cycles and at lower loads than expected *in vivo* over the lifetime of the implant.

Following a THR surgery, the surgeon will usually give advice to the patient to aid recovery in the first 8-12 weeks (Healy, et al., 2008; NHS, 2019). These recommendations could, for example, include keeping hip flexion below 90° during any activity, avoid crossing one leg over the other and to avoid a number of high RoM athletic activities which could increase the risk of impingement and potential dislocation (Healy, et al., 2008; NHS, 2019). These recommendations by the surgeon are given on a patient-specific basis, therefore the geometric models in this study could identify particularly problematic activities and aid in their decision-making for recommendations to the patient post-surgery. This could include the restriction of certain activities which recorded a high likelihood of impingement in the geometric model.

The way in which THR patients move could be a factor in the severity of damage found clinically. With THR's being implanted into younger patients, the demand on the implant including the higher RoM needed for the patient increases the need for improved preoperative planning and correct component placement.

7.4 The potential of the use of the geometric models as a THR preoperative planning tool

The geometric models developed in this thesis could have the potential to be developed further for potential use as a clinical THR preoperative planning tool. The bony geometry of a patient (Chapter 4) as well as the individual kinematic data of a patient's high RoM activities of daily living (Chapter 5) has been demonstrated to affect the occurrence and severity of impingement. A 3D preoperative planning tool could be developed which uses the techniques developed in this thesis to create a geometric model of a patient's bony geometries from a CT scan and apply a dynamic assessment using their activity data to preoperatively plan optimal positions and orientations for the THR components. The differences in occurrences of impingement at different cup orientations during a subject's individual kinematic data could be used for recommending optimal acetabular cup orientations which was demonstrated

in this thesis (Chapter 5). The typical decisions carried out using current methods in 2D and 3D templating such as leg length, offset and component size could also be carried out with the geometric models. The current geometric models would need to be developed further however to have confidence in a clinical system such as this.

A 3D preoperative planning THR system from the literature which is currently in clinical use is the Corin Optimized Positioning System™ (Corin Group, Cirencester, UK)(OPS). The information about this system is not fully detailed in scientific literature, however after reviewing the online product material, the system uses radiographs of the patient in a sitting position leaning as far forward as possible, a standing position and one leg in 90° flexion position, to measure the pelvic tilt range (Pierrepont, et al., 2017; Langston, et al., 2018). A CT scan is then used with a virtual THR to simulate a flexion/extension movement to create a contact patch area which uses the pelvic tilt range measurements from the radiographs to recommend a cup orientation which minimises edge loading. Prosthetic impingement is also analysed using this method. This system is limited by its impingement assessment as it only analyses a flexion/extension rotation and also does not analyse any anterior dislocation-prone activities. The range of activities which include internal/external rotations and adduction/abduction angles alongside high flexion from the kinematic datasets used in this thesis, as well as the activities prone to anterior dislocation have demonstrated that impingement can occur during many different types of activities.

To gain confidence in a clinical use of the geometric models, they would need to be developed further to include features such as soft tissue and pelvic rotations. The lack of soft tissue in the current models could limit the conclusions around the RoM and the likelihood of impingement. Soft tissue has been reported to reduce the RoM in THR and therefore increase the likelihood of impingement (Hayashi, et al., 2012; Woerner, et al., 2017). The use of pelvic rotations during different activities has been reported to change the functional cup orientation and therefore change the relative positions of the femur and pelvis (McCarthy, et al., 2017; Pierrepont, et al., 2017; Ike, et

al., 2018; Langston, et al., 2018). The activity data in this thesis already had pelvic tilt in the kinematic data as the markers measured the relative position of the pelvis and femur. However it could be a useful development to include pelvic movements so that the variation of pelvic motion could be investigated with the geometric models.

As a tool for assessing individual patient's bony geometries and producing a personalised geometric model which can assess RoM and impingement likelihood at different cup orientations, the geometric models in this thesis have the potential to be developed for clinical use to aid in the preoperative planning of a THR.

7.5 *In vitro* consequences of impingement during clinically-relevant motions

The volumetric overlap of bone and/or components in the geometric models were used as a measure of the severity of impingement during a number of different activities of daily living (Chapters 4 and 5). The severity of impingement predictions by the geometric model of three squat activities were compared to the damage to THR components in a hip simulator (Chapter 6). A higher severity of impingement predicted by the geometric model resulted in a larger penetration depth and therefore more severe damage to the THR components (Chapter 6). The geometric model also predicted the location of the impingement around the acetabular liner rim to within 3.8° when impingement occurred. The subject variation in the kinematic data of different squat activities had an effect on the severity of the impingement damage to the THR components in a hip simulator.

A clinically-relevant impingement test was developed which could apply dynamic impingement and repetitively replicate three different squat activities under load. The developed inputs for the impingement test included a clinically-relevant setup of THR components and applied clinically-relevant motion and load inputs. The impingement tests in the literature included a setup of components and simple motions and loads to generate impingement

damage which had little clinical relevance (Holley, et al., 2005; ASTM F2582, 2020). The impingement test developed in this thesis allowed for three different activities to be applied as well as displacement measurements in the medial-lateral and anterior-posterior direction during the impingement event, allowing for an increased understanding of separation of the femoral head during high RoM impingement events unlike the impingement tests from the literature (Holley, et al., 2005; Pryce, 2019; ASTM F2582, 2020).

The standard for impingement testing (ASTM F2582, 2020) applies simple motions under constant load in a non-clinical setup of THR components. The starting position of the test places the THR components in impingement contact, and therefore the same test conditions would be applied regardless of the design of the liner, therefore the standard appears to only test fatigue damage in the material and not clinical function of the liner. The test therefore does not differentiate between liner designs and the likelihood of impingement in a clinical scenario (i.e. a sub-hemispheric cup *in vivo* is likely to impinge less than a cup with more coverage such as a lipped liner). This raises questions to the ability of the test to compare different designs in a clinically relevant scenario. In contrast, the impingement test developed in this thesis provided a more clinically-relevant investigation into the conditions of impingement than those found in the literature (Holley, et al., 2005; Pryce, 2019; ASTM F2582, 2020) and therefore tested the clinical function of acetabular liners including being able to apply test conditions to different liner designs with different outcomes expected. As the impingement test in the current study did not test for fatigue damage, it is suggested that *in vitro* testing for impingement could use a combination of the standard for impingement testing (ASTM F2582, 2020) and a developed impingement test from the current study to provide comprehensive impingement testing methods that can be used in the development process of new THR materials and designs.

7.6 Limitations

Some limitations of the current project:

- The bony geometries of the CT scans used to develop the geometric models were different individuals to the subjects which were used in the kinematic activity data from the literature. It is not known whether a matched CT scan and kinematic data from the same individual would result in the same outcomes found in this thesis.
- There was no connective tissue such as muscles or ligaments included in the geometric models. A study found that soft tissue limited the RoM in patients by 20° when measured intraoperatively (Woerner, et al., 2017). The inclusion of this soft tissue which surrounds the hip would have reduced the RoM stated in this thesis further, and therefore possibly increase the likelihood and severity of impingement and potential subluxation. The inclusion of soft tissue could also change the types of impingement reported in this thesis.
- There was no soft tissue such as adipose or fleshy tissue included in the geometric models. A study has shown that obese patients who have additional adipose and fleshy tissue around the hip joint have reduced implant-on-implant impingement but increased soft tissue impingement which may increase the risk of subluxation and dislocation (Hayashi, et al., 2012). Another study also found that increased BMI in THR patients was attributed to a decrease in stability in a finite element study (Elkins, et al., 2013). The addition of this type of soft tissue would have affected the RoM stated in this thesis as well as the types of impingement recorded.
- The simulator conditions used to investigate the *in vitro* consequences of impingement on THR components were limited due to the constraints of the simulator. To prevent unwanted damage to the simulator, dislocation was undesirable and therefore the conditions had to be carefully monitored to ensure this would not occur. To ensure the components themselves could be mounted at high RoM, lower loads

were used so that the setup was not compromised. A simplification of the kinematic data was also required so that there were no vibrations in the simulator which could have contributed to the dislocation risk. The damage observed on the acetabular liners is therefore limited by the constraints of the simulator.

- The number of cycles used in the developed impingement test was 40,000 cycles, however it is not known whether this is representative of the frequency in which patients carry out high RoM activities over the lifetime of their THR.
- The outputs from the geometric models in this thesis included the occurrence of impingement, consisting of a “pass/fail” for impingement from the overlap of geometries in the model. However there were occurrences where impingement was narrowly missed during a motion or activity, however the output for this was the same as if impingement had been widely missed. Therefore there was some lost value in “near-misses” in the geometric models.

7.7 Future Work

The following future work should be considered following the current project to further investigate the conditions of impingement and inform on patient-specific risks to THR:

- There should be development of the THR geometric models to include soft tissue and pelvic movements to improve our understanding of the conditions of impingement.
- If impingement is detected in the geometric models, a separate FEA model could be developed to investigate the applied stress and damage these conditions could cause to the THR components by using the forces included with the data used in this study. This could also include forces of any soft tissue which could be developed into the models.

- A study matching the CT scans with kinematic datasets from the same individuals should be obtained to address this limitation and improve on the findings in this thesis.
- There should be investigation into more bony features such as the lesser trochanter to further analyse the conditions around bone-on-bone impingement and the effect that individual bony geometry has on the impingement in THR's.
- To improve the understanding of the relevancy of high RoM activities, future work should focus on the investigating the frequency of the kinematic data of activities of daily living including the frequency with which these activities occur in patient's daily lives which is most likely patient-specific.
- Different activities should be applied to THR components in the hip simulator test including those that have a range of sliding distances to improve our understanding of the consequences of impingement and improve the testing capability of impingement damage.
- The hip simulator study should be run for a higher number of cycles to analyse the damage over time and compare to the standard for impingement testing (ASTM F2582, 2020) for fatigue analysis (1 million cycles).

7.8 Conclusions

The conclusions from the current project were:

- The THR geometric models which were developed from CT scan data were an effective method of investigating impingement conditions across multiple bony geometries and outputting relevant measurable data on impingement.
- The location of the anterior inferior iliac spine (AIIS) on the pelvis affected the RoM before bone-on-bone impingement in a series of THR geometric models, particularly the lateral protrusion of the AIIS which could be used as a predictor for this type of impingement.

- The anteversion angle of the natural acetabulum affected the likelihood of bone-on-bone impingement in a series of THR geometric models and could be used as a predictor for this type of impingement.
- The shape of the bony geometries in the THR geometric models had an effect on the occurrence, type and severity of impingement during clinically-relevant dislocation-prone activities of daily living. The THR geometric models could be developed further for use in predicting the occurrence and severity of impingement in THR patients given the relevant CT scan and kinematic data.
- The kinematic data of individual subjects resulted in different occurrences of impingement at different acetabular cup orientations. This change in impingement occurrences at different cup orientations could result in a change in the recommended ideal cup position for each patient. This data suggested that ultimately a clinically validated subject-specific approach would be the best way to reduce impingement and potential dislocations in THR's.
- The risk of impingement is subject-specific with some subjects risking impingement even at clinically-relevant cup orientations. Dynamic assessment of patients during THR preoperative planning could be a useful tool to identify the patients who could be at a high risk of impingement because of the RoM of their activities of daily living.
- A clinically-relevant impingement test was developed which could apply dynamic impingement and replicate three different squat activities repetitively under load. This test could be developed to provide comprehensive impingement testing methods alongside existing standards to be used in the development process of new THR materials and designs.
- The kinematics of three individual squat activities in a hip simulator resulted in different severities of impingement damage suggesting that the kinematics of a patient could affect the likelihood and severity of impingement damage to their THR clinically.

List of References

- Abdel, M. P. et al., 2016. What Safe Zone? The Vast Majority of Dislocated THAs Are Within the Lewinnek Safe Zone for Acetabular Component Position. *Clinical orthopaedics and related research*, 474(2), pp. 386-391.
- Abu-Amer, Y., Darwech, I. & Clohisy, J. C., 2007. Aseptic loosening of total joint replacements: mechanisms underlying osteolysis and potential therapies. *Arthritis research & therapy*, 9 Suppl 1(Suppl 1), pp. S6-S6.
- Al-Hajjar, M. et al., 2013a. Wear of 36-mm BIOLOX® delta ceramic-on-ceramic bearing in total hip replacements under edge loading conditions. *Proceedings of the Institution of Mechanical Engineers, Part H: Journal of Engineering in Medicine*, 227(5), pp. 535-542.
- Al-Hajjar, M. et al., 2013b. Effect of femoral head size on the wear of metal on metal bearings in total hip replacements under adverse edge-loading conditions. *Journal of biomedical materials research. Part B, Applied biomaterials*, 101(2), pp. 213-222.
- Ali, M., Al-Hajjar, M., Fisher, J. & Jennings, L. M., 2019. The Influence of Kinematic Conditions and Variations in Component Positioning on the Severity of Edge Loading and Wear of Ceramic-on-Ceramic Hip Bearings. *Ceramics*, 2(3), pp. 488-501.
- Anda, S., Svenningsen, S., Grøntvedt, T. & Benum, P., 1990. Pelvic Inclination and Spatial Orientation of the Acetabulum: A Radiographic, Computed Tomographic and Clinical Investigation. *Acta Radiologica*, 31(4), pp. 389-394.
- Arthritis Research UK, 2013. *Osteoarthritis in general practice: data and perspectives*, Chesterfield, UK: Arthritis Research UK.
- ASTM F2582, 2020. *F2582-20:Standard Test Method for Dynamic Impingement Between Femoral and Acetabular Hip Components*, United States: ASTM International.
- Balazs, G. C. et al., 2017. Morphological Distribution of the Anterior Inferior Iliac Spine in Patients With and Without Hip Impingement: Reliability, Validity, and Relationship to the Intraoperative Assessment. *The American Journal of Sports Medicine*, 45(5), pp. 1117-1123.
- Barrack, R. L., 2003. Dislocation After Total Hip Arthroplasty: Implant Design and Orientation. *JAAOS - Journal of the American Academy of Orthopaedic Surgeons*, 11(2).
- Barrack, R. L., Butler, R. A., Laster, D. R. & Andrews, P., 2001. Stem design and dislocation after revision total hip arthroplasty: Clinical results and computer modeling. *The Journal of Arthroplasty*, 16(8, Supplement 1), pp. 8-12.
- Barsoum, W. K. et al., 2007. A computer model of the position of the combined component in the prevention of impingement in total hip replacement. *The Journal of Bone and Joint Surgery. British volume*, 89-B(6), pp. 839-845.
- Bartz, R. L., Noble, P. C., Kadakia, N. R. & Tullos, H. S., 2000. The Effect of Femoral Component Head Size on Posterior Dislocation of the Artificial Hip Joint*. *JBJS*, 82(9).

- Bergmann, G. et al., 2001. Hip contact forces and gait patterns from routine activities. *Journal of Biomechanics*, 34(7), pp. 859-871.
- Birman, M. V. et al., 2005. Cracking and Impingement in Ultra-High-Molecular-Weight Polyethylene Acetabular Liners. *The Journal of Arthroplasty*, Volume 20, pp. 87-92.
- Blizzard Daniel, J. et al., 2017. The Impact of Lumbar Spine Disease and Deformity on Total Hip Arthroplasty Outcomes. *Orthopedics*, 40(3), pp. e520-e525.
- Blom, A. W., Madhavan, P., Lee, M. & Learmonth, I. D., 2006. Thirty-two Millimetre Heads and Accelerated Polyethylene Wear in Total Hip Arthroplasty. *HIP International*, 16(3), pp. 207-209.
- Bono, J. V., 2004. Digital Templating in Total Hip Arthroplasty. *JBJS*, 86(suppl_2).
- Brooks, P. J., 2013. Dislocation following total hip replacement. *The Bone & Joint Journal*, 95-B(11_Supple_A), pp. 67-69.
- Browne, J. A. & Pagnano, M. W., 2012. Surgical technique: a simple soft-tissue-only repair of the capsule and external rotators in posterior-approach THA. *Clinical orthopaedics and related research*, 470(2), pp. 511-515.
- Brown, T. D. & Callaghan, J. J., 2008. Impingement in Total Hip Replacement: Mechanisms and Consequences. *Current orthopaedics*, 22(6), pp. 376-391.
- Brown, T. D., Elkins, J. M., Pedersen, D. R. & Callaghan, J. J., 2014. Impingement and dislocation in total hip arthroplasty: mechanisms and consequences. *The Iowa orthopaedic journal*, Volume 34, pp. 1-15.
- Burroughs, B. R. et al., 2005. Range of Motion and Stability in Total Hip Arthroplasty With 28-, 32-, 38-, and 44-mm Femoral Head Sizes: An In Vitro Study. *The Journal of Arthroplasty*, 20(1), pp. 11-19.
- Byström, S., Espehaug, B., Furnes, O. & Havelin, L., 2003. Femoral head size is a risk factor for total hip luxation A study of 42,987 primary hip arthroplasties from the Norwegian Arthroplasty Register. *Acta Orthopaedica Scandinavica*, 74(5), pp. 514-524.
- Callaghan, J. J., Brown, T. D., Pedersen, D. R. & Johnston, R. C., 2002. Choices and Compromises in the Use of Small Head Sizes in Total Hip Arthroplasty. *Clinical Orthopaedics and Related Research*®, Volume 405.
- Cebatorius, A. et al., 2015. Choice of approach, but not femoral head size, affects revision rate due to dislocations in THA after femoral neck fracture: results from the Lithuanian Arthroplasty Register. *International Orthopaedics*, 39(6), pp. 1073-1076.
- Cherian, J. J. et al., 2015. What Host Factors Affect Aseptic Loosening After THA and TKA?. *Clinical Orthopaedics and Related Research*®, 473(8).
- Cho, M.-R., Choi, W. K. & Kim, J. J., 2016. Current Concepts of Using Large Femoral Heads in Total Hip Arthroplasty. *Hip & pelvis*, 28(3), pp. 134-141.

- Cinotti, G. et al., 2011. Do large femoral heads reduce the risks of impingement in total hip arthroplasty with optimal and non-optimal cup positioning?. *International Orthopaedics*, 35(3), pp. 317-323.
- Cobb, T. K., Morrey, B. F. & Ilstrup, D. M., 1996. The Elevated-Rim Acetabular Liner in Total Hip Arthroplasty: Relationship to Postoperative Dislocation*. *JBJS*, 78(1).
- Colombi, A., Schena, D. & Castelli, C. C., 2019. Total hip arthroplasty planning. *EFORT open reviews*, 4(11), pp. 626-632.
- Cooper, H. J. & Della Valle, C. J., 2014. Large diameter femoral heads. *The Bone & Joint Journal*, 96-B(11_Supple_A), pp. 23-26.
- Crawford, R. W. & Murray, D. W., 1997. Total hip replacement: indications for surgery and risk factors for failure. *Annals of the Rheumatic Diseases*, 56(8), p. 455.
- Crowninshield, R. D. et al., 2004. Biomechanics of Large Femoral Heads: What They Do and Don't Do. *Clinical Orthopaedics and Related Research*®, Volume 429.
- Cuckler, J. M. et al., 2004. Large versus small femoral heads in metal-on-metal total hip arthroplasty. *The Journal of Arthroplasty*, 19(8, Supplement), pp. 41-44.
- Danoff, J. R. et al., 2016. Redefining the Acetabular Component Safe Zone for Posterior Approach Total Hip Arthroplasty. *The Journal of Arthroplasty*, 31(2), pp. 506-511.
- Davidovitch, R. I., DeSole, E. M. & Vigdorichik, J. M., 2015. Subspine Impingement: 2 Case Reports of a Previously Unreported Cause of Instability in Total HIP Arthroplasty. *HIP International*, 25(2), pp. e24-e29.
- Davies, H., Foote, J. & Spencer, R. F., 2007. Accuracy of Femoral Templating in Reproducing Anatomical Femoral Offset in Total Hip Replacement. *HIP International*, 17(3), pp. 155-159.
- DePuy Synthes, 2019. *PINNACLE® Hip Solutions: Surgical technique*, Warsaw, IN, USA: DePuy Synthes.
- Di Schino, M. et al., 2009. Anterior dislocation of a total hip replacement. Radiographic and CT-scan assessment. Behavior following conservative management. *Orthopaedics & Traumatology: Surgery & Research*, 95(8), pp. 573-578.
- D'Lima, D. D. et al., 2000. The Effect of the Orientation of the Acetabular and Femoral Components on the Range of Motion of the Hip at Different Head-Neck Ratios*. *JBJS*, 82(3).
- Dorr, L. D., Malik, A., Dastane, M. & Wan, Z., 2009. Combined anteversion technique for total hip arthroplasty. *Clinical orthopaedics and related research*, 467(1), pp. 119-127.
- Efe, T. et al., 2011. Precision of preoperative digital templating in total hip arthroplasty. *Acta orthopaedica Belgica*, Volume 77, pp. 616-621.
- Elkins, J. M. et al., 2013. Morbid Obesity May Increase Dislocation in Total Hip Patients: A Biomechanical Analysis. *Clinical Orthopaedics and Related Research*®, 471(3).

- Elkins, J. M., Pedersen, D. R., Callaghan, J. J. & Brown, T. D., 2012. Bone-on-bone versus hardware impingement in total hips: a biomechanical study. *The Iowa orthopaedic journal*, Volume 32, pp. 17-21.
- Enocson, A. et al., 2009. Dislocation of total hip replacement in patients with fractures of the femoral neck. *Acta orthopaedica*, 80(2), pp. 184-189.
- Ezquerria, L. et al., 2017. Range of Movement for Impingement and Dislocation Avoidance in Total Hip Replacement Predicted by Finite Element Model. *Journal of Medical and Biological Engineering*, 37(1), pp. 26-34.
- Fisher, J., 2011. Bioengineering reasons for the failure of metal-on-metal hip prostheses. *The Journal of Bone and Joint Surgery. British volume*, 93-B(8), pp. 1001-1004.
- Flecher, X., Ollivier, M. & Argenson, J. N., 2016. Lower limb length and offset in total hip arthroplasty. *Orthopaedics & Traumatology: Surgery & Research*, 102(1, Supplement), pp. S9-S20.
- Gamble, P., de Beer, J., Petruccioli, D. & Winemaker, M., 2010. The Accuracy of Digital Templating in Uncemented Total Hip Arthroplasty. *The Journal of Arthroplasty*, 25(4), pp. 529-532.
- Ghaffari, M., Nickmanesh, R., Tamannaee, N. & Farahmand, F., 2012. The impingement-dislocation risk of total hip replacement: Effects of cup orientation and patient maneuvers. *2012 Annual International Conference of the IEEE Engineering in Medicine and Biology Society*, pp. 6801-6804.
- Girard, J. et al., 2013. Primary total hip arthroplasty revision due to dislocation: Prospective French multicenter study. *Orthopaedics & Traumatology: Surgery & Research*, 99(5), pp. 549-553.
- Hailer, N. P., Weiss, R. J., Stark, A. & Kärrholm, J., 2012. The risk of revision due to dislocation after total hip arthroplasty depends on surgical approach, femoral head size, sex, and primary diagnosis. An analysis of 78,098 operations in the Swedish Hip Arthroplasty Register. *Acta orthopaedica*, 83(5), pp. 442-448.
- Hamada, H., Takao, M., Sakai, T. & Sugano, N., 2018. Morphological variation of the anterior inferior iliac spine affects hip range of motion in flexion after rotational acetabular osteotomy. *International Orthopaedics*, 42(6), pp. 1247-1252.
- Hayashi, S. et al., 2012. Obese patients may have more soft tissue impingement following primary total hip arthroplasty. *International Orthopaedics*, 36(12), pp. 2419-2423.
- Healy, W. L., Sharma, S., Schwartz, B. & Iorio, R., 2008. Athletic Activity After Total Joint Arthroplasty. *JBJS*, 90(10).
- Hemmerich, A. et al., 2006. Hip, knee, and ankle kinematics of high range of motion activities of daily living. *Journal of Orthopaedic Research*, 24(4), pp. 770-781.
- Hetsroni, I. et al., 2013. Anterior inferior iliac spine morphology correlates with hip range of motion: a classification system and dynamic model. *Clinical orthopaedics and related research*, 471(8), pp. 2497-2503.

- Holley, K. G. et al., 2005. Impingement of Acetabular Cups in a Hip Simulator: Comparison of Highly Cross-Linked and Conventional Polyethylene. *The Journal of Arthroplasty*, Volume 20, pp. 77-86.
- Holliday, M. & Steward, A., 2021. Pre-operative templating for total hip arthroplasty: How does radiographic technique and calibration marker placement affect image magnification?. *Journal of Medical Radiation Sciences*, 68(3), pp. 228-236.
- Holzer, L. A. et al., 2019. The accuracy of digital templating in uncemented total hip arthroplasty. *Archives of orthopaedic and trauma surgery*, 139(2), pp. 263-268.
- Hua, X. et al., 2014. Contact mechanics of modular metal-on-polyethylene total hip replacement under adverse edge loading conditions. *Journal of Biomechanics*, 47(13), pp. 3303-3309.
- Hunter, D. J. & Felson, D. T., 2006. Osteoarthritis. *BMJ*, 332(7542), p. 639.
- Ike, H. et al., 2018. Spine-Pelvis-Hip Relationship in the Functioning of a Total Hip Replacement. *JBJS*, 100(18).
- Jahani, F. et al., 2021. Importance of dynamics in the finite element prediction of plastic damage of polyethylene acetabular liners under edge loading conditions. *Medical Engineering & Physics*, Volume 95, pp. 97-103.
- Jameson, S. S. et al., 2011. Lower rates of dislocation with increased femoral head size after primary total hip replacement. *The Journal of Bone and Joint Surgery. British volume*, 93-B(7), pp. 876-880.
- Ji, H.-M. et al., 2012. Dislocation After Total Hip Arthroplasty: A Randomized Clinical Trial of a Posterior Approach and a Modified Lateral Approach. *The Journal of Arthroplasty*, 27(3), pp. 378-385.
- Jinno, T. et al., 2017. Intraoperative evaluation of the effects of femoral component offset and head size on joint stability in total hip arthroplasty. *Journal of Orthopaedic Surgery*, 25(1), p. 2309499016684298.
- Ji, W.-T., Tao, K. & Wang, C.-T., 2010. A three-dimensional parameterized and visually kinematic simulation module for the theoretical range of motion of total hip arthroplasty. *Clinical Biomechanics*, 25(5), pp. 427-432.
- Johnson, C. D. et al., 2008. Accuracy of CT Colonography for Detection of Large Adenomas and Cancers. *New England Journal of Medicine*, 359(12), pp. 1207-1217.
- Kaku, N., Tanaka, A., Tagomori, H. & Tsumura, H., 2020. Finite Element Analysis of Stress Distribution in Flat and Elevated-Rim Polyethylene Acetabular Liners. *Clinics in orthopedic surgery*, 12(3), pp. 291-297.
- Kanazawa, M. et al., 2016. Pelvic tilt and movement during total hip arthroplasty in the lateral decubitus position. *Modern Rheumatology*, 26(3), pp. 435-440.
- Kapoor, M. et al., 2011. Role of proinflammatory cytokines in the pathophysiology of osteoarthritis. *Nature Reviews Rheumatology*, 7(1), pp. 33-42.

- Kessler, O. et al., 2008. Bony impingement affects range of motion after total hip arthroplasty: A subject-specific approach. *Journal of Orthopaedic Research*, 26(4), pp. 443-452.
- Klasan, A. et al., 2019. The prevalence of a prominent anterior inferior iliac spine. *Archives of orthopaedic and trauma surgery*, 139(8), pp. 1045-1049.
- Ko, B.-H. & Yoon, Y.-S., 2008. Optimal orientation of implanted components in total hip arthroplasty with polyethylene on metal articulation. *Clinical Biomechanics*, 23(8), pp. 996-1003.
- Koyanagi, J. et al., 2011. In vivo kinematic analysis of squatting after total hip arthroplasty. *Clinical Biomechanics*, 26(5), pp. 477-483.
- Kristoffersson, E., Otten, V. & Crnalic, S., 2021. The accuracy of digital templating in cementless total hip arthroplasty in dysplastic hips. *BMC Musculoskeletal Disorders*, 22(1), p. 942.
- Krushell, R. J., Burke, D. W. D. & Harris, W. H., 1991. Elevated-rim acetabular components. Effect on range of motion and stability in total hip arthroplasty. *The Journal of Arthroplasty*, Volume 6 Suppl, pp. S53-8.
- Kubiak-Langer, M. et al., 2007. Range of Motion in Anterior Femoroacetabular Impingement. *Clinical Orthopaedics and Related Research*®, Volume 458.
- Lachiewicz, P. F. et al., 2009. Femoral head size and wear of highly cross-linked polyethylene at 5 to 8 years. *Clinical orthopaedics and related research*, 467(12), pp. 3290-3296.
- Lakstein, D. et al., 2016. Pre-Operative Planning of Total Hip Arthroplasty on Dysplastic Acetabuli. *HIP International*, 27(1), pp. 55-59.
- Langston, J., Pierrepont, J., Gu, Y. & Shimmin, A., 2018. Risk factors for increased sagittal pelvic motion causing unfavourable orientation of the acetabular component in patients undergoing total hip arthroplasty. *The Bone & Joint Journal*, 100-B(7), pp. 845-852.
- Larson, C. M., Kelly, B. T. & Stone, R. M., 2011. Making a Case for Anterior Inferior Iliac Spine/Subspine Hip Impingement: Three Representative Case Reports and Proposed Concept. *Arthroscopy: The Journal of Arthroscopic & Related Surgery*, 27(12), pp. 1732-1737.
- Layton, R. B., Messenger, N. & Stewart, T. D., 2021. Analysis of hip joint cross-shear under variable activities using a novel virtual joint model within Visual3D. *Proceedings of the Institution of Mechanical Engineers, Part H: Journal of Engineering in Medicine*, 235(10), pp. 1197-1204.
- Lecerf, G. et al., 2009. Femoral offset: Anatomical concept, definition, assessment, implications for preoperative templating and hip arthroplasty. *Orthopaedics & Traumatology: Surgery & Research*, 95(3), pp. 210-219.
- Lee, S. H., Lim, C. W., Choi, K. Y. & Jo, S., 2019. Effect of Spine-Pelvis Relationship in Total Hip Arthroplasty. *Hip & pelvis*, 31(1), pp. 4-10.

- Lee, Y.-K. et al., 2011. Metal neck and liner impingement in ceramic bearing total hip arthroplasty. *Journal of Orthopaedic Research*, 29(2), pp. 218-222.
- Leng, J. et al., 2017. Dynamic virtual simulation of the occurrence and severity of edge loading in hip replacements associated with variation in the rotational and translational surgical position. *Proceedings of the Institution of Mechanical Engineers, Part H: Journal of Engineering in Medicine*, 231(4), pp. 299-306.
- Leslie, I. J. et al., 2009. High cup angle and microseparation increase the wear of hip surface replacements. *Clinical orthopaedics and related research*, 467(9), pp. 2259-2265.
- Lewinnek, G. E. et al., 1978. Dislocations after total hip-replacement arthroplasties. *JBJS*, 60(2).
- Lin, H.-C. et al., 2015. Theoretical Analysis of Total Hip Dislocation and Comparison of Hemispherical Cup and Newly Developed Cup. *Journal of Medical and Biological Engineering*, 35(5), pp. 661-669.
- Liu, F., Williams, S. & Fisher, J., 2015. Effect of microseparation on contact mechanics in metal-on-metal hip replacements-A finite element analysis. *Journal of biomedical materials research. Part B, Applied biomaterials*, 103(6), pp. 1312-1319.
- Lopez, D., Leach, I., Moore, E. & Norrish, A. R., 2017. Management of the Infected Total Hip Arthroplasty. *Indian journal of orthopaedics*, 51(4), pp. 397-404.
- Malik, A., Maheshwari, A. & Dorr, L. D., 2007. Impingement with Total Hip Replacement. *JBJS*, 89(8).
- Maratt, J. D. et al., 2016. No Difference in Dislocation Seen in Anterior Vs Posterior Approach Total Hip Arthroplasty. *The Journal of Arthroplasty*, 31(9, Supplement), pp. 127-130.
- Marchetti, E. et al., 2011. Component impingement in total hip arthroplasty: Frequency and risk factors. A continuous retrieval analysis series of 416 cup. *Orthopaedics & Traumatology: Surgery & Research*, 97(2), pp. 127-133.
- Matsushita, A. et al., 2009. Effects of the Femoral Offset and the Head Size on the Safe Range of Motion in Total Hip Arthroplasty. *The Journal of Arthroplasty*, 24(4), pp. 646-651.
- McCarthy, T. F. et al., 2017. The Effect of Pelvic Tilt and Femoral Head Size on Hip Range-of-Motion to Impingement. *The Journal of Arthroplasty*, 32(11), pp. 3544-3549.
- McLawnhorn, A. et al., 2015. Targeting a New Safe Zone: A Step in the Development of Patient-Specific Component Positioning for Total Hip Arthroplasty. *American journal of orthopaedics (Belle Mead, N.J.)*, Volume 44, pp. 270-276.
- Mellon, S. J., Liddle, A. D. & Pandit, H., 2013. Hip replacement: Landmark surgery in modern medical history. *Maturitas*, 75(3), pp. 221-226.
- Minoda, Y., Kadowaki, T. & Kim, M., 2006. Acetabular Component Orientation in 834 Total Hip Arthroplasties Using a Manual Technique. *Clinical Orthopaedics and Related Research*®, Volume 445.

- Mjaaland, K. E. et al., 2017. Implant Survival After Minimally Invasive Anterior or Anterolateral Vs. Conventional Posterior or Direct Lateral Approach: An Analysis of 21,860 Total Hip Arthroplasties from the Norwegian Arthroplasty Register (2008 to 2013). *JBJS*, 99(10).
- Montiel, V. et al., 2020. Total Hip Arthroplasty Digital Templating: Size Predicting Ability and Interobserver Variability. *Indian journal of orthopaedics*, 54(6), pp. 840-847.
- Moretti, V. M. & Post, Z. D., 2017. Surgical Approaches for Total Hip Arthroplasty. *Indian journal of orthopaedics*, 51(4), pp. 368-376.
- Morris, W. Z. et al., 2018. Hip morphology predicts posterior hip impingement in a cadaveric model. *HIP International*, 29(3), pp. 322-327.
- Murray, D. W., 1993. The definition and measurement of acetabular orientation. *The Journal of Bone and Joint Surgery. British volume*, 75-B(2), pp. 228-232.
- Nadzadi, M. E. et al., 2003. Kinematics, kinetics, and finite element analysis of commonplace maneuvers at risk for total hip dislocation. *Journal of Biomechanics*, 36(4), pp. 577-591.
- Nadzadi, M. E. et al., 2003. Kinematics, kinetics, and finite element analysis of commonplace maneuvers at risk for total hip dislocation. *Journal of Biomechanics*, 1 4, 36(4), pp. 577-591.
- Nakahara, I. et al., 2011. Gender differences in 3D morphology and bony impingement of human hips. *Journal of Orthopaedic Research*, 29(3), pp. 333-339.
- National Joint Registry, 2020. *17th annual report*, England, Wales and Northern Ireland: National Joint Registry.
- NHS, 2019. *Overview - Hip Replacement*. [Online] Available at: <https://www.nhs.uk/conditions/hip-replacement/> [Accessed 20 October 2022].
- Novikov, D. et al., 2019. Can some early revision total hip arthroplasties be avoided?. *The Bone & Joint Journal*, 101-B(6_Supple_B), pp. 97-103.
- O'Dwyer Lancaster-Jones, O. et al., 2018. An in vitro simulation model to assess the severity of edge loading and wear, due to variations in component positioning in hip joint replacements. *Journal of biomedical materials research. Part B, Applied biomaterials*, 106(5), pp. 1897-1906.
- Ogawa, T. et al., 2018. Soft tissue tension is four times lower in the unstable primary total hip arthroplasty. *International Orthopaedics*, 42(9), pp. 2059-2065.
- Padgett, D. E., Lipman, J., Robie, B. & Nestor, B. J., 2006. Influence of Total Hip Design on Dislocation: A Computer Model and Clinical Analysis. *Clinical Orthopaedics and Related Research*®, Volume 447.
- Palan, J. et al., 2009. Which approach for total hip arthroplasty: anterolateral or posterior?. *Clinical orthopaedics and related research*, 467(2), pp. 473-477.
- Palit, A. et al., 2017. Femur First navigation can reduce impingement severity compared to traditional free hand total hip arthroplasty. *Scientific Reports*, 7(1), p. 7238.

- Patel, A. B. et al., 2010. Guidelines for Implant Placement to Minimize Impingement During Activities of Daily Living After Total Hip Arthroplasty. *The Journal of Arthroplasty*, 25(8), pp. 1275-1281.e1.
- Patsiogiannis, N., Kanakaris, N. K. & Giannoudis, P. V., 2021. Periprosthetic hip fractures: an update into their management and clinical outcomes. *EFORT open reviews*, 6(1), pp. 75-92.
- Pedersen, D. R., Callaghan, J. J. & Brown, T. D., 2005. Activity-dependence of the "safe zone" for impingement versus dislocation avoidance. *Medical Engineering & Physics*, 27(4), pp. 323-328.
- Pierrepoint, J. et al., 2017. Variation in functional pelvic tilt in patients undergoing total hip arthroplasty. *The Bone & Joint Journal*, 99-B(2), pp. 184-191.
- Pryce, G. M., 2019. *PhD: Polyethylene acetabular liner rim damage in total hip replacements*. Leeds, UK: White Rose eTheses Online.
- Pryce, G. M. et al., 2022. Impingement in total hip arthroplasty: A geometric model. *Proceedings of the Institution of Mechanical Engineers. Part H, Journal of engineering in medicine*, 236(4), pp. 9544119211069472-9544119211069472.
- Ro, J., Kim, P. & Shin, C. S., 2018. Optimizing total hip replacement prosthesis design parameter for mechanical structural safety and mobility. *International Journal of Precision Engineering and Manufacturing*, 19(1), pp. 119-127.
- Saputra, E., Anwar, I. B., Jamari, J. & van der Heide, E., 2013. Finite Element Analysis of Artificial Hip Joint Movement During Human Activities. *Procedia Engineering*, Volume 68, pp. 102-108.
- Sariali, E., Lazennec, J. Y., Khiami, F. & Catonné, Y., 2009. Mathematical evaluation of jumping distance in total hip arthroplasty: influence of abduction angle, femoral head offset, and head diameter. *Acta orthopaedica*, 80(3), pp. 277-282.
- Sariali, E. et al., 2012. Accuracy of the preoperative planning for cementless total hip arthroplasty. A randomised comparison between three-dimensional computerised planning and conventional templating. *Orthopaedics & Traumatology: Surgery & Research*, 98(2), pp. 151-158.
- Schiffner, E. et al., 2018. Is computerised 3D templating more accurate than 2D templating to predict size of components in primary total hip arthroplasty?. *HIP International*, 29(3), pp. 270-275.
- Schwarz, J. et al., 2022. Effect of Pelvic Sagittal Tilt and Axial Rotation on Functional Acetabular Orientation. *Orthopedics*, 0(0), pp. 1-4.
- Sechriest, V. F. et al., 2007. Activity Level in Young Patients With Primary Total Hip Arthroplasty: A 5-Year Minimum Follow-up. *The Journal of Arthroplasty*, 22(1), pp. 39-47.
- Shoji, T. et al., 2017. Factors affecting the potential for posterior bony impingement after total hip arthroplasty. *The Bone & Joint Journal*, 99-B(9), pp. 1140-1146.

- Shoji, T. et al., 2016. Anterior Inferior Iliac Spine Bone Morphology in Hip Dysplasia and Its Effect on Hip Range of Motion in Total Hip Arthroplasty. *The Journal of Arthroplasty*, 31(9), pp. 2058-2063.
- Shoji, T. et al., 2013. Bony impingement depends on the bone morphology of the hip after total hip arthroplasty. *International Orthopaedics*, 37(10), pp. 1897-1903.
- Shon, W. Y. et al., 2005. Impingement in Total Hip Arthroplasty: A Study of Retrieved Acetabular Components. *The Journal of Arthroplasty*, 20(4), pp. 427-435.
- Sierra, R. J., Raposo, J. M., Trousdale, R. T. & Cabanela, M. E., 2005. Dislocation of Primary THA Done through a Posterolateral Approach in the Elderly. *Clinical Orthopaedics and Related Research*®, Volume 441.
- Sikes, C. V. et al., 2008. Instability After Total Hip Arthroplasty: Treatment with Large Femoral Heads vs Constrained Liners. *The Journal of Arthroplasty*, 23(7, Supplement), pp. 59-63.
- Singh, G. et al., 2018. Manufacturing, oxidation, mechanical properties and clinical performance of highly cross-linked polyethylene in total hip arthroplasty. *HIP International*, 28(6), pp. 573-583.
- Smith, T., Davies, L., Ingham, C. & Mann, C., 2012. What activities cause hip dislocation? A review of 100 total hip replacement dislocations*. *European Journal of Physiotherapy*, Volume 14.
- Stigler, S. K. et al., 2017. Digital templating in total hip arthroplasty: Additional anteroposterior hip view increases the accuracy. *World journal of orthopedics*, 8(1), pp. 30-35.
- Stroh, D. A. et al., 2013. Reduced Dislocation Rates and Excellent Functional Outcomes With Large-Diameter Femoral Heads. *The Journal of Arthroplasty*, 28(8), pp. 1415-1420.
- Sugano, N. et al., 2012. Dynamic Measurements of Hip Movement in Deep Bending Activities After Total Hip Arthroplasty Using a 4-Dimensional Motion Analysis System. *The Journal of Arthroplasty*, 27(8), pp. 1562-1568.
- Tabata, T., Kaku, N., Tagomori, H. & Tsumura, H., 2019. Influence of hip center position, anterior inferior iliac spine morphology, and ball head diameter on range of motion in total hip arthroplasty. *Orthopaedics & Traumatology: Surgery & Research*, 105(1), pp. 23-28.
- Takao, M., Nishii, T., Sakai, T. & Sugano, N., 2016. Postoperative Limb-Offset Discrepancy Notably Affects Soft-Tissue Tension in Total Hip Arthroplasty. *JBJS*, 98(18).
- Tannast, M. et al., 2005. Anatomic Referencing of Cup Orientation in Total Hip Arthroplasty. *Clinical Orthopaedics and Related Research*®, Volume 436.
- Tateuchi, H. et al., 2017. Daily cumulative hip moment is associated with radiographic progression of secondary hip osteoarthritis. *Osteoarthritis and Cartilage*, 25(8), pp. 1291-1298.
- Tower, S. S. et al., 2007. Rim Cracking of the Cross-Linked Longevity Polyethylene Acetabular Liner After Total Hip Arthroplasty. *JBJS*, 89(10).

- Tsikandylakis, G. et al., 2018. Head size in primary total hip arthroplasty. *EFORT open reviews*, 3(5), pp. 225-231.
- Turley, G. A., Williams, M. A., Wellings, R. M. & Griffin, D. R., 2013. Evaluation of range of motion restriction within the hip joint. *Medical & biological engineering & computing*, 51(4), pp. 467-477.
- Usrey, M. M. et al., 2006. Does Neck/Liner Impingement Increase Wear of Ultrahigh-Molecular-Weight Polyethylene Liners?. *The Journal of Arthroplasty*, 21(6, Supplement), pp. 65-71.
- Valle, A. G. D., Slullitel, G., Piccaluga, F. & Salvati, E. A., 2005. The precision and usefulness of preoperative planning for cemented and hybrid primary total hip arthroplasty. *The Journal of Arthroplasty*, 20(1), pp. 51-58.
- Waddell, B. S. et al., 2018. Have large femoral heads reduced prosthetic impingement in total hip arthroplasty?. *HIP International*, 29(1), pp. 83-88.
- Weber, M. et al., 2016. Current standard rules of combined anteversion prevent prosthetic impingement but ignore osseous contact in total hip arthroplasty. *International Orthopaedics*, 40(12), pp. 2495-2504.
- Weeden, S. H., Paprosky, W. G. & Bowling, J. W., 2003. The early dislocation rate in primary total hip arthroplasty following the posterior approach with posterior soft-tissue repair1 1No benefits or funds were received in support of this study. *The Journal of Arthroplasty*, 18(6), pp. 709-713.
- Widmer, K. H. & Majewski, M., 2005. The impact of the CCD-angle on range of motion and cup positioning in total hip arthroplasty. *Clinical Biomechanics*, 20(7), pp. 723-728.
- Williams, S., Al-Hajjar, M., Isaac, G. H. & Fisher, J., 2013. Comparison of ceramic-on-metal and metal-on-metal hip prostheses under adverse conditions. *Journal of Biomedical Materials Research Part B: Applied Biomaterials*, 101B(5), pp. 770-775.
- Williams, S. et al., 2003. Wear and deformation of ceramic-on-polyethylene total hip replacements with joint laxity and swing phase microseparation. *Proceedings of the Institution of Mechanical Engineers, Part H: Journal of Engineering in Medicine*, 217(2), pp. 147-153.
- Williams, S. et al., 2022. *LIPPED LINERS IN TOTAL HIP ARTHROPLASTY: THE EFFECT OF LIP ORIENTATION*. Bournemouth, UK, The British Editorial Society of Bone & Joint Surgery, p. 9.
- Woerner, M. et al., 2017. Soft tissue restricts impingement-free mobility in total hip arthroplasty. *International Orthopaedics*, 41(2), pp. 277-282.
- Wu, G. et al., 2002. ISB recommendation on definitions of joint coordinate system of various joints for the reporting of human joint motion—part I: ankle, hip, and spine. *Journal of Biomechanics*, 35(4), pp. 543-548.
- Wyatt, M. C. et al., 2020. Are Lipped Polyethylene Liners Associated with Increased Revision Rates in Patients with Uncemented Acetabular Components? An Observational Cohort Study. *Clinical orthopaedics and related research*, 478(3), pp. 581-589.

Wylde, V. et al., 2009. Prevalence and functional impact of patient-perceived leg length discrepancy after hip replacement. *International Orthopaedics*, 33(4), pp. 905-909.

Yamaguchi, M., Akisue, T., Bauer, T. W. & Hashimoto, Y., 2000. The spatial location of impingement in total hip arthroplasty. *The Journal of Arthroplasty*, 15(3), pp. 305-313.

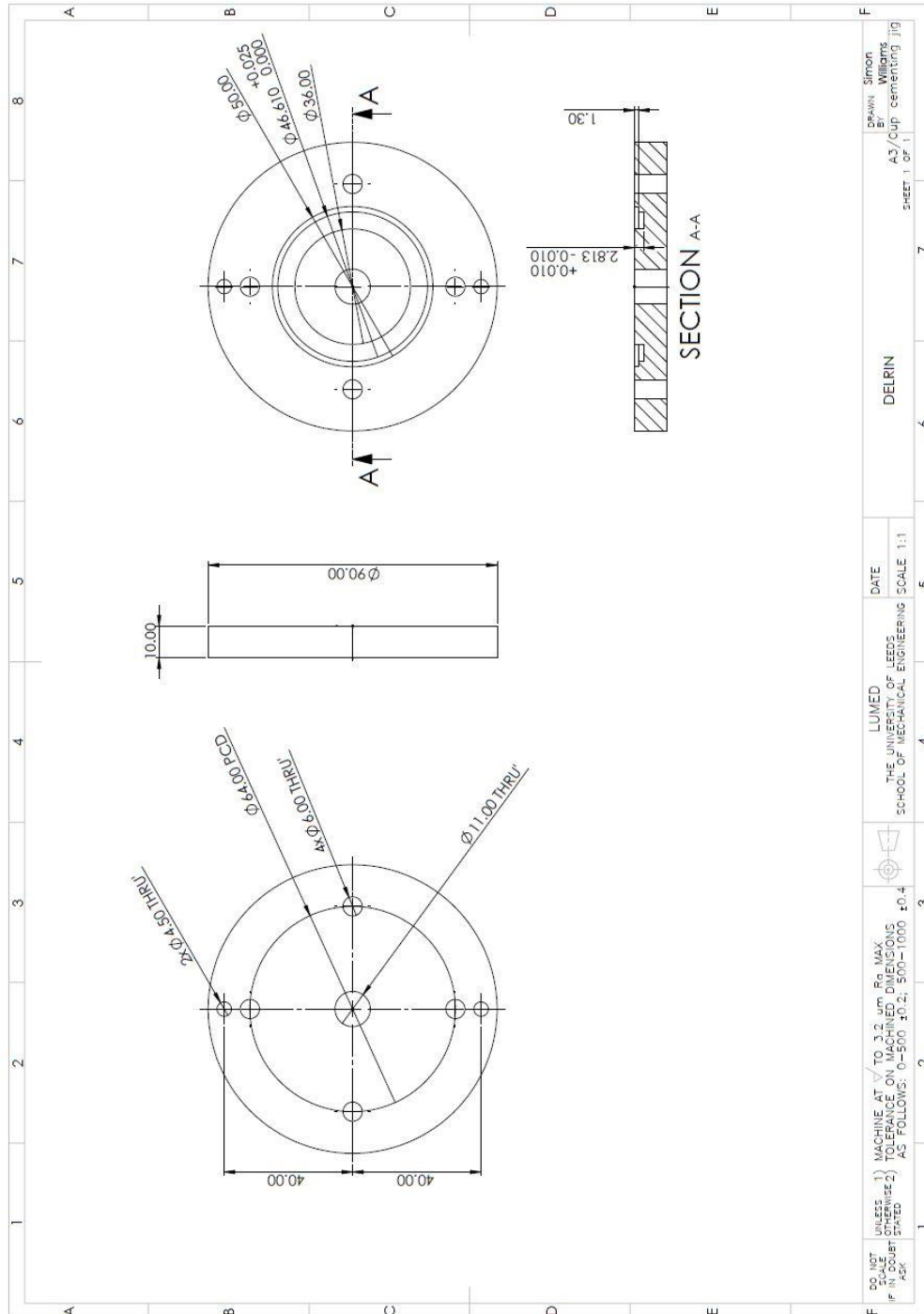
Yoshimine, F. & Ginbayashi, K., 2002. A mathematical formula to calculate the theoretical range of motion for total hip replacement. *Journal of Biomechanics*, 35(7), pp. 989-993.

Zhou, H. et al., 2013. Motion performance and impingement risk of total hip arthroplasty with a simulation module. *Journal of Zhejiang University. Science. B*, 14(9), pp. 849-854.

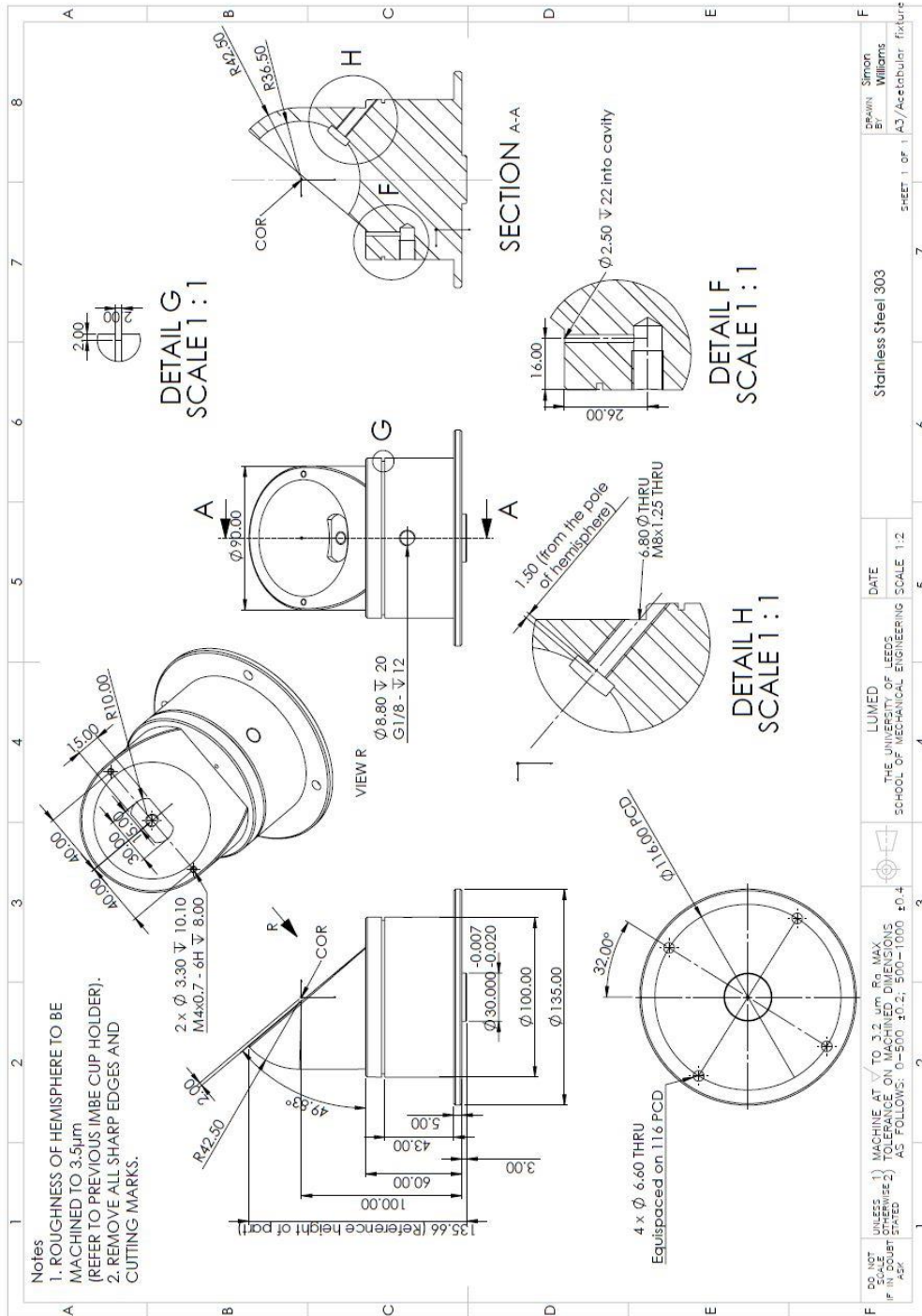
Zijlstra, W. P. et al., 2017. Effect of femoral head size and surgical approach on risk of revision for dislocation after total hip arthroplasty. *Acta orthopaedica*, 88(4), pp. 395-401.

Appendix A: Engineering drawings for hip simulator study (Chapter Six)

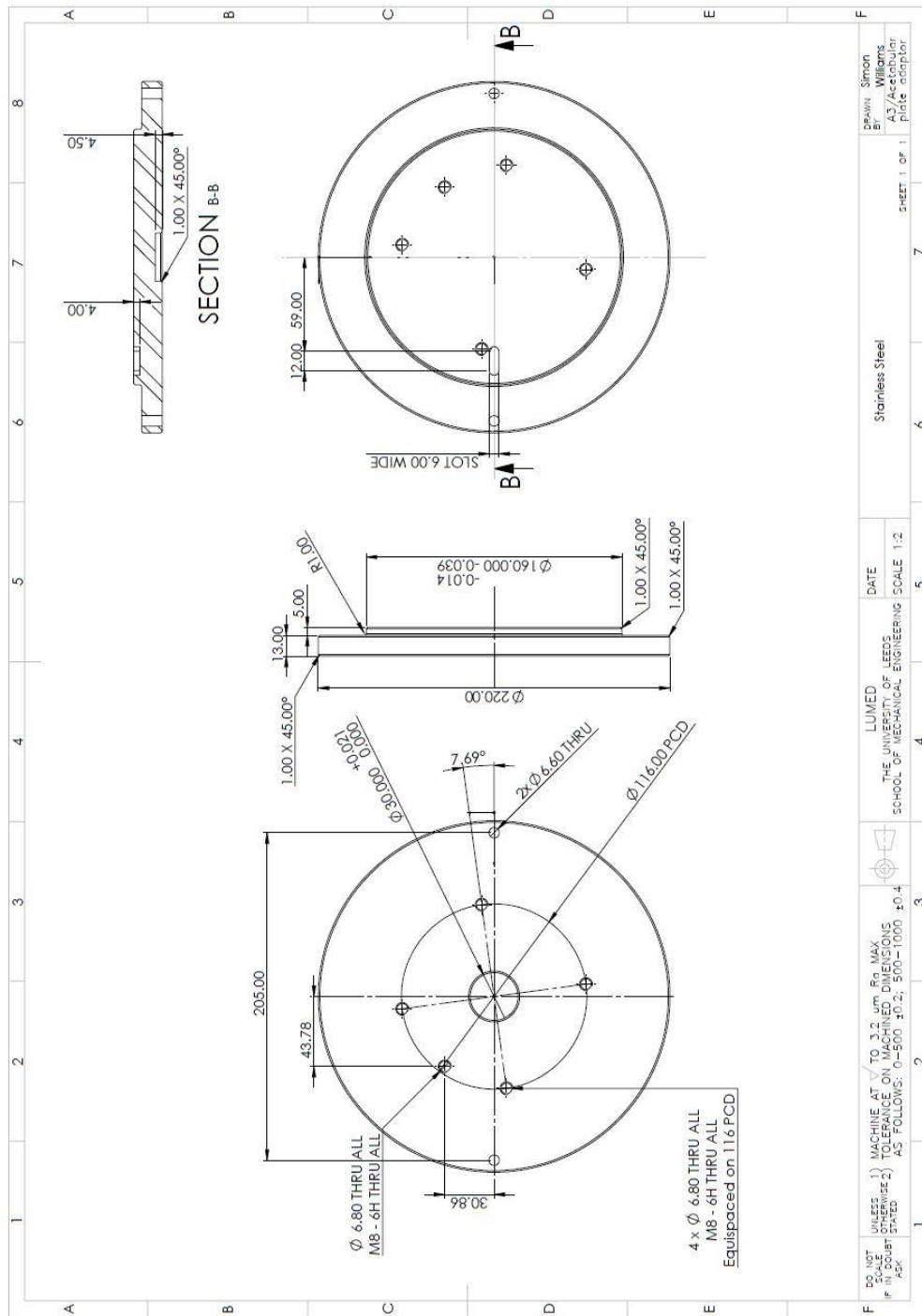
Cup cementing jig (Delrin)



Cup holder (Stainless Steel 303)



Acetabular plate adaptor (Stainless Steel 303)



Femoral plate adaptor (Stainless Steel 303)

